

**An automated computer-assisted approximation of the nose in
South Africans from CBCT (Cone Beam Computed Tomography)
scans**

Submitted by:

Alison Ridel

A thesis submitted to the Department of Anatomy, School of Medicine, Faculty of Health
Sciences, University of Pretoria, in fulfilment of the requirements for the degree

of

PhD in Anatomy

Pretoria, 2018

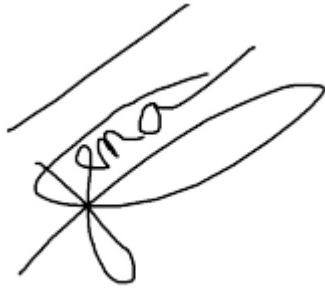
Supervisor: Prof. A.C. Oettlé

Co-supervisors: Prof. E.N. L'Abbé & Dr. F. Demeter

DECLARATION

I, Alison Ridel, declare that this dissertation is my own work. It is being submitted for the degree of PhD in Anatomy at the University of Pretoria. It has not been submitted before for any other degree or examination at this or any other institution.

Sign:

A handwritten signature in black ink, appearing to read 'Alison Ridel', written over a horizontal line. The signature is stylized and cursive.

This 06 Day of December, 2018

Thesis supervisor

Prof. A.C. Oettlé

Associate professor.

Department of Anatomy and Histology, School of Medicine, Sefako Makgatho Health Sciences University, Ga-Rankuwa, Pretoria, South Africa.

Extraordinary lecturer.

Department of Anatomy, Faculty of Health Sciences, University of Pretoria, Pretoria, South Africa.

Thesis co-supervisors

Prof. E.N. L'Abbé

Full Professor.

Section: Physical anthropology, Department of Anatomy, Faculty of Health Sciences, University of Pretoria, Pretoria, South Africa.

Dr. F. Demeter

Researcher.

Musée de l'Homme, UMR7206, 17 Place du Trocadéro, 75116 Paris, France.

Natural History Museum of Denmark, University of Copenhagen, Copenhagen, Denmark.

Extraordinary lecturer, Department of Anatomy, Faculty of Health Sciences, University of Pretoria, Pretoria, South Africa.

Statistical assistance:

Prof. D. Vandermeulen

Associate Professor.

Center for Processing Speech and Images (PSI), Department of Electrical Engineering (ESAT), KU Leuven, Belgium.

Extraordinary professor.

Department of Anatomy, Faculty of Health Sciences, University of Pretoria, Pretoria, South Africa.

The Research Ethics Committee, Faculty Health Sciences, University of Pretoria complies with ICH-GCP guidelines and has US Federal wide Assurance.

- FWA 00002567, Approved dd 22 May 2002 and Expires 20 Oct 2016.
- IRB 0000 2235 IORG0001762 Approved dd 22/04/2014 and Expires 22/04/2017.



UNIVERSITEIT VAN PRETORIA
UNIVERSITY OF PRETORIA
YUNIBESITHI YA PRETORIA

Faculty of Health Sciences Research Ethics Committee

18/08/2016

**Approval Certificate
New Application**

Ethics Reference No.: 301/2016

Title: An automated computer assisted approximation of the nose in South Africans from CBCT (Cone Beam Computer Tomography) scans

Dear Alison Fany Ridel

The **New Application** as supported by documents specified in your cover letter dated 12/08/2016 for your research received on the 15/08/2016, was approved by the Faculty of Health Sciences Research Ethics Committee on its quorate meeting of 17/08/2016.

Please note the following about your ethics approval:

- Ethics Approval is valid for 3 years
- Please remember to use your protocol number (**301/2016**) on any documents or correspondence with the Research Ethics Committee regarding your research.
- Please note that the Research Ethics Committee may ask further questions, seek additional information, require further modification, or monitor the conduct of your research.

Ethics approval is subject to the following:

- The ethics approval is conditional on the receipt of **6 monthly written Progress Reports**, and
- The ethics approval is conditional on the research being conducted as stipulated by the details of all documents submitted to the Committee. In the event that a further need arises to change who the investigators are, the methods or any other aspect, such changes must be submitted as an Amendment for approval by the Committee.

Additional Conditions:

- Approval is conditional upon the Research Ethics Committee receiving the PhD Committee approval letter

We wish you the best with your research.

Yours sincerely

*** Kindly collect your original signed approval certificate from our offices, Faculty of Health Sciences, Research Ethics Committee, Tswelopele Building, Level 4-60*

Dr R Sommers; MBChB; MMed (Int); MPharMed, PhD

Deputy Chairperson of the Faculty of Health Sciences Research Ethics Committee, University of Pretoria

The Faculty of Health Sciences Research Ethics Committee complies with the SA National Act 61 of 2003 as it pertains to health research and the United States Code of Federal Regulations Title 45 and 46. This committee abides by the ethical norms and principles for research, established by the Declaration of Helsinki, the South African Medical Research Council Guidelines as well as the Guidelines for Ethical Research: Principles Structures and Processes 2004 (Department of Health).

☎ 012 356 3084 ✉ deepeka.behari@up.ac.za / fnsethics@up.ac.za 🌐 <http://www.up.ac.za/healthethics>
✉ Private Bag X323, Arcadia, 0007 - Tswelopele Building, Level 4, Room 60, Gezina, Pretoria

SUMMARY

Each year in the Gauteng province of South Africa, approximately 1300 bodies are incinerated without a known identity (Bloom, 2015; Krüger *et al.*, 2018). Because of various socio-economic reasons, identification is not always possible with conventional methods such as DNA comparisons and fingerprints. Therefore, more creative methods, including facial reconstruction, have been implemented to assist in the identification of unknown persons from their skeletal remains in South Africa.

The aim of this thesis was to provide an automated computer-assisted method, independent of any forensic artistic interpretations, to create accurate statistical models for predicting nasal soft-tissue shape from information about the underlying skull substrate. The acquisition and extraction of the relevant anatomical structures (hard- and soft-tissue) were performed using an automatic dense landmarking procedure and analysed by geometric morphometrics.

In this research, a validation of the precision of the automatic placement of landmarks, demonstrated its utilisation as a convenient prerequisite for geometric morphometric based shape analysis of the nasal complex. The automatic landmark positioning on hard- and soft-tissue 3D surfaces offered increased objectivity and the possibility of standardisation. In addition to reducing measurement errors in landmark placements, automatic landmarking, achieved a better precision for facial approximation, enabling the possibility to include more samples and populations with ease.

A detailed study of the influence of factors (ancestry, sex, ageing and allometry) on the variability of the mid-facial skeleton among two South African ancestral groups were performed, revealing their statistically significant influences on the overall shape variation of the nose. Ancestry was found to be a very important factor in shape variation within the sample emphasising ancestral-specific differences. In addition, the expression of sexual dimorphism and effect of aging appeared to be different on distinct elements of the shape of the mid-facial region. From the findings, the two South African groups differed significantly regarding hard- and soft-tissue nasal complex morphology and their correlations, emphasising the importance

of considering ancestry, sex and age as factors in the process of approximating the nose and highlighting the need for population specific accurate and reliable 3D statistical nose prediction methods.

This study provided accurate statistical models using Partial Least Squared Regression (PLSR) algorithms which were optimised by including additional information such as ancestry, sex and age. Age and sex appeared to be important factors to be considered as additional information in order to improve the quality of the prediction. The predictions were based on a sample of 200 specimens resulting in an error when using the landmark-to-landmark distances on non-trained data, ranging between 2.139 mm and 2.833 mm for black South Africans at the tip of the nose and the alae, while they ranged from 2.575 mm to 2.859 mm for white South Africans.

This research is the first attempt at a computer-assisted facial approximation of the nose with an automatic landmarking approach for the development of valid and reliable South African population specific standards using Cone Beam Computer-Tomography scans.

Key words: Statistical modelling; Non-rigid surface registration; Automatic landmarking; Shape variation; Geometric morphometrics; Partial Least Squared Regression; Identification of unknown individuals; Templates; Craniometric landmarks; Capulometric landmarks.

*À ma petite Maman, Françoise Ridel (5 Juillet 1955-12 Août 2014),
«Rechoisis, en son nom, ta vie,
et tu honoreras sa mort.»*

ACKNOWLEDGMENTS

This doctoral research was a particularly rewarding personal and professional experience, but one which would not have been possible without the contribution of so many. The following acknowledgements are addressed to all the people and institutions who, through their kindness, collaboration and support, contributed to the achievement of this doctoral dissertation.

First, I would like to thank Professor Anna Oettlé (SMU, Pretoria, South Africa; UP, Pretoria, South Africa), main supervisor of this doctoral dissertation, for offering me the opportunity to work on this fascinating research topic, and for her tutelage during these last three years. My sincerest thanks for her scientific support, her patience and her availability, and for her meticulous, critical and educational reviews of the various manuscripts. My special thanks for having welcomed me to this beautiful country and for all those efforts to make me feel at home. Thank you for these past three years; it has been a wonderful adventure..

I would like to express my deepest gratitude to Professor Ericka L'Abbé (UP, Pretoria, South Africa), co-director of this thesis, for her support throughout the last three years. I am extremely grateful for her investment in manuscript improvements. I also warmly thank Professor Ericka L'Abbé for her scientific support, which has greatly contributed to strengthening my scientific reflections. I thank her for her warm welcome to our team and her determination to provide me with a more than ideal framework.

I would like to thank Dr. Fabrice Demeter (NHMD, Copenhagen, Danmark; MNHN, Paris, France; UP, Pretoria, South Africa), also co-director of this thesis, for the opportunity to be an integral part of this great project. I thank him for his trust, and for giving me the opportunity to work on this research topic. I also thank him for his warm welcome to the Museum of Man during my many visits to Paris.

My thanks also to Professor Dirk Vandermeulen (KU Leuven, Leuven, Belgium; UP Pretoria, South Africa) for his meticulous supervision concerning all the statistical procedures used in this thesis. Our discussions were invaluable to advance my scientific reflections throughout the last three years. I thank him for his patience, his advice and his availability. I also thank him for welcoming me very warmly to the University of Leuven.

To Dr. Peter Claes (KU Leuven, Leuven, Belgium), thank you for presenting our four oral presentations at the international conference of International IACI (International Association of Craniofacial Identification) held in Brisbane (Australia) in July 2017.

This work would not have been possible without the full funding of my three years thesis by the project AESOP + Erasmus Mundus Program, and for that I would like to particularly thank Professor José Braga (AMIS, Toulouse), coordinator of the project. I would also like to thank Elodie Balonas (Manager, AESOP +) for her availability in organising bookings and processing expenses related to this thesis during the last three years.

I would like to thank Dr. Amélie Vialet (UMR 7194, MNHN, Paris, CERPT, Tautavel) for her valuable advice and support, especially for initiating my meeting with Dr. Fabrice Demeter (MNHN, UP) without which none of this would have been possible.

This research work has benefited from the investment of various researchers, engineers and technicians who, by their availability, greatly facilitated access to collections and imaging platforms and contributed to the constitution of the sample of this thesis. My heartfelt thanks to Dr. André Uys (Oral and Dental Hospital, University of Pretoria) and Dr. Sarel Botha (Medical Centre, Life Groenkloof Hospital, Pretoria) for generously granting me access to a large database of tomographic acquisitions of modern South African specimens. I also thank them for their trust in providing me with the necessary equipment to conduct my analyses. I would also like to thank the entire radiology team of the Oral Hospital of the University of Pretoria for their availability and their goodwill.

I am very grateful to Jade Liebenberg in her role of research assistant during the first two years of this thesis, and for her considerable contribution to the measurement of observer errors. Thank you for your patience and your availability.

I would like to express my deepest gratitude to Dr. Manon Galland (MNHN, Paris, France; UP, Pretoria, South Africa) for her support in the study of the validation of the landmarks placed automatically by the performance of the observer errors. I must also thank her for our debates on geometric morphometric that greatly contributed to the development of the statistical analysis protocol of this thesis. Thank you, Manon, for your support and your availability.

I extend my thanks to Professor Carl Stephan (UQ, Brisbane, Australia), to whom I am extremely grateful for his investment in providing corrections and improvements on the first article of this thesis published in the Forensic Science International journal.

I thank Dr. Jean Dumoncel (CNRS, AMIS, Toulouse) for having welcomed me to the AMIS laboratory (Molecular Anthropology and Imaging Synthesis) of the University of Toulouse III at the beginning of this thesis, and for contributing to its inception. I thank him for his advice, patience and our discussions which greatly contributed to my training in morphometric geometry and to the inception of the statistical analysis protocol of this thesis.

I would also like to thank Dr. Clément Zanolli (CNRS, AMIS, Toulouse) for our discussions that contributed to the inception of this thesis project. I thank him for his support and availability over the last three years.

I would especially like to thank Dr. Gaël Becam (HNHP, Paris, France; EPCC / CERP, Tautavel; MNHN, Paris, France) who, by agreeing to supervise my master's degree five years ago, gave me the opportunity to continue in the field of research. Thank you, Gaël, for your support and your friendship throughout the past five years.

I warmly thank all the members of the Department of Anatomy of the University of Pretoria, who welcomed me during these three years, for their kindness and their consideration. I would especially like to thank Charlotte Theye (UP, Pretoria) for her daily presence, support and friendship. In particular, I think of our enriching discussions which greatly contributed to the construction of my scientific reflexions. I thank her for her invaluable help in organizing my arrival and settling in South Africa. Thank you, Charlotte, for being with me (in the same boat!) these last three years.

I also extend my thanks to Dr. Marie Dussault (UP, Pretoria) for our discussions, her advice and her availability, especially during the last year of this study . I thank her for her support and for our daily discussions, which greatly contributed to the development of this thesis.

I extend my thanks to Dr. Marine Cazenave (AMIS, Toulouse, UP, Pretoria) for our discussions and for her friendship throughout these three years. I thank her for her support and for our daily discussions which greatly contributed to the construction of my scientific reflexions.

I also warmly thank Dr. Amelie Beaudet (University of the Witwatersrand, Johannesburg) for our discussions, her advice and availability.

Of course, my heartfelt thanks to all these friends, and for all the great times spent together over these last years: Christelle, Gaël, Khier, Olive, Nico, Agnes, Aurelio, Constance, Cyril (Planchand), Clementine , Sophie, Romain, Jean-Marc, Leáne, Benjamin, Charlotte; Marine, Amelie, Clement, Jean, Marie, Gabi, Clarissa, Delia, Francois, Gaetan, Orian, Juliette, Manon, Cyril (Viallet), Cyrielle, Djibril, Julien, Loic, Daniela, Arnaud, Carole, Pierre. I especially thank my friend Zakia, for putting up me all those nights during my many trips to the MNHN in Paris.

My special thanks for my friends who, through shared experiences and over time have become as important to me as my own family: Christelle, Gaël, Olive, Nico, Khier, Agnes, Aurel, Constance, Hugo, Pauline, Gratien, Sophie, Romain, Jean Marc, Noam, Sasha, Leáne,

Benjamin, Samuel, Eloïse and Lucky (my “twin Sotho brother”). I thank you with all my heart for your unconditional support, your friendship and your presence during the good and the not so good moments of my life, even when we found ourselves 8 000 km apart.

This work could not have been done without the full support of my family: Jose, my father, Fany, my sister, Leo and Elliott, my brothers. I also thank my brother-in-law Nicolas and my sister-in-law Marlene, as well as my nieces: Zia, Lune, Lucie, Lola, Marie, Victoria and my nephew Carles. Thank you for supporting me and encouraging me throughout my studies and even more in the last three years. I would also like to thank Philippe and Christine, my parents-in-law and all the members of my family-in-law, especially Clément, Marion, Jessica, and Martine (la nounne).

I especially thank my sister Fany, for her daily presence, her encouragement to pursue my goals, whatever the circumstances. I thank her for her unconditional love, her kindness, for caring about me since forever. Most of all I thank her for just being there.

My infinite thanks to my father, who has, without doubt, contributed greatly to my passion for research. I thank him for our endless debates and discussions, since I was small. I thank him for teaching me the desire to learn, which for so many years has fuelled me everyday.

Lastly, my thanks to the one who shares my daily life, Gratien. I cannot thank you enough for your incredible patience over the past five years. I will never be able to thank you enough for agreeing to come with me to the other side of the world to let me pursue my passion. Thank you for all your encouragement, for your support, and for just being there. Without you, I would never have come so far.

These acknowledgements cannot be complete without dedicating a moment to my late mother, who will never read these words, but without whom, they could not have been written.

REMERCIEMENTS

Ce travail de doctorat a été une expérience personnelle et professionnelle, particulièrement enrichissante, mais il a été bien évidemment une aventure humaine inestimable. Les remerciements de cette thèse sont adressés à toutes les personnes et institutions qui, par leur accueil, leur collaboration et leur soutien, ont contribué à la réalisation de ce travail.

En premier lieu, je souhaiterais remercier le Professeur Anna Oettlé (SMU, Pretoria, South Africa; UP, Pretoria, South Africa), directrice de ce travail de thèse, pour son encadrement durant ces trois années, pour m'avoir offert l'opportunité de travailler sur ce sujet de recherche passionnant et accueilli au sein de son équipe. Je la remercie chaleureusement pour son accompagnement scientifique, sa patience et sa disponibilité. Je remercie également le Professeur Oettlé pour ses relectures minutieuses, critiques et pédagogiques des différents manuscrits. Je la remercie énormément de m'avoir accueillie dans ce beau pays et pour tous ses efforts afin que je me sente ici comme chez moi. Merci pour ces trois années riches en expériences à la fois professionnelles et humaines.

Je souhaiterais exprimer ma profonde gratitude au Professeur Ericka L'Abbé (UP, Pretoria, South Africa), codirectrice de cette thèse, pour son soutien tout au long de ces trois dernières années. Je lui suis extrêmement reconnaissante pour son investissement dans les corrections et améliorations des manuscrits et ses conseils formateurs. Je remercie également très chaleureusement le Professeur Ericka L'Abbé pour son accompagnement scientifique qui a grandement contribué à renforcer mes réflexions scientifiques. Je la remercie pour son accueil chaleureux au sein de son équipe et pour sa détermination à me fournir un cadre de travail plus qu'idéal. Merci pour ces trois années enrichissantes à la fois humainement et professionnellement.

Je tiens à remercier le Dr Fabrice Demeter (NHMD, Copenhagen, Danmark; MNHN, Paris, France; UP, Pretoria, South Africa), également codirecteur de cette thèse, pour m'avoir donné l'opportunité de faire partie intégrante de ce grand projet. Je le remercie pour sa confiance et de m'avoir offert l'opportunité de travailler sur ce sujet de recherche. Je le remercie également pour son accueil chaleureux au Musée de l'Homme lors de mes nombreuses visites à Paris et pour ses déplacements en Afrique du Sud.

Je souhaiterais remercier infiniment le Professeur Dirk Vandermeulen (KU Leuven, Leuven, Belgium; UP Pretoria, South Africa) pour son encadrement dans toutes les procédures statistiques. Je le remercie pour nos échanges qui ont fait avancer mes réflexions scientifiques

tout au long de ces trois dernières années. Je le remercie pour sa confiance, sa patience, ses précieux conseils et sa disponibilité. Je le remercie également de m'avoir accueillie très chaleureusement à l'université de Leuven et pour ses nombreux déplacements en Afrique du Sud.

J'adresse aussi mes remerciements au Dr Peter Claes (Center for Processing Speech and Images (PSI), Department of Electrical Engineering (KU Leuven, Leuven, Belgium) pour avoir assuré quatre présentations orales relatives à notre projet à la conférence internationale de IACI (International Association of Craniofacial Identification) internationale qui a eu lieu à Brisbane (Australie) en juillet 2017. Je le remercie infiniment pour son professionnalisme et sa disponibilité.

Ce travail n'aurait pu être possible sans le financement complet de mes trois années de thèse par le projet AESOP + Erasmus Mundus Programme. Je tiens tout particulièrement à adresser mes remerciements au Professeur José Braga (AMIS, Toulouse) coordinateur de ce beau projet. Je tiens à remercier également Elodie Balonas (Manager, AESOP+) pour sa disponibilité dans les réservations et les remboursements de tous les déplacements liés à cette thèse durant les trois dernières années.

Je souhaiterais remercier le Dr Amélie Vialet (UMR 7194, MNHN, Paris, CERPT, Tautavel, France) pour ses précieux conseils, son soutien et d'avoir initié ma rencontre avec le Dr. Fabrice Demeter (NHMD, Copenhagen, Danmark; MNHN, Paris, France; UP, Pretoria, South Africa). Merci, sans cette rencontre rien de cela n'aurait été possible.

Ce travail de recherche a bénéficié de l'investissement de différents chercheurs, ingénieurs et techniciens qui ont, par leur disponibilité, grandement facilité l'accès aux collections et aux plateformes d'imagerie et contribué à la constitution de l'échantillon de cette thèse. Je remercie infiniment le Dr André Uys (Oral and Dental Hospital, University of Pretoria) et le Dr Sarel Botha (Medical Centre, Life Groenkloof Hospital, Pretoria) de m'avoir généreusement accordé l'accès à une base de données importante d'acquisitions tomographiques de spécimens sud-africains actuels. Je les remercie de leur confiance et d'avoir mis à ma disposition le matériel nécessaire. Je souhaiterais remercier également toute l'équipe de radiologie de l'hôpital bucco-dentaire de l'université de Prétoria pour leur disponibilité et leur bienveillance.

Je remercie infiniment Jade Liebenberg qui a assuré la position d'assistante de recherche au cours des deux premières années de cette thèse et qui a grandement contribué aux mesures des erreurs intra observateurs. Merci pour ta patience et ta disponibilité.

Je souhaiterais exprimer ma profonde gratitude au Dr Manon Galland (MNHN, Paris, France; UP, Pretoria, South Africa) pour sa disponibilité dans l'étude de la validation des points de repère placés automatiquement par la performance rigoureuse des erreurs intra observateurs. Je la remercie également pour nos intéressants échanges sur la géométrie morphométrique qui ont largement contribué à l'élaboration du protocole d'analyse statistique de cette thèse. Merci Manon pour ton soutien et ta disponibilité.

J'adresse mes remerciements au Professeur Carl Stephan (UQ, Brisbane, Australia) Je lui suis extrêmement reconnaissante pour son investissement dans les corrections et améliorations du premier article de cette thèse en tant qu'éditeur au forensic science international journal.

Je remercie le Dr Jean Dumoncel (CNRS, AMIS, Toulouse, France) pour m'avoir accueillie au sein du laboratoire AMIS (Anthropologie Moléculaire et Imagerie de Synthèse) de l'Université de Toulouse III au début de cette thèse et pour avoir contribué à la construction de ce projet. Je le remercie pour nos échanges, ses conseils et sa disponibilité lors de ses nombreux déplacements en Afrique du Sud. Je le remercie également pour sa patience et son aide qui ont grandement contribué à ma formation en géométrie morphométrique et à l'élaboration du protocole d'analyse statistique de cette thèse.

Je souhaiterais également remercier le Dr Clément Zanolli (CNRS, AMIS, Toulouse, France) pour nos échanges qui ont contribué à l'élaboration de ce projet de thèse. Je le remercie pour son soutien et sa disponibilité ces trois dernières années.

Je tiens tout particulièrement à remercier le Dr Gaël Becam (HNHP, Paris, France; EPCC / CERP, Tautavel; MNHN, Paris, France) qui, en acceptant d'encadrer mon travail de master il y a cinq ans, m'a donné l'opportunité de poursuivre mon travail dans le domaine de la recherche. Merci, Gaël, pour, ton soutien, nos échanges et ton amitié tout au long de ces cinq dernières années.

Je remercie chaleureusement tous les membres du département d'anatomie de l'université de Pretoria, qui m'ont accueillie pendant ces trois années, pour leur gentillesse et leur attention à mon égard. Je tiens à remercier tout particulièrement Charlotte Theye (UP Pretoria, South Africa) pour sa présence quotidienne, nos échanges, son soutien et son amitié. Je la remercie grandement pour nos discussions enrichissantes qui ont fortement contribué à la construction de mes réflexions scientifiques. Je la remercie pour son aide, vraiment précieuse, dans l'organisation de mon départ et de mon installation en Afrique du Sud. Merci Charlotte d'avoir été avec moi (sur le même bateau...) ces trois dernières années.

J'adresse également mes remerciements au Dr Marie Dussault (UP Pretoria, South Africa) pour ses échanges, ses conseils et sa disponibilité, surtout lors de cette dernière année de thèse. Je la remercie pour son soutien et pour nos discussions quotidiennes qui ont grandement contribué à l'élaboration de ce travail de thèse. J'adresse mes remerciements au Dr Marine Cazenave (AMIS, Toulouse, France ; UP, Pretoria, South Africa) pour nos échanges et son amitié tout au long de ces trois années de thèse. Je la remercie pour son soutien et pour nos discussions quotidiennes qui ont grandement contribué à la construction de mes réflexions scientifiques. Je remercie également très chaleureusement le Dr Amélie Beaudet (University of the Witwatersrand, Johannesburg) pour ses échanges, ses conseils et sa disponibilité.

Je remercie également tous les membres de l'équipe du Centre Européen de Recherches Préhistoriques de Tautavel pour leur gentillesse et leur attention à mon égard.

Bien évidemment, j'adresse mes remerciements à tous mes amis pour tous ces très bons moments passés ensemble et pour leur soutien ces dernières années : Christelle, Gaël, Khier, Olive, Nico, Agnès, Aurelio, Constance, Cyril (Planchand), Clémentine, Sophie, Romain, Jean-Marc, Leane, Benjamin, Charlotte, Marine, Amélie, Clément, Jean, Marie, Gabi, Clarissa, Delia, François, Gaëtan, Orian, Juliette, Manon, Cyril (Viallet), Cyrielle, Djibril, Julien, Loïc, Daniela, Arnaud, Carole, Pierre. Je remercie tout particulièrement mon amie Zakia pour m'avoir hébergé lors de mes nombreux déplacements au Musée de l'Homme à Paris.

Je souhaiterais remercier plus particulièrement certains de mes amis qui sont devenus avec le temps tout aussi importants que ma propre famille : Christelle, Gaël, Olive, Nico, Khier, Agnes, Aurel, Constance, Hugo, Pauline, Gratien, Sophie, Romain, Jean Marc, Noam, Sasha, Leane, Ben, Samuel, Eloise. Je vous remercie de tout mon cœur pour votre soutien inconditionnel, votre amitié, votre présence dans les bons comme dans les moins bons moments de ma vie et cela même quand on se trouve parfois à 8 000 km de distance.

Ce travail n'aurait pas pu être mené à bien sans le soutien inconditionnel de ma famille : José, mon père, Fany, ma sœur, Léo et Elliott, mes frères. Je remercie également mon beau-frère Nicolas et ma belle-sœur Marlène, ainsi que mes nièces : Zia, Lune, Lucie, Lola, Marie, Victoria et mon neveu Carles. Merci de m'avoir soutenue et encouragée tout au long de mes études et encore plus ces trois dernières années. Je souhaite également remercier Philippe et Christine, mes beaux-parents ainsi que tous les membres de ma belle-famille et plus particulièrement Clément, Marion, Jessica, et Martine (la nounou).

Je remercie tout particulièrement ma grande sœur Fany pour sa présence quotidienne, ses encouragements à poursuivre mes objectifs quelles que soient les circonstances. Je la

remercie pour son amour inconditionnel pour sa bienveillance envers moi depuis toujours et je la remercie d'être là tout simplement.

Je souhaite remercier infiniment mon père, qui a sans aucun doute grandement contribué à ma passion pour la recherche. Je le remercie pour nos interminables débats et discussions depuis que je suis toute petite, pour nos longues nuits à contempler les étoiles et à prendre conscience du monde qui nous entoure. Je le remercie de m'avoir transmis l'envie d'apprendre car c'est grâce à lui qu'aujourd'hui j'en ai fait le moteur de mon quotidien.

Bien évidemment, je remercie celui qui partage mon quotidien, ma vie, Gratien. Je te remercie pour ton incroyable patience à mon égard tout au long de ces cinq dernières années. Je ne te remercierai jamais assez d'avoir accepté de m'accompagner jusqu'au bout du monde pour poursuivre mes études. Je te remercie infiniment pour tes encouragements et ta présence au quotidien. Sans toi, je ne serais certainement jamais arrivée jusque-là.

Ces remerciements ne peuvent s'achever sans une tendre pensée pour ma petite maman qui ne lira jamais ces mots mais sans qui, aucun d'eux n'auraient pu être écrits.

TABLE OF CONTENTS

DECLARATION	i
SUMMARY	iv
ACKNOWLEDGMENTS	vii
TABLE OF CONTENTS	xvi
LIST OF FIGURES	xx
LIST OF TABLES	xxvi
Chapter 1. INTRODUCTION	1
1.1. Problem statement	1
1.2. Scope of the thesis	8
Chapter 2. LITERATURE REVIEW	11
2.1. Methods of craniofacial reconstruction (CFR)	11
2.1.1. Introduction.....	11
2.1.2. Traditional manual methods of 2D/3D-CFR	12
2.1.2.1. Traditional manual 2D/3D CFR of nasal reconstruction	14
2.1.3. Computer-based CFR methods	20
2.1.3.1. Computer-based CFR methods of nasal reconstruction	26
2.2. References used in craniofacial reconstruction methods.....	31
2.2.1. Introduction.....	31
2.2.2. CT scans.....	32
2.2.3. CBCT scans	34
2.3. Anthropological examination	36
2.3.1. Introduction.....	36
2.3.2. Anatomical description of the region of interests	36
2.3.2.1. Facial skeleton anatomy.	37
2.3.2.2. External nose and nares	38
2.3.3. Previous studies on nasal shape variation	39
2.3.3.1. Ancestry	39
2.3.3.2. Age	41
2.3.3.3. Sex.....	42
2.4. Approach proposed in this thesis.....	43

Chapter 3. INTRODUCTORY MATERIALS & METHODS	46
3.1. Introduction	46
3.2. Materials	47
3.2.1. Data acquisition	47
3.2.2. Distribution of age, sex and ancestry	48
3.3. Methods	49
3.3.1. Data processing: segmentation and construction of surface meshes	49
3.3.2. Surface mesh initialisation	50
3.3.3. Non-rigid surface registration process	53
3.3.4. Template generation process	53
3.3.5. Anatomical templating	53
3.3.5.1 Landmarks	54
3.3.5.1.1. Craniometric landmarks	54
3.3.5.1.2. Capulometric landmarks	57
3.4. Statistical analysis	61
3.4.1. Study on nasal complex shape variation	61
3.4.1.1. Generalised Procrustes Analysis	62
3.4.1.2. Principal Component Analysis	62
3.4.1.3. Multivariate normality	63
3.4.1.4. Analysis of covariation between nasal hard- and soft- tissue and its dependence on ancestry	63
3.4.1.5. Quantification and visualisation of covariance between nasal complex shape and the covariates: population differences, sexual dimorphism and age effects	63
3.4.1.6. Allometry	64
3.4.2. Statistical modelling	68
3.4.3. Cross-validation testing	69
3.5. Software	71
3.5.1. Data processing	71
3.5.2. Initialisation	72
3.5.3. Surface registration process	73
3.5.4. Anatomical templating	74
3.5.5. Statistical analysis	74

Chapter 4. VALIDATION OF THE AUTOMATIC LANDMARKING	75
4.1. Introduction	75
Automatic landmarking as a convenient prerequisite for geometric morphometrics.	
Validation on cone beam computed tomography (CBCT)- based shape analysis of the nasal complex.	75
AF RIDEL, F DEMETER, M GALLAND, EN L'ABBÉ, D VANDERMEULEN, AC OETTLÉ.	
<i>Manuscript submitted for publication to Forensic Science International.</i>	
Chapter 5. PRELIMINARY ANALYSIS	107
5.1. Introduction	107
Skeletal dimensions as predictors for the shape of the nose in a South African sample: a cone-beam computed tomography (CBCT) study.....	107
AF RIDEL, F DEMETER, J LIEBENBERG, EN L'ABBÉ, D VANDERMEULEN, AC OETTLÉ.	
<i>Published in Forensic Science International.</i>	
Chapter 6. VARIATION OF THE NASAL COMPLEX SHAPE	117
6.1. Introduction	117
6.2. Statistical preliminaries	119
6.2.1. Reproducibility testing.....	119
6.2.2. General Procrustes Analysis (GPA).....	124
6.2.3. Principal Component Analysis (PCA)	124
6.2.3.1. Population differences.....	125
6.2.3.2. Assessment of sexual dimorphism, age effect and allometry.	128
6.2.3.2.1. Black South African subsample	128
6.2.3.2.2. White South African subsample	131
6.2.4. Multivariate normality	133
6.2.4.1. Population differences.....	133
6.2.4.2. Assessment of sexual dimorphism, age effect and allometry	136
6.2.4.2.1. Black South African subsample	136
6.2.4.2.2. White South African subsample.....	138
Shape analysis of the nasal complex among South African groups from Cone-Beam Computed Tomography (CBCT) using geometric morphometric.	141
AF RIDEL, F DEMETER, EN L'ABBÉ, D VANDERMEULEN, AC OETTLÉ.	
<i>Manuscript submitted for publication to Forensic Science International.</i>	

Chapter 7. STATISTICAL MODELS FOR	189
SOUTH AFRICAN NOSE RECONSTRUCTION	189
7.1. Introduction	189
Nose approximation among South African groups from Cone-Beam Computed Tomography (CBCT) using a new computer-assisted method based on automatic landmarking.	189
AF RIDEL, F DEMETER, EN L'ABBÉ, D VANDERMEULEN, AC OETTLÉ.	
<i>Manuscript submitted for publication to Forensic Science International.</i>	
Chapter 8. CONCLUSION.....	232
Chapter 9. REFERENCES.....	235
Appendix A. LIST OF SPECIMENS	253
Appendix B. RESEARCH OUTPUT	262

LIST OF FIGURES

Chapter 2.

Figure 2. 1. Traditional 2D/3D CFR of nasal reconstruction (Rynn & Wilkinson, 2009; Stephan et al., 2003).	18
Figure 2. 2. General workflow of computerised craniofacial reconstruction techniques (Claes et al., 2010a).	22
Figure 2. 3. Computed-tomography scan. a) CT-scanner; b) X-ray beam; c) Slice; d) 3D image.	33
Figure 2. 4. Cone beam-computed tomography. a) CBCT-scanner; b) Cone beam; c) Slice; d) 3D image.	35
Figure 2. 5. Anatomical description of the hard-tissue regions of interest. a) mid-facial skeleton; b) zygoma; c) nasal bones; d) anterior nasal aperture; e) maxilla.	37
Figure 2. 6. Anatomical description of the soft-tissue region of interests. a) external nose; b) nares.	38

Chapter 3.

Figure 3. 1. Age distribution of sample by population group.	48
Figure 3. 2. Surface mesh initialisation procedure. a) hard- and soft-tissue floating surfaces; b) hard- and soft-tissue target surfaces; c) hard- and soft-tissue initialised surfaces. po: porion; rhi: rhinion; ns: nasospinale; pr: prosthion; ex': exocanthion; en': endocanthion; pr': pronasale; ch': cheilion.	52
Figure 3. 3. Landmarks placed on the hard- tissue region of interest. Landmarks placed on the hard- tissue region of interest.	56
Figure 3. 4. Soft-tissue region of interest. a) frontal view of the soft-tissue region of interest; b) inferior view of the nose; c) anterior view of the nose; d) lateral view of the nose.....	59
Figure 3. 5. Workflow of the automatic landmarking procedure.	60
Figure 3. 6. Shape variation analysis on the complete sample.	66
Figure 3. 7. Shape variation analysis on subsamples (population groups separately).	67
Figure 3. 8. Statistical modelling and cross-validation testing analysis.	70

Figure 3. 9. Example of hard-tissue data processing in MeVisLab 2.7.1. a) All modules used; b) Viewer SoExaminerViewer module for visualisation of the segmentation process; c) WEMIsoSurface module for the determination of threshold values between segmented components..... 71

Figure 3. 10. Example of hard-tissue initialization in MeVisLab 2.7.1. a) All modules used; b) Floating. c) Target; d) Initialisation. 72

Figure 3. 11. Example of the hard-tissue registration process. a) All modules used; b) Visualisation of the hard-tissue registration. 73

Figure 3. 12. Example of hard-tissue anatomical templating. a) All modules used for the automatic projection; b) Automatic recording of the coordinates resulting of the automatic landmarking; c) Visualisation of the hard- tissue anatomical templating. 74

Chapter 4.

Automatic landmarking as a convenient prerequisite for geometric morphometrics. Validation on cone beam computed tomography (CBCT)- based shape analysis of the nasal complex.

AF RIDEL, F DEMETER, M GALLAND, EN L’ABBÉ, D VANDERMEULEN, AC OETTLÉ. *Manuscript submitted for publication to Forensic Science International.*

Figure 1. Landmarks placed on the hard- and soft-tissue region of interest. 82

Figure 2. Workflow of the automatic landmarking procedure. a) segmentation process; b) initialisation process; c) non-rigid surface registration process; d) templates generation; e) definition of the region of interest on templates; f) automatic landmarking..... 85

Figure 3. Boxplots of the dispersion for automatic and manual craniometric landmarking. Craniometric landmark definitions (1-41): cf Table 1. 89

Figure 4. Boxplots of the dispersion of automatic and manual capulometric landmarking. Capulometric landmark definitions (1-41): cf Table 1..... 90

Figure 5. Correlation between the dispersion (per landmark) on the automatically indicated landmarks and the dispersion on the corresponding landmarks on the templates. The solid (dashed) horizontal and vertical lines represent the global median dispersion for hard(skull) – and soft-(skin) landmarking (on target subjects and templates, respectively). 91

Figure 6. Scatterplots of Procrustes craniometric shape coordinates (PC) onto the first two principal components. Left: colored according to method and observer, middle: colored according to method, right: colored according to individual. 92

Figure 7. Scatterplots of Procrustes capulometric shape coordinates (PC) onto the first two principal components. Left: colored according to method and observer, middle: colored according to method, right: colored according to individual. 93

Chapter 6.

Figure 6. 1. Graphical comparison between the mean SE results for both INTRA-OE and INTER-OE of all craniometric landmarks positioning on hard-tissue templates and surface. 120

Figure 6. 2. Graphical comparison between the mean SE results for both INTRA-OE and INTER-OE of all capulometric landmarks positioning on soft-tissue templates and surfaces. 121

Figure 6. 3. Variance explained by each PC of the hard- tissue mid-facial (left) and the soft-tissue external nose (right) shape component. 125

Figure 6. 4. Variance explained by each PC of the nasal bones shape component. a) nasal bones; b) nasal bone left; c) nasal bone right. 127

Figure 6. 5. Variance explained by each PC of the anterior nasal aperture shape component. a) anterior nasal aperture; b) anterior nasal aperture left; c) anterior nasal aperture right. 127

Figure 6. 6. Variance explained by each PC of the zygomatic shape component. a) zygomatic; b) zygomatic left; c) zygomatic right. 127

Figure 6. 7. Variance explained by each PC of the maxillary shape component. a) maxilla; b) maxillary left; c) maxillary right. 128

Figure 6. 8. Variance explained by each PC of the mid-facial hard- tissue (left) and the external nasal soft-tissue (right) shape component. 128

Figure 6. 9. Variance explained by each PC of the nasal bones shape component. a) nasal bones; b) nasal bone left; c) nasal bone right. 130

Figure 6. 10. Variance explained by each PC of the anterior nasal aperture shape component. a) anterior nasal aperture; b) anterior nasal aperture left; c) anterior nasal aperture right. 130

Figure 6. 11. Variance explained by each PC of the zygomatic shape component. a) zygoma; b) zygomatic left; c) zygomatic right. 130

Figure 6. 12. Variance explained by each PC of the maxillary shape component. a) maxilla; b) maxillary left; c) maxillary right.....	130
Figure 6. 13. Variance explained by each PC of the hard- tissue mid-facial (left) and the soft-tissue external nose (right) shape component.	131
Figure 6. 14. Variance explained by each PC of the nasal bones shape component. a) nasal bones; b) nasal bone left; c) nasal bone right.	132
Figure 6. 15. Variance explained by each PC of the anterior nasal aperture shape component. a) anterior nasal aperture; b) anterior nasal aperture left; c) anterior nasal aperture right.	132
Figure 6. 16. Variance explained by each PC of the zygomatic shape component. a) zygoma; b) zygomatic left; c) zygomatic right.	132
Figure 6. 17. Variance explained by each PC of the maxillary shape component. a) maxilla; b) maxillary left; c) maxillary right.....	133
Figure 6. 18. Q-Q-plots of the residuals of the linear model “hard-tissue mid-facial shape (left) versus population” and the linear model “external nasal soft-tissue shape (right) versus population”.....	134
Figure 6. 19. Q-Q-plots of the residuals of the linear model “nasal bones shape versus population”. a) nasal bones; b) nasal bone left; c) nasal bone right.	134
Figure 6. 20. Q-Q-plots of the residuals of the linear model “anterior nasal aperture shape versus population”. a) anterior nasal aperture; b) anterior nasal aperture left; c) anterior nasal aperture right.	135
Figure 6. 21. Q-Q-plots of the residuals of the linear model “zygomatic shape versus population”. a) zygoma; b) zygomatic bone left; c) zygomatic bone right.....	135
Figure 6. 22. Q-Q-plots of the residuals of the linear model “maxillary shape versus population”. a) maxilla; b) maxillary bone left; c) maxillary bone right.	135
Figure 6. 23. Q-Q-plots of the residuals of the linear model “hard-tissue mid-facial shape (left) versus population” and the linear model “soft-tissue external nose shape (right) versus population”.....	136
Figure 6. 24. Q-Q-plots of the residuals of the linear model “nasal bones shape versus population”. a) nasal bones; b) nasal bone left; c) nasal bone right.	137
Figure 6. 25. Q-Q-plots of the residuals of the linear model “anterior nasal aperture shape versus population”. a) anterior nasal aperture; b) anterior nasal aperture left; c) anterior nasal aperture right.	137
Figure 6. 26. Q-Q-plots of the residuals of the linear model “zygoma shape versus population”. a) zygoma; b) zygomatic bone left; c) zygomatic bone right.....	137

Figure 6. 27. Q-Q-plots of the residuals of the linear model “maxillary shape versus population”. a) maxilla; b) maxillary bone left; c) maxillary bone right. 138

Figure 6. 28. Q-Q-plots of the residuals of the linear model “hard-tissue mid-facial shape (left) versus population” and the linear model “soft-tissue external nose shape (right) versus population” 138

Figure 6. 29. Q-Q-plots of the residuals of the linear model “nasal bones shape versus population”. a) nasal bones; b) nasal bone left; c) nasal bone right. 139

Figure 6. 30. Q-Q-plots of the residuals of the linear model “anterior nasal aperture shape versus population”. a) anterior nasal aperture; b) anterior nasal aperture left; c) anterior nasal aperture right. 139

Figure 6. 31. Q-Q-plots of the residuals of the linear model “zygomatic shape versus population”. a) zygoma; b) zygomatic bone left; c) zygomatic bone right. 139

Figure 6. 32. Q-Q-plots of the residuals of the linear model “maxillary shape versus population”. a) maxilla; b) maxillary bone left; c) maxillary bone right. 140

Shape analysis of the nasal complex among South African groups from Cone-Beam Computed Tomography (CBCT) using geometric morphometric.
 AF RIDEL, F DEMETER, EN L’ABBÉ, D VANDERMEULEN, AC OETTLÉ.
Manuscript submitted for publication to Forensic Science International.

Figure 1. Workflow of the automatic landmarking procedure. a) segmentation process; b) initialisation process; c) non-rigid surface registration process; d) templates generation; e) definition of the region of interest on templates; f) automatic landmarking..... 149

Figure 2. Hard-tissue region of interest. a) frontal view of the mid-facial hard-tissue region of interest; b) nasal bones; c) anterior nasal aperture; d) zygomatic bones; e) maxillary bones (cf. Table 1). 152

Figure 3. Soft-tissue region of interest. a) frontal view of the soft-tissue region of interest; b) inferior view of the nose; c) anterior view of the nose; d) lateral view of the nose (cf. Table 2). 154

Figure 4. Black and white South African templates. a) black hard-tissue template; b) black soft-tissue template; c) white hard-tissue template; d) white soft-tissue template..... 155

Figure 5. Pairwise scatterplots of the scores from the first three hard-tissue mid facial PCs and the first three external nasal soft-tissue PCs. a) mid-facial hard-tissue; b) external nasal soft-tissue. Red circle: Black South African; Green triangle: White South African..... 159

Figure 6. Boxplots of Centroid sizes of the mid facial hard-tissue and the external nasal soft-tissue shape components for population group comparison. a) mid facial hard-tissue; b) external nasal soft-tissue. Red: Black South African; Green: White South African..... 160

Figure 7. Between group PCA of mid facial hard-tissue and external nasal soft-tissue shape components grouped by sex and population. a) mid facial hard-tissue; b) external nasal soft-tissue. Purple circle: black female; blue triangle: black male; yellow plus: white female; orange cross: white male. 163

Figure 8. Boxplots of Centroid sizes grouped by sex and population for the mid facial hard-tissue and the external nasal soft-tissue shapes. a) mid facial hard-tissue; b) external nose soft-tissue. Purple: black female; yellow: white female; blue: black male; orange: white male. . 164

Figure 9. Mid-facial hard-tissue and external nasal soft-tissue shapes differences between populations, sex and age averages..... 172

Chapter 7.

Nose approximation among South African groups from Cone-Beam Computed Tomography (CBCT) using a new computer-assisted method based on automatic landmarking.

AF RIDEL, F DEMETER, EN L'ABBÉ, D VANDERMEULEN, AC OETTLÉ.

Manuscript submitted for publication to Forensic Science International.

Figure 1. Workflow of the automatic landmarking procedure. a) segmentation process; b) initialisation process; c) non-rigid surface registration process; d) templates generation; e) definition of the region of interest on templates; f) automatic landmarking..... 200

Figure 2. Landmarks placed on hard- and soft-tissue templates. a,b: Hard-and soft-tissue black South African templates; c,d: Hard-and soft-tissue white South African templates. . 204

LIST OF TABLES

Chapter 2.

Table 2. 1. A list of 3D computerised CFR techniques over the past 30 years in a quasi-chronological order (Claes et al., 2010a; Tilotta et al., 2010; Guyomarc'h, 2011; Guyomarc'h et al., 2013; Schlager, 2014).....	21
Table 2. 2. Computer-based CFR methods for nasal reconstruction.	27
Table 2. 3. Definition and reproducibility of landmarks (craniometric and capulometric) used by Tilotta and colleagues (2008); Schlager (2013) and Guyomarc'h and colleagues (2013) for creating computer-based CFR methods of nasal reconstruction.	30
Table 2. 4. The approach proposed in this dissertation as compared to the existing computer-based CFR methods of nasal reconstructions.....	45

Chapter 3.

Table 3. 1. Definitions, abbreviations, nature and type of landmarks used for the surface meshes initialisation.	51
Table 3. 2. Craniometric landmarks used (Schlager, 2013; Guyomarc'h et al., 2014; Buikstra & Ubelaker, 1994; Caple & Stephan, 2016).	55
Table 3. 3. Capulometric landmarks used (Schlager, 2013; Guyomarc'h et al., 2014; Buikstra & Ubelaker, 1994; Caple & Stephan, 2016).	58

Chapter 4.

Automatic landmarking as a convenient prerequisite for geometric morphometrics. Validation on cone beam computed tomography (CBCT)- based shape analysis of the nasal complex.

AF RIDEL, F DEMETER, M GALLAND, EN L'ABBÉ, D VANDERMEULEN, AC OETTLÉ. *Manuscript submitted for publication to Forensic Science International.*

Table 1. Definition, abbreviation and nature of landmarks used. [15,16,25,26].....	80
Table 2. Measurement errors (global mean and median dispersion in mm) for hard- and soft-tissue landmarks. Right column: mean dispersion for template landmarking.	88
Table 3. Three-way Procrustes ANOVA for craniometric landmarks.	94
Table 4. Three-way Procrustes ANOVA for capulometric landmarks.	94

Chapter 6.

Table 6. 1. Dispersion errors (mm) of craniometric and capulometric landmarks positioning on hard-and soft-tissue black and white surfaces.	120
Table 6. 2. Definition and reproducibility of craniometric landmarks placed automatically and used in this dissertation.	122
Table 6. 3. Definition and reproducibility of capulometric landmarks placed automatically and used in this dissertation.	123

Shape analysis of the nasal complex among South African groups from Cone-Beam Computed Tomography (CBCT) using geometric morphometric.

AF RIDEL, F DEMETER, EN L'ABBÉ, D VANDERMEULEN, AC OETTLÉ.

Manuscript submitted for publication to Forensic Science International.

Table 1. Craniometric landmarks used [3, 19, 44, 45].	151
Table 2. Capulometric landmarks used [3, 19, 44, 45].....	153
Table 3. Hard- and soft-tissue population differences results.	161
Table 4. Hard- and soft-tissue sexual dimorphism in the complete sample and within population.....	165
Table 5. Hard- and soft-tissue shape change associated with age in the complete sample and within population.....	167
Table 6. Hard- and soft-tissue shape changes associated with size in the complete sample and within population.....	169
Table 7. Results of covariation between hard-and soft-tissue and its dependence on ancestry.	174

Chapter 7.

Nose approximation among South African groups from Cone-Beam Computed Tomography (CBCT) using a new computer-assisted method based on automatic landmarking.

AF RIDEL, F DEMETER, EN L'ABBÉ, D VANDERMEULEN, AC OETTLÉ.

Manuscript submitted for publication to Forensic Science International.

Table 1. Definition and reproducibility of craniometric landmarks placed automatically and used in this study.	202
Table 2. Definition and reproducibility of capulometric landmarks placed automatically and used in this study.	203
Table 3. Hard- and soft-tissue shape analysis results.	209
Table 4. Prediction errors (in mm) of the predicted capulometric landmarks in the complete sample, calculated on 200 individuals, based on training and on non-trained data.	210
Table 5. Prediction errors (in mm) of the predicted capulometric landmarks in the black South African sample, calculated on 200 individuals, based on the training and on the non-trained data.	212
Table 6. Prediction errors (in mm) of the predicted capulometric landmarks in the white South African sample, calculated on 200 individuals, based on the training and on the non-trained data.	213
Table 7. Population dependent quality of prediction (mm) of the predicted capulometric landmarks, calculated on 200 individuals, on the training and on non-trained data.	214

Appendix A

Table 1. Sample details of 10 CBCT scans used for the validation of the automatic landmarking analysis.	253
Table 2. Sample details of 120 CBCT scans used in the preliminary analysis.	254
Table 3. Sample details of 200 CBCT scans used in this dissertation.....	257

Chapter 1

INTRODUCTION

1.1. Problem statement

Each year in the Gauteng province of South Africa, approximately 1300 bodies are incinerated without a known identity (Bloom, 2015; Krüger *et al.*, 2018). With unknown persons, identification is not always possible with conventional methods such as DNA comparisons and fingerprints. Additionally, many poor South Africans do not have dental/hospital records or identification documents. Further compounding these circumstances is a high incidence of migrant labour in South Africa which is associated with the country's socio-political and mining history (L'Abbé *et al.*, 2005). Therefore, more creative methods, including facial reconstruction, have been implemented to assist in the identification of unknown persons from their skeletal remains in South Africa. In collaboration with the Victim Identification Centre (VIC) of the South African Police Service (SAPS), the Forensic Anthropology Research Centre (FARC) at the University of Pretoria has worked hard toward finding solutions for many of the challenges in the identification of unknown skeletal remains found within the South African context. In particular, attention has been given to the development of South African standards for establishing a biological profile (age, sex, stature and ancestry) in adults and children; the validation of current research methodologies and improvements of methods used in craniofacial reconstruction and skull-to-photo superimposition (Stephan *et al.*, 2008; Stephan, 2014; Steyn *et al.*, 2016; Stephan, 2017; Krüger *et al.*, 2018).

Craniofacial reconstruction (CFR)¹ methods are employed to estimate the ante-mortem appearance of an individual from their skeletal remains, providing information about an individual which can be conveyed to the public. Craniofacial reconstruction is a useful tool in the identification of a corpse that is unrecognisable due to its state of decomposition, soft-tissue mutilation or incineration, and with no available evidence for positive identification (Vandermeulen *et al.*, 2012). Yet, prior to reconstructing a face from the cranial substrate, the practitioner needs information as to the individual's biological profiles which includes estimations of ancestry, sex, age and stature. These skeletal estimations are then used to provide a presumptive identification of the deceased.

In the South African context, the estimation of ancestry from unknown remains is an important component of the biological profile, due to the socio-cultural identity background of the country (Petersen *et al.*, 2013). Indeed, in South Africa, the socio-cultural identity is based on the strict social categories assigned to people during the apartheid era, namely “White,” “Black,” “Coloured,” and “Indian”. People in these different categories were originally from different geographical backgrounds and already displayed a variety of cultural and biological distinct traits. “White” individuals were mostly descendants from European settlers, native from the Netherlands, France, Germany and Britain (L’Abbé *et al.*, 2011). “Black” individuals were the descendants of Nguni, Sotho, Venda and Shangaan-Tsonga migrants who arrived in southern Africa due to the migration of Bantu speaking groups from western and central Africa (Franklin *et al.*, 2007; Liebenberg *et al.*, 2015). Although racial classification is no longer legally imposed in South Africa, modern South Africans continue to socially self-identify as one of the previously prescribed groups. A need to self-identify is pervasive in all aspects of life and is an important part of a person's cultural place in the country's citizenship. Therefore, the majority of the population in South Africa self-classifies today as black (80.5%), coloured (8.8%), white (8.3%), and Indian/Asian (2.5%) South Africans (Statistics South Africa, 2015).

¹ Craniofacial reconstruction (CFR) is based on the assumed morphological relationship between the soft- tissue envelope and the underlying skull substrate (Schlager, 2013).

The presumptive identification of an unknown individual is based on the presence of biological features (human variation) of the skeleton and the relationship of these features to the individual's socio-cultural identity. Assortative mating within South African groups strengthened the already notable biological variation between groups and engendered the perpetuation of skeletal variation within the population such, that forensic anthropologists are able to classify an unknown individual into three main socially identified groups: a black, a coloured, or a white South Africans (Sutherland, 2016).

The current situation of unidentified persons in South Africa will greatly benefit from research into human variation of South African groups, with the intention of creating accurate and reliable identification guidelines such using South African standard facial reconstruction methods (Steyn *et al.*, 2016). The history and development of craniofacial reconstruction methodology, as well as its applications, has exposed the depth of human variation within and between populations and forms the foundation for the current development of valid and reliable population specific standards.

Currently, the craniofacial reconstruction division of the SAPS uses facial sculpting with modelling software to construct three-dimensional (3D) manual approximation of faces following the estimation of the biological profile (sex, age and ancestry) by anthropologists at the FARC, University of Pretoria. The facial reconstruction process involves a 3D surface scan of the target skull (unidentified skull) with a Metrascan 210. The 3D surface of the target skull is then transposed onto Freeform modelling software and soft-tissue thicknesses are manually applied at specific craniometric points using a 3D stylus. Facial features are adjusted on the skull, using the same process, according to North American databases of soft-tissue thicknesses derived from cadaver studies. After the final touches by the forensic artists, the final 3D facial reconstruction is printed and presented to the family for possible recognition. The main critiques of this current facial approximation techniques are the inherent subjectivity in manual methods, the references used, the non-consideration of population specificities, the lack of standardisation and the poor correlations between facial bony structures and facial soft features, which limit the objectivity and the accuracy of the estimation.

The scientific community in the field of CFR recognised that manual reconstruction methods require a high degree of anatomical and sculptural expertise and remain difficult and subjective in practice. The manual 3D CFR technique used by the VIC in South Africa relies

on the expertise of a forensic artists to manipulate a 3D stylus. Therefore, the interpretations of two different forensic artists from the same skull can result in the creation of two substantially different faces (Tyrrell *et al.*, 1997; Stephan, 2003; Verzé, 2009; Ullrich & Stephan, 2011; Vandermeulen *et al.*, 2012; Guyomarc'h *et al.*, 2014). According to Davy and collaborators (2005), this point is further illustrated by Haglund & Reay (1991), who reported that multiple facial reconstructions of several victims of the Green River serialkiller were created. The results were highly variable between practitioners and little success was achieved when the reconstructions were shown to the public. Furthermore, manual reconstructions are time consuming, and are therefore often limited to a single reconstruction. Traditional 2D or 3D manual techniques of CFR are thus now considered to be unsuitable for application to the judicial system, which requires precision, reliability and knowledge of possible quantisation errors (Vandermeulen *et al.*, 2012).

The reliability of the craniofacial reconstruction methods used by the VIC in South Africa, is further challenged by the reference sample used to create guidelines. The utilisation of guidelines derived from cadavers, subjected to desiccation or swelling and gravity limits, greatly affect the accuracy of the reconstruction. The use of cadavers for recording soft-tissue thicknesses has been extensively criticised in recent craniofacial identification literature. Poor relationships were reported between cadaver-based and *in vivo* measurements due to tissue deformation from post-mortem changes, (Todd & Lindala, 1928) namely dehydration and shrinkage, as well as swelling with the onset of putrefaction (Manhein *et al.*, 2000; Wilkinson, 2002; Chen *et al.*, 2011; Wilkinson, 2004; De Greef *et al.*, 2005, 2009; Lee *et al.*, 2011; Vandermeulen *et al.*, 2006). In addition, the utilisation of guidelines derived from populations other than South Africans, is also problematic. The non-consideration of South African standards, taking into account the population specificities in current facial features, approximation techniques such as the approximation of the nose, limits the objectivity and the accuracy of the reconstruction, and by extension, the success of the recognition.

The nose is of particular interest as it is a projecting feature, displaying much variation. Its reconstruction could be invaluable in the identification of unknown individuals. The nose is an important feature to accurately predict in facial recognition, especially in in profile view and in three-quarter view (Bruce, 1989). However, reconstruction of the nose poses specific challenges, because of its less clear relationship with the underlying skeletal features. The morphology of the nose is often manually reconstructed from the shape and size of the nasal

aperture, represented by the position of the pronasale, subnasale, and alare landmarks (Gerasimov, 1955; Krogman, 1962; Krogman & Iscan, 1986; Macho, 1986; George, 1987; Prokopic & Ubelaker, 2002; Stephan *et al.*, 2003). These nasal profile prediction methods are time consuming, often limited to a single reconstruction and has been demonstrated to be highly varied and subjective, rendering their applications not suitable to the judicial system (Stephan *et al.*, 2003).

In order to assess with accuracy, the structural and functional coherence of correlations between facial bony structures and facial soft-tissue, a definition of a biologically meaningful region of interest, not limited to the nasal aperture and the nasal bones, for the approximation of the nose, is proposed in this thesis. During craniofacial development, from birth to death, the morphology of the nose is influenced by the remodelling of the underlying skeletal structure, (Albert *et al.*, 2007) emphasizing the fact that the components of the nose cannot be considered as independent elements of the craniofacial skeleton. In addition, in nasal approximation, a biologically meaningful region of interest is rarely considered. A biologically meaningful region of interest is defined as a skeletal region which demonstrates important shape variation, impacting on the external morphology, and is influenced by factors such as age, sex, ancestry. In the scientific literature, it has been demonstrated that the growth and development of the human craniofacial skeleton results from the interdependence of its different components, which are influenced by multifactorial processes involving hormonal, genetic and epigenetic factors such as age, sex, ancestry and external stimuli (Moss & Young, 1960; Atchley & Hall, 1991; Enlow & Hans, 1997; Moss, 1997a, 1997b, 1997c, 1997d; Lieberman *et al.*, 2002; Klingenberg *et al.*, 2003; Tomoyasu *et al.*, 2009; Lieberman, 2011; Gröning *et al.*, 2013). According to the literature, differences in the rate of soft-tissue facial aging exists, and varies according to the decade of life, sex and ancestry (Taylor, 2000; Akgül *et al.*, 2002). Recent studies on the facial approximation of the nose among South African groups (Ridel *et al.*, 2018) and on other European and Asian populations (Schlager, 2013), demonstrate the importance of considering factors such as sex and ancestry in the approximation of the nose.

Nasal shape variations present a challenge for facial reconstruction. Effective techniques taking into account the effects of population, sexual dimorphism and of aging on the morphology of the nose, need to be developed. Failure to account for this suite of variation impacts on the accuracy of the final facial reconstruction.

To further improve the accuracy of facial approximation of the nose in the South African population, this thesis proposes the development of a computer-based method using large databases of 3D representations of hard- and soft-tissues of the face. In general, all computer-based methods share the foundational premise that information about the complete skull versus information of the skin is used for mapping a template face onto a dry skull (Claes *et al.*, 2010a). The prediction is performed by using a soft-tissue representation generated from the database by applying a deformation, based on the correlation between skin and skull-surfaces incorporated in the database.

As compared to a human expert, a computer is consistent and objective. The computer integrates all the modelling assumptions and repeatedly generates the same output data. As compared to forensic artists, some procedures can be automated, such as the creation of multiple reconstructions from the same target skull, using different modelling assumptions (ancestry, age, sex). An additional advantage of using computer-based CFR is the convenience of visualisation. Furthermore, the CFR process is more accessible to a wide range of forensic experts without the need for extensive expertise in computer science or computer-based CFR fields. In practice, the development of software for computerised facial reconstructions of an individual could benefit law enforcement agencies by allowing faster, easier and more efficient generation of multiple representations of an individual.

Tilotta *et al.*, (2009) and Schlager (2013) developed computer-assisted methods for the prediction of the structure of the external surface of the nose, based on conventional computer tomography (CT) scans. Compared to manual methods, automation of facial approximation of the nose, using large 3D surface samples, offered increased objectivity and the possibility of standardisation. However, the use of conventional CT scans as initial references for CFR methods is influenced by supination effects on the face, due to the horizontal position of the patient during scanning (Iblher *et al.*, 2013; Marin *et al.*, 2015; Munn & Stephan, 2018). Munn & Stephan (2018) have recently shown important differences in the shape of the face between upright and supine postures (1-4.0 mm) using high-resolution Dimensional Imaging DI3D stereo-photographs. This recent study (Munn & Stephan, 2018) demonstrates that the actual standard collection of facial soft-tissue thicknesses in the supine position is unusable when the measurements are intended for use in the context of an upright subject (Munn & Stephan, 2018). Postural effects need to be taken into consideration when developing approaches in all CFR methods. In addition, the slice thickness of conventional CT scans, which generally ranges from

0.6 mm to 1.5 mm (Tilotta, 2008; Schlager, 2013; Guyomarc'h *et al.*, 2014), may induce errors in the manual landmark placement on the 3D hard- and soft-tissue surfaces. Although automation of facial approximation of the nose increased objectivity as compared to the traditional manual methods, the manual placements of landmarks on large 3D surface samples affected the accuracy of the standardisation. Indeed, these methods for approximation of the nose involve manual placements of landmarks for the definition of the region of interest (Tilotta, 2008; Schlager, 2013). Manual placement of landmarks is extremely time consuming on large 3D surface samples and may induce important observer subjectivity and errors in placing the landmarks. As a result, manual landmarking may render the analysis less repeatable and accurate for the facial approximation process.

In the light of the great demand for the identification of unknown remains in South Africa, a need exists to establish reliable facial approximation techniques that will not only take into account sex and age, but most importantly be specific for the South African population. Current nose approximation techniques, used in South Africa, have proved disappointing in practice. Three possible reasons include that the guidelines were derived 1) from populations other than South Africans, or 2) from cadavers subjected to desiccation or swelling and gravity and 3) from CT scans subjected to the effects of gravity and subjectivity in defining 3D landmarks manually. In order to improve the accuracy of facial approximation of the nose, this study proposes the development of an automated three-dimensional (3D) method based on an automatic dense landmarking procedure. Instead of using conventional CT for the acquisition and extraction of the relevant anatomical structures, we used cone beam CT (CBCT). By means of the semi-automatic computer-assisted technique proposed in this study, the reconstruction of a complex feature, such as the nose, may be actualised. In this way, the potential of this novel automatic computer-based method may be demonstrated. The research question therefore is: will such an automatic computer-based method render nasal shape approximations more reliable, in practice?

1.2. Scope of the thesis

The thesis aims to provide an accurate computer-assisted method for the prediction of the nasal soft-tissue shape, based on the shape of the underlying skull substrate. The first objective is to improve the standardisation, accuracy and objectivity in the methods of the facial approximation of the nose by developing an accurate automatic landmarking procedure, using CBCT-scans. The second objective is to find the statistical interrelationship between the hard- and soft-tissue of the nasal complex, attributed to factors such as sex, age and ancestry. This research requires the collection and compilation of a large 3D surface database for the creation of statistical models and for estimating the most probable soft-tissue shape, based on the known hard-tissue information.

The specific objectives of this research were the following:

1. *Creation of a large CBCT-scan database.* Cone beam computed tomography scans of South African individuals were collected from the Oral and Dental Hospital, University of Pretoria, South Africa and the Life Groenkloof Hospital, Pretoria, South Africa.
2. *Extraction of 3D soft- and hard-tissue surfaces from CBCT-scans.* The segmentation of 3D hard-tissue and soft-tissue surface meshes on the same individuals was performed.
3. *Creation of hard- and soft-tissue templates using a non-rigid surface registration process.* Reference hard- and soft-tissue templates were created from hard- and soft-tissue 3D surface meshes using a non-rigid surface registration process.
4. *Definition of hard- and soft-tissue regions of interest (mid-facial skeleton and external nose).* Craniometric and capulometric landmarks (Caple & Stephan, 2016) were selected and distributed on the facial skeleton and the external nose, creating a hard- and soft-tissue region of interest. The hard-tissue region of interest was demarcated by the facial skeleton comprising the nasal bones, the nasal aperture, the maxillae and the zygomatic bones. The soft-tissue region of interest was demarcated by the surface anatomy as related to the hard-tissue, including mainly the external nose and the nares.
5. *Hard- and soft-tissue anatomical templating (automatic landmarking projection onto every subject's surface using a warping procedure).* The reference templates

were created in an iterative fashion, akin to the generation of the mean shape in a generalized procrustes superimposition (GPS) procedure. As a by-product of this template generation process, every individual surface was ‘templated’: every point on these surfaces is associated with the anatomically corresponding point on the template. Alternatively, the templates can be independently generated from the population under study and the template warping applied in a subsequent step. This procedure was applied to the automatic placement of discrete landmarks as follows: The landmarks of interest were indicated once on the template, which were then projected onto every subject’s surface using a warping procedure. The coordinates of the warped landmarks were then recorded and saved in an Excel file for further statistical analysis.

6. *Preliminary analysis: characterisation of the nasal complex morphology among 120 South African individuals (18-30 years).*

In order to facilitate nasal soft-tissue reconstruction and to characterise the morphological differences among South African groups (black and white South Africans), the prediction of the displacements of capulometric landmarks in a sub-sample, using linear measurements, was performed.

7. *Validation of the automatic landmarking.* The aim of this analysis was to validate the automatic landmarking method by comparing the intra-observer errors (INTRA-OE) and inter-observer errors (INTER-OE) between automatic and manual landmarking.

8. *Anthropological study on nasal shape variation.* The determination of the influence of factors such as age, size, sex and ancestry on nasal complex shape variation was assessed. The approach taken in this study was to calculate regression models, based on the hard- and soft-tissue shape information stored in the database, and on additional factors (ancestry, sex, age and size), using geometric morphometric.

a. Analysis of covariation between nasal hard- and soft- tissue and its dependence on ancestry.

b. Quantification of covariance between nasal complex shape and the covariates: ancestry and sex, as well as, age and size.

9. *Creation of statistical models based on relationships between hard- and soft-tissue and additional factors/covariates.* Statistical models were calculated using a Projection onto Latent Structures Regression (PLSR) algorithm, that allow for

establishing the statistical relationship predictors (hard-tissue shape, age, sex and ancestry) and response variables (soft-tissue information).

10. Validation procedure to test the accuracy of prediction models. The validation of prediction models was performed using cross validation testing with the calculation of the Mean Squared Error (MSE) using leave-one-out cross-validation (LOOCV).

Chapter 2

LITERATURE REVIEW

2.1. Methods of craniofacial reconstruction (CFR)

2.1.1. Introduction

In forensic investigations, the identification of an unknown person is obtained by various identification techniques, which are predominantly based on comparisons of ante- and post-mortem data such as medical files, dental records, radiographs, fingerprints or DNA. However, the identification of an unknown person is not always possible with conventional methods. In the South African context, for instance, reliable ante-mortem data are often missing because of the poor socio-economic status of many victims. Therefore, other methods, including facial reconstruction, have been implemented to assist in the identification of unknown persons from their skeletal remains. Following the recommendations of the Scientific Working Group for Forensic Anthropology (SWGANTH), facial reconstruction methods are employed to estimate the ante-mortem appearance of an individual from skeletal remains, provide a presumptive identification of the individual and convey the result to the public.

Craniofacial reconstruction (CFR) is based on the assumed morphological relationship between soft-tissue and the underlying bone. Three categories of facial reconstruction techniques exist and include: 2D facial reconstruction, 3D manual facial reconstruction, and 3D computer-based facial reconstruction. Two-dimensional facial reconstruction involves the creation of a 2D image, either by drawing (Taylor, 2000), or application of computer-assisted methods (Wittwer-Backofen, 2004; Wittwer-Backofen *et al.*, 2007), 3D manual methods, defined as the simulation of soft-tissue onto a 3D skull replica uses clay or plasticine (Snow *et al.*, 1970; Gerasimov, 1971; Lebedinskaya *et al.*, 1993; Prag & R. Neave, 1997; Wilkinson,

2004; Wilkinson, 2010), or 3D modelling software (Wilkinson, 2003; Lee *et al.*, 2012). As both the traditional manual 2D and 3D facial reconstruction techniques are dependent on the unique knowledge and skills of the forensic artist, they are often subsumed into the broader category of traditional manual methods.

The final category and the main purpose of this thesis constitutes the computer-based 3D reconstructions, defined as (semi) -automated procedures for estimating the surface of the face and for which a large and reliable 3D hard- and soft-tissue surface database is used. Computer-based CFR approaches exclude any possible subjectivity produced by forensic artistic interpretations. The following describes, in detail, the CFR methods which are available for practitioners to use in forensic case analysis. All realistic representation of the individual from any of these methods may be presented to the public for possible identification.

2.1.2. Traditional manual methods of 2D/3D-CFR

A 2D reconstruction is defined as the creation of a 2D-image, either by drawing (Taylor, 2000) or application of 2D computer superimposition methods (Wittwer-Backofen, 2004; Wittwer-Backofen *et al.*, 2007).

A 2D facial reconstruction consists of hand-drawn facial images. The drawings are based on ante-mortem photographs of the skull and any other detail available of the unknown individual. During the 1980's, Karen T. Taylor created a method of 2D facial reconstruction commonly used today (Taylor, 2000). Taylor's method involves applying tissue depth markers on an unidentified skull at various anthropological landmarks. The skull is then photographed from a frontal and lateral view (Taylor, 2000). Facial drawings are made on tracing paper which are overlaid onto the frontal and lateral photographic prints. A second method for 2D facial reconstruction is the 2D computer superimposition method, described by Wittwer-Backofen (Wittwer-Backofen, 2004; Wittwer-Backofen *et al.*, 2007). Virtual 2D faces are produced by using different facial contours and features selected from a photographic database of existing people, and following the skeletal structure of the target skull.

The traditional manual method of 3D-CFR is defined as the simulation of soft-tissue onto a 3D skull replica using clay or plasticine (Snow *et al.*, 1970; Gerasimov, 1971; Lebedinskaya *et al.*, 1993; Prag & R. Neave, 1997; Wilkinson, 2004; Wilkinson, 2010), or 3D modelling software (Wilkinson, 2003; Lee *et al.*, 2012). In the literature, these traditional reconstructions have been commonly classified as “Russian”, “American” or “Combination” methods (Stephan, 2006). The Russian anthropologist Gerasimov (1971) was one of the first to use a manual reconstruction method where he modelled the complete facial anatomy of muscles and soft tissues covered by a thin layer, mimicking skin, onto the skull. This anatomical or ‘Russian’ technique, also referred to as the morphoscopic technique (Snow *et al.*, 1970), was further refined by Lebedinskaya and collaborators (1993). During the same period, an alternative technique was developed in the USA, called the morphometric, or American method (Snow *et al.*, 1970). This technique consists of building the soft-tissue layer in bulk, without much regard to the detail of the underlying anatomy, approximating tabulated average tissue depths at a sparse set of landmarks on the skull and interpolating clay in between the landmarks at previously described depths. In the late 20th century, Richard Neave used both the Russian and American methods in his facial reconstructions, which laid the foundation for the combined technique, or combination method (Prag & Neave, 1997). The advocates of the combined method claim that as the face is reconstructed according to anatomical principles, artistic subjectivity in areas between tissue-depth landmarks is greatly reduced (Wilkinson, 2010). Generally, the soft tissue is estimated using average thickness values, taking into account age, sex and ancestry. Currently, all 3D CFR methods are widely applied in forensics and for museum presentations - permanently refined, as seen in the Hominin reconstructions done by the paleoartist Elisabeth Daynès, such as the reconstruction of the *Australopithecus afarensis* “Lucy” or “the little lady of flores” (Jungers *et al.*, 2009).

Recently, Wilkinson (Wilkinson, 2003; Lee *et al.*, 2012) developed a virtual sculptural CFR method which utilises a 3D modelling system (Freeform Modelling PlusTM; Sensable Technologies Wilmington, MA) with haptic feedback (Phantom DesktoTM Haptic Device; Sensable Technologies). This method has been applied to forensic case work (Wilkinson, 2003; Wilkinson, 2010; Lee *et al.*, 2012). The method mimics the 3D manual CRF methods, described above, and enables practitioner-led facial reconstruction. An image of the target skull (unidentified skull) is imported into FreeForm Plus as a stereolithography (STL) file, converted originally from Digital Imaging and Communication in Medicine (DICOM) data, or an object file translated from laser scan data (e.g. Metrascan). Then, soft-tissue thicknesses are manually

applied at specific craniometric points and modelled using a 3D stylus. Facial features are adjusted, using the same process, on the skull according to available databases of soft tissue thicknesses for that population. After the final touches by the forensic artists, the 3D facial reconstruction is printed and presented to the family for possible recognition.

2.1.2.1. Traditional manual 2D/3D CFR of nasal reconstruction

Following the literature, facial features have been determined to be important for perceiving and remembering faces (Shepherd *et al.*, 1981; Bruce 1988; Zhao *et al.*, 2003). Several studies using frontal images have shown that the nose plays an insignificant role in face recognition in frontal view (Haig, 1986, 2013; Zhao *et al.*, 2003; Fraser & Parker, 1986). However, in face recognition using profiles and three-quarter views, a distinctive nose shape could be more important than the eyes or mouth (Bruce, 1988). Moreover, it has also been found that the upper part of the face (eyes and nose) is more useful for face recognition than the lower part (mouth) in frontal view (Shepherd *et al.*, 1981).

In order to estimate the location of a specific landmark such as the nose, on the face, the position of well-defined cephalometric landmarks (pronasale, subnasale, and alare), are predicted from analysing metric values taken from a dry skull. As most reconstruction practitioners highly value the pronasale landmark for estimating the nasal profile, methods of prediction of the pronasale from the underlying bone structure has been highly prioritised in current nose approximation research. Gerasimov (1955) was the first researcher to estimate nasal landmarks with the use of metric measures of the underlying bone tissue, known as the “two-tangent” method (Figure 2.1.a). In this method, a line is projected anteriorly following the direction of the nasal spine. A second line, which is a tangent to the most distal portion of the nasal bones, is projected inferiorly. The intersection between the two lines forms the tip of the nose (pronasale). In later years, this method was reported to be highly unreliable and often resulted in an overestimation of nose projection (Stephan *et al.*, 2003). In addition, the technique has been demonstrated to be very subjective and imprecise, because it relies on the “general directions” of two bones, and is therefore not useable in facial reconstruction of the soft-tissue of the nose (Stephan *et al.*, 2003). Following on the method established by Gerasimov (1955), a variety of approaches dealing with angles and relations between metric measurements have been proposed (Krogman, 1962; Krogman & Iscan, 1986; Macho, 1986; George, 1987; Prokopec & Ubelaker, 2002; Stephan *et al.*, 2003). The traditional 2D/3D CFR methods for

nasal reconstruction are illustrated in Figure 2.1. Evaluation concerning the accuracy of these different methods can be found in articles by Rynn & Wilkinson (2009) and Stephan *et al.*, (2003).

In 1962, Krogman developed a method for pronasale prediction (Figure 2.1.b), which consists of projecting a line, that follows the direction of the nasal spine (Krogman & Iscan, 1986). The length of the nasal spine, from the junction with the vomer to the tip, is tripled and added to the transferred depth, which is the average soft-tissue depth at midphiltrum on the lip (Krogman & Iscan, 1986). However, Stephan *et al.*, (2003) found the method to perform with low accuracy in predicting nasal shape. These authors (Stephan *et al.*, 2003) demonstrate three important limitations of the Krogman method: 1) the Krogman method (Krogman & Iscan, 1986) involves the multiplying of the nasal spine length by 3, which increases any error by 3; 2) the utilisation of the midphiltrum soft-tissue depth seems illogical, because it is not directly related to the nose; and 3) the midphiltrum depth so that it follows the general direction of the nasal spine, seems problematic, since the soft-tissue midphiltrum is actually located inferior to the hard-tissue midphiltrum (George, 1993). For all these reasons, this method should not be used in future facial approximations (Stephan *et al.*, 2003).

An alternative method to predict nasal position and dimensions was suggested by Macho (1986) (Figure 2.1.c). Measurements were taken of the external nose and bony nasal aperture in the nasion-sella plane² (NSP). Seven craniometric measurements of the nasal aperture in profile view, were compared to external measurements of height (from soft nasion to soft subnasale), length (from soft nasion to pronasale), and depth (pronasale to soft subnasale), which forms a triangle describing the external nose. Soft-tissue depths from hard to soft nasion, and from hard to soft subnasale, were taken as an aid to placement of the triangle of the external nose. The two sets of measurements were then used to generate regression equations for calculation of the shape of the nose. This method has proven impractical for facial

² Two tracings recorded the soft profile and bony profile together, including the porion (superior border of the external auditory meatus), to obtain the Frankfurt horizontal plane (FHP) between the porion and the lower border of the eye socket, and the sella turcica, to obtain the nasion-sella plane (NSP).

reconstruction, as the soft-tissue measurements are measured from the bony landmark to the soft-tissue landmark, rather than perpendicular to the bone surface (Rynn & Wilkinson, 2009).

George (1987) described a “balanced” nasal projection method (Figure 2.1.d) which was based on the “aesthetic” methods of facial surgery according to Goode (Powell & Humphreys, 1984). The method uses the measurement of the distance from the nasion (Pt.)A to point of maximum flexion on maxilla in profile. A percentage of this distance from (Pt.)X to (Pt.)A (60.5% for males and 56% for females) marks the point of intersection (Pt. AA) of a line drawn parallel to the Frankfurt horizontal plane³ (FHP) (line F) (George, 1987; Stephan *et al.*, 2003). (Pt.) AA also indicates the midpoint of the inferior slope of the anterior nasal spine. A line perpendicular to the Frankfurt horizontal is placed at the level of predicted nose projection. This method was found to be more accurate than the methods of Gerasimov (1955), Krogman (1962) and Macho (1986) (Stephan *et al.*, 2013).

Prokopec and Ubelaker (2002) (Figure 2.1.e) suggested another method to predict the shape of the nasal profile. The technique is as follows: on an image of the profile view of the nasal aperture, a line is drawn to indicate the nasion-prosthion plane (line A) and then parallel to line A, a tangent at the rhinion, line B is indicated. Horizontal lines, perpendicular to lines A and B are drawn, dividing the nasal aperture into seven equal segments. Each distance of the horizontal line from line B to the edge of aperture posteriorly, is measured and mirrored anteriorly. Two millimeters are added to each of these measurements; midline average soft-tissue depths at nasion, midnasal bone, rhinion and subnasale (Helmer, 1984) are added. The points are then joined, allowing the profile shape of nose, and hence its projection, to be estimated (Prokopec & Ubelaker, 2002). Stephan and colleagues (2003) found this method to be reliable at predicting pronasale projection in the FHP as compared to the other techniques previously described, but suggested that this method should be used with much caution when employing to predict profile nose shape.

Stephan and colleagues (2003) noted that the methods described by Prokopec and Ubelaker (2002), as well as George (2002), were more effective and reliable in predicting nasal profile shape than those of Gerasimov (1971) and Krogman (1962). Like their predecessor, Stephan and colleagues (Stephan *et al.*, 2003) created a new technique (Figure 2.1.f) to estimate nasal profile which uses various soft- and hard- tissue measurements to generate regression equations to predict nasal shape for a particular population, as the shape is age, sex and population specific (Stephan *et al.*, 2003). However, Stephan and colleagues (2003) emphasised

that the creation of regression equations for the approximation of the nose using dry skull databases has its limitations. Indeed, some measurements which are not easily taken from dry skulls directly, such as the nasal bone angle (which require planes to travel through the nasal bones), are excluded and this may affect the accuracy of the external nose prediction. Consequently, [Stephan and colleagues \(2003\)](#) conclude that the three-dimensional (3D) computer techniques for nose approximation will probably become the method of choice for many reasons: 1) by performing indirect measurements using 3D planes; 2) by considering many variables; 3) and by generating 3D nose approximations. Therefore, a need exists for facial approximation practitioners to move away from traditional three- and two-dimensional techniques and for 3D computer techniques to be further developed [Stephan and colleagues \(2003\)](#).

Recently, [Lee and colleagues \(2014\)](#) investigated the relationship between the hard- and soft- dimensions of the nose, as to predict the position of the nose in a Korean population. The authors used CBCT-scans obtained from 60 adult Korean. As CBCT scans are taken with the patient in an upright position, the authors eliminated errors involved with supination and post-mortem artifacts. Three-dimensional placements of the nasal soft structures (pronasale, subnasale, alare) from the nasal hard structures (nasal bone, nasal cavity) were manually measured in order to compute the regression equations so as to find the most probable position of the pronasale, subnasale, and alare. These results suggest that hard and soft tissue relation data from CBCT scans can be useful for predicting the position of the nose.

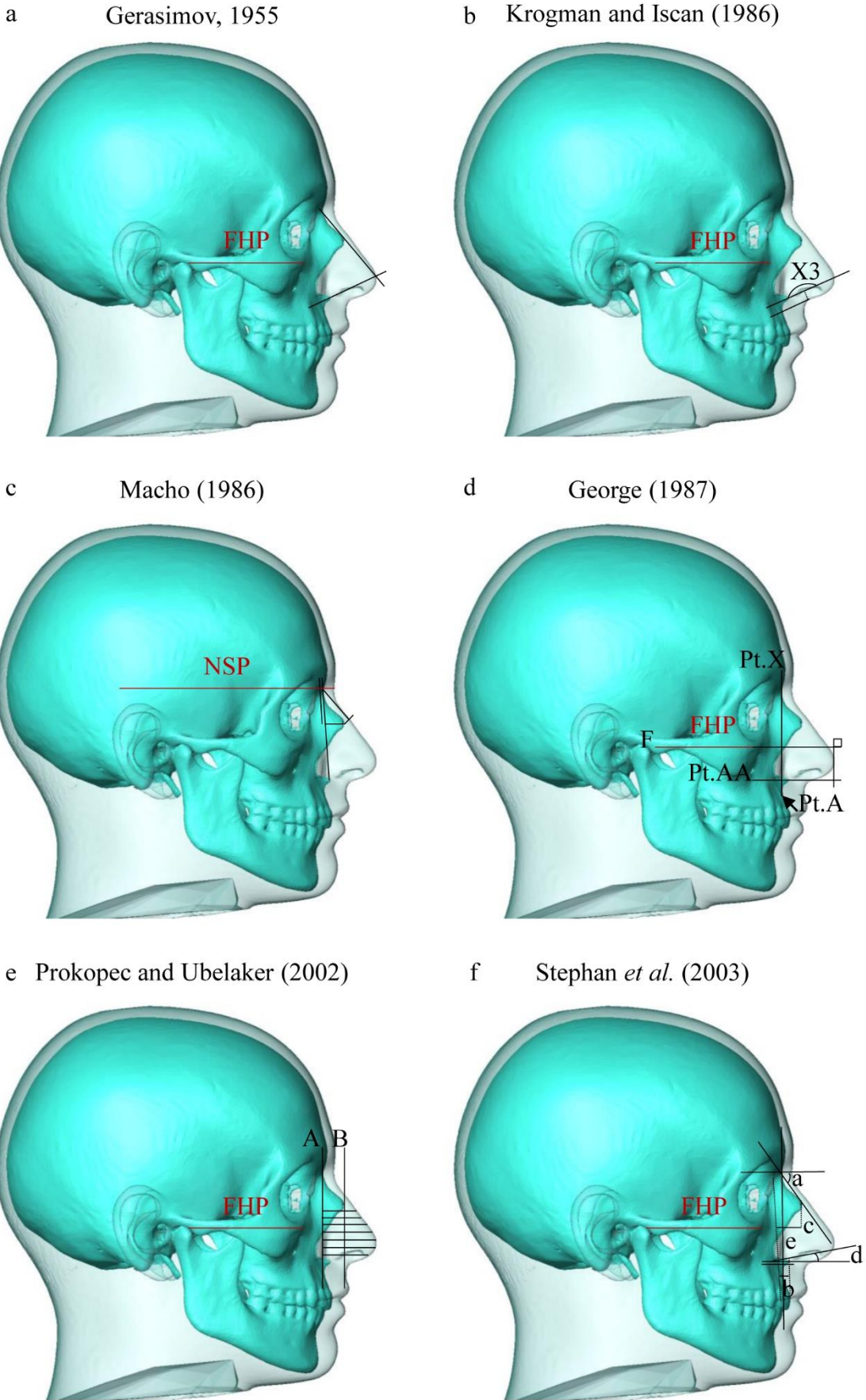


Figure 2. 1. Traditional 2D/3D CFR of nasal reconstruction (Rynn & Wilkinson, 2009; Stephan *et al.*, 2003).

The scientific community in the field of CFR recognised that manual reconstruction methods require a high degree of anatomical and sculptural expertise and remain difficult and subjective in practice (Tyrrell *et al.*, 1997; Stephan, 2003; Verzé, 2009; Ullrich and Stephan, 2011; Vandermeulen *et al.*, 2012; Guyomarc'h *et al.*, 2014). The interpretations of two different forensic artists of the same skull can result in the creation of two substantially different faces (Tyrrell *et al.*, 1997; Stephan, 2003; Verzé, 2009; Ullrich and Stephan, 2011; Vandermeulen *et al.*, 2012; Guyomarc'h *et al.*, 2014). According to Davy and collaborators (Davy *et al.*, 2005), this point is further illustrated by Haglund and Reay (1991), who stated that multiple facial reconstructions of several victims of the Green River serial-killer were created. The results were highly variable between practitioners and little success was achieved when the reconstructions were shown to the public. Furthermore, manual reconstructions are time consuming and are therefore often limited to a single reconstruction. Traditional 2D or 3D manual techniques of CFR are now considered to be unsuitable for application to the judicial system, which requires precision, reliability and knowledge of possible quantisation errors (Vandermeulen *et al.*, 2012).

2.1.3. Computer-based CFR methods

Recent developments in computer science and the improvement of medical imaging technique such as surface scanning, MRI-scanning, CT- and CBCT-scanning have resulted in the collection of large databases of 3D representations of hard- and soft-tissues of living human heads. Researchers in the field of CFR utilise these technological advances to develop alternative computer-based CFR methods to improve objectivity of facial reconstructions during criminal investigations.

As compared to a human expert, a computer is consistent and objective. The computer integrates all the modelling assumptions and repeatedly generates the same output data. As compared to forensic artists, some procedures can be automated, such as the creation of multiple reconstructions from the same target skull using different modelling assumptions (ancestry, age, sex). An additional advantage of using computer-based CFR is the convenience of visualisation. Furthermore, the CFR process is more accessible to a wide range of forensic experts without the need for extensive expertise in computer science or computer-based CFR fields. In practice, the development of software for computerised facial reconstructions of an individual could benefit law enforcement agencies by allowing faster, easier and more efficient generation of multiple representations of an individual.

Compared to manual methods, automation of facial approximation of the nose using large 3D surface samples, offers increased objectivity and the possibility of standardisation. In general, all computer-based methods share the foundational premise that information about the complete skull versus information of the skin is used for mapping a template face onto a dry skull. More precisely, the prediction is performed by using a soft-tissue representation generated from the database by applying a deformation, based on the correlation between skin and skull-surfaces, incorporated in the database. A recent review of computerised CFR methods by [Claes and colleagues \(2010a\)](#) offers an interpretation and classification of previously published computer-based CFR methods in use, and in progress (Table 2.1). As compared to the manual approaches, the computer-based methods exclude forensic artistic interpretation, and instead, use information from a large database. Consequently, the accuracy of the methodology is dependent on the accuracy of the database, and of the underlying algorithms. Following the review of computerised CFR methods by [Claes and colleagues \(2010a\)](#), the computer-based methods can be compartmentalised into six components (a–f) (Figure 2.2).

Table 2. 1. A list of 3D computerised CFR techniques over the past 30 years in a quasi-chronological order (Claes *et al.*, 2010a; Tilotta *et al.*, 2010; Guyomarc'h, 2011; Guyomarc'h *et al.*, 2013; Schlager, 2014).

Method	Reference	Craniofacial model (CFM)			Target skull representation
		Craniofacial template (CFT)	Craniofacial Information (CFI)	Craniofacial Deformation (CFD)	
Vanezis	Vanezis (1989)	Single/specific	Face	Generic/non uniform scaling	Sparse/tissue dowels+growth
	Vanezis <i>et al.</i> , (2000)	Single/specific	Face	Generic/-	Sparse/tissue dowels
Evenhouse	Evenhouse <i>et al.</i> , (2000)	Single/-	Face	Generic/polygon based deformations	Sparse/tissue dowels
Evison	Evison (1996); Evison (2000)	Single/specific	Face	Generic/-	
Michael	Michael and Chen (1996)	Single/specific	Face	Generic/volume distortion functions	
Shahrom	Shahrom <i>et al.</i> , (1996)	Single/generic	Face	Generic/-	Sparse/tissue dowels
Archer	Archer (1997); Archer <i>et al.</i> , (1998)	Single/generic	Face	Generic/radial basis functions	Sparse/tissue dowels
Quatrehomme	Quatrehomme (1997)	Single/generic	Face/skull	Generic/radial basis functions	Dense/crest-lines
Seibert	Seibert, (1997)	Single/generic	Face/skull	Generic/radial basis functions	Dense/feature points
Nelson	Nelson and Michael (1998)	Single/generic	Face	Generic/local cylindrical coordinate	Dense/feature points
Attardi	Attardi <i>et al.</i> , (1999)	Single/generic	Face/skull	Generic/diffused scattered motion fields	Sparse/tissue dowels+extra
Bullock	Bullock (1999)	Single/generic	Face	Generic/radial basis function	Sparse/tissue dowels+growth
Plasencia	Plasencia, (1999)	Single/-	Face	Generic/polygon based deformations	Sparse/tissue dowels+growth
Jones	Jones (2001)	Single/specific	Face/skull	Generic/-	Dense/feature points
Kähler	Kähler <i>et al.</i> , (2003)	Single/generic	Face/muscles	Generic/-	Sparse/tissue dowels
Claes	Claes <i>et al.</i> , (2004a;2004b);(2005a; 2005b);(2006a;2006	Multiple/generic	Face/tissue thicknesses	Face-specific/PCA	Sparse
	Claes (2007);Claes <i>et al.</i> , (2010a)	Multiple/generic	Face/tissue thicknesses	Face-specific/PCA	Implicit/signed distance transform
Vandermeulen	Vandermeulen <i>et al.</i> , (2005a, 2005b)	Multiple/specific	Face/skull	Generic/digital cosine transformations	Implicit/signed distance transform
	Vandermeulen <i>et al.</i> , (2006)	Multiple/specific	Face/skull	Generic/ radial basis functions	Implicit/signed distance transform
Pei	Pei <i>et al.</i> , 2004	Single/generic	Face/skull	Generic/ radial basis functions	
	Pei <i>et al.</i> , 2008	Single/specific	Face	Generic/-	Dense/ range image
Andersson	Andersson and Valfridsson (2005)	Single/generic	Face	Generic/-	Sparse/tissue dowels + growth
Berar	Berar <i>et al.</i> , (2005a, 2005b, 2006a)	Multiple/generic	Face/skull	Face-specific/PCA	Dense/feature points
Davy	Davy <i>et al.</i> , (2005)	Single/generic	Face	Generic/radial basis functions	Sparse/tissue dowels+extra
Muller	Muller <i>et al.</i> , (2005); Mang <i>et al.</i> , (2006)	Single/specific	Face/skull	Generic/radial basis functions	Sparse/tissue dowels
Subsol	Subsol and Quatrehomme (2005)	Single/specific	Face/skull	Generic/radial basis functions	Dense/crest-lines
Tu	Tu <i>et al.</i> , (2005);Tu <i>et al.</i> , (2007)	Multiple/specific	Face/skull	Generic/radial basis functions	Dense/ range image
Turner	Turner <i>et al.</i> , (2005)	Multiple/specific	Face	Generic/radial basis functions	Dense/crest-lines
Paysan	Paysan <i>et al.</i> , (2009)	Multiple/generic	Face/skull	Face-specific/PCA	Dense/feature points
Tilotta	Tilotta <i>et al.</i> , (2010)	Multiple/specific	Face/skull	Generic/ Local semi-rigid	Implicit/Extended Normal Vector Field
Guyomarc'h	Guyomarc'h, (2011); Guyomarc'h <i>et al.</i> , (2013)	Multiple/generic	Face/tissue thicknesses	Face-specific/PCA	Dense/feature points
Schlager	Schlager, (2014)	Multiple/specific	Face/Skull	Generic/ radial basis functions	Implicit/signed distance transform

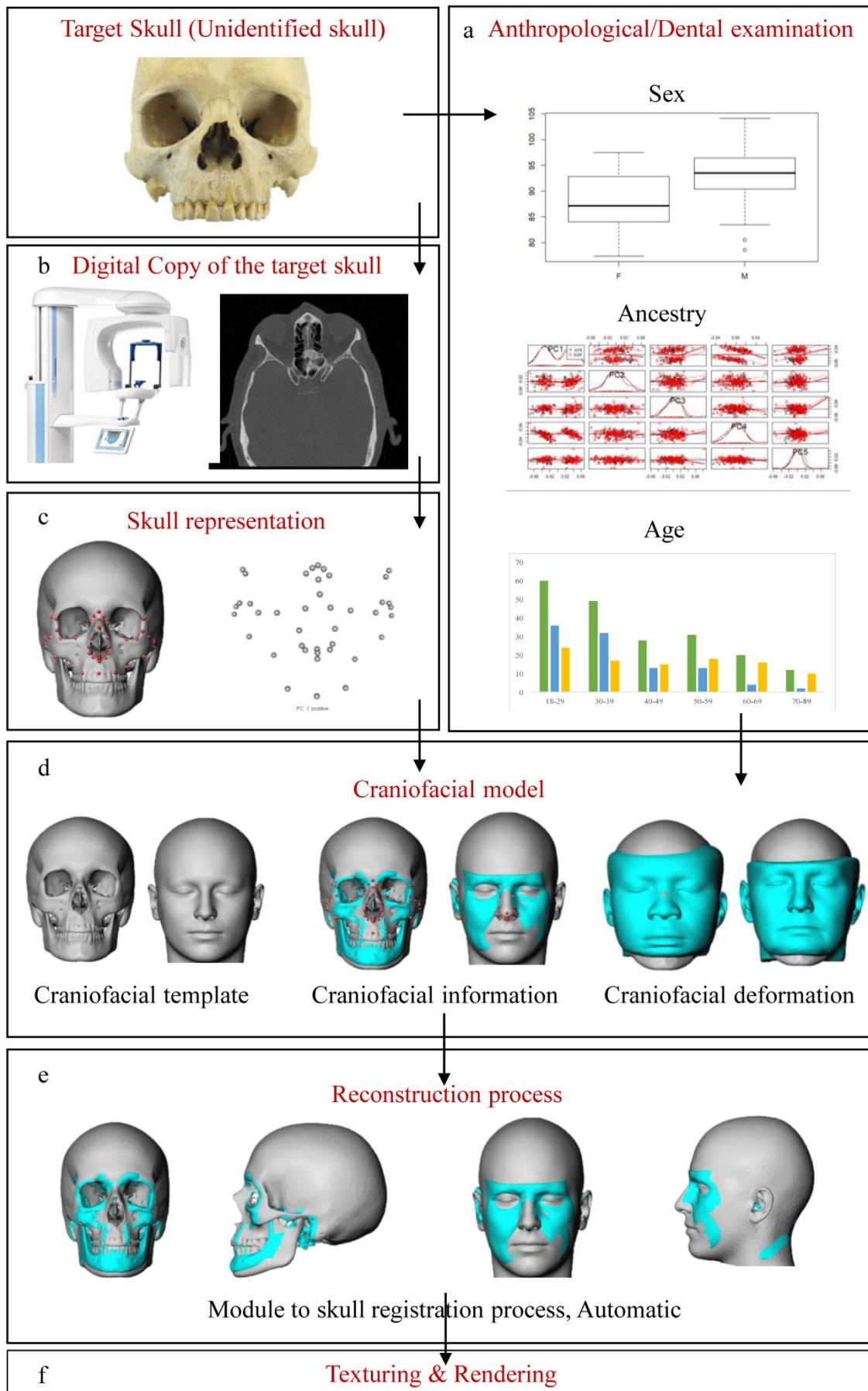


Figure 2. 2. General workflow of computerised craniofacial reconstruction techniques (Claes et al., 2010a).

The skull is the basic source of information for any craniofacial reconstruction because it has a morphometric individuality as distinctive as a fingerprint (Schimmler *et al.*, 1993). Forensic anthropologists examine the target skull so as to estimate biological parameters such as age, sex, pathological influences, and ancestry (Wilkinson, 2004). Firstly, an anthropological examination is performed on the target skull (Figure 2.2.a). The anthropological examination results are taken into account when adjusting parameters of the reconstruction.

A virtual copy of the target skull (Figure 2.2.b) is then obtained by digitisation. A computer-readable format of the skull shape is obtained for further statistical processing, depiction and visualisation. The production of a 3D replica avoids destruction or mutilation of the original skull and, therefore, possible evidence. The digitisation of a target skull for computerised 3D craniofacial reconstruction purposes was first performed by Vanezis (1989) using a laser scanning system. More recently, computerised reconstruction techniques made use of a CT-or CBCT-scanner which became scientifically recognised as a practical and accurate alternative for acquiring a digital copy of the target skull (Claes *et al.*, 2010a).

The accuracy of computer-based methods relies on the craniofacial model (CFM), while the accuracy of the CFM relies on the anthropological properties of the target skull (Figure 2.2.d). Knowledge about human facial shapes and their relationship to the underlying skull, as acquired from a representative database of living subjects, provides the anthropological inputs needed for the CFM. A CFM contains three components: i) craniofacial template (CFT); ii) craniofacial information (CFI); and iii) craniofacial deformation (CFD).

A craniofacial template (CFT) is a computer representation of the shape of a human face. Single or multiple CFT's can be used, and it can be represented as a holistic view or a collection of partial features separately (nose, mouth, eyes, ears) of the face.

In the single template setup, the knowledge of only one reference face is used. The template can either be a generic/average, or a specific individual (similar to the target skull in terms of age, sex, ancestry) created from a database. In a multiple template setup, two approaches are observed. The first or "specific" approach generates a reconstruction per specific reference head in a database, resulting in multiple reconstructions of the unknown skull. A final result is generated by combining all the reconstructions into a single reconstruction. The second or "generic" approach combines the knowledge of multiple reference heads beforehand and then makes a single reconstruction based on that combined knowledge.

Craniofacial information (CFI) is defined as the explicit information contained in the CFM, relating faces to the underlying skull substrates. This knowledge can consist of facial surfaces, tissue thicknesses, skull surfaces and/or facial muscles. For example, in [Claes and colleagues \(2004a, 2004b, 2005a, 2005b, 2006a, 2006b, 2007, 2010b\)](#) combined the facial surface knowledge with soft-tissue thicknesses measured at 52 anatomical landmarks according to de Greef and colleagues ([De Greef *et al.*, 2005, 2006](#)). The accuracy of CFI is dependent on the type of scanning equipment (CT or CBCT scan) used to scan subjects for creating the CFM.

The craniofacial deformation (CFD), used by all computer-based CFR methods, is defined as the manner by which the CFT is allowed to be deformed or transformed. Two different approaches, affine or rigid transformation, can be applied on templates in order to geometrically align them with the target skull into the same coordinate system. The affine transformation, is defined as the application of multiple modifications (rotation, translation, scale and the skew) to deform the facial template. The rigid transformation entails only the application of a translation and rotation to manipulate the CFT. The majority of recent computer-based methods use a generic non-rigid deformation (affine transformation), which are mathematically well defined and easy to use.

A reconstruction is obtained by finding the geometrical relationship between the CFM and the target skull, based on an appropriate choice of skull representation ([Figure 2.2.c](#)). The target skull representation (TSR) is strongly related to the choice of the craniofacial model. The skull representation can be parameterised in different ways depending on the type of CFI (relationship between soft and hard-tissues) incorporated in the CFM.

An important step in the computer-based CFR methods is the registration process, also called fitting or matching ([Figure 2.2.e](#)). The registration is defined as the process of finding and applying the geometrical relationship or transformation between the CFM and the target skull. This process allows for the measurement of a similarity, expressing the closeness-of-fit of the CFT to the skull. During the registration process, the CFD model is combined with the similarity measure into an objective function by increasing the similarity measure within the range of possible transformations, as coded by the CFD. Finally, the CFT can be deformed/warped/morphed/adapted towards the target skull specimen to generate an estimate of the unknown facial geometry. Additionally, the reconstructed facial

shape can be textured (skin colour) and visually represented (Figure 2.2.f) in order to generate images for further distribution and recognition.

The computerised reconstruction technique must be validated for utilisation in real-investigation situations. The performance of the methods and the success of the identification of the final reconstruction must be tested. The performance of the computer-based CFR method can be assessed by estimating the mean squared error (MSE) using leave-one-out cross-validation (LOOCV) testing. A recognition test can be performed by comparing the CFR result with a database of candidates, including the actual person. The goal is to retrieve the actual person from the database.

2.1.3.1. Computer-based CFR methods of nasal reconstruction

Recently, [Tilotta and colleagues \(2010\)](#) and [Schlager \(2013\)](#) developed computer-assisted methods for the prediction of the structure of the external surface of the nose, based on conventional computer tomography (CT) scans. Compared with manual methods, automation of facial approximation offers increased objectivity and the possibility of standardisation ([Guyomarc'h *et al.*, 2014](#)). Computer-based CFR methods of nasal reconstruction are presented in Table 2.2.

Table 2. 2. Computer-based CFR methods for nasal reconstruction.

Method	Reference	Sample	Slice thickness	Voxel size	Landmarking	Region of interest (hard-tissue)	Region of interest (soft-tissue)	Meaningful region of interest	Suppination effect
Tilotta	Tilotta <i>et al.</i> , (2008)	CT-scan/European	0.7 mm	-	Manual	External nose and nares	Nasal superior and inferior (patches)	X	✓
Schlager	Schlager, (2013)	CT-scan/European/Chinese	0.7-1.5 mm	-	Manual	External nose and nares	Nasal superior and inferior	✓	✓
Guyomarc'h	Guyomarc'h, (2014)	CT-scan/European	0.7-1.5 mm	-	Manual	Face/Facial features/External nose	Facial skeleton	✓	✓

Tilotta (Tilotta, 2008; Tilotta *et al.*, 2010) published a method for an automatic patch extraction and surface estimation using European CT-scans. The estimation is localised on hard- and soft-tissue patches delimited by surface geodesics between four anatomical landmarks on the skull (nasion, rhinion, anterior nasal spine, nasospinale) (see Table 2.3 for the definition and the reproducibility of the landmarks used). The technique relies on a continuous representation of the individual surfaces embedded in the vectorial space of extended normal vector fields, allowing to compute deformations and averages of surfaces. The method consists of estimating the soft-tissue surface over patches delimited by surface geodesics between anatomical points of the skull. In the Tilotta approach (Tilotta *et al.*, 2010), the main bias is the utilisation of a non-biologically meaningful region as a region of interest. Indeed, in the Tilotta approach (Tilotta *et al.*, 2010), the rectangular region is based on geometrical, rather than biological region and it does not account for structural or functional coherence.

Schlager (Schlager, 2013) provides a new approach of predicting nasal soft tissue shape, based on the shape of the underlying bone by using a large database of European and Chinese CT-scans. This approach involves the definition of a biologically, hence anatomically, meaningful substructure by extracting shape information using landmarks and semi-landmarks. In Schlager's (Schlager, 2013) study, 14 craniometric landmarks (nasospinale, subspinale, nariale, nasomaxillofrontale, maxillofrontale, nasion, alare, nasomaxillare, rhinion) and 15 capulometric landmarks (nasal-depth, sellion, pronasale, mid-nostril, alar-crest-sub, alar-crest-lateral, alagenion, end-of-alar-crest) placed manually on the nasal complex (see Table 2.3 for the definition). The main directive is to find the statistical interrelationship between soft-tissue and hard-tissue implying a large database for building statistical models, estimating the most probable soft-tissue shape, based on the known hard-tissue information. This method takes into account the co-variation of soft and hard tissue and the effect of age, sex and ancestry on the morphology of the nose. Although Schlager provides a very promising approach for predicting nasal soft-tissue shape for the European and Chinese populations only, the use of conventional CT scans as initial references is influenced by supination effects on the face due to the horizontal position of the patient during scanning. In addition, the manual placements of landmarks on large 3D surface samples may induce important observer subjectivity and errors in placing the landmarks rendering the analysis less repeatable. In Schlager approach (Schlager, 2013), the subspinal (craniometric landmark) and the nasal depth (capulometric landmark) have shown important observer errors (> 2 mm) with a manual placement. The reproducibility of the landmarks used is detailed in Table 2.3. The manual placements of landmarks on large 3D

surface samples derived from CT scans affect the objectivity of the standardisation, and by extension, the accuracy of the nose approximation process.

More recently, Guyomarc'h (Guyomarc'h, 2011; Guyomarc'h *et al.*, 2014) presented a new computerised method for estimating facial shape based on computed tomography (CT) scans of 500 French individuals referred to as the Anthropological Facial Approximation in Three Dimension (AFA3D). A holistic approach was followed, incorporating geometric morphometrics (GGM) and statistical models with FSTD and facial feature estimation to produce a cloud of 100 cutaneous landmarks that are transformed into facial shape through the warping of a single generic template. In this study, correlations between the external shape of the nose and the underlying bone structure were assessed using GMM. A set of craniometric landmarks (nasion, mid-nasal, rhinion, nasomaxillofrontale, mid-nasomaxillare, nasomaxillare, apertion, piriform curvature, akanthion, nariale, nasospinale superior, subspinale) and capulometric landmarks (pronasale, inferonasale, midseption, subnasale, external alar curvature, superior alar curvature, alagenion, alare, alacrepidon, seption) were manually placed on the hard- and soft-tissue nasal complex (see Table 2.3 for the definition the landmarks used). Although Guyomarc'h (Guyomarc'h, 2011; Guyomarc'h *et al.*, 2014) provides a very promising approach for predicting nasal soft-tissue shape for the French individuals only, as for the Schlager approach, the manual placement of landmarks on large 3D surface samples derived from CT scans affects the objectivity of the standardisation, and by extension, the accuracy of the nose approximation process. Indeed, in the approach of Guyomarc'h (Guyomarc'h, 2011; Guyomarc'h *et al.*, 2014), some craniometric landmarks such as the subspinal and the apertion, as well as the following capulometric landmarks: the external alare curvature, the superior alar curvature and the alare, have shown important observer errors (> 2 mm) with manual placement on CT scan surfaces. The reproducibility of the landmarks used is detailed in Table 2.3.

Table 2. 3. Definition and reproducibility of landmarks (craniometric and capulometric) used by Tilotta and colleagues (2008); Schlager (2013) and Guyomarc'h and

	Landmarks	Definition	Method			Observer errors on CT-scans
			Tilotta	Schlager	Guyomarc'h	
Craniometric	nasion	Intersection of Sutura internasalis and Sutura frontonasalis ² / Midline point on the nasofrontal suture ^{1,3}	✓	✓	✓	<1mm
	rhinion	Midline point at the inferior free end of the internasal suture ^{1,2,3}	✓	✓	✓	<1mm
	anterior nasal spine	End of the anterior nasal spine ¹	✓			/
	nasospinale	Tip of spina nasale anterior ²		✓		<1mm
	nasospinale superior	Midline point on the inferior border of the piriform aperture at the intermaxillary suture ^{1,3}	✓		✓	1-2mm
	subspinale	Transition of frontal downward edge of the Spina nasalis anterior into the processus alveolaris ² / Inferior midline point at the maximum of curvature of the nasal spine ³		✓	✓	2-3mm
	nariale	Beginning of the transition of the lower border of the Apertura nasalis into the structure of the Nasospinale ² / Most inferior point of the piriform aperture ³		✓	✓	1-2mm
	nasomaxillofrontale	Intersection of Sutura frontonasalis and Sutura nasomaxillaris ² / Point at the intersection of the frontal, maxillary, and nasal bones ³		✓	✓	1-2mm
	maxillofrontale	Intersection of Sutura frontomaxillaris and the Anterior lacrimal crest ² / Point at the intersection of the fronto-maxillary suture and the anterior lacrimal crest ³		✓		1-2mm
	alare	Most lateral positions of the apertura nasalis ²		✓		1-2mm
	nasomaxillare	Distal end point of the sutura nasomaxillaris ² / Most inferior point of the nasomaxillary suture on the nasal aperture ³		✓	✓	1-2mm
	mid-nasal	Midline point on the internasal suture midway between nasion and rhinion ³			✓	<1mm
	mid-nasomaxillare	Point of the nasomaxillary suture between the nasomaxillare and the nasomaxillofrontale ³			✓	1-2mm
	apertion	Most lateral point of the piriform aperture ³			✓	3-4mm
	piriform curvature	Most infero-lateral point of the piriform aperture ³			✓	1-2mm
	akanthion	Most anterior midline point of the nasal spine ³			✓	<1mm
	Capulometric	nasal-depth	Most medial point of the transition nose/eye ²		✓	
sellion		"Soft-tissue Nasion" ²		✓		<1mm
pronasale		Most anterior point on the tip of the nose ^{2,3}		✓	✓	<1mm
Subnasale		Point of maximum curvature at transition of philtrum and columella ² / Most postero-superior midline point of the nasal septum (maximum of curvature) ³		✓	✓	1-2mm
mid-nostril		Midpoint of maximal nostril width - projected on the transition nostril/philtrum ²		✓		<1mm
alar-crest-sub		Alar crest at the most downward point of the Alae ²		✓		<1mm
alar-crest-lateral		Alar crest at the most lateral downward point ²		✓		<1mm
alagenion		Most posterior point of the Alar crest ² / Most posterior point of the nasal wing ³		✓	✓	1-2mm
end-of-alar-crest		Upper anterior end point of the alar crest ²		✓		<1mm
inferonasale		Most antero-inferior midline point of the nose ³			✓	1-2mm
midseption		Midline point of the columella between the two nostrils ³			✓	1-2mm
external alare curvature		Most anterior point of the nasal wing at the maximum of curvature ³			✓	2-3mm
superior alar curvature		Most superior point of the nasal wing ³			✓	2-3mm
alare		Most lateral point of the nasal wing ³			✓	2-3mm
alacrepidon		Most inferior point of the nasal wing in anterior view ³			✓	1-2mm
seption	Medial point of the nostril, at the smallest width of the nasal septum ³			✓	1-2mm	

2.2. References used in craniofacial reconstruction methods

2.2.1. Introduction

The reliability of the craniofacial reconstruction method depends greatly on the characteristics of the reference sample used. Traditionally, CFR methods used facial soft tissue thicknesses (FSTT) references, which are typically measured at sparsely located craniofacial landmarks. FSTT provides a quantitative description of the envelope of soft tissue around the skull (Stephan *et al.*, 2018), and this tissue depth thickness can be measured using a variety of techniques (Stephan & Preisler, 2018) including: 1) insertion of needles or blades into cadavers (Welcker *et al.*, 1883; His, 1895; Kollmann *et al.*, 1898; Suazo *et al.*, 2008) ; 2) radiography/CT (Dumont , 1986; Bulut *et al.*, 2014; Garlie & Saunders, 1999; Hwang *et al.*, 2012) ; 3) magnetic resonance imaging (Sahni *et al.*, 2002; Sahni *et al.*, 2008; Sipahioglu *et al.*, 2012), and 4) ultrasound (Helmer, 1984; Baillie *et al.*, 2016).

The use of cadavers for recording soft-tissue thicknesses has been extensively criticised in the recent craniofacial identification literature (Manhein *et al.*, 2000; Wilkinson, 2002; Wilkinson,2004; De Greef *et al.*, 2005; Vandermeulen *et al.*, 2006; De Greef *et al.*, 2009; Lee *et al.*, 2011; Chen *et al.*, 2011). Poor relationships have been reported between cadaver-based and in vivo measurements. Tissue deformation due to post-mortem changes (Todd & Lindala, 1928), namely dehydration and shrinkage, as well swelling with the onset of putrefaction, have been thought to be responsible for the discrepancy in these findings.

Recent developments in digital imaging techniques have resulted in the collection of large databases of 3D representations of hard- and soft-tissues of the face. The accuracy of the tissue depth data, as well as the development of research on the statistical relationship between hard- and soft-tissue, was greatly improved with the arrival of in vivo, non-invasive databases (Vandermeulen *et al.*, 2006) such as lateral cephalometric radiography, ultrasound (Helmer, 1984; Baillie *et al.*, 2016), magnetic resonance imaging (Sahni *et al.*, 2002; Sahni *et al.*, 2008; Sipahioglu *et al.*, 2012), CT- and CBCT-scanning (Dumont, 1986; Garlie & Saunders, 1999; Tilotta *et al.*, 2010; Hwang *et al.*, 2012; Schlager, 2013; Gyomarc'h *et al.*, 2014; Bulut *et al.*, 2014), providing very detailed information about the structures represented. Researchers in the field of 3D computer-assisted methods for CFR utilise these sources of information to improve objectivity in the reconstruction process by mainly the creation of approaches using living

specimens (Vanezis *et al.*, 1989; Vanezis and Vanezis, 2000; Evenhouse *et al.*, 1991; Evison, 1996, 2001; Michael and Chen, 1996; Shahrom *et al.*, 1996; Archer, 1997; Quatrehomme *et al.*, 1997; Nelson *et al.*, 1998; Forte, 1999; Bullock, 1999; Jones, 2001; Kähler *et al.*, 2003; Claes *et al.*, 2004a, 2004b, 2005a, 2005b, 2006a, 2006b, 2007, 2010b; Vandermeulen *et al.*, 2005a, 2005b; Andersson & M.Valfridsson, 2005; Berar *et al.*, 2005, 2006a, 2006b; Davy *et al.*, 2005; Muller *et al.*, 2005; Mang *et al.*, 2006; Subsol & Quatrehomme, 2005; Tu *et al.*, 2005; Turner *et al.*, 2005; Pei *et al.*, 2008; Paysan *et al.*, 2009; Tilotta *et al.*, 2009; Schlager, 2013; Guyomarc'h *et al.*, 2014; Lee *et al.*, 2014; Ridel *et al.*, 2018) .

2.2.2. CT scans

Computer-based CFR methods for the prediction of the external nose are based on conventional computer tomography (CT) scans (Figure 2.3). Computed tomography, also originally called computed axial tomography, produces the complete image volume of an object from a large series of two-dimensional X-ray images taken around a single axis of rotation. In a conventional CT, there is an X-ray source, mounted on a rotatable ring, and a line of detectors on the opposite side of the ring. X-rays are emitted at the source, pass through the object, and are recorded by the array of detectors, while the ring rotates at the same time. The object itself is placed on a table that moves along the rotational axis (Figure 2.3.a). Information about the interior of the object comes from information on the attenuation of radiation resulting from absorption and scattering caused by the object (Figure 2.3.b,c). For a more technical descriptions of CT see [Gonzales & Woods \(2008\)](#); [Brant & Helms \(2012\)](#) and [Oppelt \(2011\)](#).

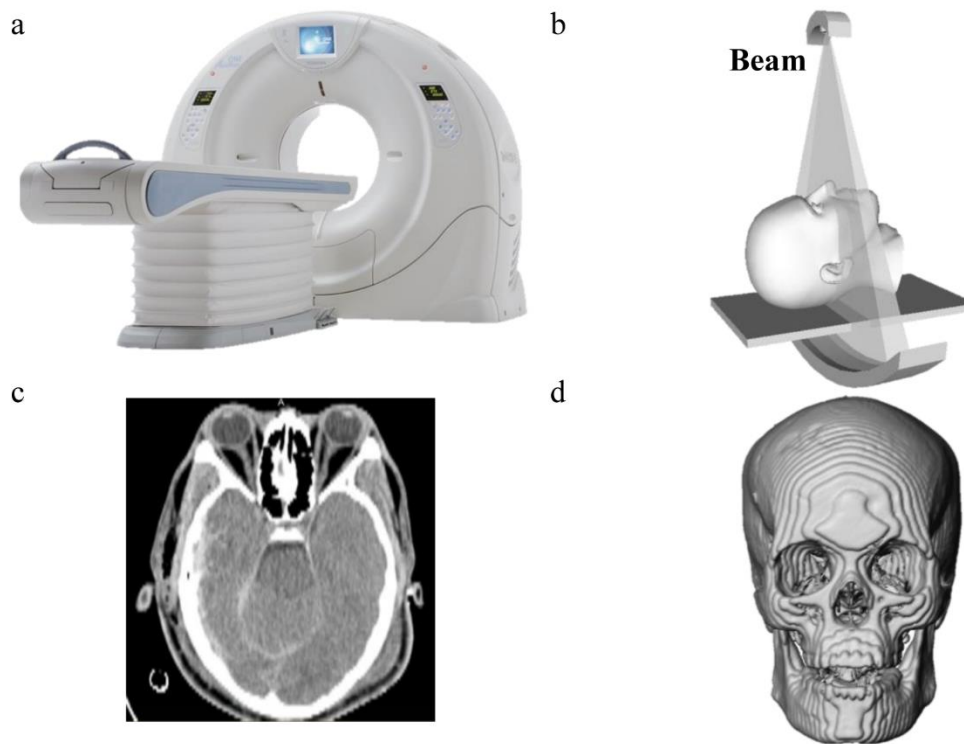


Figure 2. 3. Computed-tomography scan. a) CT-scanner; b) X-ray beam; c) Slice; d) 3D image.

The use of conventional CT scans as initial references for CFR methods is influenced by supination effects on the face due to the horizontal position of the patient during scanning (Iblher *et al.*, 2013; Marin *et al.*, 2015; Munn & Stephan, 2018). Patterns of nasal contour change with posture. This is important important for disciplines concerned with soft tissue morphology, such as facial approximation of the nose, because measurements in one position (e.g., supine) cannot serve as upright models in computerised face prediction programmes (Tu *et al.*, 2003, 2005). The disregard of the supination effect when developing approaches in computerised nose prediction programmes, may add errors to the methods. Munn & Stephan (2018) has recently shown important differences in the shape of the face between upright and supine postures (1-4.0 mm), using high-resolution non-contact 3D stereophotogrammetry (Dimensional Imaging DI3D, Glasgow, Scotland) to investigate facial surface changes in a set of young and old adults, both in frontal and profile views. This outcome demonstrates that the actual standard collection of facial soft-tissue thicknesses in the supine position is less applicable when these measurements are intended for use in the subject-upright context (Munn & Stephan, 2018). This research emphasises the need to take postural effects into consideration in the reference used, when developing approaches in all methods for CFR.

2.2.3. CBCT scans

Cone Beam-CT is a more recent technology used for CFR (Figure. 2.4). In the literature, however, only one manual CFR method for the prediction of the nose is based on CBCT scans. Furthermore, no reports regarding a computer-based CFR method for the approximation of the nose, using CBCT-scans for the acquisition and extraction of the relevant anatomical structure, could be found. Cone Beam-CT imaging is accomplished by using a rotating gantry to which an X-ray source and detector are fixed. A divergent pyramidal- or cone-shaped source of ionising radiation is directed through the middle of the area of interest onto an area x-ray detector on the opposite side. The X-ray source and detector rotate around a rotation fulcrum fixed within the centre of the region of interest (Figure 2.4.a). During the rotation, multiple (from 150 to more than 600) sequential planar projection images of the field of view (FOV) are acquired in a complete, or sometimes partial, arc (Scarfe & Farman, 2008).

This procedure varies from a traditional medical CT for several reasons. Firstly, the traditional medical CT uses a fan-shaped X-ray beam in a helical progression to acquire individual image slices of the FOV and then stacks the slices (Figure 2.4.b) to obtain a 3D representation (Figure 2.4.c). Each slice requires a separate scan and separate 2D reconstruction, while CBCT exposure incorporates the entire FOV. Only one rotational sequence of the gantry is necessary to acquire enough data for image reconstruction. The patient is thus also exposed to a reduced dosage of radiation. A further advantage of CBCT, as compared to CT, includes higher spatial resolution (0.1 mm to 0.4 mm) and isotropic volumetric data for the accurate placement of 3D landmarks (Scarfe & Farman, 2008). Finally, during a CT-scan, the patient is in a supine position, while during a CBCT scan acquisition, the patient is in an upright position and the scanner rotates around the head, which minimises gravitational effects on soft-tissue deformations. Unfortunately, as for the previous studies on the approximation of the nose using CT-scan, the CBCT-scans analysed in this thesis do not contain any information whatsoever related to the body mass index (BMI) of the scanned individuals. However, recent publications by De Greef *et al.*, (2006, 2009) imply that there is no evidence that the facial region is affected by the BMI, as soft-tissue thickness measurements regarding the nose are not dependent on BMI.

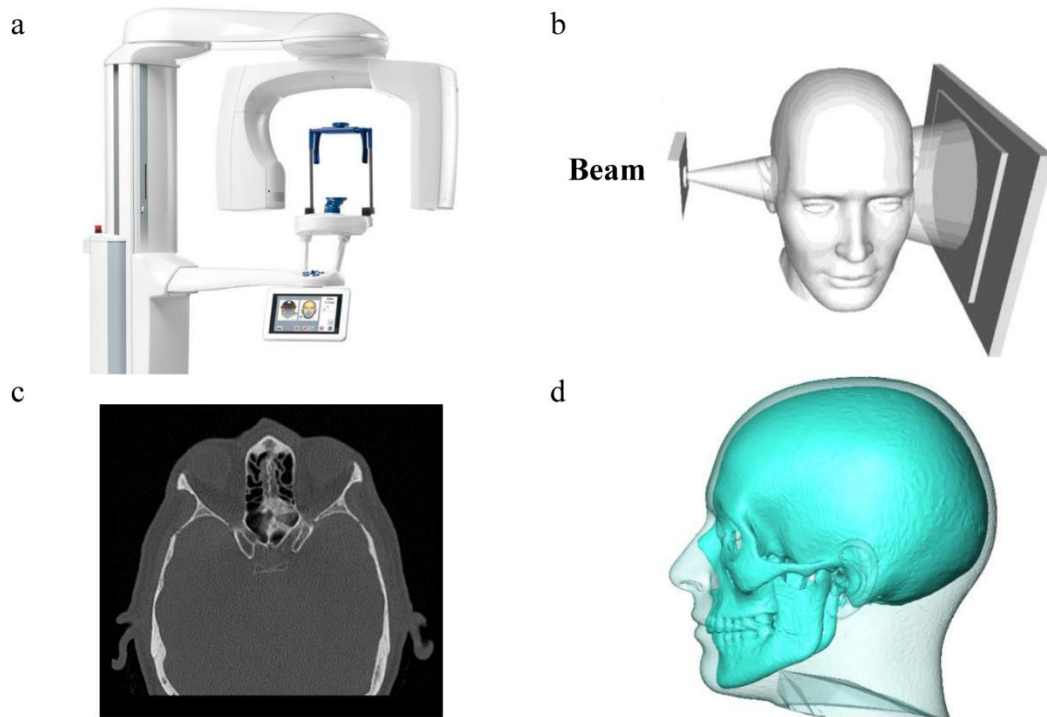


Figure 2. 4. Cone beam-computed tomography. a) CBCT-scanner; b) Cone beam; c) Slice; d) 3D image.

2.3. Anthropological examination

2.3.1. Introduction

Ignorance of population specificities in current facial approximation techniques, used by the VIC (Victim Identification Centre) of the SAPS, limits the objectivity and accuracy of the reconstruction performed. Recent studies on the facial approximation of the nose among South African groups (Ridel *et al.*, 2018) and on other European and Asian populations (Schlager, 2013), demonstrate the importance of considering factors such as sex, age and ancestry in the approximation of the nose. The failure of consideration of biological parameters when developing approximations, will impact on the accuracy of the final facial reconstruction.

2.3.2. Anatomical description of the region of interests

The skull is the most complex part of the skeleton and is of major importance in physical anthropology. The skull, houses and protects the brain and accomodates the senses of sight, smell, taste and hearing. The cranium can be divided into the neurocranium (the cranial vault), which encloses the brain and meninges and the viscerocranium (the facial skeleton), which contains the organs of the various senses. The osteology is usually described from five standard perspectives, namely the norma verticalis (vertical view), the norma lateralis (lateral view), the norma occipitalis (posterior view), the norma frontalis (anterior view) and the norma basilaris (inferior view). The morphological structure of the cranium is dependent on transformations related to both ontogeny and senescence. In this study, only the splanchnocranium (the facial skeleton) will be considered (Figure 2.5.a), comprising: the nasal bones; the anterior nasal aperture; the zygomatic bone; and the maxillae. (White *et al.*, 2011). The convention used in orientating the skull is the Frankfurt Horizontal Plane (FHP) which is defined by three points: the right and left porion points (located at the summit of each external acoustic meatus) and the left orbitale (located at the bottom of the left orbit).

2.3.2.1. Facial skeleton anatomy.

The nasal bones (Figure 2.5. c) are located on either side of the midline below the glabellar region of the frontal bone, with their inferior ends forming the superior margin of the anterior nasal aperture (White *et al.*, 2011). The nasal bones articulate superiorly with the frontal bones, with each other medially, with the frontal processes of the maxillae laterally and with the ethmoid bones posteriorly. The anterior nasal aperture (Figure 2.5.d) is piriform in shape, with the nasal bones delimiting its upper boundary, while the lower boundary is formed by the maxillae (Standring *et al.*, 2009). The maxillae (Figure 2.5.e) form the dominant elements of the facial skeleton. Functionally, the maxillae accommodate the tooth roots and form most of the boundaries of the nasal aperture. They articulate with the zygomatic bones, and the nasal bones. The zygomatic bones (Figure 2.5.b) form the prominent corners of the face and articulate with the frontal, sphenoidal, temporal and maxillary bones.

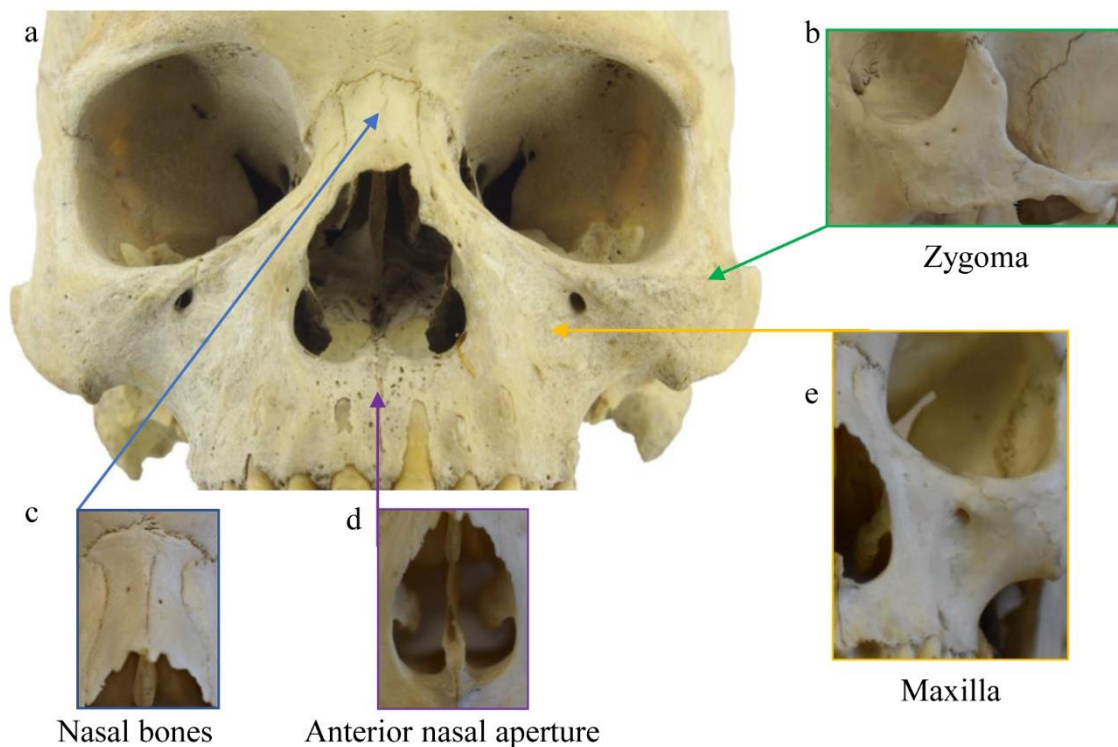


Figure 2. 5. Anatomical description of the hard-tissue regions of interest. a) mid-facial skeleton; b) zygoma; c) nasal bones; d) anterior nasal aperture; e) maxilla.

2.3.2.2. External nose and nares

The external nose extends the nasal cavities onto the front of the face and positions the nares so that they point downward. The nose is pyramidal in shape, with its apex anteriorly. The upper angle of the nose, between the openings of the orbits, is continuous with the forehead. Like the posterior regions, the anterior parts of the nasal cavities found within the nose are held open by a skeletal framework composed partly of bone and partly of cartilage. The supporting bony parts are located where the nose is continuous with the skull and is composed of the nasal bones and parts of the maxillae and frontal bones. Anteriorly, a single septal cartilage in the midline forms the anterior part of the nasal septum. On each side, support is provided by the lateral processes of the septal cartilage, the major alar and three or four minor alar cartilages. (Figure 2.6). The nares are oval apertures on the inferior aspect of the external nose and are the anterior openings of the nasal cavities. They are held open by the surrounding alar cartilages and septal cartilage, and by the inferior nasal spine and adjacent margins of the maxillae. Although the nares are continuously open, they can be widened further by the action of the related muscles of facial expression (nasalis, depressor septi nasi, and levator labii superioris alaeque nasi) (Standring *et al.*, 2009; White *et al.*, 2011).

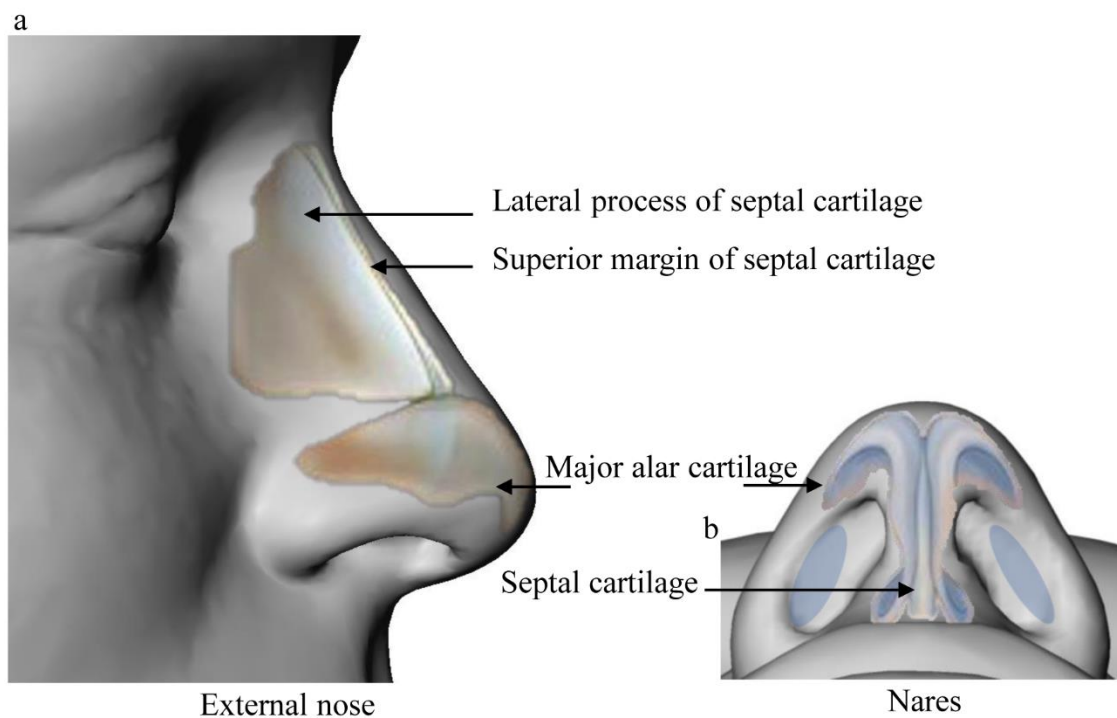


Figure 2. 6. Anatomical description of the soft-tissue region of interests. a) external nose; b) nares.

2.3.3. Previous studies on nasal shape variation

Nasal shape variation results from the divergent growth and development of the human craniofacial skeleton. Growth of the components of the craniofacial skeleton are interdependent and are influenced by multifactorial processes involving hormonal, genetic and epigenetic factors, as well as external stimuli (soft tissue growth, dental maturation and biomechanical factors) (Moss & Young, 1960; Atchey & Hall, 1991; Enlow & Hans, 1996; Moss, 1997a, 1997b, 1997c, 1997d; Lieberman *et al.*, 2002; Klingenberg *et al.*, 2003; Tomoyasu *et al.*, 2009; Lieberman, 2012; Groming *et al.*, 2013). During craniofacial development, from birth to death, the morphology of the nose is influenced by the remodelling of the underlying skeletal structure (Albert *et al.*, 2007), emphasising the fact that the components of the nose cannot be considered as independent elements of the craniofacial skeleton. According to the literature, differences in the rate of soft tissue facial aging exist that varies according to the decade of life, sex and ancestry (Taylor, 2000; Akgül *et al.*, 2002). These variations present a challenge for facial reconstruction. Effective techniques, taking into account the effects of ancestry, sexual dimorphism and aging on the morphology of the nose, need to be developed.

2.3.3.1. Ancestry

The estimation of ancestry is based on the geographical origin of a person's ancestors. A few hundred years of migration is not enough time to eliminate the geographic variation, particularly in societies with historically restricted interracial mating as in South Africa (Ousley *et al.*, 2009). From 1913 to 1983, approximately 60 segregation acts were implemented to control and to segregate the populations of South Africa (Thompson, 2001; Lemon, 2002). These segregation acts concerning race, influenced employment, education, land tenure and geography, inter-racial marriage, political representation and state security. The geographical separation of socially defined groups inhibited gene flow, resulting in distinct morphological variation between ancestral groups, still existing among South African population groups. The three largest socially identified population groups are Black (80%), Coloured (9%), and White (8%) (Statistics South Africa, 2015). In this thesis, only two South African groups (black and white) were studied and the terms "black" and "white" South Africans are used as these social terms are required when reporting and describing a missing person (Sauer, 1992).

While no discrete pattern of biological variation exists among humans, clinal morphological variation, which is often driven by social and cultural aptitudes, is observed in geographical distances (Hall *et al.*, 1983; Dubow, 1995; Ousley *et al.*, 2009; L'Abbé *et al.*, 2013). The influence of environmental factors on nasal shape has been demonstrated by many bioanthropological studies. The general hypothesis is that the shape of the external nose and the nasal aperture plays an important role in climate adaptation by regulating air temperature in order to protect the lungs from extreme temperature and excessive desiccation (Thomson & Buxton, 1923; Weiner, 1954; Franciscus & Long, 1991). Ousley and collaborators (Ousley *et al.*, 2009) demonstrated that the morphological variability among population groups is quantifiable and may be useful in order to provide a probable classification of an unknown person. In forensics, estimation of ancestry from unknown skeletal remains is important to the development of a biological profile (Hefner, 2009). Steyn and colleagues (Steyn *et al.*, 2016) have demonstrated that the South African white population is osteologically distinct from their European counterparts. From the recent literature, distinct differences in mid-facial size and shape have already been observed among all South Africans groups (L'Abbé *et al.*, 2011; McDowell *et al.*, 2012; McDowell *et al.*, 2015). Indeed, in several osteometric analyses, some discrete traits from the mid-face, such as nasal width, inter-orbital breadth, nasal bone structure and alveolar prognathism have been shown to have a significant relationship with ancestry for South African groups (L'Abbé *et al.*, 2011; McDowell *et al.*, 2012; McDowell *et al.*, 2015).

Variation in nasal hard- and soft-tissue morphologies has been described in other populations as well (Schlager, 2013), for instance, a difference of hard- and soft-tissue nasal shapes between Chinese and Europeans populations. While the nasal complexes in Chinese are smoother and incorporated into the skull, the European nasal shapes are quite prominent (Schlager, 2013). In the craniofacial reconstruction literature, no research has focused on the development of methods for prediction of the nose, taking into account the ancestry-related shape changes. The failure of consideration of ancestral variation when developing approximation approaches, may impact on the accuracy of the final facial reconstruction.

2.3.3.2. Age

During human development, and in order to maintain the function and the proportionate growth, the skeletal components of the face involve changes in their shape and size, as well as their relative position within the craniofacial complex system (O' Higgins *et al.*, 1991; Enlow & Hans, 1996; Mc Collum, 2008; Lieberman, 2011). During growth, the skull evolves through two simultaneous and interrelated processes: modelling and displacements of the skeletal components. In general, the adult face shows downward and forward growth directions (Bastir, 2008) due to the bone growth dynamics of the facial skeleton, such as the resorption of the nasal area, the canine fossae and the inferior margin of the zygomatic region. During adulthood and with advancing age, the remodelling of the underlying skeletal structure (Albert *et al.*, 2007) and changes in the facial musculature (e.g. gravity and hyperdynamic facial expressions effects) may influence the morphology of the nose (Albert *et al.*, 2007).

In general, the studies on the change in morphology with age concentrate on the analysis of classical metric data (Zankl *et al.*, 2002; Chen *et al.*, 2011) and/or additional volume and area measurements (Sforza *et al.*, 2011) of the soft-tissue of the nose. These studies report the prolongation and the widening of the nose (increase of nasal breadth and length) (Damon *et al.*, 1972; Sforza *et al.*, 2011; Chen *et al.*, 2011) and a change in angles (Sforza *et al.*, 2011). Only two studies, one on a French sample (Guyomarc'h *et al.*, 2014) and one on a Chinese and a European sample (Schlager, 2013), demonstrated the presence of age-related changes of the nasal soft-tissue dimensions in human adults using geometric morphometric analysis. The results are consistent with previous studies, using classic anthropometric methods. Schlager (Schlager, 2013) found differences in the ageing changes in the nasal features between populations (Chinese and European), which could be explained by general shape differences: as the tissue weakens with age, it follows gravity downwards. The effect of gravity with advancing age is present in all populations and has an effect on the general shape change, independent of population differences.

2.3.3.3. Sex

Accurate sex estimation is based on interpreting and quantifying the expression of sexual dimorphism in a population (Loth *et al.*, 2000; Gapert *et al.*, 2009). These questions are of basic anthropological interest, as they can provide information about human patterns of sexual selection. At birth, in general, a slight sexual dimorphism exists, but the major divergence does not occur until puberty. As the adolescent growth spurt occurs approximately two years earlier in females than in males, creating a significant sexual dimorphism in many body measures. Therefore, variations in the dimensions of the nose are not unexpected (Chronicle *et al.*, 1995; Enlow & Hans, 1996; Lieberman, 2011). In recent literature on this topic, methods of standard morphometrics are used, based on distances and angles (see for example Troncoso Pazos *et al.*, 2008; Rynn *et al.*, 2009; Sforza *et al.*, 2011) or soft-tissue thickness (Chen *et al.*, 2011), that address a link between asymmetry and facial masculinity (Troncoso Pazos *et al.*, 2008; Rynn *et al.*, 2009; De Greef *et al.*, 2009). In craniofacial reconstruction, dimensions of the nose are important in distinguishing male and female faces and are useful in establishing an accurate facial approximation of a missing person. (Chronicle *et al.*, 1995). In the literature, only one method, developed by Schlager (2013) on a Chinese and European sample, involves geometric morphometrics having been applied to these issues for nasal reconstruction purposes.

Schlager (Schlager, 2013) found that the expression of sexual dimorphism in the variation of the shape of the nose among Chinese and European groups seems to be influenced statistically by ancestry, but he emphasised that, from a biological point of view, this influence is small. However, he demonstrated that the amount of asymmetry differs significantly in both groups between sexes, both in hard- and soft-tissue, supporting the hypothesis that asymmetry is linked to facial masculinity (Scheib *et al.*, 1999; Gangestad & Thornhill, 2003). In the South African research context, distinct differences in facial skeletal morphology (size and shape) between the sexes have been demonstrated in many research studies (Guyomarc'h & Bruzek, 2010; L'Abbé *et al.*, 2011; Schlager, 2013; Lee *et al.*, 2014; McDowell *et al.*, 2015; Schlager & Rüdell, 2015), using standard morphometric methods. These studies demonstrate that sexual dimorphism may be less pronounced in the black South African population than in other groups (white and coloured) (L'Abbé *et al.*, 2011; McDowell *et al.*, 2012). From the literature, no studies could be found concerning the analysis of sex-related shape changes of the nose by means of geometric morphometrics among South African populations.

2.4. Approach proposed in this thesis

The main critiques of current facial approximation techniques, which are used in South Africa, are (1) the inherent subjectivity in manual methods, (2) the references used, (3) the lack of standardisation, (4) the non-consideration of population specificities, and (5) the poor correlations between facial bony structures and facial soft features. These factors limit the objectivity and the accuracy of the estimation.

Faced with the inherent subjectivity in the 2D/3D manual methods in CFR, an automated three-dimensional (3D) method, independent of any forensic artistic interpretations was developed. Moreover, in order to improve the reliability of the CFR method, great care was taken to select the reference sample used. In this study, in vivo cone beam CBCT-scans were used instead of using cadavers, ultrasound, MRI or CT-scan references for the acquisition and extraction of the relevant anatomical structures. During a CBCT acquisition, the patient is in an upright position and the machine rotates around the head, capturing images using a cone-shaped X-ray beam. The construction of a large and reliable database using in vivo CBCT scanning compared to other conventional reference bases (cadavers, ultrasound, MRI or CT-scans), allowed us to have access to accurate living data, excluding any possible gravitational effect on soft-tissue deformations. The CBCT-scans also provide higher spatial resolution (0.1 mm to 0.4 mm) for the placement of 3D landmarks on 3D surfaces.

The main aim of this thesis, following the trends of the recent research to improve the standardisation in the facial features approximation process, is to propose an accurate automatic placement of landmarks on 3D surfaces. Contrary to the previous recent research on nasal shape approximation using a manual placement of landmarks, an automatic dense landmarking procedure, using a non-rigid registration process, was used.

In addition, unlike current facial approximation techniques used in South Africa, great care was taken in this research to consider population specificities and correlations between facial bony structures and facial soft features, by the quantification and visualisation of covariance between the nasal complex shape variations and factors such as age, size, sex and ancestry, using GMM.

Statistical models are needed that allow for establishing the statistical relationship predictors (hard-tissue shape, age, sex and ancestry) and response variables (soft-tissue information). The evaluation and application of different statistical modelling procedures was performed, in order to obtain an optimally adjusted prediction algorithm. This included the finding of an optimal amount of variables and factors in order to achieve reliable prediction results for unknown cases. Finally, the methodology was applied by predicting an unknown hard-tissue, which is not from the initial database, but with known related soft-tissue surface. The main elements of the approach proposed in this thesis as compared to the actual computer-based CFR methods of nasal reconstruction, are reported in Table 2.4.

Table 2. 4. The approach proposed in this thesis as compared to the existing computer-based CFR methods of nasal reconstructions.

Method	Reference	Sample	Slice thickness	Voxel size	Landmarking	Region of interest (hard-tissue)	Region of interest (soft-tissue)	Meaningful region of interest	Suppination effect
Tilotta	Tilotta <i>et al.</i> , (2008)	CT-scan/European	0.7 mm	-	Manual	External nose and nares	Nasal superior and inferior (patches)	X	✓
Schlager	Schlager, (2013)	CT-scan/European/Chinese	0.7-1.5 mm	-	Manual	External nose and nares	Nasal superior and inferior	✓	✓
Guyomarc'h	Guyomarc'h, (2014)	CT-scan/European	0.7-1.5 mm	-	Manual	Face/Facial features/External nose	Facial skeleton	✓	✓
Ridel	Ridel, (2018)	CBCT-scan/South African	-	0.4 mm	Automatic	External nose and nares	Mid-facial skeleton	✓	X

Chapter 3

INTRODUCTORY MATERIALS & METHODS

3.1. Introduction

The main purpose of this thesis was to provide an accurate computer-assisted method for the prediction of the nasal soft-tissue shape, from the morphological features of the underlying skull substrate. The development of this method relied on the creation of sound statistical models, which estimate the most probable soft-tissue shape from the known hard-tissue information. To this end, a large CBCT-scan database was established, comprising two hundred and sixty adult South Africans collected from different institutions located in Pretoria. The main methodology used to collect 3D hard- and soft-tissue shape data involved an automatic landmarking procedure. The validation of the automatic landmarking procedure is provided in Chapter 4 “*Automatic landmarking as a convenient prerequisite for geometric morphometrics. Validation on cone beam computed tomography (CBCT)- based shape analysis of the nasal complex.*”, while the complete workflow is detailed in this chapter. The statistical approach in this chapter involves calculation of statistical models, based on the hard- and soft-tissue shape information and the additional factors (age, size, sex and ancestry), using geometric morphometrics. Further statistical procedures applicable to the anthropological aspects, statistical modelling and cross-validation testing are described in this chapter.

A preliminary analysis described in Chapter 5 “*Skeletal dimensions as predictors for the shape of the nose in a South African sample: a cone-beam computed tomography (CBCT) study.*” was performed on a sub-sample of 120 South African individuals (18-30 years), extracted from this CBCT-scan database, which allows for characterising the morphological

differences among South African groups, using linear measurements. As one of our objectives was to find the statistical interrelationship between the hard- and soft-tissue of the nasal complex attributed ancestry, sex and age, statistical models were needed to establish the statistical relationship predictors (hard-tissue shape, ancestry, sex, age and size (allometry)) and response variables (soft-tissue information). Therefore, an evaluation and a quantification of shape differences attributed to known factors (ancestry, sex, age and size (allometry) and covariates was performed on the complete CBCT sample, both on hard- and soft-tissue shape using GMM. The results of this analysis are discussed in Chapter 6 “*Shape analysis of the nasal complex among South African groups from Cone-Beam Computed Tomography (CBCT) using geometric morphometrics.*” The validation of prediction models was performed using cross-validation testing with the calculation of the Mean Squared Error (MSE), using leave-one-out cross-validation (LOOCV). The results are described in Chapter 7 “*Statistical models for South African nose reconstruction*”.

3.2. Materials

The materials used in this thesis consisted exclusively of CBCT-scans of adult South Africans. The data acquisition (collection and general properties) and the distribution of age, sex and ancestry (complete sample, black South African sample, white South African sample) are described in the following sections.

3.2.1. Data acquisition

The data used in this thesis originated from CBCT-scans as retrospective records collected at two institutions: the *Oral and Dental Hospital, University of Pretoria, South Africa* and the *Life Groenkloof Hospital, Pretoria, South Africa*. The data were anonymised, and only age, sex and ancestry used in the further analysis. In order to standardise the acquisition, all subjects were scanned in a seated position with their eyes closed and with a relaxed facial expression. Subjects were excluded if they presented with any condition that could affect the morphology of the face (e.g. orthodontic treatment, pathological conditions, facial asymmetry or any facial interventional reconstructive surgery). As the scope of this thesis was not concerned with the analysis of ontogenetic processes, only individuals between 18 and 80 years

of age were selected. This resulted in 200 usable datasets. All cone beam computer tomography scans used in this research were obtained using a CBCT-scanner (Planmeca ProMax ® 3D, Pretoria, South Africa) with the following properties: 90 kV, 11.2 mA, voxel size of 0.4 mm, and field of view of 230 x 260 mm. CBCT images in DICOM format were imported into MeVisLab © v. 2.7.1 software for segmentation and 3D surface mesh generation.

3.2.2. *Distribution of age, sex and ancestry*

The average age of the complete sample was 40.51 years. The database contained 200 individuals of which 100 were black South Africans (33 females, 67 males) and 100 were white South Africans (65 females, 35 males) (Figure 3.1). The average age of the black South African sample was 36.07 years, with females being slightly older (39.45 years) than males (34.40 years) (Figure 3.1). Individuals in the white South African sub-sample were slightly older in average compared to the black South African sub-sample. The average of the white South African group was 45.01 years, with females being slightly older (45.78 years) than males (43.60 years) (Figure 3.1).

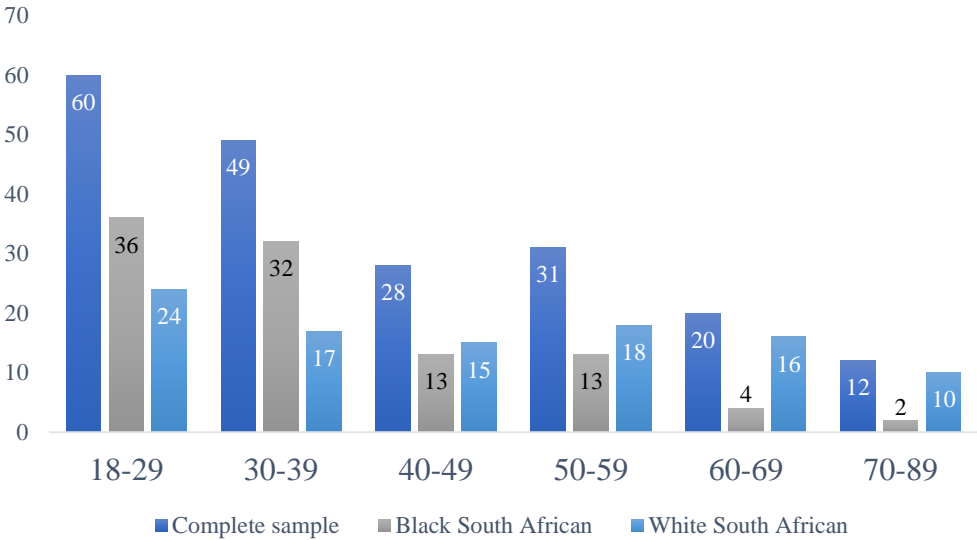


Figure 3. 1. Age distribution of sample by ancestral group.

3.3. Methods

The automatic landmarking method proposed was from the procedure introduced by [Claes and colleagues \(2006a, 2006b; Claes, 2007\)](#). The basic concept involved using a reference template (floating surface) of the anatomical surface of interest, containing a dense set of (quasi-) landmarks. These (quasi-) landmarks are a dense equivalent of the traditional anatomical landmarks which are sparse, discrete and well-defined. During the anatomical templating process, this reference template is warped non-rigidly to the anatomically corresponding surface (target surface) of each subject. The non-rigid (robust) surface registration software used for this warping was developed using the MeVisLab © v. 2.7.1 software ([Snyders et al., 2014](#)). The warping is performed iteratively starting with a rigid alignment, followed by gradually more flexible registration steps. At the same time, non-matching parts, due to incomplete scanning, foreign objects or artefacts, are detected and left out of the warping process. At the end of this process every (quasi-) landmark of the template is projected onto the surface of every subject, thus establishing a dense point-based anatomical correspondence between all subjects. The complete workflow, including the data processing (segmentation and construction of surface meshes), the surface mesh initialisation, the non-rigid surface registration process and the template generation process, is detailed in the following section and illustrated in [Figure 3.5](#). Landmarks (craniometric and capulometric) and the software programs (modules on MeVisLab © v. 2.7.1 and packages for R. studio software version 1.0.44-®2009-2016 for Windows (R Core Team, 2012)) used, are described in this section.

3.3.1. Data processing: segmentation and construction of surface meshes

CBCT images in DICOM format were imported into MeVisLab © v. 2.7.1 software for segmentation and 3D surface mesh generation. The grey values encode the density of the material observed - analogous to a common radiographic image: the lighter the grey value, the denser the intrinsic structure of the tissue. Based on an initially defined grey value threshold, and given all the different layers, MeVisLab © v. 2.7.1 software program estimated a three-dimensional representation of the object in question. As one was dealing with distinct slices, the space between them had to be interpolated by the software. A process called threshold-segmentation allows an observer to define grey value intervals, within which a given tissue (e.g. hard- and soft- tissue) is displayed. The segmentation of different elements (hard- and soft-

tissue) were obtained by finding the threshold values between segmented components according to the “Half Maximum Height” (HMH) quantitative iterative thresholding method (Spoor *et al.*, 1993). For this thesis, threshold values for hard-tissue varied between 1200-1250 and for the soft-tissue between 400-450. The segmentation process is illustrated in Figure 3.5. a.

After segmentation of hard- and soft-tissues, 3D-triangular surface meshes were constructed. Triangular meshes consist of a finite number of connected triangles, forming a three-dimensional hull representing a solid object (Schneider & Eberly, 2002). In this way, 400 usable 3D surfaces (200 hard- tissue 3D surfaces and 200 soft-tissue 3D surfaces) were created for further analysis and manipulations.

3.3.2. Surface mesh initialisation

Surface mesh initialisation refers to the repositioning of all the surfaces into the same coordinate system (Figure 3.5.b). Prior to registration, the floating surface (Figure 3.2. a) is to be brought into the vicinity of the target surface (Figure 3.2.b) by repositioning the floating surface, using an affine transformation, into the coordinate system of the target surface (Figure 3.2.c). In this thesis, the initialisation was performed manually by indicating a set of landmarks on floating and target surfaces in order to interactively rotate and translate the surfaces to bring them into proximity of each other. The definitions, abbreviations, nature and type of landmarks used for the surface mesh initialisation are indicated in Table 3.1.

For the initialisation, five landmarks (one bilateral: porion, and three median: rhinion, nasospinale, prosthion) were indicated on the hard-tissue floating and target surfaces, and seven landmarks (three bilateral: exocanthion, endocanthion, cheilion, and one median: pronasale) on the soft-tissue floating and target surface.

Table 3. 1. Definitions, abbreviations, nature and type of landmarks used for the surface meshes initialisation.

	Landmark	Abbreviation	Nature	Definition
Cranio-metric	Porion	po	Bilateral	Most superior point on the upper margin of the external auditory meatus.
	Rhinion	rhi	Median	Most rostral (end) point on the internasal suture. Cannot be determined accurately if nasal bones are broken distally.
	Nasospinale	ns	Median	The point where a line drawn between the inferior most points of the nasal aperture crosses the median plane. Note that this point is not necessarily at the tip of the nasal spine.
	Prosthion	pr	Median	Median point between the central incisors on the anterior most margin of the maxillary alveolar rim.
Capulo-metric	Exocanthion	ex'	Bilateral	Most lateral point of the palpebral fissure, at the outer commissure of the eye; best seen when subject is gazing upward.
	Endocanthion	en'	Bilateral	Most lateral point of the head, located in the parietal region.
	Pronasale	pr'	Median	The most anteriorly protruded point of the apex nasi. In the case of a bifid nose, the more protruding tip is chosen.
	Cheilion	ch'	Bilateral	Outer corners of the mouth where the outer edges of the upper and lower vermilions meet.

These transformations map the coordinates of each point of the floating surface into the coordinate space of the target surface. The non-rigid surface registration results are dependent on the quality of this initialisation procedure.

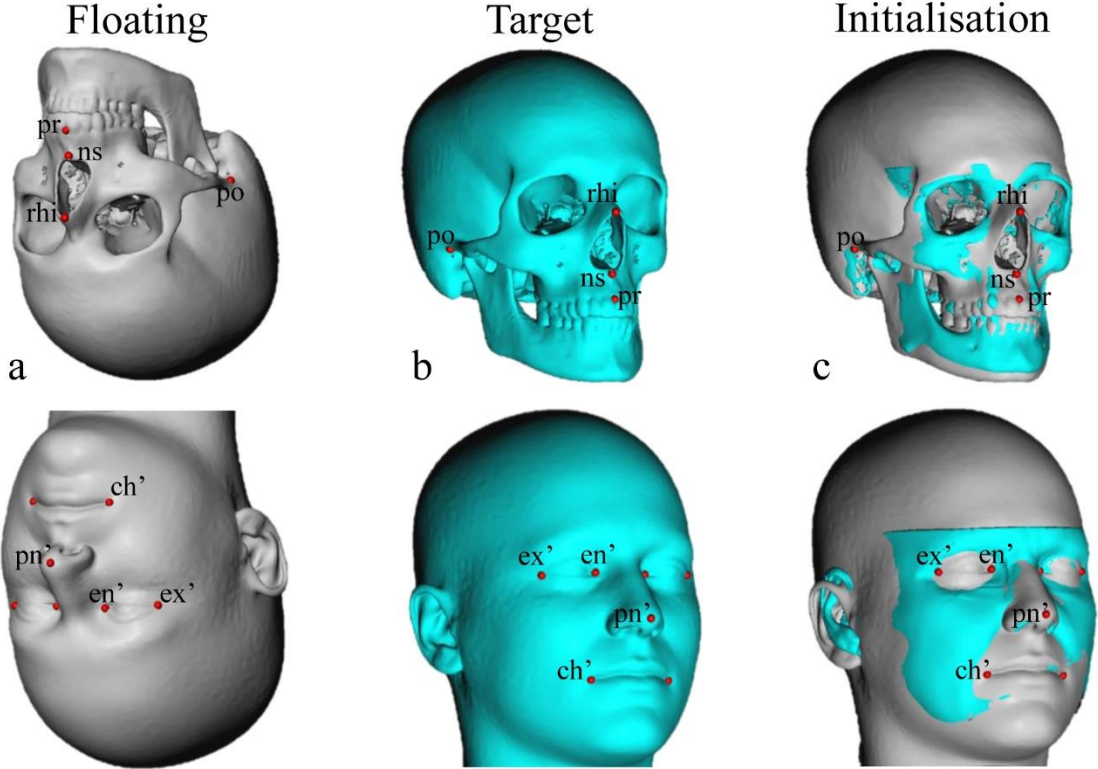


Figure 3. 2. Surface mesh initialisation procedure. a) hard- and soft-tissue floating surfaces; b) hard- and soft-tissue target surfaces; c) hard- and soft-tissue initialised surfaces. po: porion; rhi: rhinion; ns: nasospinale; pr: prosthion; ex': exocanthion; en': endocanthion; pr': pronasale; ch': cheilion.

3.3.3. Non-rigid surface registration process

Surface registration refers to the establishment of the geometrical relationship between two or more surfaces (Claes, 2007) that aligns the surfaces as well as possible. All surfaces in the database have to be registered non-rigidly to perform a statistical analysis of 3D shape information. A surface is represented by a dense set of connected 3D points. Registered surfaces share the same number of 3D points with the same connectivity. For this, the 3D points with known connectivity of a carefully constructed generic reference surface (initial generic template) are mapped onto the surfaces in the database by finding dense point correspondences. The result is that every facial surface in the database is represented by the same number of points with the same connectivity, such, that for every point on one surface, the corresponding point on every other surface in the database is known.

3.3.4. Template generation process

The reference templates are created in an iterative fashion, akin to the generation of the mean shape in a Generalized Procrustes Superimposition (GPS) procedure (Kendall, 1984; Slice, 2001), the main difference being the insertion of a point-correspondence establishment step determined by the non-rigid registration process. Starting from an initial generic template, this template is iteratively updated as the GPA-mean, till convergence, thus eliminating any possible bias in the selection of the initial generic surfaces. As a by-product of this template generation process (template), every individual surface has been ‘templated’ (warped surfaces): every point on these warped surfaces is associated with the anatomically corresponding point on the template. Alternatively, one can generate the templates independently from the population under study and apply the template warping in a subsequent step. The template generation process is illustrated in Figure 3.5. c,d.

3.3.5. Anatomical templating

As the main interest of this thesis is finding a quantitative approach to estimate soft-tissue shape from information given by the underlying bone structure, information encoded in 3D-surface representations has to be extracted and made comparable. The approach taken is that of landmark-based geometric morphometrics, which exploit the entire geometric

information encoded within landmarks. Therefore, the landmark coordinates are recorded within a common coordinate system for further analysis. The anatomical templating is illustrated in Figure 3.5. e,f.

3.3.5.1 Landmarks

Following the facial approximation literature (Schlager, 2013; Guyomarch' *et al.*, 2014), and in order to conserve homology and comparability between studies, classic craniometric and capulometric landmarks (type I, II, and III (Buikstra & Ubelaker, 1994; Schlager, 2013; Guyomarch' *et al.*, 2014; Caple & Stephan, 2016) were used.

The landmarks selected were distributed on the facial skeleton and the external nose, creating a hard- and soft-tissue region of interest.

3.3.5.1.1. Craniometric landmarks

The hard-tissue region of interest was delimited on the facial skeleton (Figure 3.3) comprising the nasal bones (Figure 3.3.b), the anterior nasal aperture (Figure 3.3.c), the zygomatic bones (Figure 3.3.d), and the maxillae (Figure 3.3.e). On the nasal bones, five craniometric landmarks (three median and two bilateral pairs), and on the anterior nasal aperture, eight craniometric landmarks (four median and four bilateral pairs) were recorded. On the zygomatic, nine craniometric landmarks (bilateral pairs) were recorded, while 10 craniometric landmarks (two median and eight bilateral pairs) were recorded on the maxillary bone. A total of 41 craniometric landmarks consisting of 17 bilateral pairs and seven median landmarks were recorded on the hard-tissue surfaces (Table 3.2).

Table 3. 2. Craniometric landmarks used (Schlager, 2013; Guyomarch' *et al.*, 2014; Buikstra & Ubelaker, 1994; Caple & Stephan, 2016).

Craniometric	Landmarks	Abbreviation	Nature	Definition
	1 Nasion	n	Median	Intersection of the nasofrontal sutures in the median plane.
	2 Mid-nasal	mn	Median	Midline point on the internasal suture midway between nasion and rhinion.
	3 Rhinion	rhi	Median	Most rostral (end) point on the internasal suture. Cannot be determined accurately if nasal bones are broken distally.
	4 Nasospinale	ns	Median	The point where a line drawn between the inferior most points of the nasal aperture crosses the median plane. Note that this point is not necessarily at the tip of the nasal spine.
	5 Subspinale	ss	Median	The deepest point seen in the profile view below the anterior nasal spine (orthodontic point A).
	6 Akanthion	ak	Median	Most anterior midline point of the nasal spine.
	7 Prosthion	pr	Median	Median point between the central incisors on the anterior most margin of the maxillary alveolar rim.
	8/9 Zygotemporale superior	zts	Bilateral	Most superior point of the zygomatico-temporal suture.
	10/11 Zygotemporale inferior	zti	Bilateral	Most inferior point of the zygomatico-temporal suture.
	12/13 Jugale	ju	Bilateral	Vertex of the posterior zygomatic angle, between the vertical edge and horizontal part of the zygomatic arch.
	14/15 Frontomalare temporale	fnt	Bilateral	Most lateral part of the zygomaticofrontal suture.
	16/17 Frontomalare orbitale	fmo	Bilateral	Point on the orbital rim marked by the zygomaticofrontal suture.
	18/19 Nasomaxillofrontale	nmf	Bilateral	Point at the intersection of the frontal, maxillary, and nasal bones.
	20/21 Ectoconchion	ec	Bilateral	Lateral point on the orbit at a line that bisects the orbit transversely.
	22/23 Orbitale	or	Bilateral	Most inferior point on the inferior orbital rim. Usually falls along the lateral half of the orbital margin.
	24/25 Zygo-orbitale	zo	Bilateral	Intersection of the orbital margin and the zygomaticomaxillary suture.
	26/27 Maxillofrontale	mf	Bilateral	Intersection of the anterior lacrimal crest with the frontomaxillary suture.
	28/29 Nasomaxillare	nm	Bilateral	Most inferior point of the nasomaxillary suture on the nasal aperture.
	30/31 Alare	al	Bilateral	Instrumentally determined as the most lateral point on the nasal aperture in a transverse plan.
	32/33 Piriform curvature	cp	Bilateral	Most infero-lateral point of the piriform aperture.
	34/35 Nariale	na	Bilateral	Most inferior point of the piriform aperture.
	36/37 Zygomaxillare	zm	Bilateral	Most inferior point on the zygomaticomaxillary suture.
	38/39 Submaxillare curvature	csm	Bilateral	Most supero-medial point on the maxillary inflexion between the zygomaxillare and the ectomolar.
	40/41 Supra-canine	sc	Bilateral	Point on the superior alveolar ridge superior to the crown of the maxillary canine.

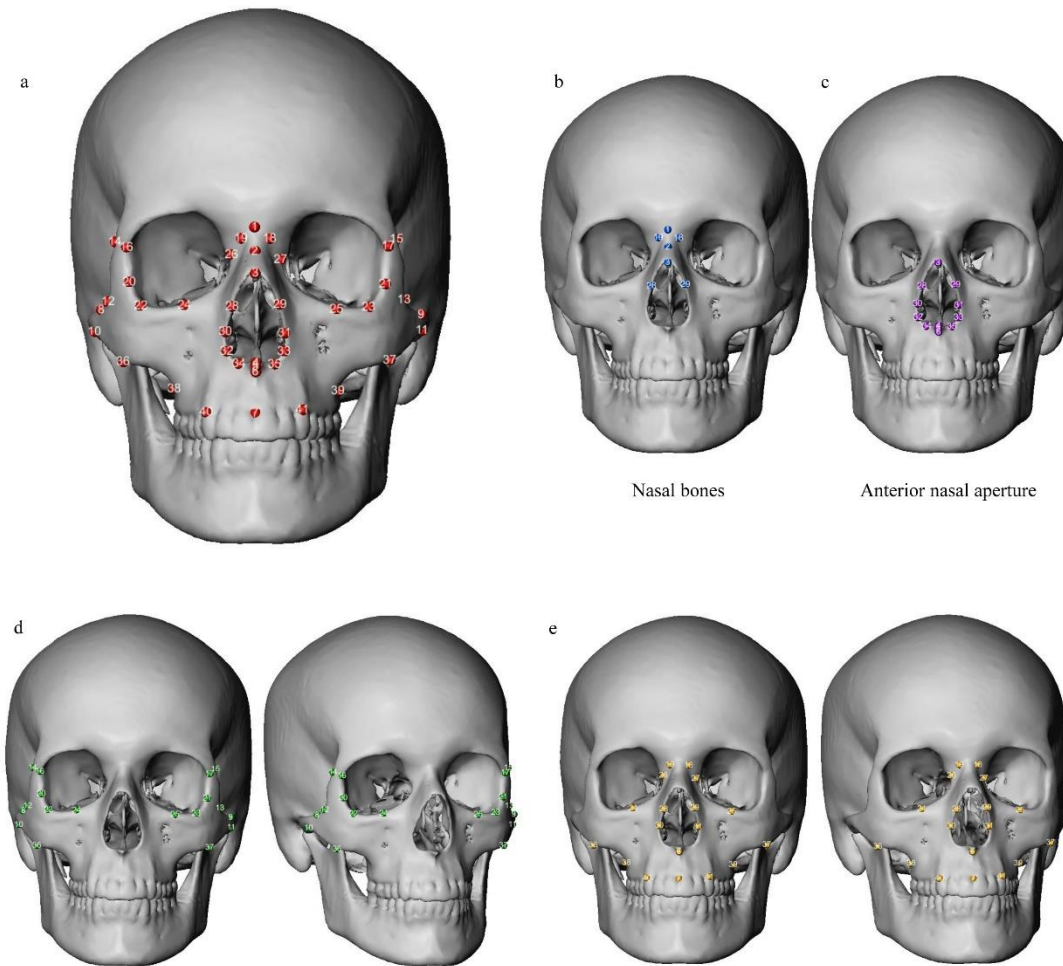


Figure 3.3. Landmarks placed on the hard-tissue region of interest. Landmarks placed on the hard-tissue region of interest.

a) Frontal view of the mid-facial hard-tissue region of interest. b) nasal bones; c) anterior nasal aperture; d) zygomatic bones; e): maxillary bones.

3.3.5.1.2. Capulometric landmarks

The soft-tissue region of interest was delimited by the surface anatomy as related to the hard-tissue (Figure 2.4), including mainly the nares (Figure 2.4. b) and the external nose (Figure 2.4 c, d). On the soft-tissue, 21 capulometric landmarks were recorded: eight bilateral pairs and five median landmarks (Table 3.3).

The procedure of automatic placement of discrete landmarks was executed as follows: the landmarks of interest were indicated once on the template, then projected onto every subject's surface using the warping procedure explained before. As a by-product of the template generation process, every individual surface was 'templated': Every landmark placed on a template was associated with the anatomically corresponding point on the warped surface. The coordinates of the warped landmarks were then recorded and saved in an Excel file for further statistical analysis.

Table 3. 3. Capulometric landmarks used (Schlager, 2013; Guyomarch' *et al.*, 2014; Buikstra & Ubelaker, 1994; Caple & Stephan, 2016).

Capulometric	Landmarks	Abbreviation	Nature	Definition
1	Pronasale	prn'	Median	The most anteriorly protruded point of the apex nasi. In the case of a bifid nose, the more protruding tip is chosen.
2	Nasale inferius	ni'	Median	Most inferior point of the apex nasi. Not locatable on upturned noses.
3	Columella	c'	Median	Midpoint of the nasal columella crest, intersecting a line between the two cs' points.
4	Subnasale	sn'	Median	Median point at the junction between the lower border of the nasal septum and the philtrum area.
5	Sellion	se'	Median	Deepest midline point of the nasofrontal angle; not a substitute for n'.
6/7	External alar curvature	eac	Bilateral	Most anterior point of the nasal wing at the maximum of curvature.
8/9	Superior alar curvature	sac	Bilateral	Most superior point of the nasal wing.
10/11	Alagenion	ag	Bilateral	Most posterior point of the nasal wing.
12/13	Alare	al'	Bilateral	The most lateral point on the nasal ala.
14/15	Alar curvature point	ac'	Bilateral	The most posterolateral point of the curvature of the base line of each nasal ala.
16/17	Mid-nostril	mn	Bilateral	Midpoint of maximal nostril width - projected on the transition nostril/philtrum.
18/19	Mid-columella	mc'	Bilateral	Midpoint of the nasal columella crest on either side, where the columella thickness is measured (equivalent to Subnasale).
20/21	Nasal-depth	nd	Bilateral	Most medial point of the transition nose/eye.

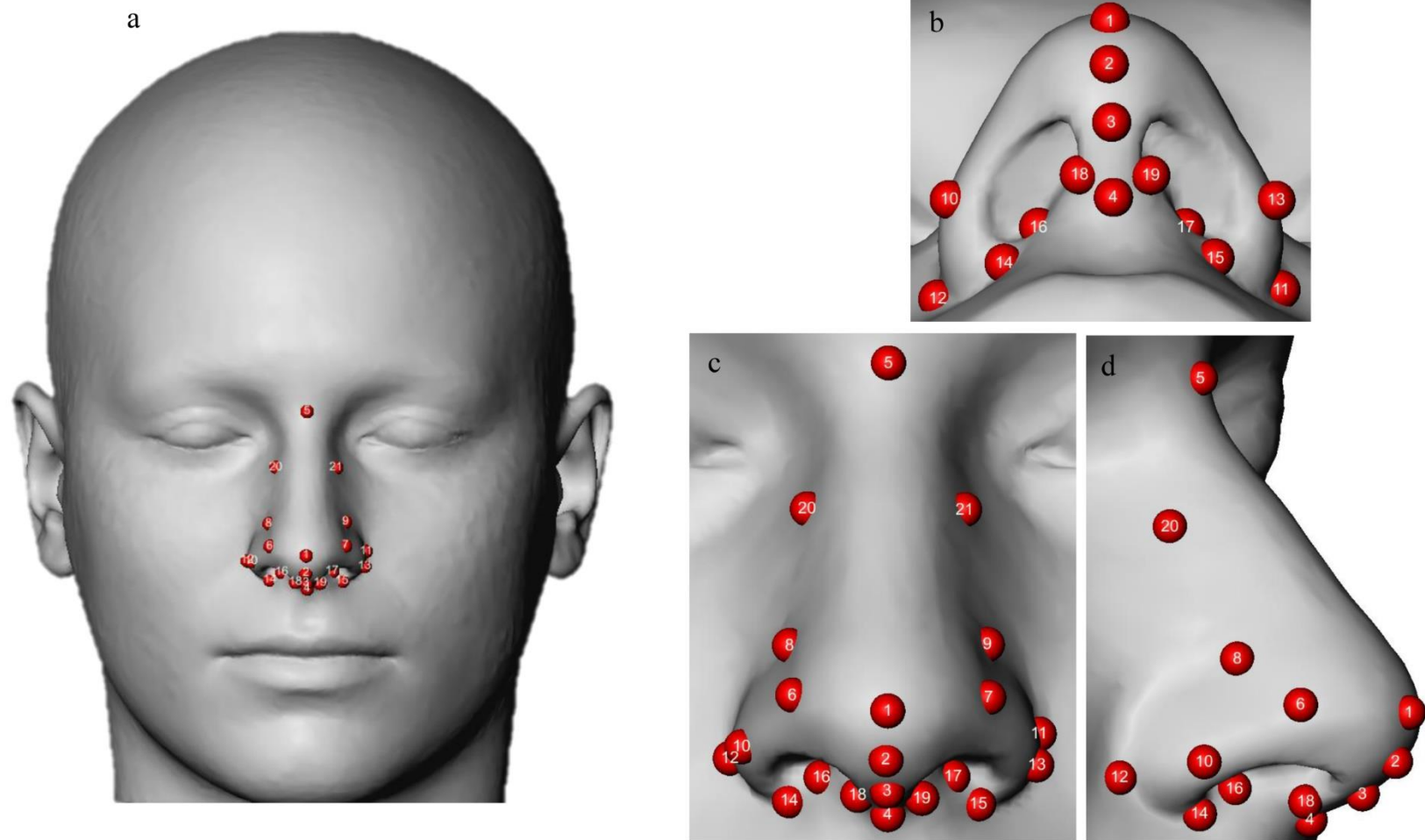


Figure 3. 4. Soft-tissue region of interest. a) frontal view of the soft-tissue region of interest; b) inferior view of the nose; c) anterior view of the nose; d) lateral view of the nose.

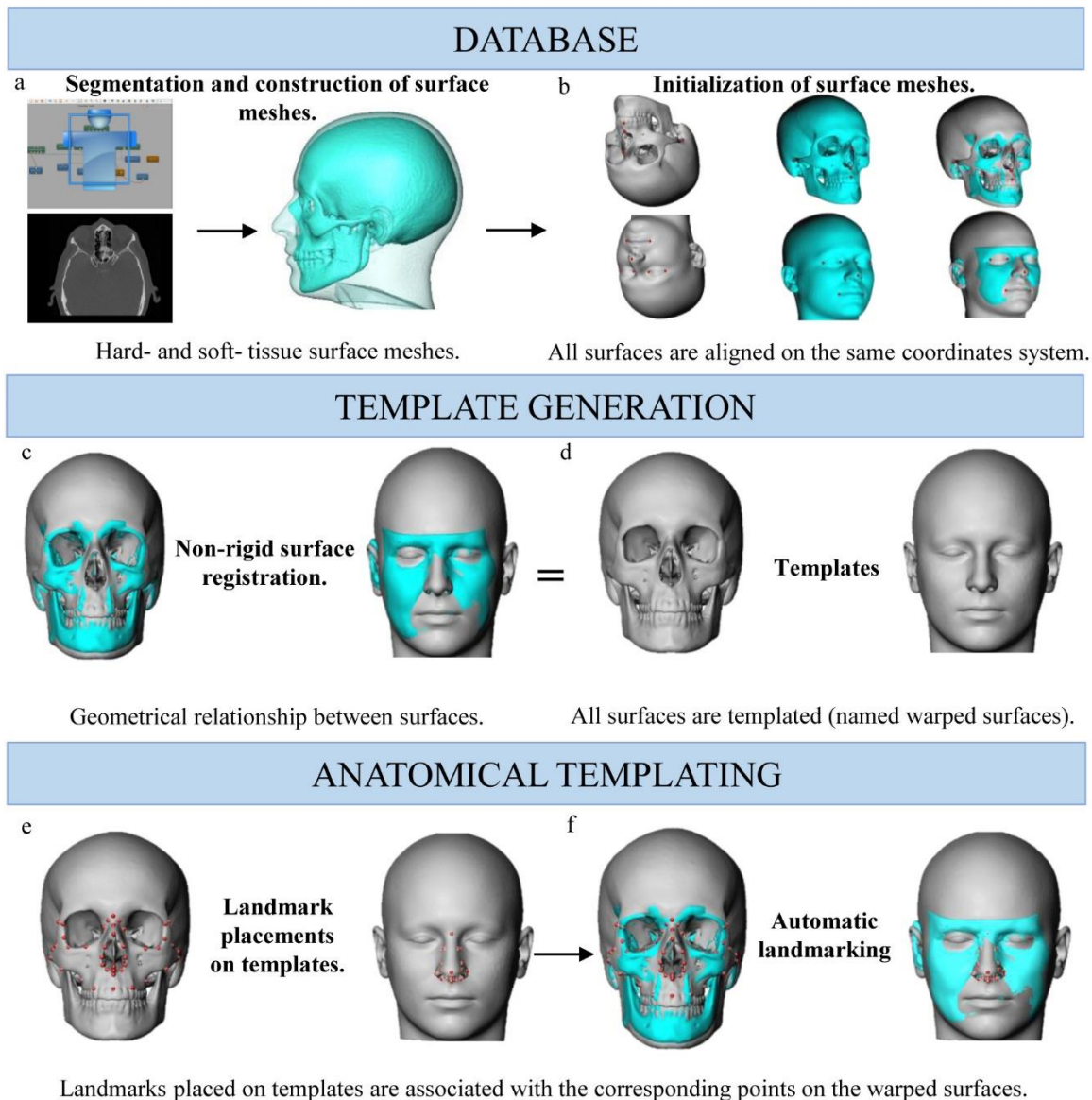


Figure 3. 5. Workflow of the automatic landmarking procedure.

3.4. Statistical analysis

All statistical analysis performed in this thesis (nasal complex shape variation, statistical modelling and cross-validation testing) are detailed in this section.

3.4.1. Study on nasal complex shape variation

In order to build statistical models for estimating nasal shape, an evaluation and a quantification of shape differences attributed to known factors (ancestry, sex, size and age) and covariates was performed both on hard- and soft-tissue shapes using GMM. In contrast to classical morphometric approaches based on linear distances and angles, geometric morphometric methods are based on the Cartesian coordinates of measurement points, the so-called landmarks. Since the geometry of the measured landmark configuration is preserved by the set of landmark coordinates, geometric morphometrics allow for effective visual representations of statistical results as actual shapes/forms or shape/form deformations (e.g. Bookstein, 1991; 1996a, 1996b; Rohlf & Marcus 1993; Zollikofer & Ponce de Leon, 2002; Adams *et al.*, 2004; Zelditch *et al.*, 2004; Slice, 2007; Mitteroecker & Gunz, 2009). In geometric morphometrics, the shape and the size of a biological structure are distinguished. The shape of an object is determined by the geometric properties that are invariant to translation, rotation and scaling. More precisely, the shape of an object is unaffected by changes in the position, the orientation and size of the object. The most common measure of size used in geometric morphometrics is centroid size (CS): the square root of the summed squared distance between all landmarks and their centroid. The centroid of a landmark configuration is the average (arithmetic mean) of all landmarks. Centroid size is a composite size measure based on all landmarks and is proportional to the square root of the summed squared interlandmark distances. It has been shown to be uncorrelated with shape for small isotropic variation at each landmark (Bookstein, 1991; Dryden & Mardia, 2016).

3.4.1.1. Generalised Procrustes Analysis

Preceding the statistical analysis, a Generalised Procrustes Analysis (GPA) (Goodall, 1991; Dryden & Mardia, 2016) was performed on the hard- and soft-tissue raw coordinates to obtain pose-invariant shape coordinates (Kendall DG, 1984; Klingenberg & McIntyre, 1998; Slice DE, 2001; Klingenberg *et al.*, 2002). The raw landmark coordinates do not only comprise information on size and shape of the landmark configurations, but also on their position and orientation. The most common approach for separating shape from size and the “nuisance parameters” position and orientation, is the Generalised Procrustes Analysis (Gower, 1975; Rohlf & Slice, 1990). This method comprises three steps: translating all landmark configurations to the same centroid, scaling all configurations to the same centroid size, and iteratively rotating all configurations until the summed squared distances between the landmarks and their corresponding sample average is a minimum. The coordinates of the resulting superimposed landmark configurations are called Procrustes shape coordinates as they only contain information about the shape of the configurations.

3.4.1.2. Principal Component Analysis

In this thesis, data reduction is achieved by Principal Component Analysis (PCA) to reduce data dimensionality and to create independent principal component (PC) scores that quantify the different shapes studied. Statistical testing was performed using the PC scores covering 95% of the sample’s overall variance of the sample. The principal component analysis (PCA) involves the examination of axes that reflect maximum variation and covariation. PCA transforms the data to a new coordinate system, such, that the greatest variance of the data lies on the first transformed new variable (the first principal component) and the second greatest variance on the second transformed variable. The orthogonal axes of the PCA summarize variation decreasing in order. Individual’s observation are plotted along axes. The score of a given observation on a given axis corresponds to the projection of the data on that axis. Examining variation on the first axes provides a way to reduce the variable space to dimensions that express most variation. Each axis corresponds to a linear combination of original variables. The first corresponds to the main direction of the variance covariance structure of individual observations.

3.4.1.3. Multivariate normality

In this study, multivariate normality testing was performed on the hard- and soft-tissue principal component scores distribution by interpreting Q-Q-plots (Scrucca, 2000), which allowed us to presume that the variables are distributed according to the distribution tested. The graphical output shows the actual values of squared Mahalanobis-distances plotted, versus those of an ideal multivariate normal distribution. The closer the values are to the diagonal line, the more probable is a multivariate normal distribution.

3.4.1.4 Analysis of covariation between nasal hard- and soft- tissue and its dependence on ancestry

The evaluation of covariation between the mid-facial hard-tissue elements (nasal bones and anterior nasal aperture; zygomatic (right and left); maxillary (right and left)) and the external soft-tissue of the nose was performed with Two Blocks Partial Least Squares (PLS) analyses. This function performs two-block partial least squares analysis to assess the degree of association between two blocks of Procrustes-aligned coordinates (or other variables) (Rohlf & Corti, 2000).

3.4.1.5. Quantification and visualisation of covariance between nasal complex shape and the covariates: population differences, sexual dimorphism and age effects

The quantification and the visualisation of covariance between nasal complex shape and the covariates: population differences, sexual dimorphism and age effects were performed on the complete sample (Figure 3.6), as well as on each ancestral groups separately (Figure 3.7). In this study, standard MANOVA, 50-50 MANOVA, permutation testing and discriminant function analysis were applied. Significance of population differences, sexual dimorphism and age effects were assessed using standard MANOVA, 50-50 MANOVA and permutation testing (all permutation tests were run with 10,000 rounds). Standard discriminant function analysis (DFA) was also applied for classification purposes. The classification accuracy was estimated by conducting a leaving-one-out cross-validation. Multivariate analysis of variance (MANOVA) is an extension of the univariate analysis of variance (ANOVA). In an ANOVA, statistical differences on one continuous dependent variable by an independent grouping

variable are examined. The MANOVA extends this analysis by taking into account multiple continuous dependent variables and bundles them together into a weighted linear combination or composite variable. The MANOVA will indicate whether or not the newly created combination differs between the different groups, or levels, of the independent variable. In this way, the MANOVA essentially tests whether or not the independent grouping variable simultaneously explains a statistically significant amount of variance in the dependent variable. We applied MANOVA using the R-packages *geomorph* (Adams *et al.*, 2018). The 50-50 MANOVA (Langsrud, 2002; Langsrud *et al.*, 2007) is a modified version of a MANOVA, designed for many (potentially correlated) response variables. We applied 50-50 MANOVA using the R-packages *ffmanova* (Langsrud & Mevik, 2012).

Permutation tests are based on resampling. A given factor (e.g. ancestry) is calculated and compared to values gained from the same sample where group membership is randomly reassigned repeatedly. As a result, the number of resampled values exceeding the “true” one is divided by the number of permutation rounds. If the value falls within the range of random grouping, the null hypothesis cannot be rejected because the measured value is not exceeding the one generated by chance (Schlager, 2013; Schlager, 2017). We applied permutation testing using the R-packages *Morpho* (Schlager, 2017). Discriminant function analysis finds linear combinations of variables that describe intergroup differences. These combinations define linear discriminant functions. The linear discriminant coefficients are defined from the non-null eigenvectors of the between group variance-covariance “scaled” by the within-group variance-covariance. Discriminant function analysis was performed using the R-packages *Morpho* (Schlager, 2017).

3.4.1.6. Allometry

Allometry is defined as shape change that can be expressed as a function of size (Bookstein, 1991; Gonzales *et al.*, 2011). In this study, allometric effects were considered when dealing with shape differences associated with sex, due to the effect of sexual dimorphism on size (Rosas & Bastir, 2002; Kimmerle & Ross, 2008; Schlager, 2013). For assessing the allometry involved, linear models (hard- and soft-tissue shape versus the factors: sex and centroid size) were calculated using the PCs from the sexual dimorphism analysis. The

significance of each variable was tested using MANCOVA (using Pillai trace) and 50-50 MANOVA.

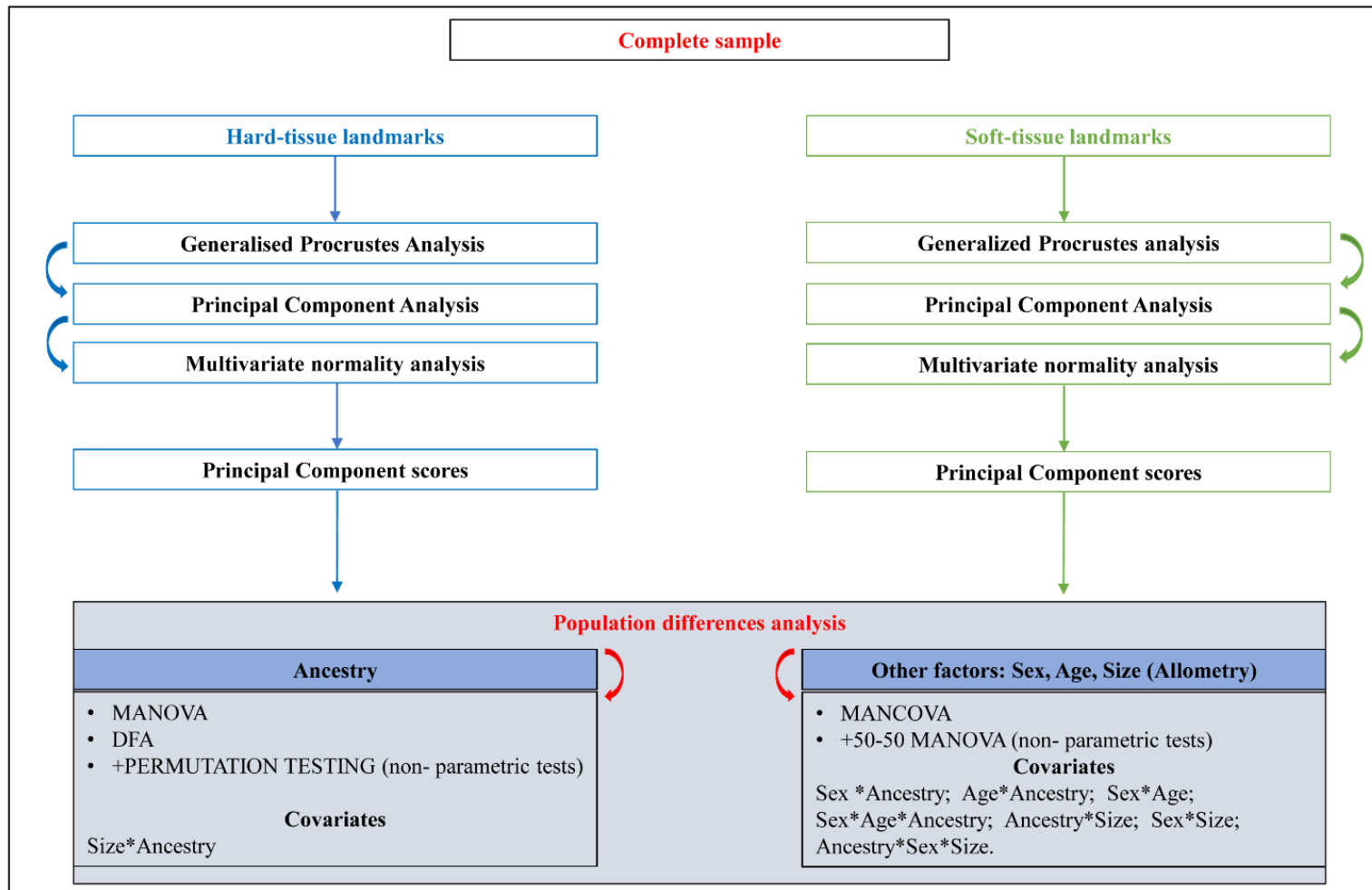


Figure 3. 6. Shape variation analysis on the complete sample.

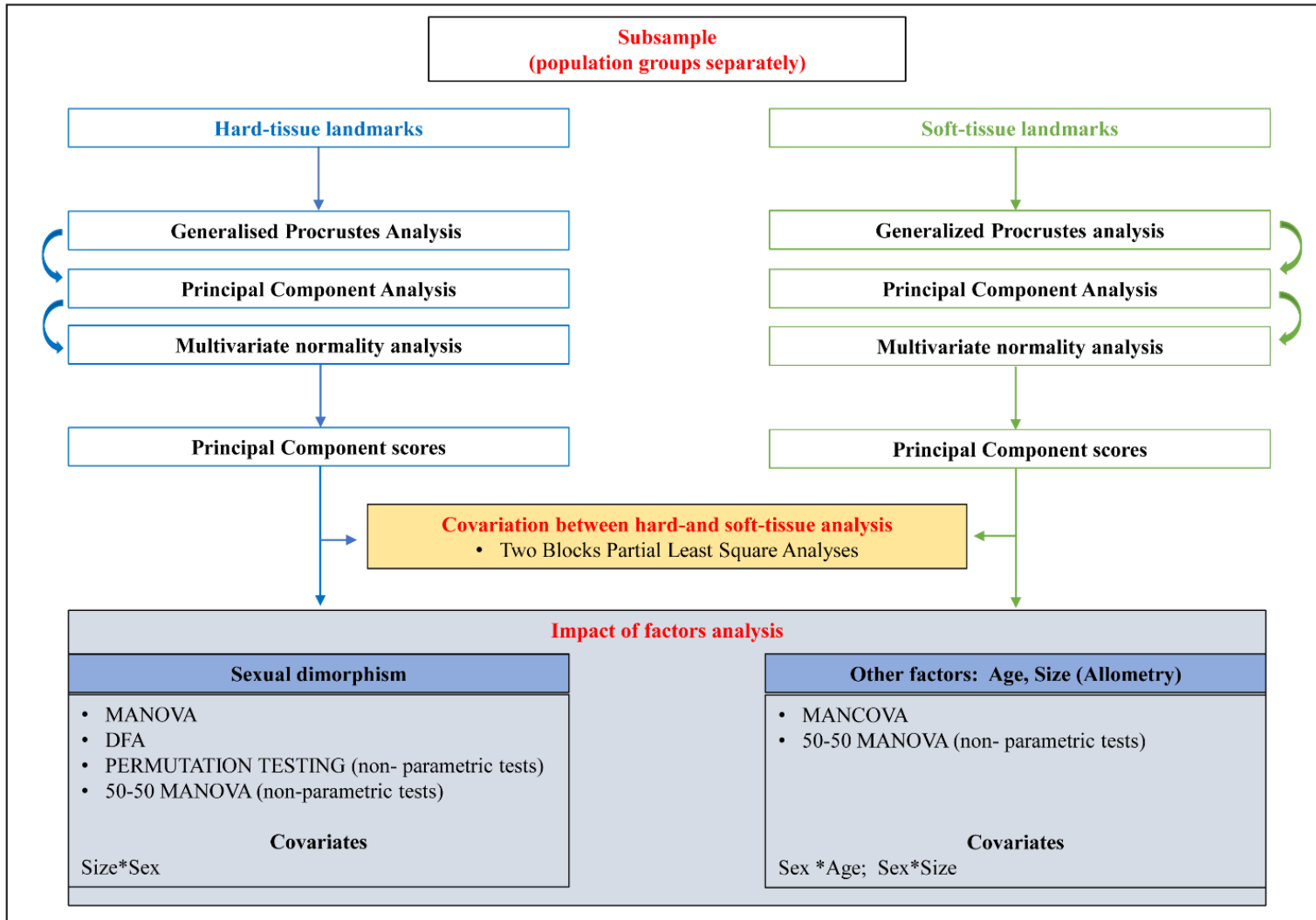


Figure 3. 7. Shape variation analysis on subsamples (ancestral groups separately).

3.4.2. Statistical modelling

In the previous section, the influence of known factors (ancestry, age, sex, allometry) on shape using geometric morphometric methods, were analysed. Two separate shape spaces, one for each type of tissue (hard- and soft-tissue) were used. In order to create a statistical model for predicting nasal soft-tissue shape from information obtained from the underlying hard-tissue configuration, both hard- and soft-tissues needed to be scaled, translated, rotated and predicted within the same space, using only the initial hard-tissue information. The adapted Generalised Procrustes Analysis used in this study was firstly introduced by Schlager in 2013 (Schlager, 2013).

Firstly, a Procrustes fit for hard-tissue configurations was calculated and the complete (soft- and hard-tissue) landmark datasets were scaled, translated and rotated onto the hard-tissue configurations by using corresponding landmarks. In a last step, the data were split up into soft-tissue and hard-tissue configuration again, allowing for a predictor hard-tissue shape and a predicted soft-tissue shape to be already aligned correctly, as they both are in the same coordinate system.

Projection onto Latent Structures Regressions (PLSR) was used in this study in order to extract information for the soft-tissue prediction and to select those linear combinations relevant for explaining the predictor variables maximising covariation between predictors (hard-tissue shape and additional factors) and response (soft-tissue shape) (Abdi, 2010, Martens & Naes, 1992, Wold *et al.*, 2001). PLSR is a method for relating two data matrices, X and Y, by a linear multivariate model. In addition, PLSR goes beyond traditional regression as it also models the structure of X and Y and analyse data with many, noisy, collinear, and even incomplete variables (Wold *et al.*, 2001). Moreover, PLSR has the property of improving the precision of the model parameters improves with the increasing number of relevant variables and observations.

In order to extract information for the soft-tissue prediction, many types of regression algorithm exist such as Principal Component Regression and Projection onto Latent Structures Regressions (PLSR). Schlager (Schlager, 2013) demonstrated that these both types of regression algorithms yielded very similar results in terms of nose prediction accuracies. It has

been emphasised that, when applying PLSR, the number of latent variables must be carefully selected due to the greater risk of overfitting, especially when sample sizes are small. Given the data analysed in this thesis, the PLSR could be safely used. The prediction accuracy could be significantly improved by adding additional information such as ancestry, sex and age as predictors.

3.4.3. Cross-validation testing

To determine the accuracy of the estimated soft-tissue nose, it has to be evaluated in terms of metric deviations. This is necessary to allow comparison with other research results. The validation of prediction models was performed using cross validation testing with the calculation of the Mean Squared Error (MSE) using leave-one-out cross-validation (LOOCV). The MSE is estimated from the training data and comparing it to the MSE of the predicted data (RMSE) (Mevik & Cederkvist (2004)). The impact of additional information such as ancestry, sex and age was evaluated by adding them to the models as predictors and comparing the resulting MSE/MSEP. The Mean Euclidean Distance (MED) per landmarks over all subjects and the MED over all landmarks and all subjects were also calculated. In addition, in order to determine if the covariation is significantly population-dependent, the soft-tissue shape of all specimens from one ancestral group was estimated by applying a regression model fit to the data of the other ancestral group.

The workflow of the statistical modelling procedure performed in this thesis is illustrated in Figure 3.8.

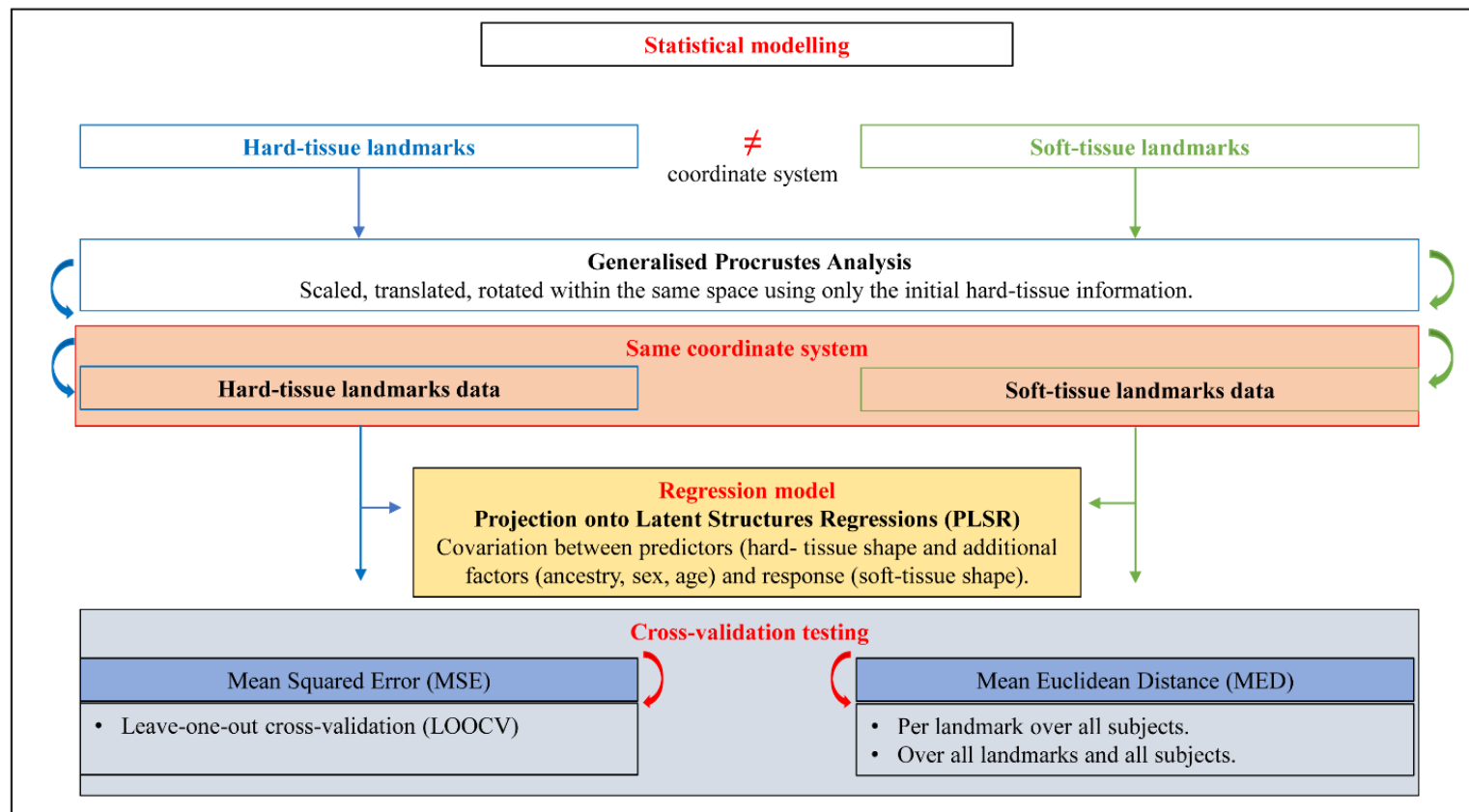


Figure 3. 8. Statistical modelling and cross-validation testing analysis.

3.5. Software

The software programs used for the placement and processing of landmarks are MeVisLab 2.7.1 and R studio. MeVisLab 2.7.1 is an open source software including a modular framework for image processing research and development with a special focus on medical imaging. It allows fast integration and testing of new algorithms and the development of clinical application prototypes. MeVisLab includes advanced software modules for segmentation, registration, volumetric, as well as quantitative morphological and functional analysis.

3.5.1. Data processing

The results of segmentation are called hard- and soft-tissue surfaces or hard- and -soft-tissue Winged Edge Mesh (WEM). The segmentation of different elements (hard- and soft-tissue WEM surfaces) were obtained using WEMIsoSurface module which generates an iso-surface as a WEM in MeVisLab 2.7.1 (Figure 3.9). Some 3D elements such as the spine, artefacts or structure of the CBCT-scanner present on 3D WEM surfaces, were removed using the WEMInteract module which removes or selects parts of the WEM.

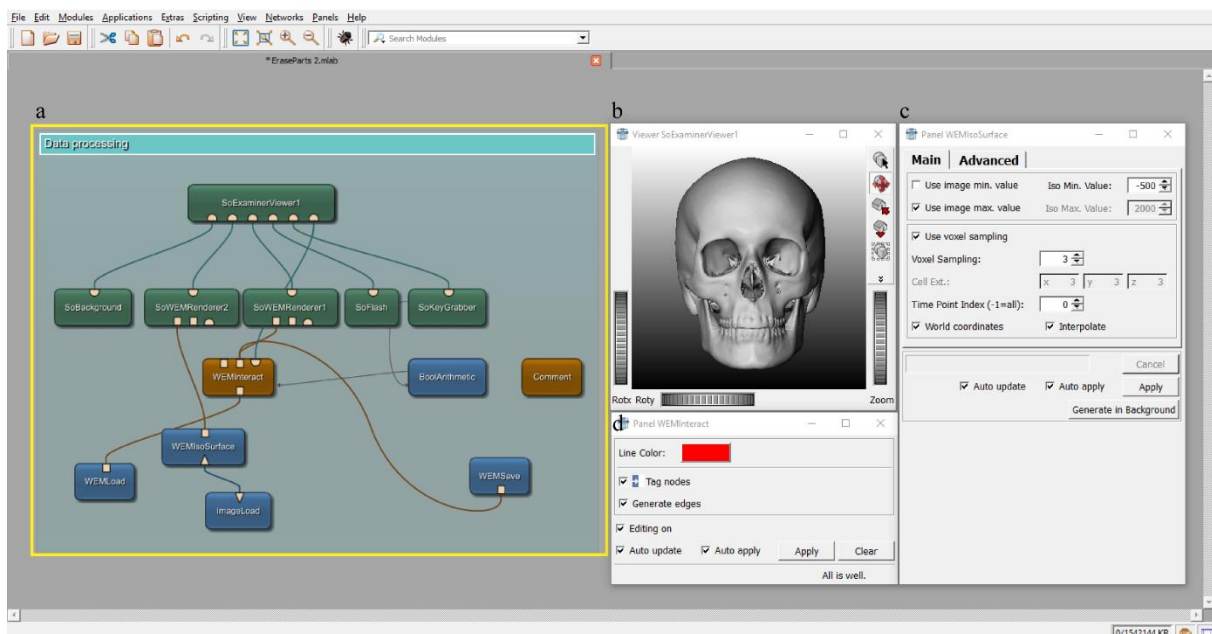


Figure 3. 9. Example of hard-tissue data processing in MeVisLab 2.7.1. a) All modules used; b) Viewer SoExaminerViewer module for visualisation of the segmentation process; c) WEMIsoSurface module for the determination of threshold values between segmented components.

3.5.2. Initialisation

The initialisation procedure was performed using the WEMMarkerInitialization module in MeVisLab 2.7.1 which rotates and translates the surfaces to bring them into the proximity of each other (Figure 3.10).

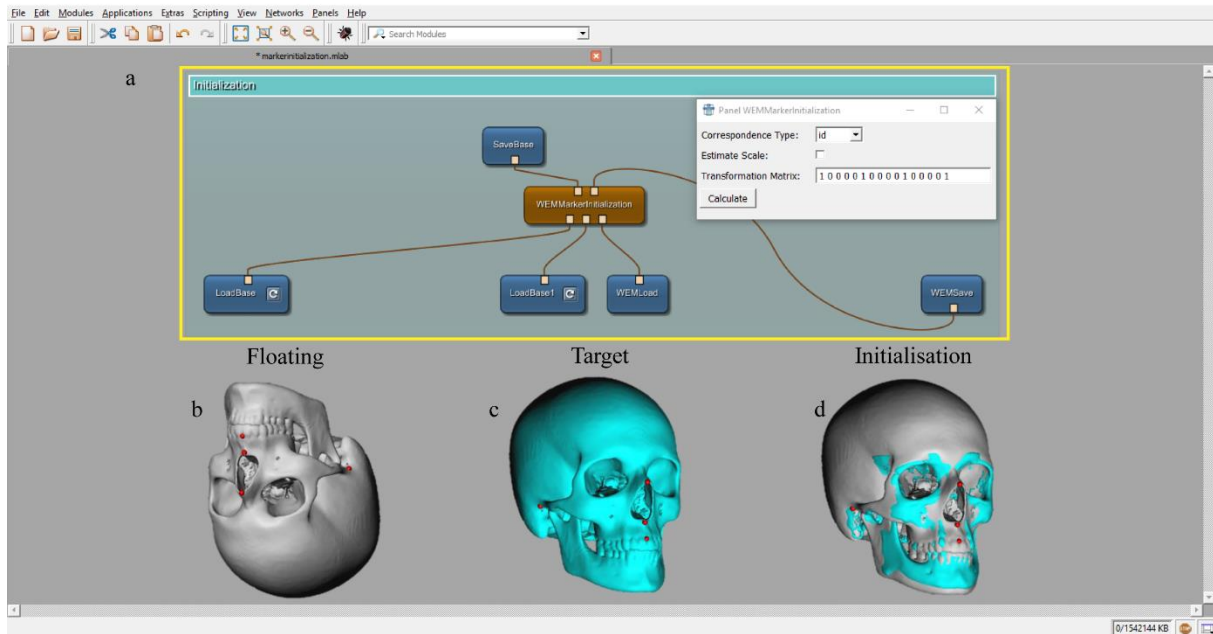


Figure 3. 10. Example of hard-tissue initialization in MeVisLab 2.7.1. a) All modules used; b) Floating. c) Target; d) Initialisation.

3.5.3. Surface registration process

The non-rigid surface registration process was applied using a module in MeVisLab 2.7.1 by Prof. Vandermeulen (Figure 3.11).

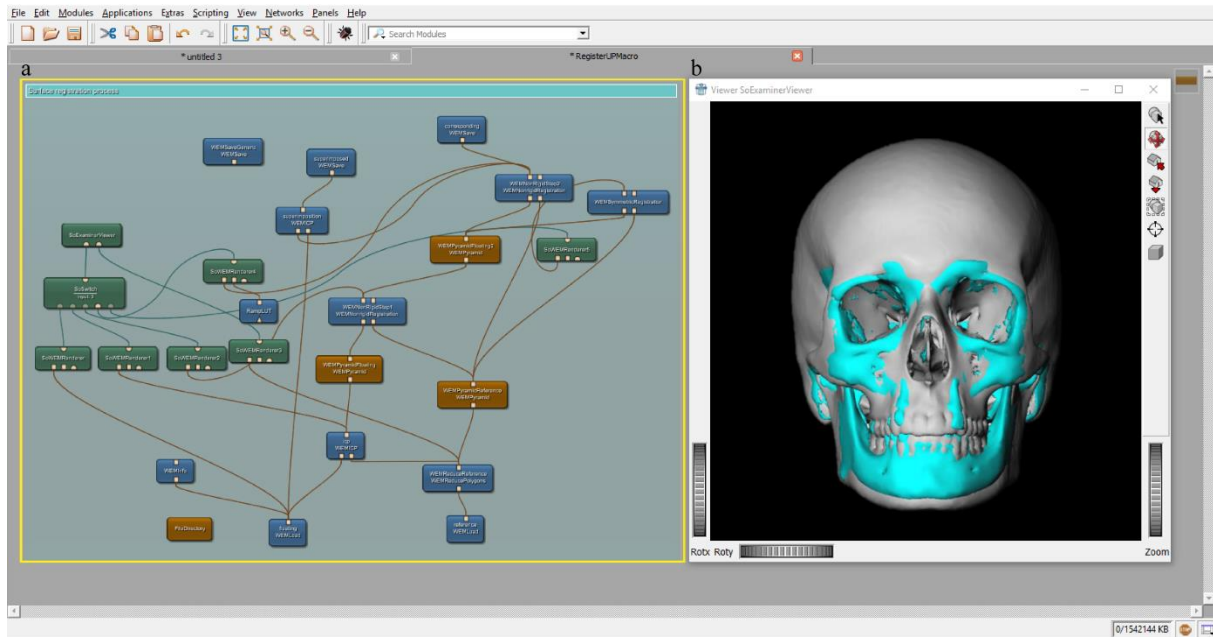


Figure 3. 11. Example of the hard-tissue registration process. a) All modules used; b) Visualisation of the hard-tissue registration.

Chapter 4

VALIDATION OF THE AUTOMATIC LANDMARKING

4.1. Introduction

The purpose of this chapter is to demonstrate the validation of the automatic landmarking procedure by comparing the intra-observer errors (INTRA-OE) and inter-observer errors (INTER-OE) between automatic and manual landmarking. This research provides a validation of the precision of the automatic placement of landmarks and demonstrates its utilization as a convenient prerequisite for geometric morphometrics, based on shape analysis of the nasal complex.

Automatic landmarking as a convenient prerequisite for geometric morphometrics. Validation on cone beam computed tomography (CBCT)-based shape analysis of the nasal complex.

AF RIDEL, F DEMETER, M GALLAND, EN L'ABBÉ, D VANDERMEULEN, AC OETTLÉ

Manuscript submitted for publication to Forensic Science International.

Abstract

Manual landmarking is used in several manual and semi-automated prediction guidelines for approximation of the nose. The manual placement of landmarks may, however, render the analysis less repeatable due to observer subjectivity and, consequently, have an impact on the accuracy of the human facial approximation. In order to address this subjectivity and thereby improve facial approximations, we are developing an automated three-dimensional (3D) method based on an automatic dense landmarking procedure using non-rigid surface registration. The aim of this study was to validate the automatic landmarking method by comparing the intra-observer errors (INTRA-OE) and inter-observer errors (INTER-OE) between automatic and manual landmarking.

Ten cone beam computed tomography (CBCT) scans of adult South Africans were selected from the Oral and Dental Hospital, University of Pretoria, South Africa. INTRA-OE and INTER-OE were analyzed by registering 41 craniometric landmarks from 10 hard-tissue surfaces and 21 capulometric landmarks from 10 soft-tissue surfaces of the same individuals. Absolute precision of the landmark positioning (both on the samples as well as the template) was assessed by calculating the ME for each landmark over different observers. Systematic error (bias) and relative random error (precision) was further quantified through repeated measures ANOVA (ANOVA-RM).

The analysis showed that the random component of the measurement errors in landmark positioning between the automatic observations were on average on par with the manual observations, except for the soft-tissue landmarks where automatic landmarking showed lower measurement error (ME) compared to manual landmarking. No bias was observed within the craniometric landmarking methods, but some bias was observed for capulometric landmarking.

In conclusion, this research provides a first validation of the precision and accuracy of the automatic placement of landmarks on 3D hard- and soft-tissue surfaces and demonstrates its utilization as a convenient prerequisite for geometric morphometrics based shape analysis of the nasal complex.

Keywords: Non-rigid surface registration; automatic craniometric landmarking; automatic capulometric landmarking; manual landmarking; intra- and inter- observer errors.

Introduction

Craniofacial reconstruction (CFR) is based on the assumed morphological relationship between the soft-tissue envelope and the underlying skull substrate. Traditional CFR methods are based on 2D or 3D manual reconstruction by physically modelling a face on a skull replica with clay or plasticine [1-6]. In the literature, these traditional reconstructions have been commonly classified as “Russian”, “American” or “Combination” methods [7]. It was recognized by the scientific community in the field of CFR that manual reconstruction methods require a high degree of anatomical and sculptural expertise and, as a result, remain difficult and subjective [8-13]. The interpretations of two different artists can result in the creation of two substantially different faces from the same skull [12]. Therefore, traditional manual techniques are unsuitable for application to the judicial system, which requires precision, reliability and knowledge of possible quantization [12].

Recent developments in digital imaging techniques have resulted in the collection of large databases of 3D representations of hard- and soft-tissues of the face. Researchers in the field of CFR utilize these sources of information to improve objectivity in the reconstruction process [14-57]. In CFR, all computer-assisted methods share the foundational premise that information about the complete skull versus information of the skin is used for mapping a template face onto a dry skull [14-59]. Recently, [Tilotta and colleagues](#) [54], [Schlager](#) [55] and [Guyomarc’h](#), [13] developed computer-assisted methods for the prediction of the structure of the external surface of the nose based on conventional computer tomography (CT) scans. Compared with manual methods, automation of facial approximation offers increased objectivity and the possibility of standardization [13]. However, the use of conventional CT scans as initial references may be influenced by supination effects on the face due to the horizontal position of the patient during scanning [60, 61]. Moreover, the slice thickness, which generally ranges from 0.6 mm to 1.5 mm [13, 55], induces errors of at least the same order of magnitude in the manual landmark placement on the 3D hard- and soft-tissue surfaces.

Previously described methods for approximation of the nose involve manual placements of landmarks for the definition of the region of interest [13, 55]. Following the results of these methods, it seems that the nasal depth, the external and superior alar curvature, the alare [13, 55] and the submaxillare curvature [13] landmark positions are prone to inter- and intra-observer errors. Manual placement of landmarks is extremely time consuming on large 3D surface

samples and may induce important observer subjectivity and errors. Errors in manual landmarking are determined by factors such as the inherent variability among individuals in the sample and the metric quality of the instruments used [62-65]. As a result, manual landmarking may render the analysis less repeatable and accurate for the facial approximation process. In the field of craniofacial reconstruction, the scientific literature concerning the utilization of automatic landmarking on 3D surfaces for the approximation of facial features (e.g. nose, eyes, mouth and ears), or the complete face, is limited. Limited research has been published regarding facial recognition implications for 2D [66-70] and 3D [71] cephalometric landmarks, whereas no research has been done on the automatic landmarking of craniometric and cephalometric landmarks on hard- and soft-tissue 3D surfaces.

The main critiques of current facial approximation techniques are the inherent subjectivity in manual methods, the references used and the lack of standardization, which limit the accuracy of the estimation [8-13]. In order to improve the accuracy of facial approximation, we are developing an automated three-dimensional (3D) method based on an automatic dense landmarking procedure. Moreover, instead of using conventional CT for the acquisition and extraction of the relevant anatomical structures, we used cone beam CT (CBCT). During a CBCT scan, the patient is in a vertical position and the scanner rotates around the head, capturing images using a cone-shaped X-ray beam. The advantages of CBCT compared to CT include lower radiation dose, lower cost and higher spatial resolution (0.1 mm to 0.4 mm) for the placement of 3D landmarks [72]. Furthermore, the patient's upright position during acquisition minimizes gravitational effects on soft-tissue deformations. The aim of this study was to evaluate the measurement error (ME) of the automatic versus the manual landmarking method, defined as the difference between repeated measurements of the same variable made by the same (i.e., INTRA-OE) or different observers (i.e., INTER-OE) [73]. A further aim of this study was to demonstrate the utilization of automatic landmarking as a convenient prerequisite for geometric morphometrics, based on shape analysis of the nasal complex.

Materials & Methods

Cone beam computer tomography scans of ten adult South Africans were selected from the Oral and Dental Hospital, University of Pretoria, South Africa. Cone beam computer tomography scans were obtained using a CBCT scanner (Planmeca ProMax ® 3D, Pretoria, South Africa) with the following properties: 90 kV, 11.2 mA, voxel size of 0.4 mm and field of view of 230 x 260 mm. In order to standardize the acquisition, the subjects were scanned in a seated position with their eyes closed and with a relaxed facial expression. Patients were excluded if they presented with any condition that could affect the morphology of the face (e.g. orthodontic treatment, pathological conditions, facial asymmetry, or any facial interventional reconstructive surgery). This research project was approved by the Main Research Ethics Committee of the Faculty of Health Sciences, University of Pretoria, South Africa (Ethics Reference No: 301/2016).

CBCT scans in DICOM format were imported into MeVisLab © v. 2.7.1 software to extract volume data and create 3D images. The segmentation of different elements (hard- and soft-tissue) were obtained by finding the threshold values between segmented components according to the “Half Maximum Height” (HMH) quantitative iterative thresholding method [74]. Threshold values for hard-tissue varied between 1200-1250 and for the soft-tissue, between 400-450. In this study, the facial skeleton will be referred to as the hard-tissue, and the external structure of the nose as the soft-tissue.

Following facial approximation literature [13, 55], and in order to conserve homology and comparability between studies, classic craniometric and capulometric landmarks (type I, II, and III [13, 55, 75, 76] were used. INTRA-OE and INTER-OE were analyzed by registering craniometric landmarks from ten hard-tissue surfaces and capulometric landmarks from ten soft-tissue surfaces of the same individuals. A total of 62 landmarks, described in Table 1 and illustrated in Figure 1 were used.

Table 1. Definition, abbreviation and nature of landmarks used. [15, 16, 25, 26].

	Landmarks	Abbreviation	Nature	Definition
Cranio-metric	1 Nasion	n	Median	Intersection of the nasofrontal sutures in the median plane.
	2 Mid-nasal	mn	Median	Midline point on the internasal suture midway between nasion and rhinion.
	3 Rhinion	rhi	Median	Most rostral (end) point on the internasal suture. Cannot be determined accurately if nasal bones are broken distally.
	4 Nasospinale	ns	Median	The point where a line drawn between the inferior most points of the nasal aperture crosses the median plane. Note that this point is not necessarily at the tip of the nasal spine.
	5 Subspinale b	ss	Median	The deepest point seen in the profile view below the anterior nasal spine (orthodontic point A).
	6 Akanthion	ak	Median	Most anterior midline point of the nasal spine.
	7 Prosthion	pr	Median	Median point between the central incisors on the anterior most margin of the maxillary alveolar rim.
	8/9 Zygotemporale superior	zts	Bilateral	Most superior point of the zygomatico-temporal suture.
	10/11 Zygotemporale inferior	zti	Bilateral	Most inferior point of the zygomatico-temporal suture.
	12/13 Jugale	ju	Bilateral	Vertex of the posterior zygomatic angle, between the vertical edge and horizontal part of the zygomatic arch.
	14/15 Frontomalare temporale	fnt	Bilateral	Most lateral part of the zygomaticofrontal suture.
	16/17 Frontomalare orbitale	fmo	Bilateral	Point on the orbital rim marked by the zygomaticofrontal suture.
	18/19 Nasomaxillofrontale	nmf	Bilateral	Point at the intersection of the frontal, maxillary, and nasal bones.
	20/21 Ectoconchion	ec	Bilateral	Lateral point on the orbit at a line that bisects the orbit transversely.
	22/23 Orbitale	or	Bilateral	Most inferior point on the inferior orbital rim. Usually falls along the lateral half of the orbital margin.
	24/25 Zygoorbitale	zo	Bilateral	Intersection of the orbital margin and the zygomaticomaxillary suture.
	26/27 Maxillofrontale	mf	Bilateral	Intersection of the anterior lacrimal crest with the frontomaxillary suture.
	28/29 Nasomaxillare	nm	Bilateral	Most inferior point of the nasomaxillary suture on the nasal aperture.
	30/31 Alare	al	Bilateral	Instrumentally determined as the most lateral point on the nasal aperture in a transverse plan.
	32/33 Piriform curvature	cp	Bilateral	Most infero-lateral point of the piriform aperture.
	34/35 Nariale	na	Bilateral	Most inferior point of the piriform aperture.
	36/37 Zygomaxillare	zm	Bilateral	Most inferior point on the zygomaticomaxillary suture.
	38/39 Submaxillare curvature	csm	Bilateral	Most supero-medial point on the maxillary inflexion between the zygomaxillare and the ectomolar.
	40/41 Supra canine	sc	Bilateral	Point on the superior alveolar ridge superior to the crown of the maxillary canine.
Capulometric	1 Pronasale	prn'	Median	The most anteriorly protruded point of the apex nasi. In the case of a bifid nose, the more protruding tip is chosen.
	2 Nasale inferius	ni'	Median	Most inferior point of the apex nasi. Not locatable on upturned noses.
	3 Columella	c'	Median	Midpoint of the nasal columella crest, intersecting a line between the two cs' points.
	4 Subnasale	sn'	Median	Median point at the junction between the lower border of the nasal septum and the philtrum area.
	5/6 External alar curvature	eac	Bilateral	Most anterior point of the nasal wing at the maximum of curvature.
	7/8 Superior alar curvature	sac	Bilateral	Most superior point of the nasal wing.
	9/10 Alagenion	ag	Bilateral	Most posterior point of the nasal wing.
	11/12 Alare	al'	Bilateral	The most lateral point on the nasal ala.
	13/14 Alar curvature point	ac'	Bilateral	The most posterolateral point of the curvature of the base line of each nasal ala.
	15/16 Mid-columella	mc'	Bilateral	Midpoint of the nasal columella crest on either side, where the columella thickness is measured (equivalent to Subnasale').
	17/18 Nasal-depth	nd	Bilateral	Most medial point of the transition nose/eye.
	19 Sellion	se'	Median	Deepest midline point of the nasofrontal angle; not a substitute for n'.
	20/21 Mid-nostril	mn	Bilateral	midpoint of maximal nostril width - projected on the transition nostril/philtrum.

Forty-one craniometric landmarks were recorded on the hard-tissue: 17 bilateral pairs and seven median landmarks. On the soft-tissue, 21 capulometric landmarks were recorded: eight bilateral pairs and five median landmarks. The landmarks selected were distributed on the facial skeleton and the external nose, creating a hard- and soft-tissue region of interest. The hard-tissue region of interest was delimited by the facial skeleton comprising the nasal bones (Figure 1.a), the nasal aperture (Figure 1.b), the maxillae (Figure 1.c) and the zygomatic bones (Fig 1.d). The soft-tissue region of interest was delimited by the surface anatomy as related to the hard-tissue, including mainly the external nose (Figure 1. e, g) and the nares (Figure 1. f, h).

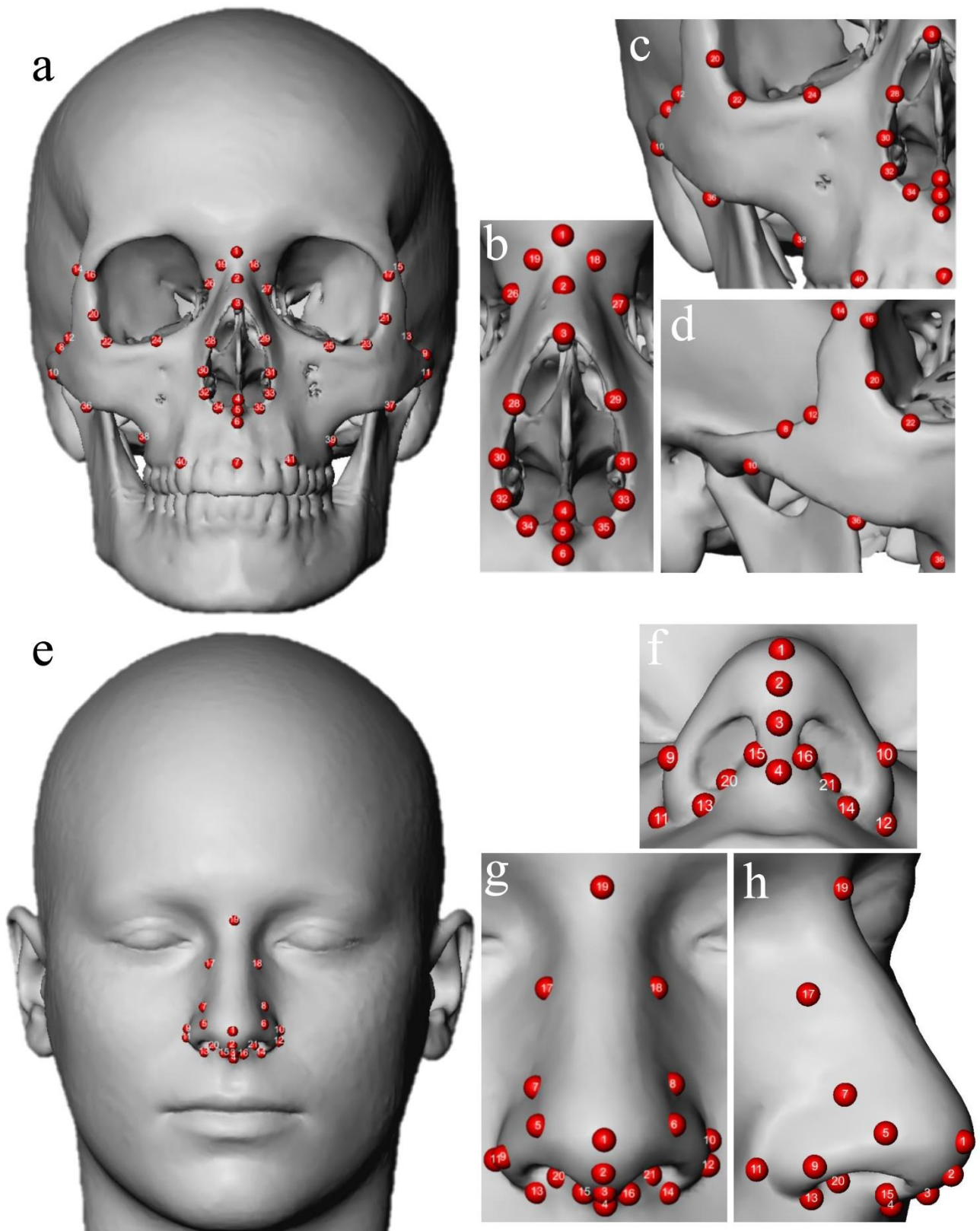


Figure 1. Landmarks placed on the hard- and soft-tissue region of interest.

a: Frontal view of the hard-tissue region of interest; b: nasal superior and inferior; c: maxillary; d: zygomatic; e: frontal view of the soft-tissue region of interest; f: inferior view of the nose; g: anterior view of the nose; h: lateral view of the nose (cf. Table 1).

Manual landmarking

The manual placement of landmarks was performed by indicating the 41 craniometric landmarks on the ten hard-tissue surfaces and the 21 capulometric landmarks on the ten soft-tissue surfaces. For the INTRA-OE, the manual placement of landmarks was performed twice by the same observer (noted AR1m and AR2m) on every subject, with an interval of two weeks. For the INTER-OE, the manual landmarking was performed twice by two different observers (noted AR1m and MGm). The manual placement was performed using MeVisLab software and the 3D coordinates of landmark points were recorded and saved in an Excel file for further analysis.

Automatic landmarking

The automatic landmarking method proposed here is adapted from the procedure introduced by Claes et al. [33-35]. The basic concept involves a reference template of the anatomical surface of interest, containing a dense set of landmarks. These landmarks are a dense equivalent of traditional sparse, discrete, well-defined, anatomical landmarks. Reference hard- and soft-tissue templates (Figure 2.d) are created using a non-rigid- surfaces registration process (Figure 2.c). Prior to registration, all the surfaces are repositioned into the same coordinate system using an initialisation mesh procedures (Figure 2.b). The initialization is performed manually with indicating a set of landmarks on floating and target surfaces in order to interactively rotate and translate the surfaces so as to bring them into each other's proximity. These transformations map the coordinates of each point of the floating surface into the coordinate space of the target surface. The non-rigid surface registration results are dependent on the quality of this initial initialization procedure. Surface registration refers to the establishment of the geometrical relationship between surfaces that aligns the surfaces between them as well as possible. Then, every individual surface is "templated" (named the warped surfaces) such that every point on all 3D surfaces is associated with the anatomically corresponding point on the reference template. Therefore, information encoded in 3D-surface representations has to be extracted and made comparable. In a last step, landmarks are indicated once on the reference templates (Figure 2.e) . Every landmark placed on the template is associated with the anatomically corresponding point on the warped surfaces.

During an anatomical templating process, the reference template is warped non-rigidly to every subject's anatomically corresponding surface (target surface). The non-rigid (robust) surface registration software used for this warping was developed using the MeVisLab © v. 2.7.1 software [77]. The warping is performed iteratively starting with a rigid alignment, and gradually following with more flexible registration steps. At the end of this process every landmark of the template is projected onto every subject's surface, thus establishing a dense point-based anatomical correspondence among all subjects (Figure 2.f). Therefore, the coordinates of all subjects are recorded within a common coordinate system which may be used for statistical analysis.

In order to estimate the precision/measurement error of this procedure, the discrete landmarks were twice indicated on the hard- and soft-tissue templates. The warped landmarks on the studied subjects were recorded (noted AR1a, AR2a, MGa). Note that the warping transformation remains the same, independent of the re-indication of the discrete landmarks. For the INTRA-OE, the landmark indication on the templates was done by the same observer (noted AR1t, AR2t), with an interval of two weeks. For the INTER-OE, the landmark indication on the templates was done independently by two different observers (noted AR1t, MGt).

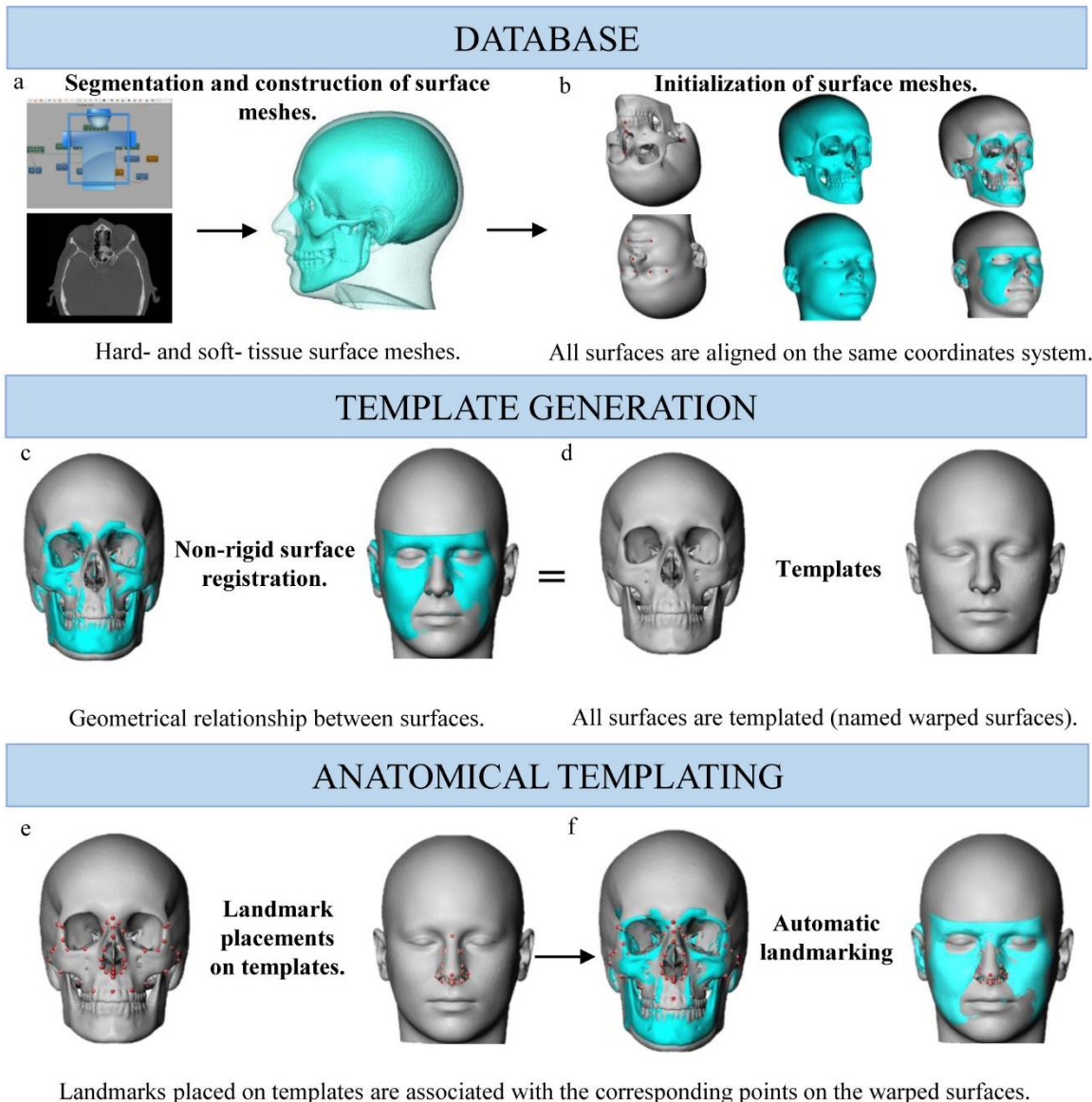


Figure 2. Workflow of the automatic landmarking procedure. a) segmentation process; b) initialisation process; c) non-rigid surface registration process; d) templates generation; e) definition of the region of interest on templates; f) automatic landmarking.

Statistical analysis

The raw coordinates resulting from the manual and automatic landmarking procedures were adjusted through a generalized Procrustes superimposition (GPS) to obtain pose-invariant shape coordinates [78, 79]. More precisely, GPS reduces the sum of the squared distances between corresponding anatomical points by aligning the configurations of landmarks and removing the differences due to translation and rotation (not size) among all individuals thus defining the remaining shape information as a set of Procrustes coordinates [80-82]. We adapted the procedure to keep the relative position (and thus measurement error) of the samples of the same individual unchanged, while their common (per subject) mean is GPA aligned with the grand mean.

We distinguish between two types of measurement errors on landmark localization: precision and accuracy. Precision refers to the random error, in measuring the degree to which repeated measurements give the same result under the same conditions. In contrast, accuracy refers to the systematic error (or bias) of the measurements compared to their true values. Random error interferes with the genuine variability by adding residual noise and increases any Type II error rate (reduction in statistical power). In our particular setting ME reflects two different components of error: reproducibility due to different methods (automatic versus manual), which induces both systematic and random errors and repeatability due to multiple observers, which induces random errors. Since we do not have a ground truth available, we limit the assessment of the systematic error by evaluating the bias between the automatic and manual landmarking.

The precision of the (manual and automatic) landmark positioning was calculated using the dispersion Δ_{ij} for each landmark i and individual j . Dispersion is defined as the Mean Euclidean Distance (MED) of the sample landmark \mathbf{p}_{ijk} to the mean $\bar{\mathbf{p}}_{ij}$ of the (x,y,z)-coordinates of landmark i over all observations k (INTER, INTRA, resp.) for subject j :

$$\Delta_{ij} = \sum_{k=1}^K \|\mathbf{p}_{ijk} - \bar{\mathbf{p}}_{ij}\|/K, \text{ with } \bar{\mathbf{p}}_{ij} = \sum_{k=1}^K \mathbf{p}_{ijk}/K$$

Boxplots of MED values are generated for automatic and manual landmarking separately, showing the variation of dispersion over different subjects. Global precision is then reported as

the global (averaged over all landmarks) mean (μ_{Δ}) and median (m_{Δ}) of the per landmark mean ($\mu_{\Delta i}$) and median ($m_{\Delta i}$) values (over all subjects) .

The precision of the manual landmarking was assessed by comparing the dispersion over the three observers (AR1m, AR2m, MGm) manually placing the landmarks on each subject. The precision of the automatic landmarking was calculated by indicating the craniometric and capulometric landmarks three times (AR1t, AR2t, MGt) on the templates and measuring the resulting dispersion on the automatically indicated landmarks (AR1a, AR2a, MGa) for each subject. In addition, the precision of the landmark positioning on the templates was similarly calculated using MED on the three measurements (AR1t, AR2t, MGt).

While these absolute (expressed in metric units (mm)) measures are valuable in comparing the precision of different methods and possibly selecting a subset of landmarks to retain for further morphometric analysis, they should be supplemented by relative measures, comparing the ME to the true shape variation in the specific data sets.

The bias between automatic and manual landmarking was assessed both visually and statistically. Plotting the Procrustes shape measures (principal components) in the PCA tangent space along the first two principal components can reveal any structural grouping due to the methods. Bias was first examined by examining differences in mean shape of the landmark configurations obtained by the two (automatic and manual) methods, considered as independent populations.

Finally, both systematic (bias) and relative random error were assessed through a three-way repeated measures Procrustes ANOVA [83-85], with individual as a factor and with observer and method as additional factors. This procedure partitions the overall variation of Procrustes aligned landmark coordinates into separate components, allowing to evaluate the impact of variation due to methods (automatic versus manual) and observers (intra and inter) relative to true morphological variation between individuals. Intra-class correlation (also termed repeatability) was obtained using a one-way ANOVA with individual as unique categorical predicting variable [86, 87].

All statistical analyses were performed using R studio software version 1.0.44-©2009-2016 for Windows [88].

Results

The global mean and median dispersion results are presented in Table 2, together with the dispersion of the three observations (AR1t, AR2t, MGt) of landmark positioning on the hard- and soft-tissue templates. While both mean and median dispersion are on par for automatic and manual craniometric landmarking (mean(median) values of 1.64 (1.64) mm vs 1.67 (1.63) mm), lower dispersion values were obtained for automatic compared to manual capulometric landmarking (1.31 (1.23) mm vs 1.66 (1.57) mm). The boxplots of the dispersion for automatic and manual craniometric and capulometric landmarking are shown in Figs. 3 and 4. These plots show that the variation in dispersion in automatic landmarking is much smaller than in manual landmarking.

Table 2. Measurement errors (global mean and median dispersion in mm) for hard- and soft-tissue landmarks. Right column: mean dispersion for template landmarking.

	Automatic		Manual		Template
	<i>Mean (mm)</i>	<i>Median (mm)</i>	<i>Mean (mm)</i>	<i>Median (mm)</i>	<i>Mean (mm)</i>
Hard-tissue	1.64	1.64	1.67	1.63	1.63
Soft-tissue	1.31	1.23	1.66	1.57	1.26

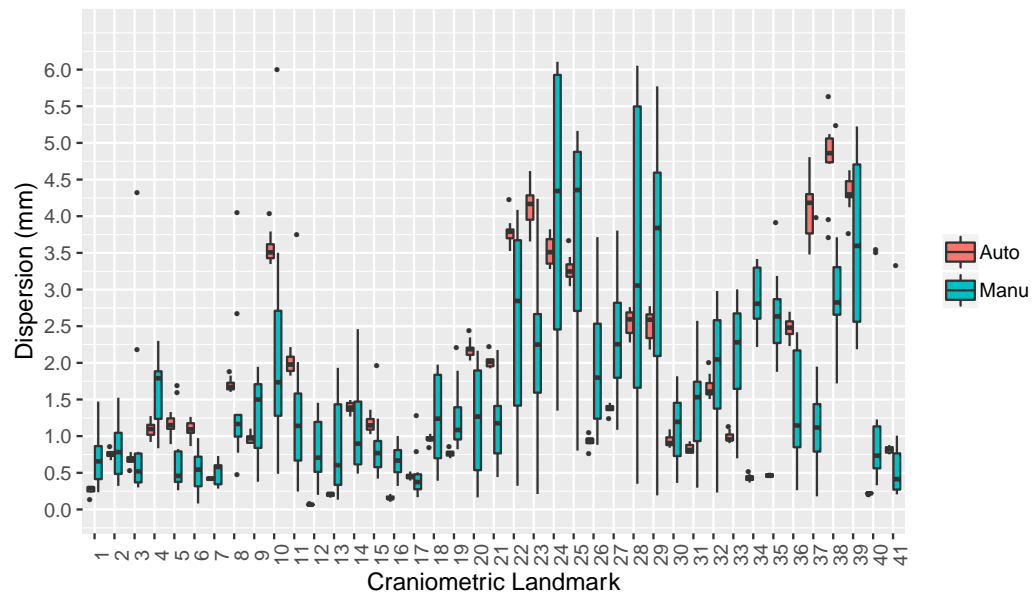


Figure 3. Boxplots of the dispersion for automatic and manual craniometric landmarking. Craniometric landmark definitions (1-41): cf Table 1.

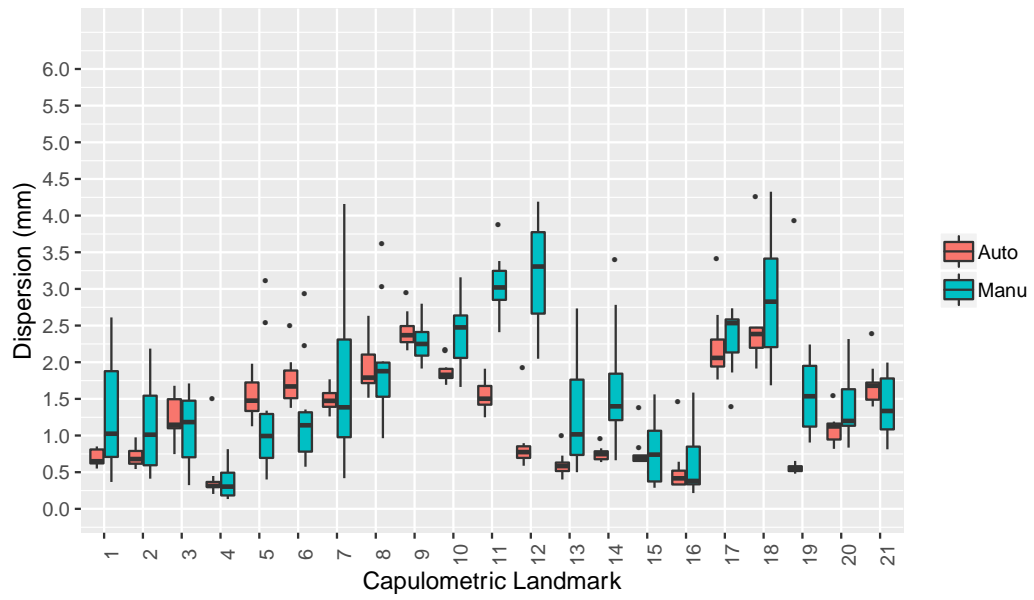


Figure 4. Boxplots of the dispersion of automatic and manual capulometric landmarking. Capulometric landmark definitions (1-41): cf Table 1.

We also plotted the median dispersion per landmark of the automatic landmarking as a function of the median dispersion per landmark due to the multi-observer landmarking on the templates for both the hard and the soft tissues Figure 5. We observe a strong linear correlation between both: automatic landmarking dispersion is almost exclusively determined by template landmarking dispersion, with little or no influence of inter-individual differences of the warping procedure.

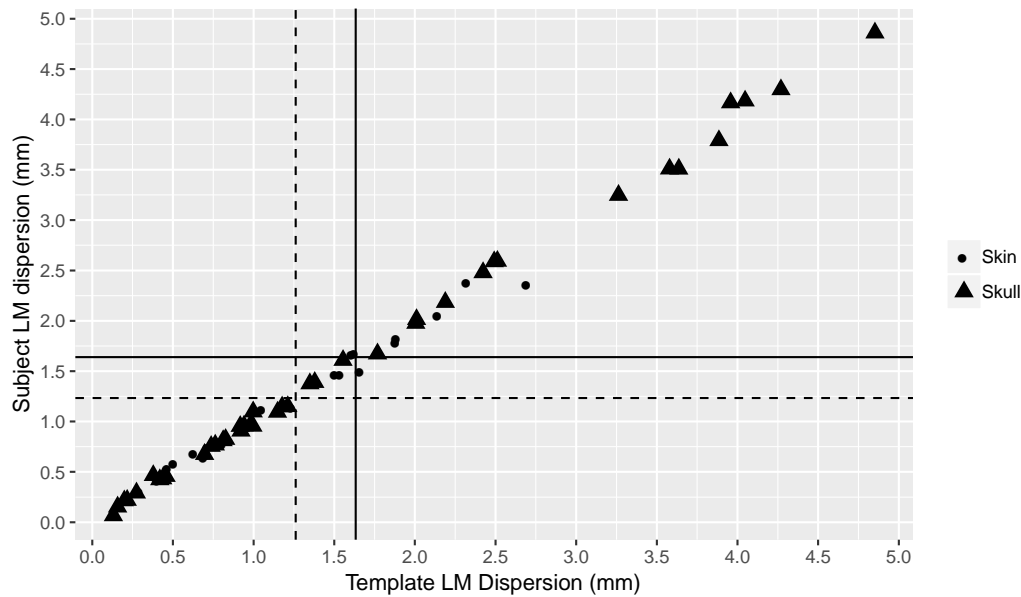


Figure 5. Correlation between the dispersion (per landmark) on the automatically indicated landmarks and the dispersion on the corresponding landmarks on the templates. The solid (dashed) horizontal and vertical lines represent the global median dispersion for hard(skull) – and soft-(skin) landmarking (on target subjects and templates, respectively).

Figures 6 and 7 shows three different plots of the Procrustes aligned craniometric /capulometric coordinates projected onto the first two principal components in tangent space, grouped according to method and observer, method and individual. The graphs for the craniometric landmarking do not provide visual evidence of biases induced by observer and/or method. However, Figure 7 indicate bias induced by method on the one hand (middle plot), and also observer, although mainly for the manual procedure (left plot).

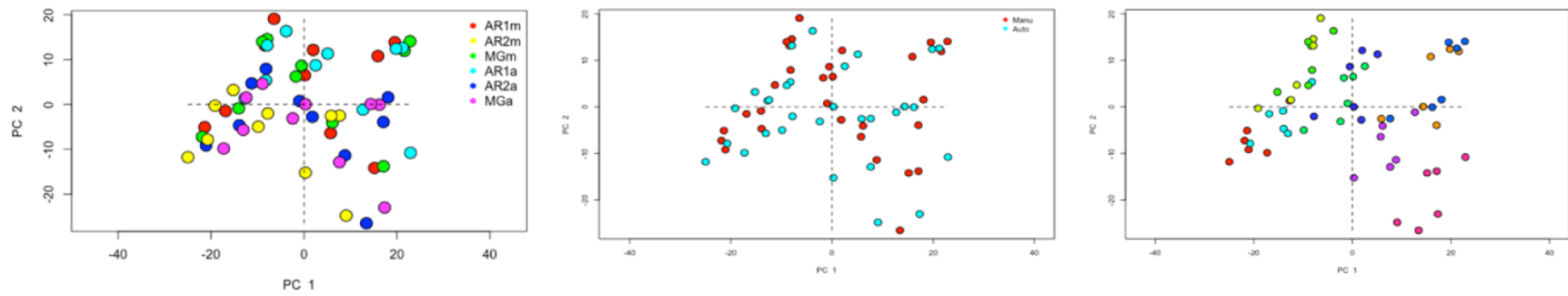


Figure 6. Scatterplots of Procrustes craniometric shape coordinates (PC) onto the first two principal components. Left: colored according to method and observer, middle: colored according to method, right: colored according to individual.

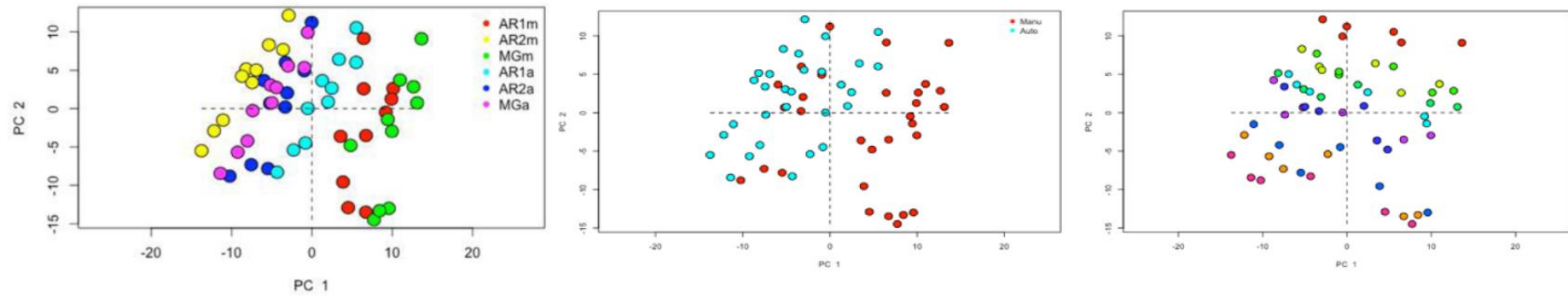


Figure 7. Scatterplots of Procrustes capulometric shape coordinates (PC) onto the first two principal components. Left: colored according to method and observer, middle: colored according to method, right: colored according to individual.

The unpaired test of equal mean shapes for the automatic and manual landmark configurations returned p-values (according to different tests) lower than 0.01, indicating no significant differences in mean shapes due to the choice of method. The results of the 3-way Procrustes ANOVA are tabulated in Table 3 and in Table 4. From these tables we read that both method and observer have a statistically non-negligible contribution to total variance. However, the observer component for craniometric landmarking is far larger than the method component. This supports the conclusion that the automatic method has little influence on the ME for craniometric landmarking in line with the findings of Table 2 and Figure 6.

Table 3. Three-way Procrustes ANOVA for craniometric landmarks.

	Df	SS	MS	Rsq	F	Z	Pr (>F)
Individual	9	22853	2539.2	0.56792	21.275	15.7904	0.001
Method	1	2259	2259.3	0.05614	18.929	7.4386	0.001
Observer	2	6587	3293.4	0.16369	27.593	11.0797	0.001
Method:Observer	2	3170	1585.1	0.07878	13.280	12.1300	0.001
Residuals	45	2112.6	46.95	0.18615			
Total	59	40 240					

Table 4. Three-way Procrustes ANOVA for capulometric landmarks.

	Df	SS	MS	Rsq	F	Z	Pr (>F)
Individual	9	4550.9	505.65	0.40100	10.7709	11.5281	0.001
Method	1	1566.2	1566.16	0.13800	33.3605	7.1559	0.001
Observer	2	2248.9	1124.46	0.19816	23.9519	9.4629	0.001
Method:Observer	2	870.2	435.12	0.07668	9.2684	10.6648	0.001
Residuals	45	2112.6	46.95	0.18615			
Total	59	11348.8					

For capulometric landmarking, however, the contribution of method attributed variance is larger, which corroborates the findings of Table 2, which indicates a lower dispersion for the automatic method and Figure 7 (middle) which indicates a bias between automatic and manual landmarking. The inter- and intra- observer ME for both types of landmarks, on the other hand, contribute to a larger extent to total ME.

Discussion

The results obtained in this study validated the accuracy (bias) and the precision of the automatic placement of landmarks, both on hard- and soft-tissue surfaces. The automatic landmarking method allows us to reduce inter- and intra-observer errors and it could be a convenient prerequisite for geometric morphometrics as an alternative to manual landmarking. More generally, automatic landmarking offers many applications in forensic and physical anthropology using 3D surfaces.

The automatic placement of landmarks, in addition to reducing measurement errors in landmark placements, allows us to achieve a better precision for facial approximation, enabling the possibility to include more samples and populations with ease. Especially in CFR, when large sample sizes are required, manual placement of landmarks could be extremely time consuming and may be biased with observer subjectivity, rendering the analysis less repeatable and impacting on the precision of the human facial approximation.

The results (both visually and statistically) show that the automatic procedure, as tested here, has similar, if not better, measurement error compared to the manual procedure. The resulting random component of ME is almost exclusively determined by the dispersion on the template landmarks. Random measurement error, in general, is known to be reduced by averaging the repeated measurements (ref Armqvist). Hence, in order to further reduce this ME for automatic landmarking, one should obtain an average template landmark configuration either by averaging multiple indications on the template or defining a consensus configuration.

Extensive work has been published on 2D landmarks [66-70], whereas less research has been done on the identification and location of landmarks on 3D surfaces [71]. Only some recent work on 3D face registration explored the use of curvature in order to find the tip of the nose [89-93] in combination with an iterative closest point (ICP) alignment algorithm. The ICP is one of most popular techniques for 3D face registration and it has been extensively used as the main procedure, or in combination with other methods [89, 90, 93]. Finally, we stress that this study is the first attempt at a computer-assisted facial approximation of the nose with an automatic landmarking approach for the South African population using CBCT scans.

Compared with manual methods, automation of facial approximation is suitable for application to the judicial system, which requires precision, reliability and knowledge of possible quantization errors. In addition, the automatic placement of landmarks on large 3D surface samples, offers the possibility of standardization and increased accuracy in the analysis of the correlations between hard- and soft-tissue facial features. In this research, we specifically used CBCT scans from living patients, since we intended to remove the limits generated by the use of dry skulls, cadavers and CT datasets as initial references, such as desiccation and supination effects. A further advantage of CBCT compared to CT includes higher spatial resolution (0.1 mm to 0.4 mm) and isotropic volumetric data for the accurate placement of 3D landmarks [72].

Finally, this research demonstrates the utilization of the automatic landmarking as a convenient prerequisite for geometric morphometrics-based shape analysis of the nasal complex. The automatic landmarking needs to be applied on different 3D anatomical elements and on different populations before it can be considered robust. When planning future research, it would be interesting to test the precision of the automatic placement of landmarks on another facial skeleton element (for instance the mandible or forehead) and on external components of the face (for instance the mouth, eye, or ear), in order to finally apply the methodology on the complete skull/face. In general, when developing approaches using automatic landmarking, it may be useful to consider factors such as sex, age and inter-population morphological differences to possibly further enhance the accuracy of the methodology.

Conclusion

This research provides a validation of the precision of the automatic placement of landmarks and demonstrates its utilization as a convenient prerequisite for geometric morphometrics-based shape analysis of the nasal complex. The automatic landmarks positioning on hard- and soft-tissue 3D surfaces offers increased objectivity and the possibility of standardization. The automatic landmarking, in addition to reducing measurement errors, allows us to achieve a better precision for facial approximation, enabling the possibility to include more samples and populations with ease. Furthermore, the automatic placement of landmarks as an accurate alternative to manual landmarking, offers many applications in forensic and physical anthropology.

Acknowledgments

The authors would like to thank Dr. André Uys from the Oral and Dental Hospital, University of Pretoria, South Africa and Dr. Sarel Botha from the Life Groenkloof Hospital, Pretoria, South Africa, for providing the CBCT-data. We acknowledge the AESOP+ consortia coordinated by Prof. José Braga from the Computer-assisted Palaeoanthropology Team, UMR 5288 CNRS- Université Paul-Sabatier, 37, allées Jules-Guesde, 31000 Toulouse, and from the Evolutionary Studies Institute and School of Geosciences, University of the Witwatersrand, Johannesburg, South Africa, for the financial support.

References

1. M.M. Gerasimov, Face Finder, CRC Press, NY, NY, 1971.
2. G. Lebedinskaya, T. Balueva, and E. Veselovskaya, Development of methodological principles for reconstruction of the face on the basis of skull material. In M. Y. İşcan and R. P. Helmer (Eds.), *Forensic Analysis of the Skull: Craniofacial Analysis, Reconstruction, and Identification*. New York, NY: Wiley-Liss, 1993.
3. C.C. Snow, B.P. Gatliff, K.R. McWilliams, Reconstruction of facial features from the skull: An evaluation of its usefulness in forensic anthropology, *American Journal of Physical Anthropology*. 33 (1970) 221–227. [Doi:10.1002/ajpa.1330330207](https://doi.org/10.1002/ajpa.1330330207).
4. J. Prag and R. Neave, *Making Faces using Forensic and Archeological Evidence*. London: British Museum Press, 1997.
5. C. Wilkinson, *Forensic facial reconstruction*, Cambridge University Press, Cambridge, UK ; New York, 2004.
6. C. Wilkinson, Facial reconstruction – anatomical art or artistic anatomy?, *Journal of Anatomy*. 216 (2010) 235–250. [Doi:10.1111/j.1469-7580.2009.01182.x](https://doi.org/10.1111/j.1469-7580.2009.01182.x).
7. C.N. Stephan, Beyond the Sphere of the English Facial Approximation Literature: Ramifications of German Papers on Western Method Concepts*, *Journal of Forensic Sciences*. 51 (2006) 736–739. [Doi:10.1111/j.1556-4029.2006.00175.x](https://doi.org/10.1111/j.1556-4029.2006.00175.x).
8. A.J. Tyrrell, M.P. Evison, A.T. Chamberlain, M.A. Green, Forensic Three-Dimensional Facial Reconstruction: Historical Review and Contemporary Developments, *Journal of Forensic Sciences*. 42 (1997) 14176J. [Doi:10.1520/JFS14176J](https://doi.org/10.1520/JFS14176J).
9. C.N. Stephan, Anthropological facial ‘reconstruction’ – recognizing the fallacies, ‘unembracing’ the errors, and realizing method limits, *Science & Justice*. 43 (2003) 193–200. [Doi:10.1016/S1355-0306\(03\)71776-6](https://doi.org/10.1016/S1355-0306(03)71776-6).
10. L. Verzé, History of facial reconstruction, 1. 80 (2009) 5–12.
11. H. Ullrich, C.N. Stephan, On Gerasimov’s Plastic Facial Reconstruction Technique: New Insights to Facilitate Repeatability*: Gerasimov’s plastic facial reconstruction techniques, *Journal of Forensic Sciences*. 56 (2011) 470–474. [Doi:10.1111/j.1556-4029.2010.01672.x](https://doi.org/10.1111/j.1556-4029.2010.01672.x).
12. D. Vandermeulen, P. Claes, S. De Greef, G. Willems, J. Clement, P. Suetens, Automated facial reconstruction. *Craniofacial Identification*, (2012) 203.
13. P. Guyomarc’h, B. Dutailly, J. Charton, F. Santos, P. Desbarats, H. Coqueugniot, Anthropological Facial Approximation in Three Dimensions (AFA3D): Computer-

- Assisted Estimation of the Facial Morphology Using Geometric Morphometrics, *Journal of Forensic Sciences*. 59 (2014) 1502–1516. [Doi:10.1111/1556-4029.12547](https://doi.org/10.1111/1556-4029.12547).
14. P. Vanezis, R.W. Blowes, A.D. Linney, A.C. Tan, R. Richards, R. Neave, Application of 3-D computer graphics for facial reconstruction and comparison with sculpting techniques, *Forensic Science International*. 42 (1989) 69–84. [Doi:10.1016/0379-0738\(89\)90200-4](https://doi.org/10.1016/0379-0738(89)90200-4).
 15. M. Vanezis, P. Vanezis, Cranio-Facial Reconstruction in Forensic Identification Historical Development and a Review of Current Practice, *Medicine, Science and the Law*. 40 (2000) 197–205. [Doi:10.1177/002580240004000303](https://doi.org/10.1177/002580240004000303).
 16. R.J. Evenhouse, M. Rasmussen, L.L. Sadler, Computer-aided forensic facial reconstruction, in: R.E. Herron (Ed.), 1991, pp. 147–156. [Doi:10.1117/12.48078](https://doi.org/10.1117/12.48078).
 17. M. Evison, Computerised 3D facial reconstruction [Online]. Research School of Archaeology and Archaeological Science, University of Sheffield, UK (1996). www.assemblage.group.shef.ac.uk/1/evison.html.
 18. M. Evison, Modeling age, obesity, and ethnicity in a computerized 3D facial reconstruction. *Forensic Science Communications*[Online], (2000) 3.
 19. S. Michael and M. Chen, The 3D reconstruction of facial features using volume distortion. 14th Eurographics UK Conference. London (1996).
 20. A.W. Shahrom, P. Vanezis, R.C. Chapman, A. Gonzales, C. Blenkinsop, M.L. Rossi, Techniques in facial identification: Computer-aided facial reconstruction using a laser scanner and video superimposition, *International Journal of Legal Medicine*. 108 (1996) 194–200. [Doi:10.1007/BF01369791](https://doi.org/10.1007/BF01369791).
 21. K. Archer, Cranio-facial reconstruction using hierarchical B-spline interpolation. Masters Thesis, The University of British Columbia (1997).
 22. K. Archer, K. Coughlan, D. Forsey, and S. Struben, Software tools for craniofacial growth and reconstruction. *Graphics Interface*. Vancouver, Canada (1998).
 23. G. Quatrehomme, S. Cotin, G. Subsol, H. Delingette, Y. Garidel, G. Grévin, M. Fidrich, P. Bailet, A. Ollier, A Fully Three-Dimensional Method for Facial Reconstruction Based on Deformable Models, *Journal of Forensic Sciences*. (1997) 42 14175J. [Doi:10.1520/JFS14175J](https://doi.org/10.1520/JFS14175J).
 24. L. Nelson, S. Michael, The application of volume deformation to three-dimensional facial reconstruction: A comparison with previous techniques, *Forensic Science International*. 94 (1998) 167–181. [Doi:10.1016/S0379-0738\(98\)00066-8](https://doi.org/10.1016/S0379-0738(98)00066-8).

25. M. Forte, 3D facial reconstruction and visualization of ancient Egyptian mummies using spiral CT data, in: ACM Press, 1999: p. 223. [Doi:10.1145/311625.312106](https://doi.org/10.1145/311625.312106).
26. W.D. Bullock, Computer assisted 3d craniofacial reconstruction, University of British Columbia, 1999. [Doi:10.14288/1.0051482](https://doi.org/10.14288/1.0051482).
27. M. Jones, Facial reconstruction using volumetric data. Proceedings of the 6th International Vision Modeling and Visualisation Conference in Stuttgart (Germany). (2001) pages 21–23.
28. K. Kähler, J. Haber, H.-P. Seidel, Reanimating the dead: reconstruction of expressive faces from skull data, in: ACM Press. 2003: pp. 554. [Doi:10.1145/1201775.882307](https://doi.org/10.1145/1201775.882307).
29. P. Claes, S. De Greef, G. Willems, D. Vandermeulen, and P. Suetens, Craniofacial statistical modelling and reconstruction. 3D Modelling, Paris, France (2004a).
30. P. Claes, D. Vandermeulen, P. Suetens, S. De Greef, and G. Willems, Computerized facial approximation using statistical models of tissue depth and 3-D facial outlook. Conference of the International Association for Craniofacial Identification, IACI. Dalian, China (2004b).
31. P. Claes, D. Vandermeulen, S. De Greef, G. Willems, and P. Suetens, Combined statistical modeling of tissue depth and 3D facial outlook for computerized facial approximation. 2nd International Conference on Reconstruction of Soft Facial Parts, RSFP. Remagen, Germany (2005a).
32. P. Claes, D. Vandermeulen, S. De Greef, G. Willems, and P. Suetens, Statistically deformable face models for cranio-facial reconstruction. Proceedings 4th International Symposium on Image and Signal Processing and Analysis, ISPA. Zagreb, Croatia (2005b).
33. P. Claes, D. Vandermeulen, S. De Greef, G. Willems, P. Suetens, Statistically Deformable Face Models for Cranio-Facial Reconstruction, Journal of Computing and Information Technology. 14 (2006) 21. [Doi:10.2498/cit.2006.01.03](https://doi.org/10.2498/cit.2006.01.03).
34. P. Claes, D. Vandermeulen, S. De Greef, G. Willems, P. Suetens, Craniofacial reconstruction using a combined statistical model of face shape and soft tissue depths: Methodology and validation, Forensic Science International. 159 (2006) S147–S158. [Doi:10.1016/j.forsciint.2006.02.035](https://doi.org/10.1016/j.forsciint.2006.02.035).
35. P. Claes, A robust statistical surface registration framework using implicit function representations: Application in craniofacial reconstruction. PhD Thesis, K.U. Leuven, Belgium 2007.

36. P. Claes, D. Vandermeulen, S. De Greef, G. Willems, J.G. Clement, P. Suetens, Bayesian estimation of optimal craniofacial reconstructions, *Forensic Science International*. 201 (2010) 146–152. [Doi:10.1016/j.forsciint.2010.03.009](https://doi.org/10.1016/j.forsciint.2010.03.009).
37. D. Vandermeulen, P. Claes, R. Suetens, S. De Greef, G. Willems, Volumetric deformable face models for cranio-facial reconstruction, in: *IEEE*, 2005: pp. 353–358. [Doi:10.1109/ISPA.2005.195437](https://doi.org/10.1109/ISPA.2005.195437).
38. D. Vandermeulen, M. Loubele, P. Claes, Q. Wang, W. Mollemans, S. Srivastava, P. Suetens, Low-dose CT-based soft tissue modeling for craniofacial reconstruction. 2nd International Conference on Reconstruction of Soft Facial Parts, RSFP. Remagen, Germany (2005b).
39. D. Vandermeulen, P. Claes, D. Loeckx, S. De Greef, G. Willems, P. Suetens, Computerized craniofacial reconstruction using CT-derived implicit surface representations, *Forensic Science International*. 159 (2006) S164–S174. [Doi:10.1016/j.forsciint.2006.02.036](https://doi.org/10.1016/j.forsciint.2006.02.036).
40. Y. Pei, H. Zha, Z. Yuan, The Craniofacial Reconstruction from the Local Structural Diversity of Skulls, *Computer Graphics Forum*. 27 (2008) 1711–1718. [Doi:10.1111/j.1467-8659.2008.01315.x](https://doi.org/10.1111/j.1467-8659.2008.01315.x).
41. B. Andersson and M. Valfridsson, Digital 3D facial reconstruction based on computer tomography. Master Thesis, Linkopings university (2005).
42. M. Berar, M. Desvignes, G. Bailly, Y. Payan, 3D statistical facial reconstruction, in: *IEEE*, 2005a, pp. 365–370. [Doi:10.1109/ISPA.2005.195439](https://doi.org/10.1109/ISPA.2005.195439).
43. M. Berar, M. Desvignes, G. Bailly, and Y. Payan, Statistical skull models from 3D X-ray images. 2nd International Conference on Reconstruction of Soft Facial Parts, RSFP. Remagen, Germany (2005b).
44. M. Berar, M. Desvignes, G. Bailly, Y. Payan, 3D Semi-Landmarks Based Statistical Face Reconstruction, *Journal of Computing and Information Technology*. 14 (2006) 31. [Doi:10.2498/cit.2006.01.04](https://doi.org/10.2498/cit.2006.01.04).
45. S. Davy, T. Gilbert, D. Schofield and M. Evison, Forensic facial reconstruction using computer modeling software. In J. G. Clement and M. K. Marks (Eds.), *Computer-Graphic Facial Reconstruction*. Amsterdam: Elsevier (2005).
46. J. Muller, A. Mang, T.M. Buzug, A template-deformation method for facial reproduction, in: *IEEE*, 2005, pp. 359–364. [Doi:10.1109/ISPA.2005.195438](https://doi.org/10.1109/ISPA.2005.195438).

47. A. Mang, J. Muller, T.M. Buzug, A Multi-Modality Computer-Aided Framework Towards Postmortem Identification, *Journal of Computing and Information Technology*. 14 (2006) 7. [Doi:10.2498/cit.2006.01.02](https://doi.org/10.2498/cit.2006.01.02).
48. G. Subsol, and G. Quatrehomme, Automatic 3D facial reconstruction by feature-based registration of a reference head. In Clement J. G. and Marks M. K., editors, *Computergraphic facial reconstruction*. Elsevier Academic Press, Amsterdam u.a. (2005), pp. 79–101.
49. P. Tu, R. Book, X. Liu, N. Krahnstoever, C. Adrian, P. Williams, Automatic Face Recognition from Skeletal Remains, in: *IEEE*, 2007: pp. 1–7. [Doi:10.1109/CVPR.2007.383060](https://doi.org/10.1109/CVPR.2007.383060).
50. P. Tu, R. Hartley, W. Lorensen, A. Alyassin, R. Gupta, Face reconstruction using flesh deformation modes. In J. G. Clement and M. K. Marks (Eds.), *Computer Graphic Facial Reconstruction*. Amsterdam: Elsevier. (2005) pp. 145–162.
51. W.D. Turner, R.E.B. Brown, T.P. Kelliher, P.H. Tu, M.A. Taister, K.W.P. Miller, A novel method of automated skull registration for forensic facial approximation, *Forensic Science International*. 154 (2005) 149–158. [Doi:10.1016/j.forsciint.2004.10.003](https://doi.org/10.1016/j.forsciint.2004.10.003).
52. Y. Pei, H. Zha, Z. Yuan, The Craniofacial Reconstruction from the Local Structural Diversity of Skulls, *Computer Graphics Forum*. 27 (2008) 1711–1718. [Doi:10.1111/j.1467-8659.2008.01315.x](https://doi.org/10.1111/j.1467-8659.2008.01315.x).
53. P. Paysan, M. Lüthi, T. Albrecht, A. Lerch, B. Amberg, F. Santini, T. Vetter, Face Reconstruction from Skull Shapes and Physical Attributes, in: J. Denzler, G. Notni, H. Süße (Eds.), *Pattern Recognition*, Springer Berlin Heidelberg, Berlin, Heidelberg, 2009, pp. 232–241. [Doi:10.1007/978-3-642-03798-6_24](https://doi.org/10.1007/978-3-642-03798-6_24).
54. F. Tilotta, F. Richard, J. Glaunès, M. Berar, S. Gey, S. Verdeille, Y. Rozenholc, J.F. Gaudy, Construction and analysis of a head CT-scan database for craniofacial reconstruction, *Forensic Science International*. 191 (2009) 112.e1-112.e12. [Doi:10.1016/j.forsciint.2009.06.017](https://doi.org/10.1016/j.forsciint.2009.06.017).
55. S. Schlager, Soft-tissue reconstruction of the human nose : population differences and sexual dimorphism = Weichteilrekonstruktion der menschlichen Nase : Populationsunterschiede und Sexualdimorphismus, Universität, Freiburg, 2013.
56. K.-M. Lee, W.-J. Lee, J.-H. Cho, H.-S. Hwang, Three-dimensional prediction of the nose for facial reconstruction using cone-beam computed tomography, *Forensic Science International*. 236 (2014) 194.e1-194.e5. [Doi:10.1016/j.forsciint.2013.12.035](https://doi.org/10.1016/j.forsciint.2013.12.035).

57. A.F. Ridel, F. Demeter, J. Liebenberg, E.N. L'Abbé, D. Vandermeulen, A.C. Oettlé, Skeletal dimensions as predictors for the shape of the nose in a South African sample: A cone-beam computed tomography (CBCT) study, *Forensic Science International*. 289 (2018) 18–26. [Doi:10.1016/j.forsciint.2018.05.011](https://doi.org/10.1016/j.forsciint.2018.05.011).
58. P. Vanezis, O. Trujillo, Evaluation of hypostasis using a colorimeter measuring system and its application to assessment of the post-mortem interval (time of death), *Forensic Science International*. 78 (1996) 19–28. [Doi:10.1016/0379-0738\(95\)01845-X](https://doi.org/10.1016/0379-0738(95)01845-X).
59. G. Subsol, A scheme for automatically building 3D morphometric anatomical atlases based on feature lines: a list of references. online. 2002.
60. N. Iblher, E. Gladilin, B.G. Stark, Soft-Tissue Mobility of the Lower Face Depending on Positional Changes and Age: A Three-Dimensional Morphometric Surface Analysis, *Plastic and Reconstructive Surgery*. 131 (2013) 372–381. [Doi:10.1097/PRS.0b013e318278d67c](https://doi.org/10.1097/PRS.0b013e318278d67c).
61. F. Marin, K.B. Mansour, F. Demeter, P. Frey, Displacement of facial soft tissues in upright versus supine positions, *Computer Methods in Biomechanics and Biomedical Engineering*. (2015) 1–2. [Doi:10.1080/10255842.2015.1069590](https://doi.org/10.1080/10255842.2015.1069590).
62. G. Arnqvist, T. Martensson, Measurement error in geometric morphometrics: empirical strategies to assess and reduce its impact on measures of shape. *Acta Zool Acad Sci Hung*. (1988) 44(1–2):73–96.
63. A. Pérez-Pérez, A. Alesan, L. Roca, Measurement error: Inter-and Intraobserver Variability. An Empiric Study, *Int. J. Anthropol*. 5 (1990) 129–135. [Doi:10.1007/BF02442082](https://doi.org/10.1007/BF02442082).
64. S.M. Yezerinac, S.C. Loughheed, P. Handford, Measurement Error and Morphometric Studies: Statistical Power and Observer Experience, *Systematic Biology*. 41 (1992) 471–482. [Doi:10.1093/sysbio/41.4.471](https://doi.org/10.1093/sysbio/41.4.471).
65. L.P. Menéndez, Comparing Methods to Assess Intraobserver Measurement Error of 3D Craniofacial Landmarks Using Geometric Morphometrics Through a Digitizer Arm, *Journal of Forensic Sciences*. 62 (2017) 741–746. [Doi:10.1111/1556-4029.13301](https://doi.org/10.1111/1556-4029.13301).
66. T.F. Cootes and C. Taylor. "Active Shape Models Search Using Grey Level Models: A Quantitative Evaluation". In *Proceedings, British Machine Vision Conference*, (1993) 2:639–648.
67. T.F. Cootes, G.J. Edwards, C.J. Taylor, Active appearance models, *IEEE Transactions on Pattern Analysis and Machine Intelligence*. 23 (2001) 681–685. [Doi:10.1109/34.927467](https://doi.org/10.1109/34.927467).

68. Y. Wang, C.-S. Chua, Y.-K. Ho, Facial feature detection and face recognition from 2D and 3D images, *Pattern Recognition Letters*. 23 (2002) 1191–1202.
[Doi:10.1016/S0167-8655\(02\)00066-1](https://doi.org/10.1016/S0167-8655(02)00066-1).
69. D. Xi, S.-W. Lee, Face Detection and Facial Component Extraction by Wavelet Decomposition and Support Vector Machines, in: *Audio- and Video-Based Biometric Person Authentication*, Springer, Berlin, Heidelberg, 2003, pp. 199–207.
[Doi:10.1007/3-540-44887-X_24](https://doi.org/10.1007/3-540-44887-X_24).
70. S. Kobayashi, S. Hashimoto, Automated feature extraction of face image and its applications, in: *IEEE*, 1995, pp. 164–169. [Doi:10.1109/ROMAN.1995.531954](https://doi.org/10.1109/ROMAN.1995.531954).
71. M.C. Ruiz, J. Illingworth, Automatic landmarking of faces in 3D-ALF, in: *IEE*, 2008, pp. 41–46. [Doi:10.1049/cp:20080280](https://doi.org/10.1049/cp:20080280).
72. W.C. Scarfe, A.G. Farman, What is Cone-Beam CT and How Does it Work?, *Dental Clinics of North America*. 52 (2008) 707–730. [Doi:10.1016/j.cden.2008.05.005](https://doi.org/10.1016/j.cden.2008.05.005).
73. J.F. Hair, R.E. Anderson, R.L. Tatham, Black, W.C. Analisis multivariante. Madrid, Spain: Prentice-Hall. (1999).
74. C.F. Spoor, F.W. Zonneveld, G.A. Macho, Linear measurements of cortical bone and dental enamel by computed tomography: Applications and problems, *American Journal of Physical Anthropology*. 91 (1993) 469–484. [Doi:10.1002/ajpa.1330910405](https://doi.org/10.1002/ajpa.1330910405).
75. J. Buikstra, D. Ubelaker, Standards for data collection from human skeletal remains: Proceedings of a seminar at the Field Museum of Natural History (Arkansas Archaeology Research Series 44). *Fayetteville Arkansas Archaeological Survey*. (1994).
76. J. Caple, C.N. Stephan, A standardized nomenclature for craniofacial and facial anthropometry, *International Journal of Legal Medicine*. 130 (2016) 863–879.
[Doi:10.1007/s00414-015-1292-1](https://doi.org/10.1007/s00414-015-1292-1).
77. J. Snyders, P. Claes, D. Vandermeulen, P. Suetens, Development and comparison of non-rigid surface registration algorithms and extensions. Technical report KUL/ESAT/PSI/1401, KU Leuven, ESAT, January (2014) Leuven, Belgium.
78. D.G. Kendall, Shape Manifolds, Procrustean Metrics, and Complex Projective Spaces, *Bulletin of the London Mathematical Society*. 16 (1984) 81–121.
[Doi:10.1112/blms/16.2.81](https://doi.org/10.1112/blms/16.2.81).
79. D.E. Slice, Landmark coordinates aligned by Procrustes analysis do not lie in Kendall's shape space. *Syst Biol*. (2001) 50(1):141–9.

80. F.L. Bookstein, *Morphometric tools for landmark data: geometry and biology*, Cambridge University Press, Cambridge [England]; New York, 1991.
81. F. Bookstein, Biometrics, biomathematics and the morphometric synthesis, *Bulletin of Mathematical Biology*. 58 (1996) 313–365. [Doi:10.1016/0092-8240\(95\)00329-0](https://doi.org/10.1016/0092-8240(95)00329-0).
82. F.L. Bookstein, Shape and the information in medical images: a decade of the morphometric synthesis, in: *IEEE*, 1996, pp. 2–12. [Doi:10.1109/MMBIA.1996.534052](https://doi.org/10.1109/MMBIA.1996.534052).
83. T.A. White, J.B. Searle, Mandible asymmetry and genetic diversity in island populations of the common shrew, *Sorex araneus*, *Journal of Evolutionary Biology*. 21 (2008) 636–641. [Doi:10.1111/j.1420-9101.2007.01481.x](https://doi.org/10.1111/j.1420-9101.2007.01481.x).
84. L.J. Leamy, C.P. Klingenberg, The Genetics and Evolution of Fluctuating Asymmetry, *Annual Review of Ecology, Evolution, and Systematics*. 36 (2005) 1–21. [Doi: 10.1146/annurev.ecolsys.36.102003.152640](https://doi.org/10.1146/annurev.ecolsys.36.102003.152640).
D.A. Schmieder, H.A. Benítez, I.M. Borissov, C. Fruciano, Bat Species Comparisons Based on External Morphology: A Test of Traditional versus Geometric Morphometric Approaches, *PLOS ONE*. 10 (2015) e0127043. [Doi: 10.1371/journal.pone.0127043](https://doi.org/10.1371/journal.pone.0127043).
85. G. Arnqvist, & T. Mårtensson, Measurement error in geometric morphometrics: Empirical strategies to assess and reduce its impact on measures of shape. *Acta Zoologica Acaemiae Scientiarum Hungaricae*, 44(1), 73–96 (1998).
86. C. Fruciano, Measurement error in geometric morphometrics. *Development Genes and Evolution*, 226(3), 139–158 (2016).
87. R Core Team. *R: a language and environment for statistical computing*. Vienna, Austria: R Foundation for Statistical Computing, (2012). <http://www.R-project.org>.
88. Kyong I. Chang, K.W. Bowyer, P.J. Flynn, Multiple Nose Region Matching for 3D Face Recognition under Varying Facial Expression, *IEEE Transactions on Pattern Analysis and Machine Intelligence*. 28 (2006) 1695–1700. [Doi:10.1109/TPAMI.2006.210](https://doi.org/10.1109/TPAMI.2006.210).
89. G. Zhang, Y. Wang, A 3D Facial Feature Point Localization Method Based on Statistical Shape Model, in: *IEEE*, (2007), p. II-249-II-252. [Doi:10.1109/ICASSP.2007.366219](https://doi.org/10.1109/ICASSP.2007.366219).
90. M.P. Segundo, C. Queirolo, O.R.P. Bellon, L. Silva, Automatic 3D facial segmentation and landmark detection, in: *IEEE*, (2007), pp. 431–436. [Doi:10.1109/ICIAP.2007.4362816](https://doi.org/10.1109/ICIAP.2007.4362816).
91. I.A. Kakadiaris, G. Passalis, G. Toderici, M.N. Murtuza, Y. Lu, N. Karampatziakis, T. Theoharis, Three-Dimensional Face Recognition in the Presence of Facial Expressions:

An Annotated Deformable Model Approach, *IEEE Transactions on Pattern Analysis and Machine Intelligence*. 29 (2007) 640–649. [Doi:10.1109/TPAMI.2007.1017](https://doi.org/10.1109/TPAMI.2007.1017).

92. Xiaoguang Lu, A.K. Jain, Automatic Feature Extraction for Multiview 3D Face Recognition, in: *IEEE*, (2006), pp. 585–590. [Doi:10.1109/FGR.2006.23](https://doi.org/10.1109/FGR.2006.23).

Chapter 5

PRELIMINARY ANALYSIS

5.1. Introduction

This preliminary analysis allows to characterise the morphology differences among South African groups in order to facilitate nasal soft-tissue reconstruction.

To this end, a sub-sample of 120 South Africans, from the original sample, were selected for this preliminary analysis. In order to exclude the possible remodelling effect of the facial skeleton with the advancement of age, only young adults ageing between 18 to 30 years old were analysed. The main purpose of this analysis is to predict the displacements of three capulometric landmarks (pronasale, subnasale and alare) for the nose approximation using linear measurements. Correlation coefficients between hard- and soft-tissue measurements were determined, and regression equations computed to predict the most probable shape and size of the nose.

Skeletal dimensions as predictors for the shape of the nose in a South African sample: a cone-beam computed tomography (CBCT) study.

AF RIDEL, F DEMETER, J LIEBENBERG, EN L'ABBÉ, D VANDERMEULEN, AC OETTLÉ.

Published in Forensic Science International.



Skeletal dimensions as predictors for the shape of the nose in a South African sample: A cone-beam computed tomography (CBCT) study



A.F. Ridel^{a,*}, F. Demeter^{a,b}, J. Liebenberg^a, E.N. L'Abbé^a, D. Vandermeulen^{a,c}, A.C. Oettlé^{a,d}

^a Department of Anatomy, Faculty of Health Sciences, University of Pretoria, Pretoria, South Africa

^b Musée de l'Homme, UMR7206, 17 Place du Trocadéro, Paris 75116, France

^c Center for Processing Speech and Images (PSI), Department of Electrical Engineering (ESAT), KU Leuven, Belgium

^d Department of Anatomy, School of Medicine, Sefako Makgatho Health Sciences University, Ga-Rankuwa, Pretoria, South Africa

ARTICLE INFO

Article history:

Available online 12 May 2018

Keywords:

Human variability
Facial approximation
Regression equations
Craniofacial landmarks
Capulometric landmarks
Plane-to-plane distances

ABSTRACT

The profile of the nose is an important feature for facial approximations. Although several manual and semi-automated prediction guidelines exist for estimating the shape of the nose, the reliability and applicability of these methods to South Africans groups are unknown.

The aim of this study was to predict the displacements of capulometric landmarks from hard-tissue planes to facilitate nasal soft-tissue reconstruction in a South African sample. Cone beam computed tomography (CBCT) scans of 120 adult South Africans were selected from the Oral and Dental Hospital, University of Pretoria, South Africa. Measurements involving craniometric and capulometric landmarks of the nose were obtained as plane-to-plane distances. Correlation coefficients between hard- and soft-tissue measurements were determined, and regression equations computed to assist in the prediction of the most probable shape and size of the nose. All hard- and soft-tissue measurements appeared significantly different between groups, except for the distance between the pronasale and nasion in the transverse plane and for the distance between the alare and the nasion in the coronal plane. The nasal height, nasal bone length and the nasal bone projection were significant predictors of the pronasale, subnasale and alare positions. More precisely, the nasal height and the nasal bone length were significant predictors of the pronasale position in both groups. Nasal bone projection was only useful for predicting shape in white South Africans. The variation in the skeletal predictors of the external shape of the nose noted between black and white South Africans and the results of the cross-validation testing emphasize the need for population specific guidelines.

© 2018 Elsevier B.V. All rights reserved.

1. Introduction

Facial features, especially the profile of the nose, are important in facial recognition and are of paramount consideration in forensic facial approximations [1–3]. Dimensions of the nose might be important in distinguishing male and female faces and are useful in establishing an accurate facial approximation of a missing person through craniofacial reconstruction [4]. Craniofacial reconstruction (CFR) focuses on the relationship between the external envelope of tissue and the internal skeletal substrate. As the nose is

a complex component, with the underlying bone being only a minor substructure of the mid-facial cranium, the region needs to be analysed separately from the rest of the mid-face so as to assess the correlation between the skeletal substructures of the nose and its external surface morphology.

The morphology of the nose is often manually reconstructed from the shape and size of the nasal aperture, represented by the position of the pronasale, subnasale, and alare landmarks [5–9]. However, the reliability of this method depends on the characteristics of the sample population [9,10]. For example, the utilization of cadaver samples may be responsible for distortion of the soft-tissue data as desiccation appears within a few hours after death [11]. To overcome the limitations of tissue desiccation in cadavers, a variety of nose approximation methods in living populations have been developed based on the recent development in digital imaging techniques such as cephalograms [9,12] and computer tomography (CT) scans [13–15]. However, the utilization of CT scans as initial references may involve a supination effect on the

* Corresponding author at: Tswelopele Building, University of Pretoria, Private Bag X323, Arcadia 0007, South Africa.

E-mail addresses: Alison.ridel.up@gmail.com (A.F. Ridel), Fabrice.demeter@mhnh.fr (F. Demeter), jadel92@hotmail.com (J. Liebenberg), Erica.Labbe@up.ac.za (E.N. L'Abbé), Dirk.vandermeulen@kuleuven.be (D. Vandermeulen), Anna.oettle@smu.ac.za (A.C. Oettlé).

<https://doi.org/10.1016/j.forsciint.2018.05.011>

0379-0738/© 2018 Elsevier B.V. All rights reserved.

face due to the horizontal position of the patient during scanning [16,17]. Moreover, the slice thickness, which generally ranges from 0.6 mm to 1.5 mm [13–15], may induce errors in the manual landmark placement on 3D surfaces.

More recently, cone-beam computed tomography (CBCT) scanning from living patients has been used. During a CBCT scan, the patient is seated in a vertical position while the X-ray source and detector rotate around the head, capturing images using a cone-shaped X-ray beam. The advantages of CBCT compared to CT include lower radiation dose, lower cost, and higher spatial resolution (0.1 mm–0.4 mm) for the placement of 3D landmarks [18]. Using in vivo CBCT scanning does not only eliminate the effect of desiccation, but also possible supination effects.

Recently, Lee et al. [19] used CBCT scans to investigate the relationship between the external- and skeletal-dimensions of the nose so as to predict the nasal morphology of a Korean population. Measurements were obtained as point-to-plane distances or plane-to-plane distances by using well defined landmarks on the nasal skeleton and the external surface of the nose. This method estimates the coordinates of capulometric landmarks from the hard-tissue by predicting the distances of the capulometric landmarks from planes defined through craniometric landmarks. For example, the 3D position of the alare can be reconstructed from its distances from three mutually orthogonal planes (e.g. sagittal, coronal and transverse planes through the hard tissue nasion landmark). However, the reproducibility of the method described by Lee et al. [19] is unknown and has not yet been tested.

The aim of our study was to predict the relative positions of capulometric landmarks from hard-tissue planes to facilitate nasal soft-tissue reconstruction in a South African sample. Distances between landmarks (craniometric and capulometric) and planes were assessed. We examined the correlations among these measurements and established regression equations. We also assessed the reproducibility of all measures, which was not done by Lee et al. [19].

2. Materials & methods

Cone beam computer tomography (CBCT) scans of 120 adult South Africans were selected from the Oral and Dental Hospital, University of Pretoria, South Africa. CBCT scans were obtained using a CBCT scanner (Planmeca ProMax[®] 3D) with the following properties: 90 kV, 11.2 mA, voxel size of 0.4 mm, and field of view of 230 × 260 mm. A total of 60 black (37 males and 23 females) and 60 white (32 males and 28 females) South Africans were selected (Table 1). In this study, the terms black and white South Africans were used as these social terms are required when describing a missing person. We selected young adults between 18 to 30 years old in order to exclude possible remodelling effect of the facial skeleton with the advancement of age. In order to obtain a standardized volume data set, the subjects were scanned in the seated position with their eyes closed and with a relaxed facial expression. Patients were excluded if they presented with any condition that could affect the morphology of the face (e.g. orthodontic treatment, pathological conditions, facial asymmetry or any facial interventional reconstructive surgery). This research project was approved by the Main Research Ethics Committee of

the Faculty of Health Sciences, University of Pretoria, South Africa (Ethics Reference No: 301/2016).

In order to obtain a standardized orientation of the planes, special care was taken in orienting all scans in the Frankfurt horizontal (FH) plane using Fiji software [20]. The FH plane is defined by the right and left porion points (located at the top of each external acoustic meatus) and the left orbital (located at the bottom of the left orbit). Then, a reslicing process was performed on all DICOM images orienting all 3D head images in the same position. These resliced CBCT scans were imported into 3D Slicer software [21], version 4.8 for Windows for all measurements. Hard- and soft-tissue surface meshes were generated by finding the threshold values between segmented components according to the "Half Maximum Height" (HMH) quantitative iterative thresholding method [22]. Threshold values for hard-tissue varied between 1200–1250, and for the soft-tissue between 400–450. Sagittal, coronal and transverse planes corresponding to the resliced images were visualized and used as an instrument of measurement. In this study, the facial skeleton will be referred to as the hard-tissue, and the external structure of the nose as the soft-tissue.

Following the literature regarding facial approximation of the nose using CBCT scans [19] and in order to conserve homology and comparability between studies, craniometric and capulometric landmarks (types I–III [23,24]) selected in the study by Lee et al. [19] were used. Four craniometric landmarks (nasion (n), rhinion (rhi), nasospinale (ns) and alare (al)) were identified on the nasal bone and periphery of the nasal aperture, while three capulometric landmarks (pronasale (pn'), subnasale (sn') and alare (al')) were considered to represent the external structure of the nose. A total of seven landmarks described in Table 2 and illustrated in Fig. 1 were used.

In order to assess the 3D external structure of the nose and related skeletal-tissue structures, a set of coronal, sagittal and transverse planes were defined through the identified landmarks. The planes on the hard-tissue included the nasion transverse plane (nTr), rhinion transverse plane (rhiTr), nasospinale transverse plane (nsTr), left alare sagittal plane (alLSa), right alare sagittal plane (alRSa), nasion coronal plane (nCor), rhinion coronal plane (rhiCor). A total of seven hard-tissue planes, described in Table 1 in supplementary material and illustrated in Fig. 2, were used. The planes on the soft-tissue included the pronasale transverse plane (pnTr), left alare transverse plane (alLTr), subnasale transverse plane (snTr), subnasale coronal plane (snCor), pronasale coronal plane (pnCor), left alare sagittal plane (alLSa), right alare sagittal plane (alRSa), left alare coronal plane (alLCor). A total of eight soft-tissue planes, described in Table 1 in Supplementary material and illustrated in Fig. 3, were used. All measurements (M) were calculated as distances (in mm) between parallel planes. Thanks to the reslicing this reduces to taking absolute differences between the x, y or z coordinate value defining the plane.

The hard-tissue measurements included the nasal dimensions: nasal width, nasal height, nasal bone length, nasal bone projection and nasal bone angle. Only the nasal bone angle measurement was calculated using 3D hand tools. In order to represent the soft-tissue, measurements between the pn' and sn' planes (pnTr, pnCor, snTr, snCor) and each hard-tissue plane (nTr and nCor) were determined

Table 1
South African sample used.

Complete sample		Black South Africans			White South Africans		
N	Age	Male	Female	Age	Male	Female	Mean age
120	Mean: 27.15 (SD: 8.12)	37	23	Mean: 27.70 (SD: 7.18)	32	28	Mean: 26.25 (SD:9.1)

Table 2
Definition and abbreviation of craniometric and capulometric landmarks used [23,24].

	Landmarks	Abbreviation	Definition
Craniometric	Nasion	n	Intersection of the nasofrontal sutures in the median plane.
	Rhinion	rhi	Most rostral (end) point on the internasal suture. Cannot be determined accurately if nasal bones are broken distally.
	Nasospinale	ns	The point where a line drawn between the inferior most points of the nasal aperture crosses the median plane. Note that this point is not necessarily at the tip of the nasal spine.
	Alare	al	Instrumentally determined as the most lateral point on the nasal aperture in a transverse plane.
Capulometric	Pronasale	Pn'	The most anteriorly protruded point of the apex nasi. In the case of a bifid nose, the more protruding tip is chosen.
	Subnasale	Sn'	Median point at the junction between the lower border of the nasal septum and the philtrum area.
	Alare	Al'	The most lateral point on the nasal ala.

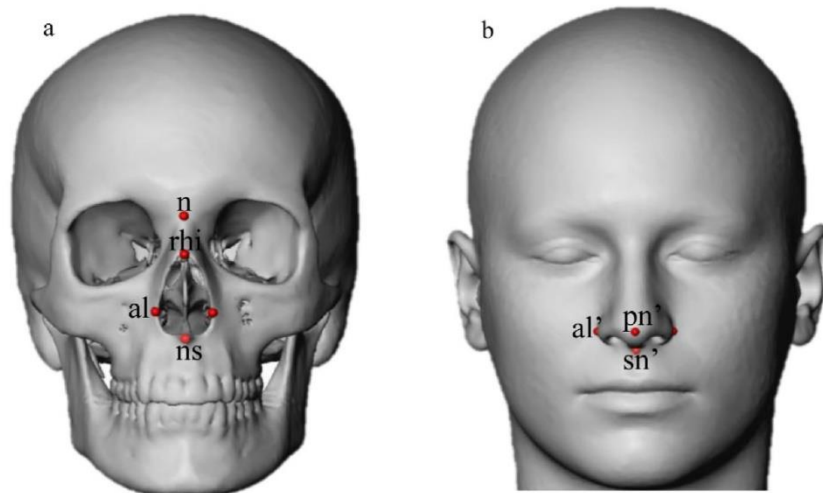


Fig. 1. Landmarks placed on the hard- and soft-tissue.
n, nasion; rhi, rhinion; ns, nasospinale; al, alare; pn', pronasale; sn', subnasale; al', alare (cf. Table 2).

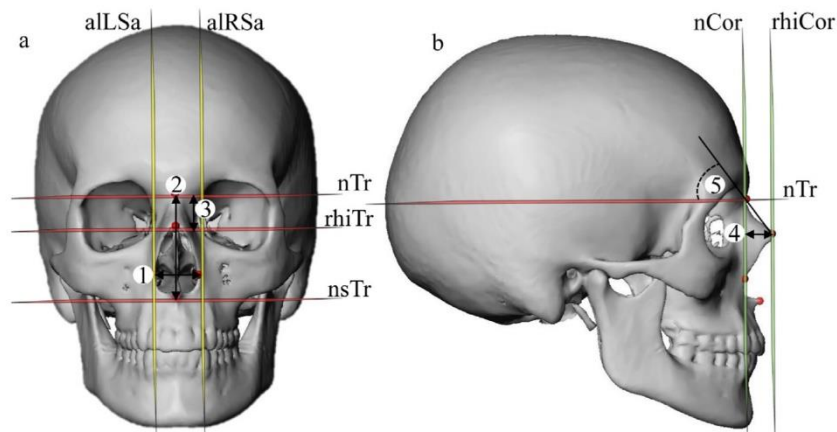


Fig. 2. Hard-tissue transverse, sagittal and coronal planes and measurements.
(a) Frontal view of the hard-tissue planes and measurements: nTr, nasion transverse plane; rhiTr, rhinion transverse plane; nsTr, nasospinale transverse plane; alSa, alare sagittal plane (left and right); 1, nasal width; 2, nasal height; 3, nasal bone length.
(b) Lateral view of the hard-tissue planes and measurements: nCor, nasion coronal plane; rhiCor, rhinion coronal plane; 4, nasal bone projection; 5, nasal bone angle (cf. Table 1 in Supplementary material).

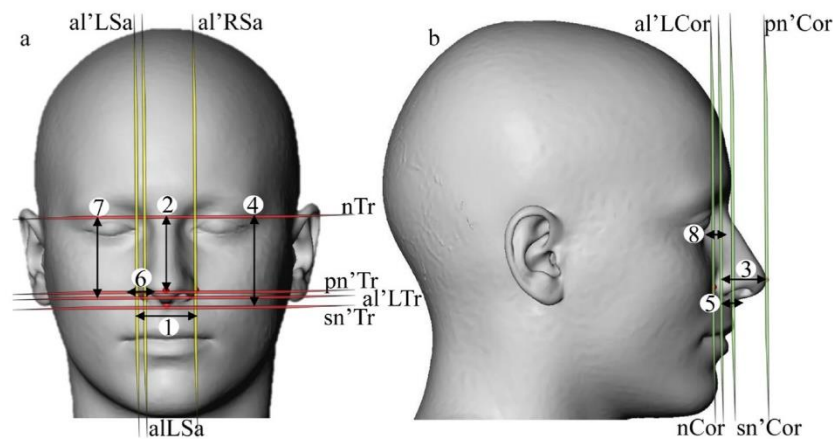


Fig. 3. Soft-tissue transverse, sagittal and coronal planes and measurements.

(a) Frontal view of the soft-tissue planes and measurements: nTr, nasion transverse plane; pnTr, pronasale transverse plane; alTr, alare transverse plane (left); snTr, subnasale transverse plane; al'Sa, alare sagittal plane (left and right); 1, alare width; 2, pronasale to nasion transverse plane; 4, subnasale to nasion transverse plane; 6, alare to right nasal cavity sagittal plane; 7, alare to nasion transverse plane.

(b) Lateral view of the soft-tissue planes and measurements: nCor, nasion coronal plane; sn'Cor, subnasale coronal plane; al'Cor, alare coronal plane (left); pn'Cor, pronasale coronal plane; 3, pronasale to nasion coronal plane; 5, subnasale to nasion coronal plane; 8, alare to nasion coronal plane (cf. Table 1 in Supplementary material).

as well as between the al' planes (al'LSa, al'LTr and al'LCor) and each hard-tissue reference plane (alLSa, nTr, and nCor). The Alare width was measured by using the al'LSa and al'RSa planes. A total of 13 measurements described in Table 1 in Supplementary material and illustrated in Figs. 2 and 3 were recorded.

2.1. Statistical analysis

In order to assess reproducibility and to have a quantification of errors induced, a test of the repeatability of the digitization in terms of inter- and intra-observer errors was performed. The method error (ME) of the double registration of all measurements was calculated using Dahlberg's [25] formula:

$$ME = \sqrt{\frac{\sum_{i=1}^n d_i^2}{2n}}$$

where d is the difference between two measurements and n is the number of subjects. For the inter-observer error, the images from 20 subjects (10 males and 10 females) were selected randomly and the measurements were performed twice by two different observers. For the intra-observer error, the images from 10 subjects (5 males and 5 females) were selected and the measurements were recorded twice with an interval of two weeks. According to the craniometric literature [26], an error will be considered acceptable in this study if the deviation is less than 2 mm. The Bland–Altman [27] plot was used to visually assess the degree of agreement between observers. In this method, the difference between the measurements is plotted against their mean. Additionally, lines corresponding to bias (defined as the mean (over all measurements) difference) and lower and upper limits of a 95% Confidence interval (CI) are plotted as well.

In order to assess the normality of the measurements, the Shapiro Wilk test was used. Means and standard deviations of measurements were computed in each South African group. An independent t-test was used to test for differences between sexes and ancestry. In order to determine whether the hard-tissue structure correlated to the soft-tissue of the nose, Pearson correlation analysis between measurements representing the position of the nose was applied. In addition, stepwise multiple

regression analysis was used to determine whether skeletal-tissue measurements were able to predict the external surface measurements. The performance of equation regressions was assessed by estimating the mean squared error (MSE) using leave-one-out cross-validation (LOOCV). The MSE is estimated from the training data and comparing it to the MSE of the predicted data (MSEP) [28]. Validation of the regression equations was also performed by using a 10-fold cross-validation process [29,30]. In each round, 90% of the subjects were used for training and 10% of the subjects are used for testing. The tests were repeated 10 times so that every subject had been tested once.

Significance was set at $p < 0.05$ for all tests. All statistical analyses were carried out with the R-studio software, version 1.0.44-⁸⁸2009-2016 for Windows [31].

3. Results

According to the Shapiro Wilk test for multivariate normality, the sample is distributed normally (Shapiro Wilk test: p -value = 0.2). Separate tests of univariate normality for each measurement were also performed (Table 1 in Supplementary material). The inter- and intra-observer tests showed that all measurements were reproducible (Table 1 in Supplementary material). Bland and Altman plots of the inter- and intra-observer errors are in Figs. 1 and 2 in Supplementary material. These plots show that, apart from a limited number of outliers, the measurements for the inter- and intra-observations were located within the 95% CI, visually indicating a high degree of inter- and intra-observer agreement.

The means and standard deviations of the measurements involving pn', sn', and al' for the South African sample are given in Tables 3 and 4. All hard- and soft-tissue measurements were significantly different between black and white South Africans (see Table 3), except for the distance between the pronasale to the nasion transverse plane and the distance between the alare to the nasion coronal plane. On account of these differences black and white South Africans were analysed separately (Table 4). For black South Africans, males and females were significantly different for nasal height and distances: pn' to nTr, sn' to nTr, al' to alLSa and nTr, whereas white South Africans males and females were significantly different for the nasal

Table 3
Means and standard deviations of the measurements in mm for the South African sample.

Measurements			Male		Female		Population difference
	Mean	SD	Mean	SD	Mean	SD	p-Value
Nasal width	25.86	2.79	26.39	2.39	25.11	3.08	0.00
Nasal height	50.68	3.76	52.05	3.83	49.05	2.96	0.04
Nasal bone length	19.39	3.54	20.03	3.61	18.62	3.33	0.01
Nasal bone projection	10.25	4.13	9.43	4.08	11.21	4.02	0.00
Nasal bone angle (°)	66.70	7.69	68.55	7.15	64.52	7.79	0.00
Alare width	39.63	6.00	42.15	5.35	36.64	5.34	0.00
Alare width/nasal width	153.72	18.23	160.09	18.29	146.25	15.37	0.00
Pronasale to nasion transverse plane	41.12	4.87	42.88	5.01	39.04	3.78	0.36
Pronasale to nasion coronal plane	28.90	7.21	28.04	7.90	29.91	6.22	0.00
Subnasale to nasion transverse plane	52.83	4.78	54.20	5.16	51.19	3.73	0.01
Subnasale to nasion coronal plane	14.87	7.18	13.40	7.51	16.60	6.40	0.00
Alare to left alare sagittal plane	6.76	2.39	7.63	2.42	5.73	1.92	0.00
Alare to nasion transverse plane	45.84	4.64	47.21	4.92	44.20	3.70	0.00
Alare to nasion coronal plane	6.60	3.84	5.81	3.25	7.52	4.34	0.34

Significant values ($p < 0.05$) are indicated in bold.

Table 4
Means and standard deviations of the measurements in mm for the black and white South African sample.

Measurements	Black South Africans					White South Africans				
	Male		Female		Sex difference	Male		Female		Sex difference
	Mean	SD	Mean	SD	p-Value	Mean	SD	Mean	SD	p-Value
Nasal width	27.34	2.28	27.83	1.94	0.37	25.13	1.95	23.17	2.13	0.00
Nasal height	51.28	3.32	47.91	2.32	0.00	53.07	4.27	49.87	3.14	0.00
Nasal bone length	20.69	3.51	19.38	2.62	0.10	19.16	3.61	18.08	3.71	0.25
Nasal bone projection	7.66	4.07	8.40	3.22	0.44	11.78	2.72	13.24	3.27	0.06
Nasal bone angle (°)	70.66	7.07	67.08	6.95	0.57	65.76	6.35	62.68	7.95	0.75
Alare width	45.78	3.52	42.06	2.95	0.33	37.34	3.06	32.74	2.47	0.00
Alare width/nasal width	168.17	14.52	151.56	11.23	0.34	149.41	17.14	142.44	16.92	0.00
Pronasale to nasion transverse plane	42.47	4.84	37.89	3.63	0.00	43.42	5.27	39.87	3.72	0.00
Pronasale to nasion coronal plane	23.97	7.27	25.46	5.22	0.36	33.41	4.98	33.11	4.78	0.81
Subnasale to nasion transverse plane	53.19	5.06	49.51	3.30	0.00	55.54	5.06	52.40	3.59	0.00
Subnasale to nasion coronal plane	10.10	7.48	13.72	6.96	0.06	17.77	4.94	18.67	5.14	0.49
Alare to left alare sagittal plane	8.65	2.22	6.97	1.67	0.00	6.27	1.98	4.83	1.57	0.00
Alare to nasion transverse plane	46.12	4.72	42.30	3.58	0.00	48.65	4.88	45.57	3.19	0.00
Alare to nasion coronal plane	6.02	3.04	6.64	4.33	0.55	5.54	3.54	8.15	4.31	0.01

Significant values ($p < 0.05$) are indicated in bold.

Table 5
Correlation coefficient between hard- and soft-tissue measurements in mm of the black South African sample.

Measurements	Black South Africans				
	Nasal width	Nasal height	Nasal bone length	Nasal bone projection	Nasal bone angle
Pn' to nTr	0.08	0.80	-0.14	0.03	-0.24
Pn' to nCor	0.08	-0.05	0.69	0.15	0.16
Sn' to nTr	0.07	0.80	0.73	0.15	-0.24
Sn' to nCor	-0.01	-0.26	-0.24	0.53	0.26
Al' to allSa	-0.30	0.02	-0.16	0.09	0.28
Al' to nTr	0.08	0.74	0.65	0.08	-0.16
Al' to nCor	-0.10	-0.21	-0.29	0.17	0.15

Significant correlations ($p < 0.05$) are indicated in bold.

width, nasal height, alare width, alare width/nasal width, and distances: pn' to nTr, sn' to nTr, al' to allSa, al' to nTr and nCor.

Correlations of the hard- and soft-tissue dimensions with the capulometric landmarks: pn', sn', and al' in black South Africans are shown in Table 5 and white South Africans in Table 6. In both groups, the measurements of pn' to nTr, sn' to nTr, and al' to nTr, indicating the inferosuperior position of the pronasale, subnasale, and alare, respectively, showed significant correlations with the nasal height and nasal bone length. The measurement of sn' to nCor, highlighting the anteroposterior position of the subnasale, also showed a significant correlation with the nasal bone projection in both groups, while the measurement of pn' to

nCor distinguishing the anteroposterior position of the pronasale showed a significant correlation with the nasal bone projection only in white South Africans. In addition, the measurement of pn' to nCor showed a significant correlation with the nasal bone length only in black South Africans. The measurements of the al' to allSa and al' to nCor respectively indicating the inferosuperior and anteroposterior position of the Alare, did not show significant correlations with any skeletal measurements in both groups. Finally, the nasal width and the nasal bone angle did not correlate significantly with any surface measurements in both groups. All significant correlations were used in creating stepwise multiple regression equations for

Table 6

Correlation coefficient between hard- and soft-tissue measurements in mm of the white South African sample.

Measurements	White South Africans				
	Nasal width	Nasal height	Nasal bone length	Nasal bone projection	Nasal bone angle
Pn' to nTr	0.31	0.80	0.76	0.05	-0.27
Pn' to nCor	0.11	0.19	-0.24	0.69	-0.07
Sn' to nTr	0.24	0.86	0.71	0.18	-0.20
Sn' to nCor	0.02	0.04	-0.31	0.64	-0.05
Al' to allSa	-0.20	0.07	0.01	-0.20	-0.07
Al' to nTr	0.33	0.81	0.64	0.09	-0.26
Al' to nCor	-0.07	-0.13	-0.42	0.49	0.07

Significant correlations ($p < 0.05$) are indicated in bold.**Table 7**

Stepwise multiple regression equations for predicting nose position of the black South African sample.

Black South Africans equation regression						Cross-validation			
		SE	R ²	p-Value	Black sample		White sample		
					MSE	Accuracy	MSE	Accuracy	
Pronasale	Pn to NaTr = -17.805 + 1.170*Nasal height	5.69	0.64	0.00	1.89	88%	2.55	82%	
	Pn to NaCor = 30.403 - 0.290*Nasal bone length	5.37	0.02	0.00	2.17	97%	8.31	87%	
Subnasale	Sn to NaTr = -5.208 + 1.140*Nasal height	0.11	0.64	0.00	1.83	87%	1.89	78%	
	Sn to NaTr = 29.723 + 1.092*Nasal bone length	2.67	0.54	0.00	1.82	91%	4.02	89%	
	Sn to NaTr = 1.270 + 0.795*Nasal height + 0.531*Nasal bone length	0.13	0.71	0.00	1.75	80%	2.32	70%	
	Sn to NaCor = 3.063 + 1.060*Nasal bone projection	0.22	0.28	0.00	2.43	100%	3.30	87%	
Alare	Al to NaTr = -7.148 + 1.036*Nasal height	0.12	0.56	0.00	1.79	84%	2.11	78%	
	Al to NaTr = 25.608 + 0.943*Nasal bone length	2.93	0.42	0.00	1.86	88%	4.16	83%	
	Al to NaTr = -2.369 + 0.782*Nasal height + 0.391*Nasal bone length	0.15	0.61	0.00	1.88	88%	2.41	83%	

SEE, standard errors of the estimates; R², coefficient of determination. Significant values ($p < 0.05$) are indicated in bold. Mean squared error (MSE) using leave-one-out cross-validation and the accuracies of the regression equations using k-folds cross-validation.**Table 8**

Stepwise multiple regression equations for predicting nose position of the white South African sample.

White South Africans						Cross-validation			
		SE	R ²	P-value	White sample		Black sample		
					MSE	Accuracy	MSE	Accuracy	
Pronasale	Pn to NaTr = -7.969 + 0.963*Nasal height	0.09	0.64	0.00	1.79	90%	2.36	82%	
	Pn to NaTr = 22.859 + 1.004*Nasal bone length	2.09	0.58	0.00	1.80	86%	3.56	84%	
	Pn to NaTr = -1.341 + 0.633*Nasal height + 0.554*Nasal bone length	0.11	0.74	0.00	1.77	83%	2.27	82%	
	Pn to NaCor = 19.616 + 1.085*Nasal bone projection	1.90	0.48	0.00	1.90	98%	4.95	92%	
Subnasale	Sn to NaTr = 2.950 + 0.991*Nasal height	0.07	0.75	0.00	1.52	86%	2.44	80%	
	Sn to NaTr = 37.287 + 0.891*Nasal bone length	2.16	0.51	0.00	1.78	92%	4.08	88%	
	Sn to NaTr = 6.850 + 0.797*Nasal height + 0.326*Nasal bone length	0.09	0.79	0.00	1.24	79%	2.54	70%	
	Sn to NaCor = 5.055 + 1.050*Nasal bone projection	0.16	0.41	0.00	1.94	100%	5.70	91%	
Alare	Al to NaTr = 1.974 + 0.876*Nasal height	0.08	0.66	0.00	1.53	82%	2.61	79%	
	Al to NaTr = 32.924 + 0.757*Nasal bone length	2.23	0.41	0.00	2.77	89%	4.16	83%	
	Al to NaTr = 4.779 + 0.737*Nasal height + 0.234*Nasal bone length	0.10	0.68	0.00	1.95	88%	2.68	83%	

SEE, standard errors of the estimates; R², coefficient of determination. Significant values ($p < 0.05$) are indicated in bold. Cross-validation testing, mean squared error (MSE) using leave-one-out cross-validation and the accuracies of the regression equations using k-folds cross-validation.

predicting the morphology of the nose of black and white South Africans.

Regression equations (Figs. 3 and 4 in Supplementary material) and the results of cross-validations for black and white South Africans are described in Tables 7 and 8. From these regression equations, the nasal height and the nasal bone length were found to be significant predictors of the pronasale, subnasale and alare positions, while the nasal bone projection appeared as a consistent predictor only for the subnasale position in black and white South Africans. In addition, the nasal bone projection was also a consistent predictor for the pronasale position in white South Africans. The MSE for the regression equations of black South

Africans ranged between 1.75 and 2.43 mm, and for white South Africans between 1.24 and 2.77 mm. The cross-validated accuracies for regression equations of black South Africans ranged between 87% and 100%, and for white South Africans between 79% and 100%. A cross-validation was also performed by applying the regression models (black/white South Africans) of one group to the other group (black/white South Africans). The regression equations of white South Africans applied to the black South African sample showed a MSE ranging between 2.27 and 5.70 mm and, between 1.89 and 8.31 mm when the black South Africans regression equations were applied to the white South African sample. The regressions equations of white South Africans applied to the black

South African sample showed accuracies ranging between 70% and 89% and, between 70% and 91% when the black South Africans regression equations were applied to the white South African sample.

4. Discussion

In the process of approximating the nose, factors such as age, sex and ancestry must be considered. The growth and development of the human craniofacial skeleton results from the interdependence of its different components, which are influenced by multifactorial processes involving hormonal, genetic and epigenetic factors; and external stimuli (soft-tissue growth, dental maturation and various biomechanical factors) [32–43].

In forensic anthropology, estimation of ancestry from unknown skeletal remains is important for the development of a biological profile [44]. Ousley et al. [45] demonstrated that the morphological variability among population groups is quantifiable and may be useful in providing a probable classification of an unknown person. Data on the nose are also relevant to South African forensic artists and forensic anthropologists, especially in profile view to enhance facial recognition.

From the findings in this study, nasal height and nasal bone length might play important roles in the prediction of the shape of the nose in the frontal view in South Africans. The extent of nasal bone projection, on the other hand, could prove useful for the shape of the South African nose on profile views. Therefore, the morphology of the nose based on the pronasale, subnasale and alare positions, can potentially be estimated in an unknown black or white South African skull from the measurements of the nasal height, nasal bone length and nasal bone projection.

Although the nasal height, nasal bone length and nasal bone projection were significant and reproducible predictors for some of the positions of pn', sn' and al' in South Africans, not all surface landmark positions correlated significantly with the related hard-tissues. It is interesting to note that the nasal width and the nasal bone angle did not show any correlations with the external surface of the nose in both South African groups, while for the Korean population, all positions of the surface landmarks on the nose showed statistically significant correlations with the nasal bone and nasal aperture structure [19]. The value of our findings in the prediction of the al' by regression equations in both groups are limited. Indeed, the prediction on the alare relied only on a single vertical height measurement (al' to nTr) and not on any of the antero-posterior and lateral measurements.

From the recent literature, distinct differences in mid-facial size and shape have already been observed among all South Africans groups [46–48]. Indeed, in several osteometric analyses, some discrete traits from the mid-face, such as nasal width, inter-orbital breadth, nasal bone structure and alveolar prognathism have been shown to have a significant relationship with ancestry for South African groups [46–52]. Our findings confirm that a significant hard- and soft-tissue morphological difference exists between black and white South Africans. The variation in the skeletal predictors of the external shape of the nose noted between black and white South Africans and the results of the cross-validation testing, emphasize the need for population specific guidelines and highlight the importance of considering ancestry as a factor in the process of approximating the nose. Variation in nasal hard- and soft-tissue morphologies has been described in other populations as well [14]. For instance, a highly significant difference of hard- and soft-tissue nasal shapes between Chinese and Europeans exists. While the nasal complexes in Chinese are smoother and incorporated into the skull, the European nasal shapes are quite prominent [14]. The failure of consideration of ancestral variation when developing approximation approaches may impact the accuracy of the final facial reconstruction.

Dimensions of the nose are important in distinguishing male and female faces and are useful in establishing an accurate facial approximation of a missing person through craniofacial reconstruction [4]. Although distinct differences in mid-facial morphology (size and shape) between the sexes are shown in many research studies [14,19,46,48,53,54], this may be less pronounced in the black South African group because of lower levels of sexual dimorphism in the cranium [46,47]. More precisely, these researchers observed that black South African males had a greater tendency for “intermediate” or “wide” nasal width and inter-orbital breadth than black South African females. In this study, the statistical analysis of sex differences in each group has shown a more important sexual dimorphism in white South Africans than in the black South African sample. It is important to emphasize that the findings on sexual dimorphism may to some extent be impacted by the sex split in each sample (60 black (23 females and 37 males) and 60 white (28 females and 32 males)). The differences between sexes observed confirm that growth for males and females is different. At birth, a slight sexual dimorphism exists, but the major divergence does not occur until puberty. As the adolescent growth spurt occurs approximately two years earlier in females than in males a longer development in males is induced, creating a significant sexual dimorphism in many body measures and therefore variations in the dimensions of the nose are not unexpected [4,33,41].

Currently, forensic artists in South Africa follow specific guidelines of soft-tissue thicknesses based on North American cadaver studies. Studies based on cadavers are influenced by desiccation, secular trends and population specificity, and the combination of these factors may affect the accuracy and validity of facial approximations in South Africa. As in the study by Lee et al. [19], we specifically used CBCT scans from living patients since we intended to remove the limits generated by the use of dry skulls, cadavers and CT datasets as initial references, such as desiccation and supination effects. A further advantage of CBCT compared to CT includes higher spatial resolution (0.1 mm–0.4 mm) and isotropic volumetric data for the accurate placement of 3D landmarks and planes as required for this study [18].

An attempt was made to enhance the reproducibility and therefore the precision of the measurements by incorporating interplane distances, using coordinate values in the correlation between hard- and soft-tissue dimensions. In addition, great care was taken in the 3D head orientation by using a reslicing process following the FH planes. The utilization of coordinate values allows us to overcome the limits generated by the utilization of 3D hand tools such as the 3D head orientation during measurements.

The methodology resulting from this preliminary study on a South African sample needs to be applied to different populations and compared more intensively with other methods before it could be considered robust. In this study, we selected young adults in order to exclude possible remodelling effects of the facial skeleton with the advancement of age. When planning future research, it would be interesting to include more individuals of different age classes with a distinction between the sexes in order to observe possible effects of these factors on the approximation of the nose and their possible significant relationship with ancestry. The utilization of CBCT scans from living patients negated the effects of desiccation and supination and provided a higher spatial resolution for the placement of 3D landmarks. It is important to emphasize that the measurement error is probably underestimated because single scans were re-measured, without rescanning the same subject.

5. Conclusion

The morphology of the nose based on the pronasale, subnasale and alare positions was found to have the potential to be estimated

in an unknown black and white South African skull. From the findings, black and white South Africans, had significantly different hard- and soft-tissue morphology inducing the need for specific regression equations for both South African groups.

This study provides a possible reliable and reproducible method using CBCT scans and illustrates the importance of considering factors such as sex and ancestry in the process of approximating the nose.

Acknowledgements

The authors would like to thank Dr. André Uys from the Oral and Dental Hospital, University of Pretoria, South Africa and Dr. Sarel Botha from the Life Groenkloof Hospital, Pretoria, South Africa, for providing the CBCT-data. We acknowledge the AESOP+ consortia coordinated by Prof. José Braga from the Computer-assisted Palaeoanthropology Team, UMR 5288 CNRS- Université Paul-Sabatier, 37, allées Jules-Guesde, 31000 Toulouse, and from the Evolutionary Studies Institute and School of Geosciences, University of the Witwatersrand, Johannesburg, South Africa, for the financial support. We also thank the three anonymous reviewers for their constructive comments.

Appendix A. Supplementary data

Supplementary data associated with this article can be found, in the online version, at <https://doi.org/10.1016/j.forsciint.2018.05.011>.

References

- [1] V. Bruce, G.W. Humphreys, Recognizing objects and faces, *Vis. Cogn.* 1 (April (2–3)) (1994) 141–180, doi:<http://dx.doi.org/10.1080/13506289408402299>.
- [2] S.H. Jeng, H.Y.M. Liao, C.C. Han, M.Y. Chern, Y.T. Liu, Facial feature detection using geometrical face model: an efficient approach, *Pattern Recognit.* 31 (March (3)) (1998) 273–282, doi:[http://dx.doi.org/10.1016/S0031-3203\(97\)00048-4](http://dx.doi.org/10.1016/S0031-3203(97)00048-4).
- [3] W. Zhao, R. Chellappa, P.J. Phillips, A. Rosenfeld, Face recognition: a literature survey, *ACM Comput. Surv.* 35 (December (4)) (2003) 399–458, doi:<http://dx.doi.org/10.1145/954339.954342>.
- [4] E.P. Chronicle, M.Y. Chan, C. Hawkins, K. Mason, K. Smethurst, K. Stallybrass, You can tell by the nose—judging sex from an isolated facial feature, *Perception* 24 (8) (1995) 969–973, doi:<http://dx.doi.org/10.1068/p240969>.
- [5] W. Krogman, M. İşcan, *The Human Skeleton in Forensic Medicine*, 2nd edition, Charles C. Thomas, Springfield, IL, 1986.
- [6] M.M. Gerasimov, *Face Finder*, CRC Press, NY, NY, 1971.
- [7] R. George, The lateral craniographic method of facial reconstruction, *J. Forensic Sci.* 32 (5) (1987) 1305–1330, doi:<http://dx.doi.org/10.1520/JFS11181> ISSN 0022-1198.
- [8] M. Prokopc, D.H. Ubelaker, Reconstructing the shape of the nose according to the skull, *Forensic Sci. Commun.* 4 (1) (2002). <https://archives.fbi.gov/archives/about-us/lab/forensic-science-communications/fsc/jan-2002/prokopc.htm>.
- [9] C.N. Stephan, M. Henneberg, W. Sampson, Predicting nose projection and pronasale position in facial approximation: a test of published methods and proposal of new guidelines, *Am. J. Phys. Anthropol.* 122 (3) (2003) 240–250, doi:<http://dx.doi.org/10.1002/ajpa.10300>.
- [10] C. Rynn, C.M. Wilkinson, Appraisal of traditional and recently proposed relationships between the hard and soft dimensions of the nose in profile, *Am. J. Phys. Anthropol.* 130 (July (3)) (2006) 364–373, doi:<http://dx.doi.org/10.1002/ajpa.20337>.
- [11] T.W. Todd, A. Lindala, Thickness of the subcutaneous tissues in the living and the dead, *Am. J. Anat.* 41 (2) (1928) 153–196, doi:<http://dx.doi.org/10.1002/aja.1000410202>.
- [12] G.A. Macho, An appraisal of plastic reconstruction of the external nose, *J. Forensic Sci.* 31 (4) (1986) 1391–1403, doi:<http://dx.doi.org/10.1002/aja.1000410202>.
- [13] F.M. Tilotta, J.A. Glaunès, F.J. Richard, Y. Rozenholc, A local technique based on vectorized surfaces for craniofacial reconstruction, *Forensic Sci. Int.* 200 (1) (2010) 50–59, doi:<http://dx.doi.org/10.1016/j.forsciint.2010.03.029>.
- [14] S. Schlager, *Soft-tissue Reconstruction of the Human Nose, Population Differences and Sexual Dimorphism*, Dissertation, Albert-Ludwigs-Universität de Fribourg, 2013. <http://d-nb.info/1120020522>.
- [15] P. Guyomarç'h, B. Dutailly, J. Charton, F. Santos, P. Desbarats, H. Coqueugnot, Anthropological facial approximation in three dimensions (AFA3D): computer-assisted estimation of the facial morphology using geometric morphometrics, *J. Forensic Sci.* 59 (6) (2014) 1502–1516, doi:<http://dx.doi.org/10.1111/1556-4029.12547>.
- [16] N. Iblher, E. Gladilin, B.G. Stark, Soft-tissue mobility of the lower face depending on positional changes and age: a three-dimensional morphometric surface analysis, *Plast. Reconstr. Surg.* 131 (2013) 372–381, doi:<http://dx.doi.org/10.1097/PRS.0b013e318278d67c>.
- [17] F. Marin, K. Ben Mansour, F. Demeter, P. Frey, Displacement of facial soft tissues in upright versus supine positions, *Comput. Methods Biomech. Biomed. Eng.* (2015), doi:<http://dx.doi.org/10.1080/10255842.2015.1069590>.
- [18] W.C. Scarfe, A.G. Farman, What is cone-beam CT and how does it work? *Dent. Clin. North Am.* 52 (2008) 707–730, doi:<http://dx.doi.org/10.1016/j.cden.2008.05.005>.
- [19] K.M. Lee, W.J. Lee, J.H. Cho, H.S. Hwang, Three-dimensional prediction of the nose for facial reconstruction using cone-beam computed tomography, *Forensic Sci. Int.* 236 (2014) 194–e1, doi:<http://dx.doi.org/10.1016/j.forsciint.2013.12.035>.
- [20] J. Shindelin, I. Arganda-Carreras, E. Frise, Fiji: an open-source platform for biological-image analysis, *Nat. Methods* 9 (7) (2012) 676–682, doi:<http://dx.doi.org/10.1038/nmeth.2019> PMID 22743772.
- [21] A. Fedorov, R. Beichel, J. Kalpathy-Cramer, J. Finet, J.C. Fillion-Robin, S. Pujol, C. Bauer, D. Jennings, F. Fennessy, M. Sonka, J. Buatti, S.R. Aylward, J.V. Miller, S. Pieper, R. Kikinis, 3D slicer as an image computing platform for the quantitative imaging network, *Magn. Reson. Imaging* 30 (November (9)) (2012) 1323–1341, doi:<http://dx.doi.org/10.1016/j.mri.2012.05.001> PMID: 22770690.
- [22] C.F. Spoor, F.W. Zonneveld, G.A. Macho, Linear measurements of cortical bone and dental enamel by computed tomography: applications and problems, *Am. J. Phys. Anthropol.* 91 (4) (1993) 469–484, doi:<http://dx.doi.org/10.1002/ajpa.1330910405>.
- [23] J. Buikstra, D. Ubelaker, Standards for data collection from human skeletal remains: Proceedings of a seminar at the Field Museum of Natural History (Arkansas Archaeology Research Series 44), Fayetteville Arkansas Archaeological Survey, 1994.
- [24] J. Caple, C.N. Stephan, A standardized nomenclature for craniofacial and facial anthropometry, *Int. J. Leg. Med.* 130 (3) (2016) 863–879, doi:<http://dx.doi.org/10.1007/s00414-015-1292-1>.
- [25] G. Dahlberg, *Statistical Methods for Medical and Biological Students*, (1940).
- [26] G. Brüner, R. Knussman, Grundlagen der Osteometrie, in: R. Knussman, R. Martin (Eds.), *Anthropologie, Handbuch der vergleichenden Biologie des Menschen*, Fisher, Stuttgart, New York, 1988, pp. 129–159.
- [27] J.M. Bland, D.G. Altman, Comparing methods of measurement: why plotting difference against standard method is misleading, *Lancet* 346 (8982) (1995) 1085–1087, doi:[http://dx.doi.org/10.1016/S0140-6736\(95\)91748-9](http://dx.doi.org/10.1016/S0140-6736(95)91748-9).
- [28] B.H. Mevik, H.R. Cederkvist, Mean squared error of prediction (MSEP) estimates for principal component regression (PCR) and partial least squares regression (PLSR), *J. Chemom.* 18 (9) (2004) 422–429, doi:<http://dx.doi.org/10.1002/cem.887>.
- [29] P. Burman, A comparative study of ordinary crossvalidation, v-fold cross-validation and the repeated learning-testing methods, *Biometrika* 76 (1989) 503–514, doi:<http://dx.doi.org/10.1093/biomet/76.3.503>.
- [30] R. Kohavi, A study of cross-validation and bootstrap for accuracy estimation and model selection, *Ijcai* 14 (2) (1995). <https://pdfs.semanticscholar.org/0be0/d781305750b37acb35fa187febd8db67bfcc.pdf>.
- [31] R. Core Team, *R: A Language and Environment for Statistical Computing*, R Foundation for Statistical Computing, Vienna, Austria, 2012. <http://www.R-project.org>.
- [32] M.L. Moss, R.W. Young, A functional approach to craniology, *Am. J. Phys. Anthropol.* 18 (4) (1960) 281–292, doi:<http://dx.doi.org/10.1002/ajpa.1330180406>.
- [33] D.H. Enlow, M.G. Hans, *Essentials of Facial Growth*, W.B. Saunders Company, 1996.
- [34] M.L. Moss, The functional matrix hypothesis revisited. 1, the role of mechanotransduction, *Am. J. Orthod. Dentofac. Orthop.* 112 (1) (1997) 8–11, doi:[http://dx.doi.org/10.1016/S0889-5406\(97\)70267-1](http://dx.doi.org/10.1016/S0889-5406(97)70267-1).
- [35] M.L. Moss, The functional matrix hypothesis revisited. 2, the role of an osseous connected cellular network, *Am. J. Orthod. Dentofac. Orthop.* 112 (2) (1997) 221–226, doi:[http://dx.doi.org/10.1016/S0889-5406\(97\)70249-X](http://dx.doi.org/10.1016/S0889-5406(97)70249-X).
- [36] M.L. Moss, The functional matrix hypothesis revisited. 3, the genomic thesis, *Am. J. Orthod. Dentofac. Orthop.* 112 (3) (1997) 338–342, doi:[http://dx.doi.org/10.1016/S0889-5406\(97\)70265-8](http://dx.doi.org/10.1016/S0889-5406(97)70265-8).
- [37] M.L. Moss, The functional matrix hypothesis revisited. 4, the epigenetic antithesis and the resolving synthesis, *Am. J. Orthod. Dentofac. Orthop.* 112 (4) (1997) 410–417, doi:[http://dx.doi.org/10.1016/S0889-5406\(97\)70049-0](http://dx.doi.org/10.1016/S0889-5406(97)70049-0).
- [38] D.E. Lieberman, B.M. McBratney, G. Krovitz, The evolution and development of cranial form in Homo sapiens, *Proc. Natl. Acad. Sci. U. S. A.* 99 (3) (2002) 1134–1139, doi:<http://dx.doi.org/10.1073/pnas.022440799>.
- [39] C.P. Klingenberg, K. Mebus, J. Auffray, Developmental integration in a complex morphological structure: how distinct are the modules in the mouse mandible? *Evol. Dev.* 5 (5) (2003) 522–531, doi:<http://dx.doi.org/10.1046/j.1525-142X.2003.03057.x>.
- [40] Y. Tomoyasu, T.T.A. Yamaguchi Tajima, T. Nakajima, I. Inoue, K. Maki, Further evidence for an association between mandibular height and the growth hormone receptor gene in a Japanese population, *Am. J. Orthod. Dentofac. Orthop.* 136 (4) (2009) 536–541, doi:<http://dx.doi.org/10.1016/j.ajodo.2007.10.054>.
- [41] D. Lieberman, *The Evolution of the Human Head*, Harvard University Press, 2011.
- [42] F. Grönberg, M. Fagan, P. O'higgins, Comparing the distribution of strains with the distribution of bone tissue in a human mandible: a finite element study, *Anat. Rec.* 296 (1) (2013) 9–18, doi:<http://dx.doi.org/10.1002/ar.22597>.

- [43] W.R. Atchley, B.K. Hall, A model for development and evolution of complex morphological structures, *Biol. Rev.* 66 (2) (1991) 101–157, doi:<http://dx.doi.org/10.1111/j.1469-185X.1991.tb01138.x>.
- [44] J.T. Hefner, Cranial nonmetric variation and estimating ancestry, *J. Forensic Sci.* 54 (2009) 985–995, doi:<http://dx.doi.org/10.1111/j.1556-4029.2009.01118.x>.
- [45] S. Ousley, R. Jantz, D. Freid, Understanding race and human variation: why forensic anthropologists are good at identifying race, *Am. J. Phys. Anthropol.* 139 (February (1)) (2009) 68–76, doi:<http://dx.doi.org/10.1002/ajpa.21006>.
- [46] E.N. L'Abbé, C. Van Rooyen, S.P. Nawrocki, P.J. Becker, An evaluation of non-metric cranial traits used to estimate ancestry in a South African sample, *Forensic Sci. Int.* 209 (1) (2011) 195–e1, doi:<http://dx.doi.org/10.1016/j.forsciint.2011.04.002>.
- [47] J.L. McDowell, E.N. L'Abbé, M.W. Kenyhercz, Nasal aperture shape evaluation between black and white South Africans, *Forensic Sci. Int.* 222 (1) (2012) 397–e1, doi:<http://dx.doi.org/10.1016/j.forsciint.2012.06.007>.
- [48] J.L. McDowell, M.W. Kenyhercz, E.N. L'Abbé, An evaluation of nasal bone and aperture shape among three South African populations, *Forensic Sci. Int.* 252 (2015) 189–e1, doi:<http://dx.doi.org/10.1016/j.forsciint.2015.04.016>.
- [49] M. Steyn, E.N. L'Abbé, J. Myburgh, *Forensic Anthropology as Practiced in South Africa*, Handbook of Forensic Anthropology and Archaeology, (2016).
- [50] M.Y. İscan, M. Steyn, Craniometric determination of population affinity in South Africans, *Int. J. Leg. Med.* 112 (2) (1999) 91–97, doi:[http://dx.doi.org/10.1016/S1353-1131\(99\)90011-1](http://dx.doi.org/10.1016/S1353-1131(99)90011-1).
- [51] H. De Villiers, *The Skull of the South African Negro: A Biometrical and Morphological Study*, Witwatersrand University Press, 1968.
- [52] M. Napoli, W. Birky, G. Gill, S. Rhine, Skeletal attribution of race: methods for forensic anthropology, *Skeletal Attribution of Race Methods Forensic Anthropology*, (1990).
- [53] S. Schlager, A. Rüdell, Analysis of the human osseous nasal shape—population differences and sexual dimorphism, *Am. J. Phys. Anthropol.* 157 (2015) 571–581, doi:<http://dx.doi.org/10.1002/ajpa.22749>.
- [54] P. Guyomarc'h, J. Bruzek, Dimorphisme sexuel du crâne de sujets identifiés (Collection Olivier, MNHN, Paris): évaluation par morphométrie géométrique, *Bull. Mem. Soc. Anthropol. Paris* 22 (3–4) (2010) 216–229, doi:<http://dx.doi.org/10.1007/s13219-010-0019-6>.

Chapter 6

VARIATION OF THE NASAL COMPLEX SHAPE

6.1. Introduction

The primary focus of this thesis was to provide an accurate computer-assisted method for the prediction of the nasal soft-tissue shape, based on the shape of the underlying skull substrate. One of our objectives was to find the statistical interrelationship between the hard- and soft-tissue of the nasal complex attributed to the factors ancestry, sex and age. Statistical models were created to establish the statistical relationship predictors (hard-tissue shape, ancestry, sex, age, and size (allometry)) and response variables (soft-tissue information). In order to build statistical models, an evaluation and a quantification of shape differences attributed to known factors (ancestry, sex, age and size (allometry)) and covariates were performed both on hard- and soft-tissue shapes using geometric morphometric methods.

The preliminary analysis of the linear measurements described in Chapter 5, revealed that black and white South Africans had significantly different hard- and soft-tissue morphology, illustrating the importance of considering factors such as ancestry in the process of approximating the nose. In order to confirm the findings of the preliminary analysis (Chapter 5 “Preliminary Analysis”), and to quantify the morphological differences in the nasal complex within ancestral groups in the complete sample on other skeletal elements, geometric morphometric methods were used and are detailed in chapter 6 as part of the manuscript to be submitted for publication. The analysis of covariation among nasal hard- and soft- tissue and its dependence on ancestry is also described in this chapter, as well as the quantification and visualisation of covariance between nasal complex shape and ancestry, sexual dimorphism, age and size (allometry).

The procedure of automatic placement of discrete landmarks was applied using two templates: one for black South Africans and one for white South Africans. The landmarks were indicated once on each template for both groups separately, and then projected onto each of the 400 surfaces (200 hard- tissue and 200 soft-tissue) using the warping procedure explained in Chapter 3. The coordinates of the landmarks were recorded for geometric morphometric analyses.

The impact of ancestry, sex, age and allometry on the hard- and soft-tissue within the complete sample was firstly determined. Then, in order to identify significant ancestral-specific differences, the sexual dimorphism expression, the ageing process and the impact of size (allometry) were analysed on each specific subsample (black and white subsamples) separately and on both hard- and soft- tissue. Finally, the covariation between nasal hard- and soft- tissue and its dependence on ancestry was analysed.

Preceding the shape analysis of the nasal complex on the complete sample and on each specific subsample, statistical preliminaries including the reproducibility testing, the Generalised Procrustes Analysis (GPA), the data reduction (Principal Component Analysis) and the multivariate normality testing are detailed in this chapter .

6.2. Statistical preliminaries

6.2.1. Reproducibility testing

In order to assess reproducibility and to have a quantification of errors induced, a test of the repeatability of the digitisation in terms of inter- and intra-observer errors was performed on the complete sample (400 surfaces). The procedure of automatic placement of discrete landmarks was applied using two different templates, one for each sample: black South Africans and white South Africans. The landmarks of interest were indicated once on each template for both groups separately, which were then projected onto each of the 400 surfaces (100 black hard-tissue surfaces; 100 white hard-tissue surface; 100 black soft-tissue surfaces; 100 white soft-tissue surface). The coordinates of the landmarks were then recorded. For the intra-observer errors, the landmark indication on templates was done by the same observer, with an interval of two weeks. For the inter-observer errors, the landmark indication on templates was done independently by two different observers.

The precision of the landmark positioning was calculated using the dispersion Δ_{ij} for each landmark i and individual j . Dispersion is defined as the Mean Euclidean Distance (MED) of the sample landmark \mathbf{p}_{ijk} to the mean $\bar{\mathbf{p}}_{ij}$ of the (x,y,z)-coordinates of landmark i over all observations k (INTER, INTRA, resp.) for subject j :

$$\Delta_{ij} = \sum_{k=1}^K \|\mathbf{p}_{ijk} - \bar{\mathbf{p}}_{ij}\| / K, \text{ with } \bar{\mathbf{p}}_{ij} = \sum_{k=1}^K \mathbf{p}_{ijk} / K$$

Regarding the mean results of the intra- and inter- measurement errors (ME) of craniometric and capulometric landmark positioning (Table 6.1), lower mean values were obtained for both black and white surfaces and for both hard- and soft-tissue. For black surfaces, the mean values ranged between 0.22 mm and 0.88 mm (Sd ranged between 0.02 mm and 0.11 mm), while the mean values for the white surfaces ranged between 0.23 mm and 0.77 mm (Sd ranged between 0.02 mm and 0.98 mm). The errors in landmark positioning were smaller for white than black surfaces. For the craniometric landmark positioning on hard-tissue surfaces, the mean values ranged between 0.22 mm and 0.68 mm (Sd ranged between 0.02 mm and 0.07 mm), while the mean values for capulometric landmarks positioning on soft-tissue ranged between 0.23 mm and 0.79 mm (Sd ranged between 0.04 mm and 0.10 mm).

Table 6. 1. Dispersion errors (mm) of craniometric and capulometric landmarks positioning on hard- and soft-tissue black and white surfaces.

Observations	Intra-observer errors				Inter-observer errors 1				Inter-observer errors 2			
	Black surfaces		White surfaces		Black surfaces		White surfaces		Black surfaces		White surfaces	
	M	Sd	M	Sd	M	Sd	M	Sd	M	Sd	M	Sd
Hard-tissue	0.68	0.07	0.57	0.05	0.65	0.06	0.53	0.05	0.22	0.02	0.23	0.02
Soft-tissue	0.79	0.10	0.77	0.98	0.88	0.11	0.70	0.10	0.23	0.04	0.23	0.04

The visualisation of the comparison between the mean values for both intra- and inter-measurement errors of all craniometric and capulometric landmark positioning on black and white hard- and soft-tissue templates and on hard- and soft-tissue surfaces is shown in Figs. 6.1 and 6.2. The mean dispersion errors result of the craniometric (Figure. 6.1) and capulometric (Figure. 6.2) landmarks positioning on templates and on warped surfaces follow the same trend, indicating that landmarks positioning on warped surfaces is dependent on the initial landmarks positioning on templates.

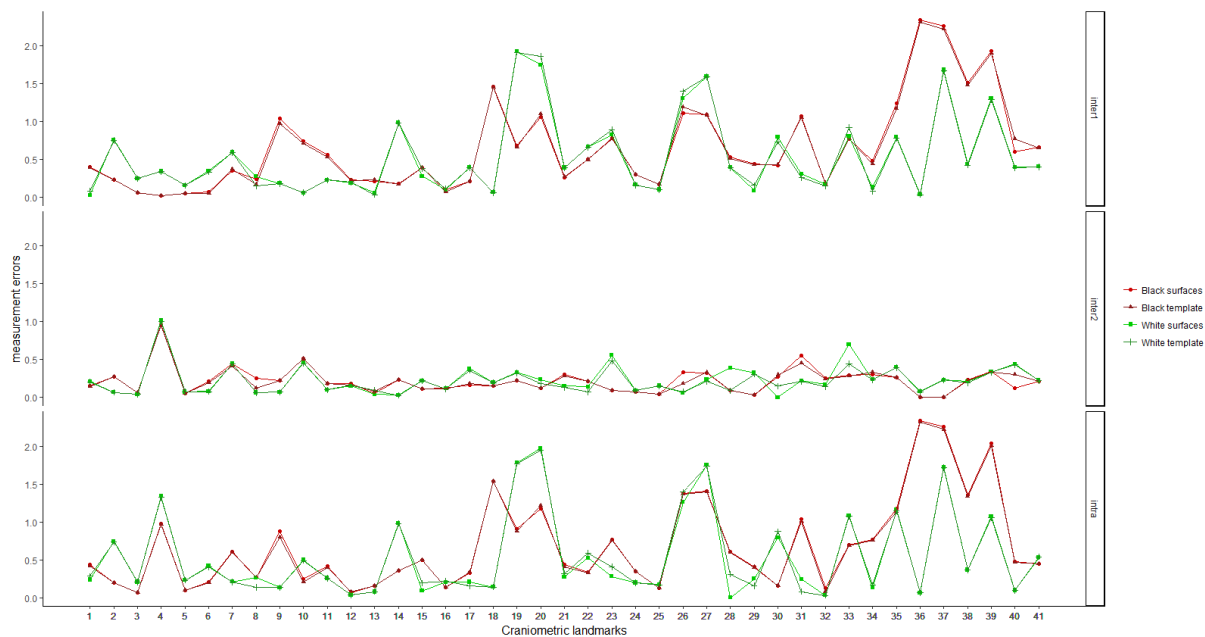


Figure 6. 1. Graphical comparison between the mean SE results for both INTRA-OE and INTER-OE of all craniometric landmarks positioning on hard-tissue templates and surfaces.

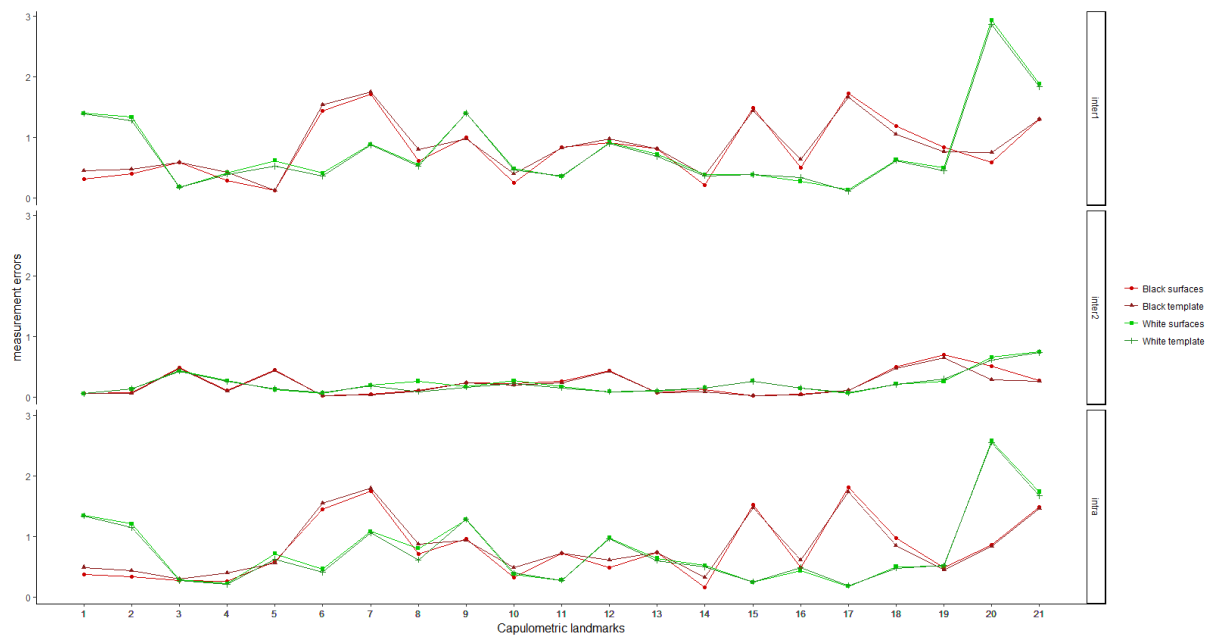


Figure 6. 2. Graphical comparison between the mean SE results for both INTRA-OE and INTER-OE of all capulometric landmarks positioning on soft-tissue templates and surfaces.

Concerning the reproducibility of each craniometric (Table 6.2) and capulometric landmark (Table 6.3) on each black and white surface analysed separately, all landmarks showed high reproducibility (< 2 mm). All craniometric and capulometric landmarks presented a measurement error less than 2 mm. Only three craniometric landmarks (nasomaxillofrontale, zygomaxillare, submaxillare curvature) placed on black surfaces and three craniometric landmarks (nasomaxillofrontale, maxillofrontale, zygomaxillare) placed on white surfaces showed a reproducibility between 1 and 2 mm. Regarding the reproducibility of each capulometric landmarks, four capulometric landmarks (superior alar curvature, mid-columella, nasal depth, mid-nostril) placed on black surfaces and only one capulometric landmark (mid-nostril) placed on white surfaces, demonstrated a reproducibility comprising between 1 and 2 mm.

Table 6. 2. Definition and reproducibility of craniometric landmarks placed automatically and used in this thesis.

Craniometric	Landmarks	Abbreviation	Nature	Definition	Observer errors	
					Black surfaces	White surfaces
	1 Nasion	n	Median	Intersection of the nasofrontal sutures in the median plane.	< 1mm	< 1mm
	2 Mid-nasal	mn	Median	Midline point on the internasal suture midway between nasion and rhinion.	< 1mm	< 1mm
	3 Rhinion	rhi	Median	Most rostral (end) point on the internasal suture. Cannot be determined accurately if nasal bones are broken distally.	< 1mm	< 1mm
	4 Nasospinale	ns	Median	The point where a line drawn between the inferior most points of the nasal aperture crosses the median plane. Note that this point is not necessarily at the tip of the nasal spine.	< 1mm	< 1mm
	5 Subspinale	ss	Median	The deepest point seen in the profile view below the anterior nasal spine (orthodontic point A).	< 1mm	< 1mm
	6 Akanthion	ak	Median	Most anterior midline point of the nasal spine.	< 1mm	< 1mm
	7 Prosthion	pr	Median	Median point between the central incisors on the anterior most margin of the maxillary alveolar rim.	< 1mm	< 1mm
	8/9 Zygotemporale superior	zts	Bilateral	Most superior point of the zygomatico-temporal suture.	< 1mm	< 1mm
	10/11 Zygotemporale inferior	zti	Bilateral	Most inferior point of the zygomatico-temporal suture.	< 1mm	< 1mm
	12/13 Jugale	ju	Bilateral	Vertex of the posterior zygomatic angle, between the vertical edge and horizontal part of the zygomatic arch.	< 1mm	< 1mm
	14/15 Frontomalare temporale	fnt	Bilateral	Most lateral part of the zygomaticofrontal suture.	< 1mm	< 1mm
	16/17 Frontomalare orbitale	fmo	Bilateral	Point on the orbital rim marked by the zygomaticofrontal suture.	< 1mm	< 1mm
	18/19 Nasomaxillofrontale	nmf	Bilateral	Point at the intersection of the frontal, maxillary, and nasal bones.	1-2 mm	1-2 mm
	20/21 Ectoconchion	ec	Bilateral	Lateral point on the orbit at a line that bisects the orbit transversely.	< 1mm	1-2 mm
	22/23 Orbitale	or	Bilateral	Most inferior point on the inferior orbital rim. Usually falls along the lateral half of the orbital margin.	< 1mm	< 1mm
	24/25 Zygo-orbitale	zo	Bilateral	Intersection of the orbital margin and the zygomaticomaxillary suture.	< 1mm	< 1mm
	26/27 Maxillofrontale	mf	Bilateral	Intersection of the anterior lacrimal crest with the frontomaxillary suture.	< 1mm	1-2 mm
	28/29 Nasomaxillare	nm	Bilateral	Most inferior point of the nasomaxillary suture on the nasal aperture.	< 1mm	< 1mm
	30/31 Alare	al	Bilateral	Instrumentally determined as the most lateral point on the nasal aperture in a transverse plan.	< 1mm	< 1mm
	32/33 Piriform curvature	cp	Bilateral	Most infero-lateral point of the piriform aperture.	< 1mm	< 1mm
	34/35 Nariale	na	Bilateral	Most inferior point of the piriform aperture.	< 1mm	< 1mm
	36/37 Zygomaxillare	zm	Bilateral	Most inferior point on the zygomaticomaxillary suture.	1-2 mm	1-2 mm
	38/39 Submaxillare curvature	csm	Bilateral	Most supero-medial point on the maxillary inflexion between the zygomaxillare and the ectomolar.	1-2 mm	< 1mm
	40/41 Supra-canine	sc	Bilateral	Point on the superior alveolar ridge superior to the crown of the maxillary canine.	< 1mm	< 1mm

Table 6. 3. Definition and reproducibility of capulometric landmarks placed automatically and used in this thesis.

Capulometric	Landmarks	Abbreviation	Nature	Definition	Observer errors	
					Black surfaces	White surfaces
	1 Pronasale	prn'	Median	The most anteriorly protruded point of the apex nasi. In the case of a bifid nose, the more protruding tip is chosen.	< 1 mm	< 1 mm
	2 Nasale inferius	ni'	Median	Most inferior point of the apex nasi. Not locatable on upturned noses.	< 1 mm	< 1 mm
	3 Columella	c'	Median	Midpoint of the nasal columella crest, intersecting a line between the two cs' points.	< 1 mm	< 1 mm
	4 Subnasale	sn'	Median	Median point at the junction between the lower border of the nasal septum and the philtrum area.	1-2 mm	< 1 mm
	5 Sellion	se'	Median	Deepest midline point of the nasofrontal angle; not a substitute for n'.	< 1 mm	< 1 mm
	6/7 External alar curvature	eac	Bilateral	Most anterior point of the nasal wing at the maximum of curvature.	< 1 mm	< 1 mm
	8/9 Superior alar curvature	sac	Bilateral	Most superior point of the nasal wing.	< 1 mm	< 1 mm
	10/11 Alagenion	ag	Bilateral	Most posterior point of the nasal wing.	1-2 mm	< 1 mm
	12/13 Alare	al'	Bilateral	The most lateral point on the nasal ala.	< 1 mm	< 1 mm
	14/15 Alar curvature point	ac'	Bilateral	The most posterolateral point of the curvature of the base line of each nasal ala.	< 1 mm	< 1 mm
	16/17 Mid-nostril	mn	Bilateral	Midpoint of maximal nostril width - projected on the transition nostril/philtrum.	1-2 mm	1-2 mm
	18/19 Mid-columella	mc'	Bilateral	Midpoint of the nasal columella crest on either side, where the columella thickness is measured (equivalent to Subnasale).	< 1 mm	< 1 mm
	20/21 Nasal-depth	nd	Bilateral	Most medial point of the transition nose/eye.	1-2 mm	< 1 mm

These reproducibility analyses provided a validation of the precision of the automatic placement of craniometric and capulometric landmarks on all 3D hard- and soft-tissue surfaces used in this thesis, for both the black and white South African subsamples.

Preceding all statistical analyses on the complete sample a GPA, a PCA and multivariate normality testing were performed on the whole sample and on complete hard- and soft-tissue sample, separately. Where differences between the two ancestral groups were noted, the data was separated into ancestral specific subsets (black South African and white South African). Then, GPA and PCA, as well as a multivariate normality testing, were performed on each ancestral specific subset and on each hard- and soft-tissue sample, separately.

6.2.2. *General Procrustes Analysis (GPA)*

Preceding the geometric morphometric analysis, a Generalised Procrustes Analysis (GPA) (Goodall, 1991; Dryden & Mardia, 2016) was performed on the hard- and soft-tissue raw coordinates to obtain pose-invariant shape coordinates (Kendall DG, 1984; Klingenberg & McIntyre, 1998; Slice DE, 2001; Klingenberg *et al.*, 2002). The raw landmark coordinates do not only comprise information on size and shape of the landmark configurations, but also on their position and orientation. The most common approach for separating shape from size and the “nuisance parameters” position and orientation, is the Generalised Procrustes Analysis (Gower, 1975; Rohlf & Slice, 1990). This method comprises three steps: translating all landmark configurations to the same centroid, scaling all configurations to the same centroid size, and iteratively rotating all configurations until the summed squared distances between the landmarks and their corresponding sample average is a minimum. The coordinates of the resulting superimposed landmark configurations are called Procrustes shape coordinates as they only contain information about the shape of the configurations.

6.2.3. *Principal Component Analysis (PCA)*

Data reduction was achieved by principal component analysis (PCA) to reduce data dimensionality and to create independent principal component (PC) scores that quantify the different shapes studied. Statistical testing was performed using the PC scores covering 95% of the sample’s overall variance of the sample. The principal component analysis (PCA) involves the examination of axes that reflect maximum variation and covariation. PCA

transforms the data to a new coordinate system, such, that the greatest variance of the data lies on the first transformed new variable (the first principal component), while the second greatest variance lies on the second transformed variable. The orthogonal axes of the PCA summarise variation decreasing in order and individual observations are plotted along axes. The score of a given observation on a given axis corresponds to the projection of the data on that axis. Examining variation on the first axes provides a way to reduce the variable space to dimensions that express the most variation. Each axis corresponds to a linear combination of original variables. The first corresponds to the main direction of the variance covariance structure of individual observations.

6.2.3.1. Population differences

For the population differences of hard- and soft-tissue shape, only those principal components (PCs) accounting for at least 95% of the variance of the sample are included in the statistical analysis. For the hard-tissue mid-facial shape (Figure 6.3), the first 39 PCs and the first 3 PCs for the soft-tissue external nose shape were selected (Figure 6.3).

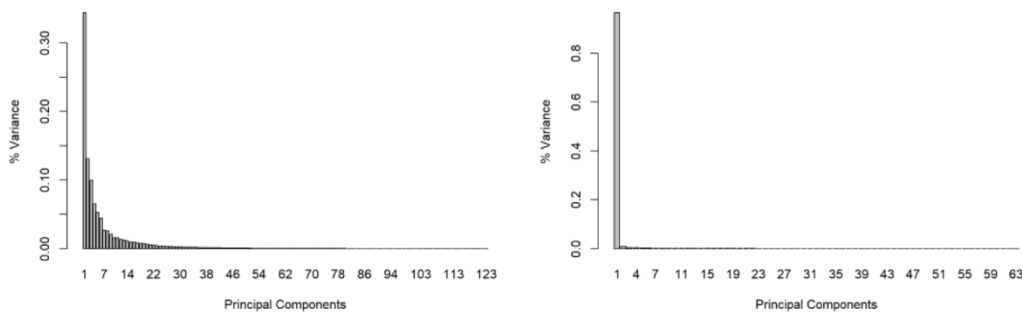


Figure 6. 3. Variance explained by each PC of the hard- tissue mid-facial (left) and the soft-tissue external nose (right) shape component.

For the population differences of separate hard-tissue mid-facial elements (nasal bones, anterior nasal aperture, zygoma and maxilla), only those principal components accounting for at least 95% of the variance of the sample were included in the statistical analysis. These are the first 12 PCs for the nasal bones shape (Figure 6.4.a) and the first eight PCs for left and right nasal bones shapes (Figure 6.4.b,c). For the anterior nasal aperture shape, the first 18 PCs were selected (Figure 6.5.a), for the left (Figure 6.5.b) and right (Figure 6.5.c) anterior nasal aperture

shapes, the first 15 and 13 PCs were selected, respectively. For the zygomatic bone shape, the first 21 PCs were used (Figure 6.6.a) and the first 13 PCs for the left and right zygomatic bone shapes (Figure 6.6. b,c). The first 31 PCs for the maxillary shape were selected (Figure 6.7.a) and the first 23 and 19 PCs were used for the left (Figure 6.7.b) and right (Figure 6.7.c) zygomatic bone shape, respectively.

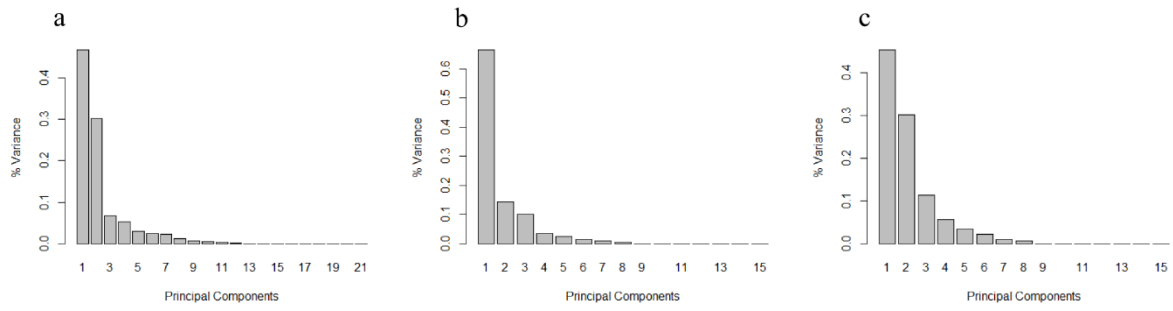


Figure 6. 4. Variance explained by each PC of the nasal bones shape component. a) nasal bones; b) nasal bone left; c) nasal bone right.

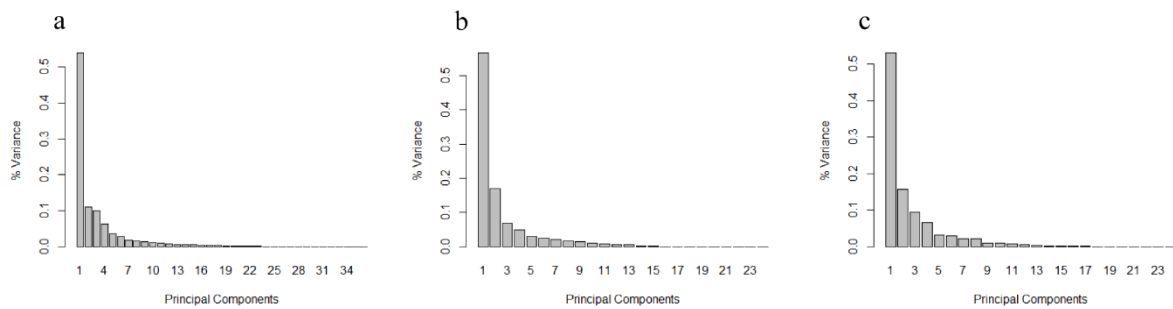


Figure 6. 5. Variance explained by each PC of the anterior nasal aperture shape component. a) anterior nasal aperture; b) anterior nasal aperture left; c) anterior nasal aperture right.

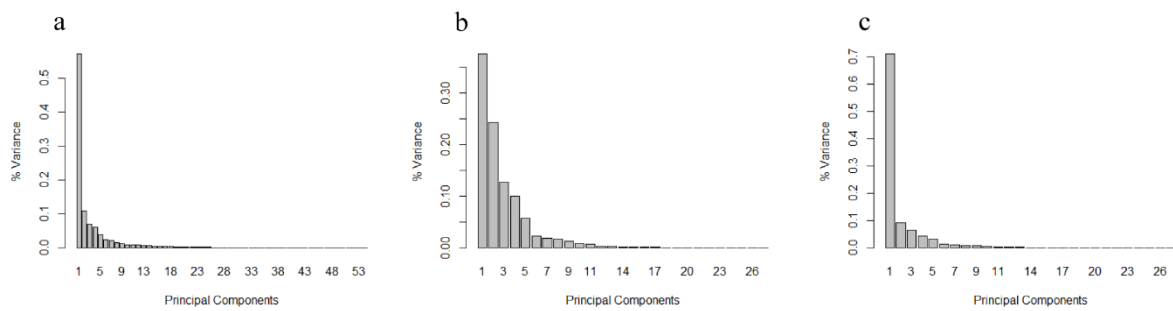


Figure 6. 6. Variance explained by each PC of the zygomatic shape component. a) zygomatic; b) zygomatic left; c) zygomatic right.

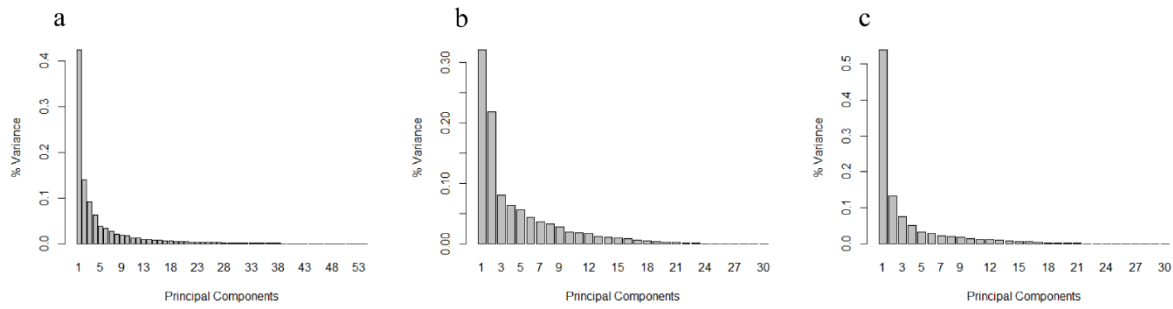


Figure 6. 7. Variance explained by each PC of the maxillary shape component. a) maxilla; b) maxillary left; c) maxillary right.

6.2.3.2. Assessment of sexual dimorphism, age effect and allometry.

In order to minimise the effects of ancestry on the data, the sample was split into population-specific subsets for assessing sexual dimorphism, age effect and allometry.

6.2.3.2.1. Black South African subsample

For assessing sexual dimorphism, age effect and allometry of hard- and soft-tissue shape in the black South African sample, only those principal components accounting for at least 95% of the variance of the sample were included in the statistical analysis. The first 45 PCs for the hard-tissue mid-facial shape (Figure 6.8) and for the external nasal soft-tissue shape (Figure 6.8) were used.

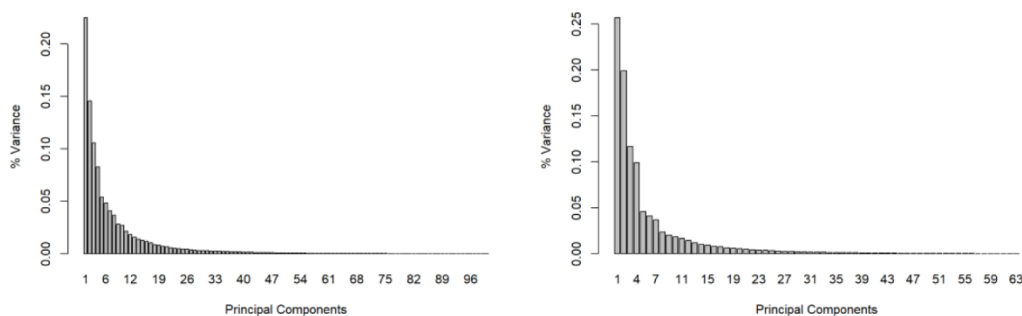


Figure 6. 8. Variance explained by each PC of the mid-facial hard- tissue (left) and the external nasal soft-tissue (right) shape component.

For assessing sexual dimorphism, age effect and allometry on hard-tissue mid-facial elements separately (nasal bones, anterior nasal aperture, zygoma and maxilla) in the black South African sample, only those principal components accounting for at least 95% of the variance of the sample were included in the statistical analysis. For the nasal bones shape, the first 13 PCs (Figure 6.9.a), and for the nasal bone left and right shapes, the first 8 PCs were selected (Figure 6.9.b,c). For the anterior nasal aperture shape the first 20 PCs were used (Figure 6.10.a), and only the 15 and the 13 first PCs were used for the left (Figure 6.10.b) and right (Figure 6.10.c) anterior nasal aperture shapes, respectively. The first 31 PCs for the zygomatic shape were selected (Figure 6.11.a), the first 19 PCs for the left zygomatic bone shape (Figure 6.11.b), and the first 16 PCs for the right zygomatic bone shape (Figure 6.11.c). For the maxillary shape, the first 31 PCs were selected (Figure 6.12.a) and for the left and right maxillary shapes, the first 23 PCs were used (Figure 6.12.b,c).

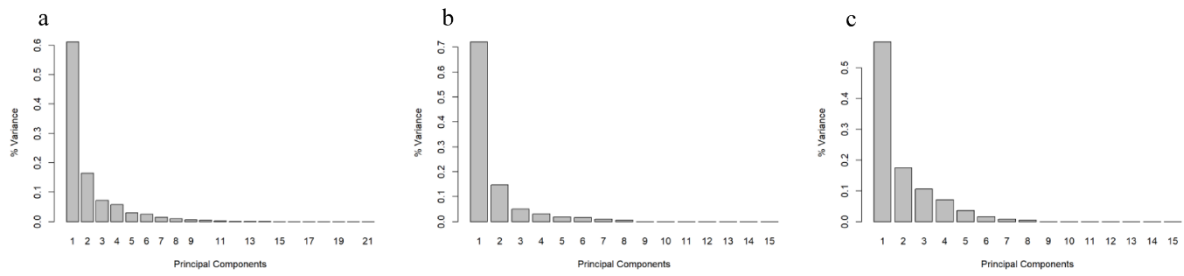


Figure 6.9. Variance explained by each PC of the nasal bones shape component. a) nasal bones; b) nasal bone left; c) nasal bone right.

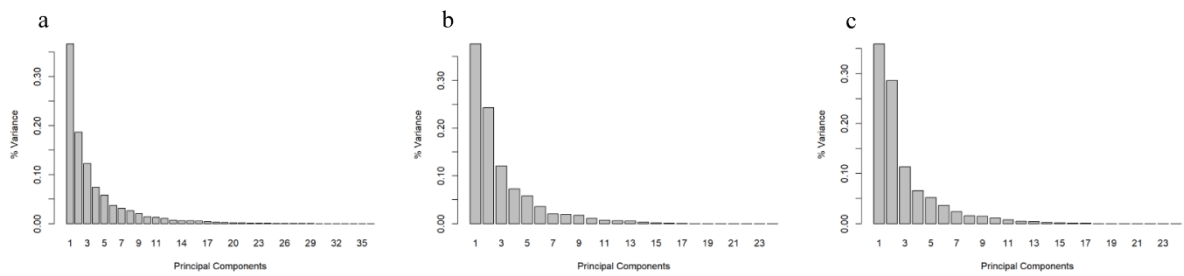


Figure 6.10. Variance explained by each PC of the anterior nasal aperture shape component. a) anterior nasal aperture; b) anterior nasal aperture left; c) anterior nasal aperture right.

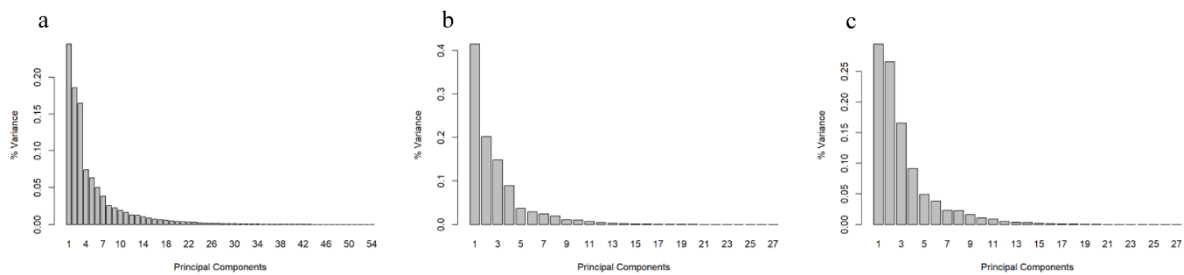


Figure 6.11. Variance explained by each PC of the zygomatic shape component. a) zygoma; b) zygomatic left; c) zygomatic right.

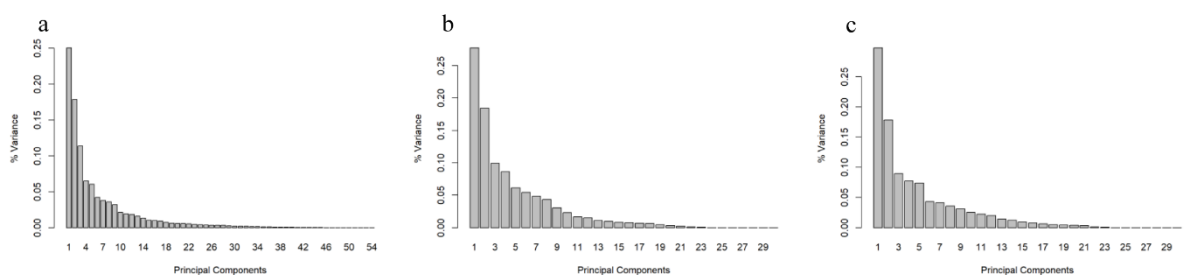


Figure 6.12. Variance explained by each PC of the maxillary shape component. a) maxilla; b) maxillary left; c) maxillary right.

6.2.3.2.2. White South African subsample

For assessing sexual dimorphism, age effect and allometry of hard- and soft-tissue shape in the white South African sample, only those principal components accounting for at least 95% of the variance of the sample are included in the statistical analysis. These are, for the hard-tissue mid-facial shape (Figure 6.13), the first 45 PCs, and the first 34 PCs for the external nasal soft-tissue shape (Figure 6.13).

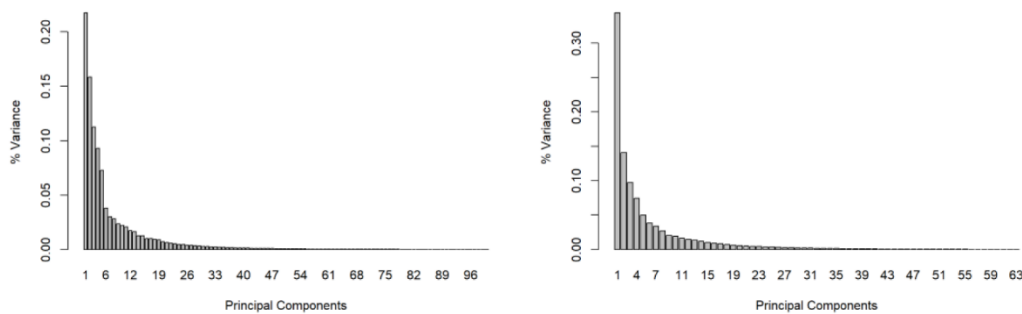


Figure 6. 13. Variance explained by each PC of the hard- tissue mid-facial (left) and the soft-tissue external nose (right) shape component.

For assessing sexual dimorphism, age effect and allometry on hard-tissue mid-facial elements separately (nasal bones, anterior nasal aperture, zygoma and maxilla) in the white South African sample , only those principal components accounting for at least 95% of the variance of the sample are included in the statistical analysis. These are the first 14 PCs for the nasal bones shape (Figure 6.14.a) and the 8 PCs for the nasal bone left and right shapes (Figure 6.14.b,c)) separately. For the anterior nasal aperture shape the first 23 PCs were used (Figure 6.15.a) and for left and the right anterior aperture shapes, the first 14 PCs were selected (Figure 6.15.b,c)). For the zygoma shape, the first 32 PCs were used (Figure 6.16.a) and the first 14 and 17 PCs were selected for the left (Figure 6.16.b) and right (Figure 6.16.c) zygomatic bone shapes respectively. The first 32 PCs were used for the maxilla shape (Figure 6.17.a), as well as the first 23 PC for the left and right maxilla shapes separately (Figure 6.17.b,c).

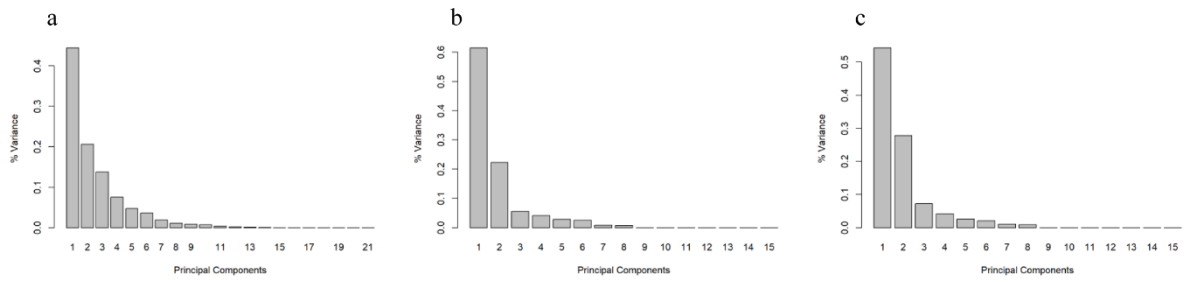


Figure 6. 14. Variance explained by each PC of the nasal bones shape component. a) nasal bones; b) nasal bone left; c) nasal bone right.

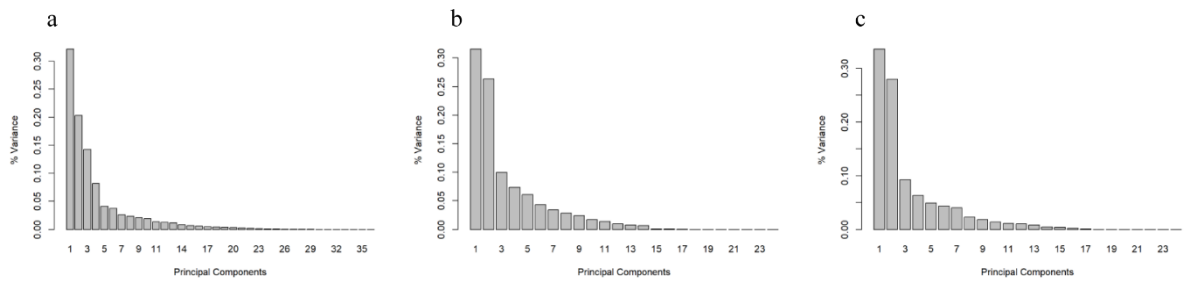


Figure 6. 15. Variance explained by each PC of the anterior nasal aperture shape component. a) anterior nasal aperture; b) anterior nasal aperture left; c) anterior nasal aperture right.

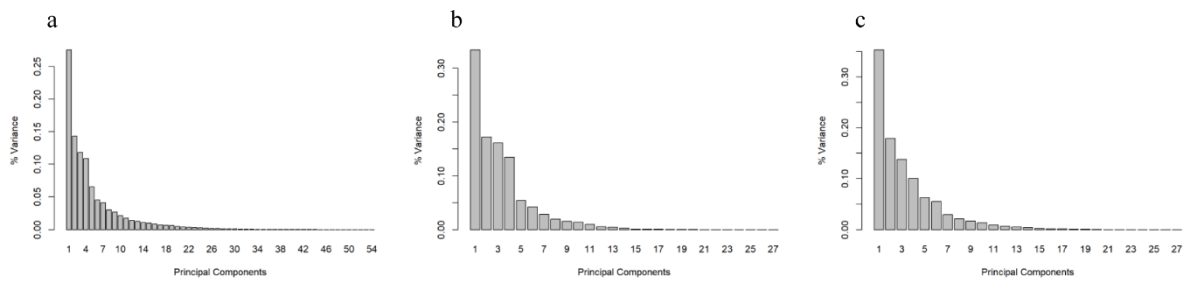


Figure 6. 16. Variance explained by each PC of the zygomatic shape component. a) zygoma; b) zygomatic left; c) zygomatic right.

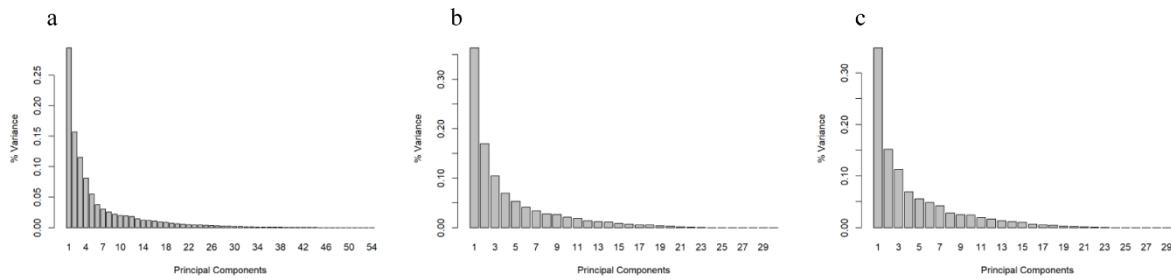


Figure 6.17. Variance explained by each PC of the maxillary shape component. a) maxilla; b) maxillary left; c) maxillary right.

6.2.4. Multivariate normality

Multivariate normality testing was performed on the hard- and soft-tissue principal component scores distribution with Q-Q-plots (Scrucca, 2000), which allow us to visually assess the distribution of the variable from normality. The graphical output shows the actual values of squared Mahalanobis-distances plotted versus those of an ideal multivariate normal distribution. The closer the values are to the diagonal line, the more probable the multivariate normal distribution.

6.2.4.1. Population differences.

For the assessment analysis of population differences, the Q-Q plots of Mahalanobis distances expected in perfectly normal distributed data versus those actually calculated from the sample, demonstrated some deviation from the normality (Figure 6.18) in the hard-tissue mid-facial component, while the external nasal soft-tissue component followed a normal distribution (Figure 6.18).

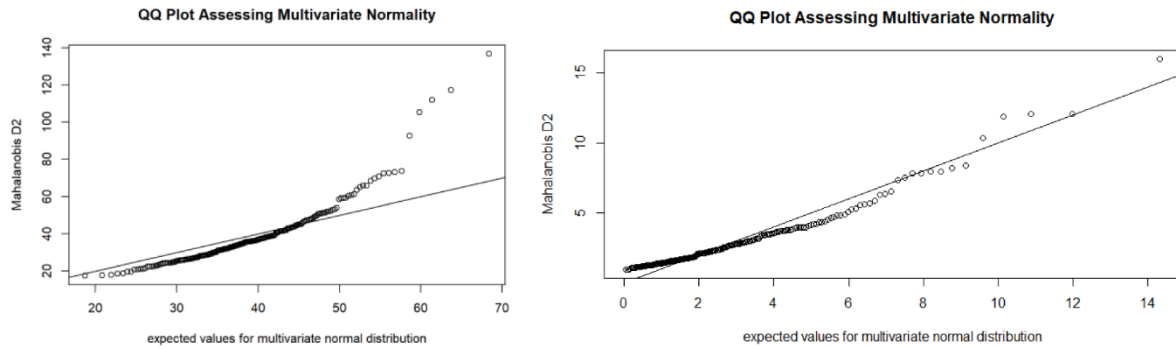


Figure 6. 18. Q-Q-plots of the residuals of the linear model “hard-tissue mid-facial shape (left) versus population” and the linear model “external nasal soft-tissue shape (right) versus population” .

For assessment of population differences of separate hard-tissue mid-facial elements (nasal bones (Figure 6.19), anterior nasal aperture (Figure 6.20), zygoma (Figure 6.21) and maxilla (Figure 6.22)), the Q-Q plots of Mahalanobis distances expected in perfectly normal distributed data versus those actually calculated from the sample, showed that only the anterior nasal aperture shape (Figure 6.20) and the maxillary shape (Figure 6.22) had a strong deviation from the normality.

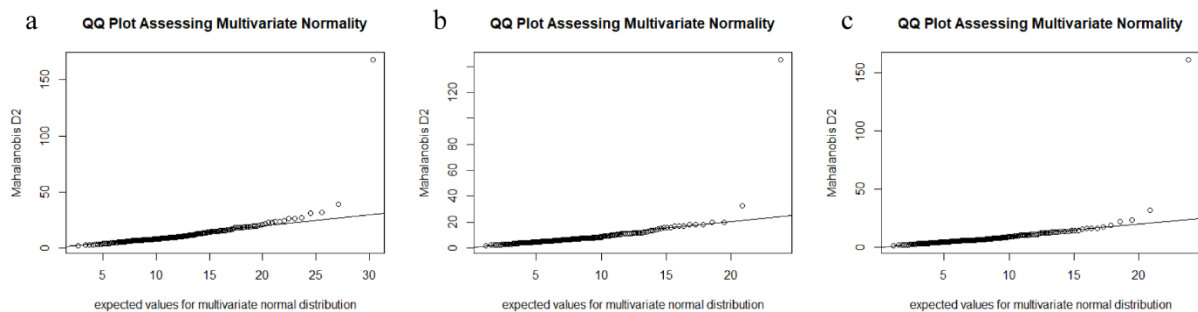


Figure 6. 19. Q-Q-plots of the residuals of the linear model “nasal bones shape versus population”. a) nasal bones; b) nasal bone left; c) nasal bone right.

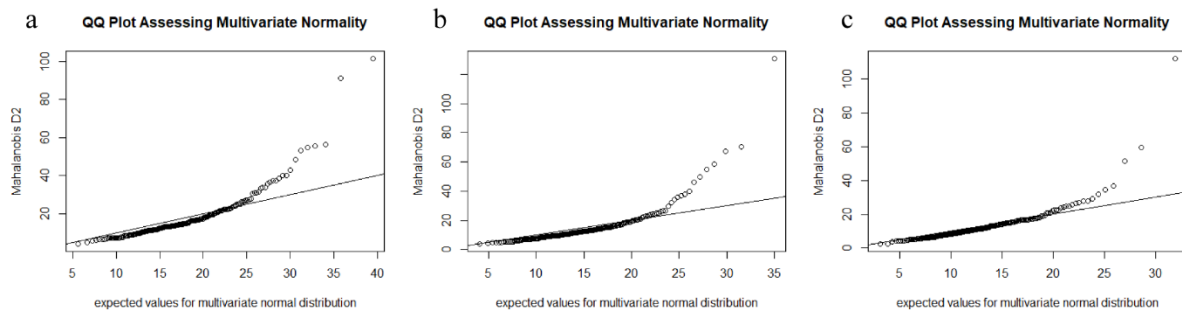


Figure 6. 20. Q-Q-plots of the residuals of the linear model “anterior nasal aperture shape versus population”. a) anterior nasal aperture; b) anterior nasal aperture left; c) anterior nasal aperture right.

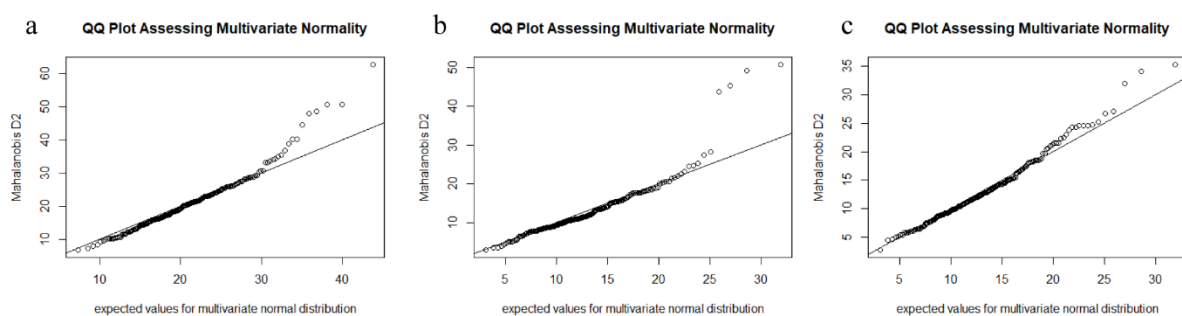


Figure 6. 21. Q-Q-plots of the residuals of the linear model “zygomatic shape versus population”. a) zygoma; b) zygomatic bone left; c) zygomatic bone right.

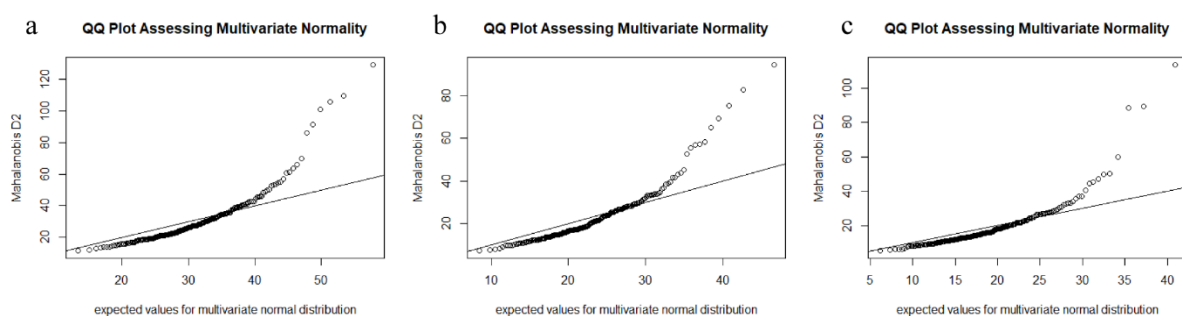


Figure 6. 22. Q-Q-plots of the residuals of the linear model “maxillary shape versus population”. a) maxilla; b) maxillary bone left; c) maxillary bone right.

6.2.4.2. Assessment of sexual dimorphism, age effect and allometry

6.2.4.2.1. Black South African subsample

For sexual dimorphism, age effect and allometric assessments in the black South African sample, the Q-Q plots of Mahalanobis distances expected in perfectly normal distributed data versus those actually calculated from the sample, showed that the hard- and soft-tissue shape components deviated somewhat from normality (Figure 6.23).

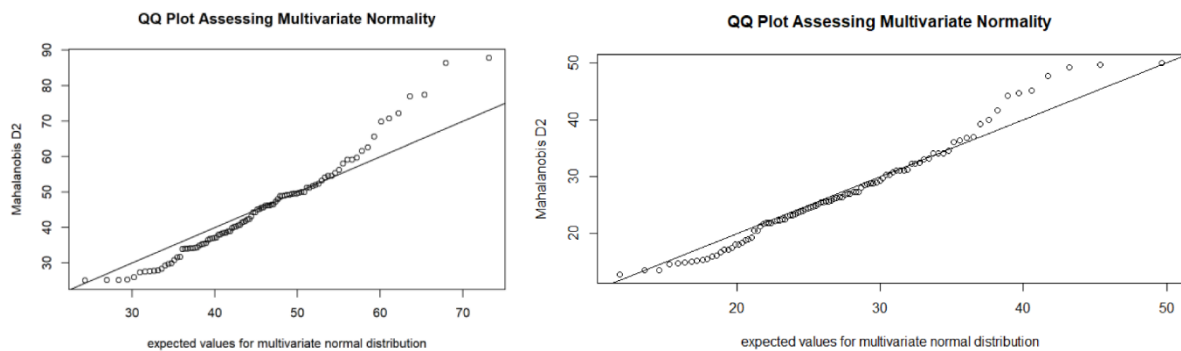


Figure 6. 23. Q-Q-plots of the residuals of the linear model “hard-tissue mid-facial shape (left) versus population” and the linear model “soft-tissue external nose shape (right) versus population” .

For sexual dimorphism, age effect and allometric assessments of mid-facial hard-tissue elements separately, only the anterior nasal aperture (Figure 6.25) and the maxillary shape (Figure 6.27) strongly deviated from normality when applying the Q-Q plots of Mahalanobis distances.

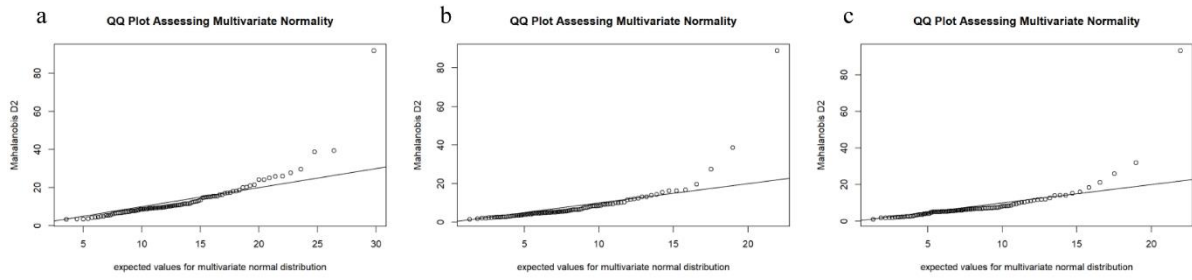


Figure 6. 24. Q-Q-plots of the residuals of the linear model “nasal bones shape versus population”. a) nasal bones; b) nasal bone left; c) nasal bone right.

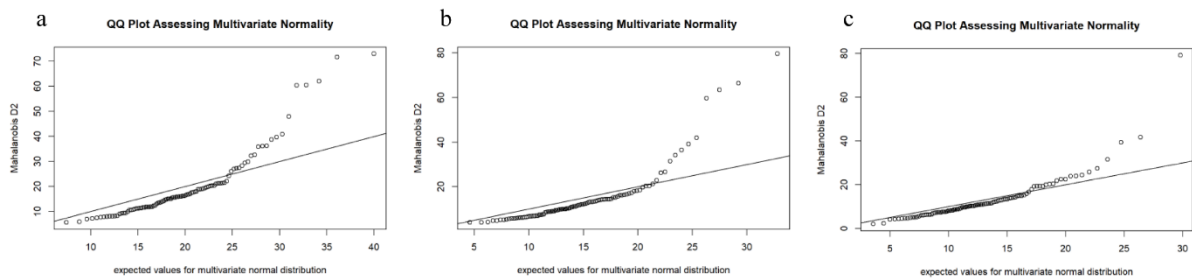


Figure 6. 25. Q-Q-plots of the residuals of the linear model “anterior nasal aperture shape versus population”. a) anterior nasal aperture; b) anterior nasal aperture left; c) anterior nasal aperture right.

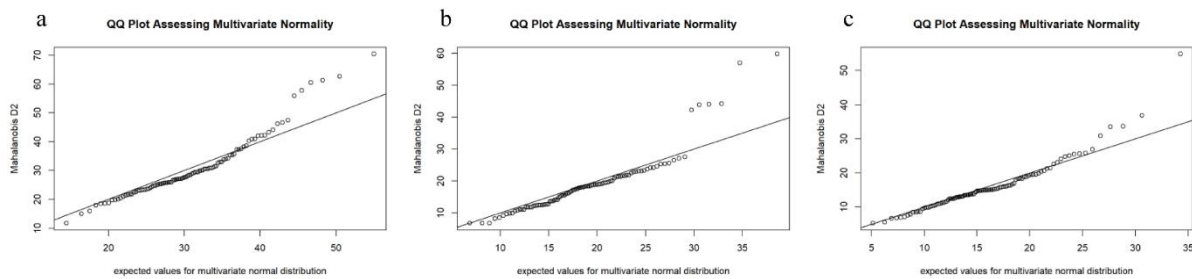


Figure 6. 26. Q-Q-plots of the residuals of the linear model “zygoma shape versus population”. a) zygoma; b) zygomatic bone left; c) zygomatic bone right.

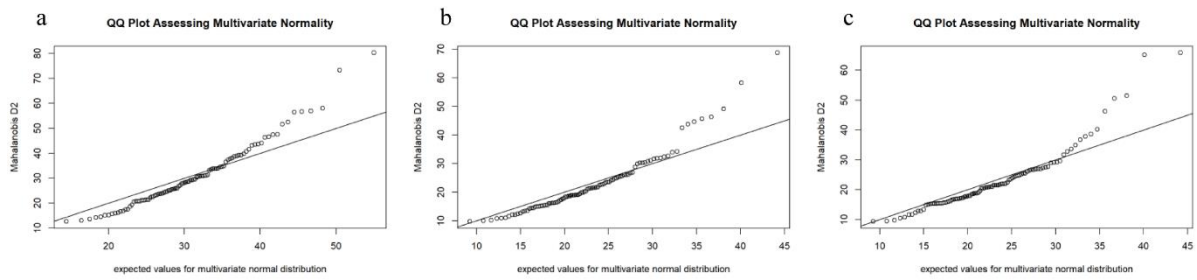


Figure 6. 27. Q-Q-plots of the residuals of the linear model “maxillary shape versus population”. a) maxilla; b) maxillary bone left; c) maxillary bone right.

6.2.4.2.2. *White South African subsample.*

For sexual dimorphism, age effect and allometric assessments in the white South African sample, the Q-Q plots of Mahalanobis distances expected in perfectly normal distributed data versus those actually calculated from the sample, showed that the hard- and soft-tissue shape components followed a normal distribution (Figure 6.28).

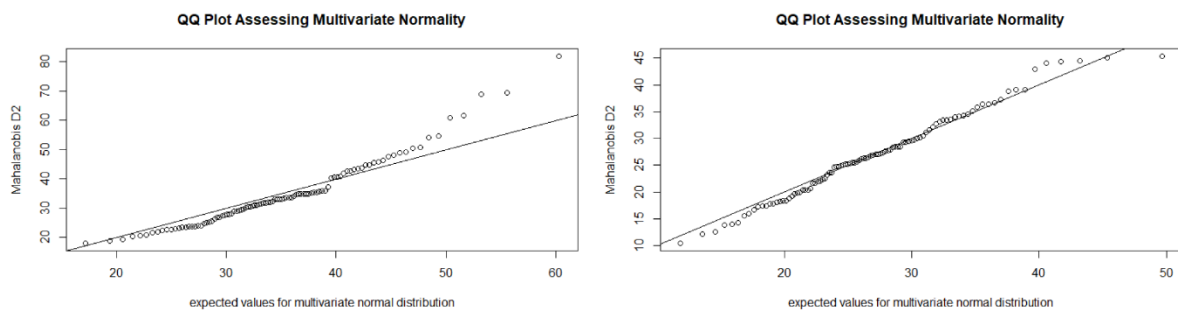


Figure 6. 28. Q-Q-plots of the residuals of the linear model “hard-tissue mid-facial shape (left) versus population” and the linear model “soft-tissue external nose shape (right) versus population” .

For sexual dimorphism, age effect and allometry assessments of mid-facial hard-tissue elements separately, only the anterior nasal aperture shape (Figure 6.30) and the maxillary shape (Figure 6.32) showed a strong deviation from the normality when applying Q-Q plots of Mahalanobis distances.

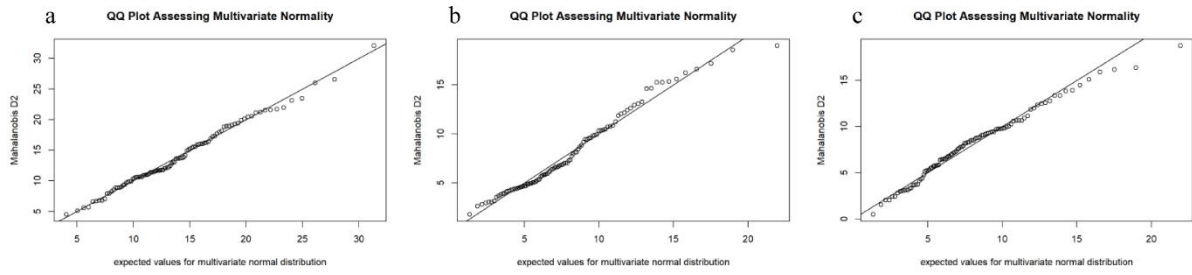


Figure 6. 29. Q-Q-plots of the residuals of the linear model “nasal bones shape versus population”. a) nasal bones; b) nasal bone left; c) nasal bone right.

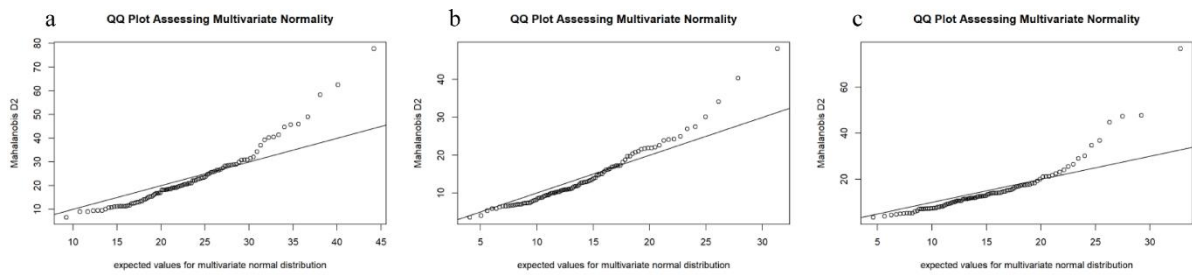


Figure 6. 30. Q-Q-plots of the residuals of the linear model “anterior nasal aperture shape versus population”. a) anterior nasal aperture; b) anterior nasal aperture left; c) anterior nasal aperture right.

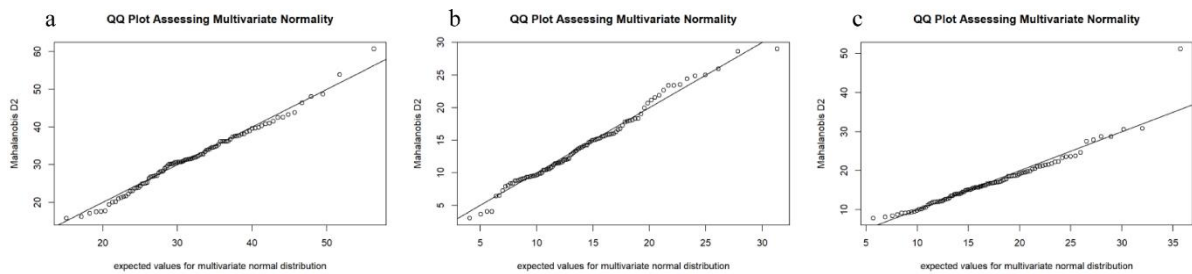


Figure 6. 31. Q-Q-plots of the residuals of the linear model “zygomatic shape versus population”. a) zygoma; b) zygomatic bone left; c) zygomatic bone right.

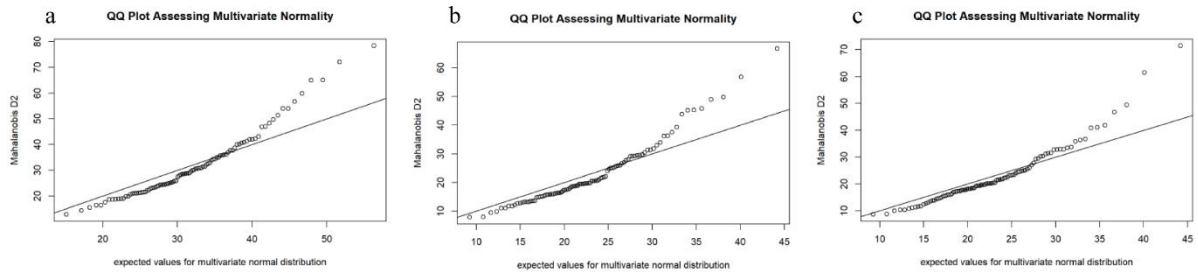


Figure 6. 32. Q-Q-plots of the residuals of the linear model “maxillary shape versus population”. a) maxilla; b) maxillary bone left; c) maxillary bone right.

The outcome of these multivariate normality analyses on the complete sample and within ancestral groups suggests that the results obtained from parametric testing should be carefully interpreted and counter-checked with non-parametric testing. Some mid-facial elements such as the anterior nasal aperture and the maxillary shapes showed a deviation from the normality when applying Q-Q plots of Mahalanobis distances for all statistical analysis and needs to be considered when interpreting the final results. For this reason, all results were double-checked using non-parametric testing and only if both tests provided a similar outcome could the results be considered reliable.

Shape analysis of the nasal complex among South African groups from Cone-Beam Computed Tomography (CBCT) using geometric morphometric.

AF RIDEL, F DEMETER, EN L'ABBÉ, D VANDERMEULEN, AC OETTLÉ.

Manuscript submitted for publication to Forensic Science International.

Abstract

In light of the great demand for the identification of unknown remains in South Africa, a dire need exists to establish reliable facial approximation techniques that will not only take into account sex and age, but most importantly be specific for the South African population. The main critiques of current facial approximation techniques, which are used in South Africa, are the inherent subjectivity in manual methods, the references used, the lack of standardisation, the poor correlations between facial bony structures and facial soft features, and the non-consideration of population specificities. The aim of this study was to assess the influence of factors such as age, size, sex and ancestry on hard- and soft-tissue shape among a South African sample using geometric morphometric methods.

The database containing 200 cone beam computer tomography (CBCT) scans, belonging to 100 black South Africans and 100 white South Africans were selected from the Oral and Dental Hospital, University of Pretoria, and the Life Groenkloof Hospital, Pretoria, South Africa. The landmarks selected were distributed on the facial skeleton (the nasal bones, the anterior nasal aperture, the zygoma, and the maxilla) and the external nose, creating a hard- and soft-tissue region of interest. On the same individuals, 41 craniometric landmarks were registered on the 200 hard-tissue surfaces and 21 capulometric landmarks on the 200 soft-tissue surfaces. The placement of landmarks on 3D surfaces were performed by an automatic landmarking procedure using MeVisLab © v. 2.7.1 software. Geometric morphometrics was used for correlations between the mid-facial hard-tissue region of interest and the external soft-tissue of the nose and comparisons between groups (ancestry, sex, age and size (allometry)).

Ancestry, sexual dimorphism, as well as age and size affected nasal complex shape. Ancestry was an considerable factor in the mid-facial region, emphasizing that shape variability was specific between the two groups, along with the expression of sexual dimorphism and effect

of aging. In addition, the two groups differed significantly regarding their hard- and soft-tissue correlations.

Variations in the nasal complex morphology between the two ancestral groups, emphasizing the need for population specific guidelines and highlights the importance of considering ancestry as a factor in the process of approximating the nose.

Keywords: Facial reconstruction; nasal shape variation; human variability; automatic landmarking.

Introduction

Each year in the Gauteng province of South Africa, approximately 1300 unidentified bodies are incinerated [1, 2]. It is not always possible to identify unknown persons with conventional methods by comparing DNA and fingerprints. Additionally, many poor South Africans do not have dental or hospital records, or identification documents. As a result, more creative methods, including facial reconstruction, have been implemented to assist in the identification of unknown persons from their skeletal remains. Craniofacial reconstruction (CFR) methods can be used to estimate the ante mortem appearance of an individual from skeletal remains, providing a presumptive identification of the individual, which can be conveyed to the public. Craniofacial reconstruction (CFR) is based on the assumed morphological relationship between the soft-tissue envelope and the underlying skull substrate [3].

In collaboration with the Victim Identification Centre (VIC) of the South African Police Service (SAPS), the Forensic Anthropology Research Centre (FARC) at the University of Pretoria has worked hard toward finding solutions for many of the challenges in the identification of unknown skeletal remains found within South African context [2]. The current situation of unidentified persons will greatly benefit from research into human variation of South African groups, with the intention of creating accurate and reliable identification guidelines such as using South African standard facial reconstruction methods [4].

The VIC, in Pretoria, performs three-dimensional (3D) manual approximation of faces by facial sculpting with modelling software. More precisely, the VIC uses a virtual sculptural method [5, 6] with a 3D modelling system (Freeform Modelling Plus™; Sensable Technologies Wilmington, MA) and haptic feedback (Phantom Deskto™ Haptic Device; Sensable Technologies). The process requires a 3D surface scan of the unidentified skull with a Metrascan 210. A 3D surface of the target skull is then transposed onto Freeform modelling software and soft-tissue thicknesses are manually applied at specific craniometric points using a 3D stylus. Using the same process, facial features are adjusted on the skull according to soft-tissue thicknesses derived from North American databases of cadaver studies. Once a forensic artist applies the final touches, and the person's biological profile, including sex, age and

ancestry has been estimated, a 3D facial reconstruction is printed and presented to the family for possible recognition [2, 4].

The accuracy of the 3D facial reconstruction depends entirely on the characteristics of the reference sample. The lack of consideration of population specificities in current facial features approximation techniques such as for the approximation of the nose limits the objectivity and the accuracy of the reconstruction. Indeed, the nose is an important feature, mainly in profile and in three-quarter view, to accurately predict in facial recognition [7].

The morphology of the nose is often manually reconstructed from the shape and size of the nasal aperture, or bony substrate represented by the position of the pronasale, subnasale, and alare landmarks [8-14]. Stephan and colleagues, [14] found that all nasal approximation methods from the nasal aperture were severely limited for accurately reconstructing the external nose. The reason for these limitations is that all these methods use dry skull reference databases and exclude data obtained from associated soft-tissue. Therefore, a need exists for facial approximation practitioners to move away from traditional three- and two-dimensional techniques and for 3D computer techniques to be further developed where the relationship between hard- and soft-tissues can be more accurately examined [14]. Stephan and colleagues [14] conclude that the three-dimensional (3D) computer techniques for nose approximation have the potential to become a CFR method of choice for many reasons, eg. for its ability to: 1) perform indirect measurements using 3D planes; 2) consider variables such as ancestry, sex and age; 3) generate 3D nose approximations.

Automation of facial approximation of the nose using large 3D surface samples offers increased objectivity and the possibility of standardization when compared to manual methods. In general, all 3D computer-based methods for nose approximation share the foundational premise that information about the complete skull versus information of the skin is used for mapping a template face onto a dry skull [15, 3]. More precisely, the prediction is performed by using a soft-tissue representation generated from the database by applying a deformation, based on the correlation between skin and skull-surfaces incorporated in the database. However, many 3D automated methods also have problems with validity and reliability because of available reference samples, the manual landmark placement on a 3D surface and the absence of a biologically meaningful region of interest [3]. For example, supination effects on the face are influenced through the use the samples from conventional CT scans [16-18]. Additionally,

the slice thickness of conventional CT scans generally range from 0.6 mm to 1.5 mm [3, 15, 19] which may contribute to errors in the time consuming process of manually placing landmarks on the 3D hard- and soft-tissue surfaces.

The nose is a projecting feature that varies considerably and is difficult to reconstruct because of its less clear relationship with the underlying skeletal features. During craniofacial development, from birth to death, the morphology of the nose is influenced by the remodelling of the underlying skeletal structure [20] emphasizing the fact that the components of the nose cannot be considered as an independent element of the craniofacial skeleton. In the scientific literature, it has been demonstrated that the growth and development of the human craniofacial skeleton results from the interdependence of its different components, which are influenced by multifactorial processes involving hormonal, genetic and epigenetic factors such as age, sex, ancestry; and external stimuli [21-32]. The shape of the nose is also influenced by soft tissue facial aging which is known to vary according to the decade of life, sex and ancestry [33, 34].

IA biologically meaningful region of interest should be considered in the prediction of the morphology of the nose. A biologically meaningful region of interest is defined as a skeletal region, demonstrating important shape variation impacting on the external morphology and influenced by factors such as age, sex, ancestry. In many 2D and 3D nose approximation methods, a biologically meaningful region of interest is rarely considered, despite numerous studies advocating the importance of considering factors such as sex and ancestry in the approximation of the nose [3, 35]. Overall, nasal complex (mid-facial skeleton and the external nose) shape variations present a challenge for developing nose reconstruction methods. The effects of ancestry, sexual dimorphism and aging on the morphology of the nose, needs to be quantified with accuracy in order to create accurate and reliable 3D South African statistical nose prediction methods in the future.

The aim of this study was to use geometric morphometrics to describe the influence of age, size, sex, ancestry, and allometry (size) on the morphology of the hard- and soft-tissues of the nasal complex.

Materials and Methods

Data were sourced from CBCT-scans as retrospective records collected at two institutions: the *Oral and Dental Hospital, University of Pretoria, South Africa* and the *Life Groenkloof Hospital, Pretoria, South Africa*. The scans were anonymized, with only details regarding age, sex and ancestry remaining. Only scans of individuals 19 years or older were selected. In order to standardise the acquisition were scanned in a seated position with their eyes closed and with a relaxed facial expression. Exclusion criteria included: any condition that affected facial morphology (e.g. orthodontic treatment, pathological conditions, facial asymmetry or any facial interventional reconstructive surgery). The database contains 200 individuals of which 100 are black South Africans (33 females, 67 males) and 100 are white South Africans (65 females, 35 males). The average age of the complete sample is 40.51 years. The average age of the black South African sample is 36.07 years, with females being slightly older (39.45 years) than males (34.40 years). Individuals in the white South African sub-sample are slightly older in average compared to the black South African sub-sample. The average of the white South African group is 45.01 years, with females being slightly older (45.78 years) than males (43.60 years). All cone beam computer tomography scans used in this research were obtained using a CBCT scanner (Planmeca ProMax ® 3D, Pretoria, South Africa) with the following properties: 90 kV, 11.2 mA, voxel size of 0.4 mm, and field of view of 230 x 260 mm.

X-ray computed tomography (CT) is a non- destructive technique that allows visualization of the internal structure of objects, determined mainly by variations in density and atomic composition [36]. Cone Beam Computed Tomography (CBCT) imagining is accomplished by using a rotating gantry to which an x-ray source and detector are fixed. A divergent pyramidal- or cone-shaped source of ionizing radiation is directed through the middle of the area of interest onto an area x-ray detector on the opposite side. The x-ray source and detector rotate around a rotation fulcrum fixed within the center of the region of interest. During the rotation, multiple (from 150 to more than 600) sequential planar projection images of the field of view (FOV) are acquired in a complete, or sometimes partial, arc [37].

CBCT images in DICOM format were imported into MeVisLab © v. 2.7.1 software for segmentation and 3D surface mesh generation. On the scans, grey values encode the density of the observed material similar to a common X-ray image; the lighter the grey value, the denser the tissue's intrinsic structure. Based on a defined grey value threshold and given all the different layers, the MeVisLab[©] v2.7.1 estimates a 3D representation of the object. The software also interpolates the spaces between the distinct slices. We defined different grey value intervals for hard and soft tissues using the "Half Maximum Height" (HMH) quantitative iterative thresholding method [38]. For this dissertation, threshold values for hard-tissue varied between 1200-1250 and for the soft-tissue between 400-450. The segmentation process is illustrated in Figure 1. a.

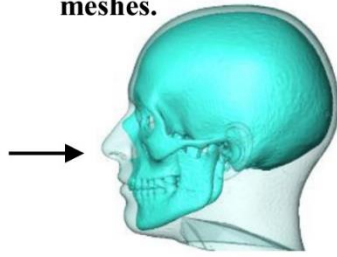
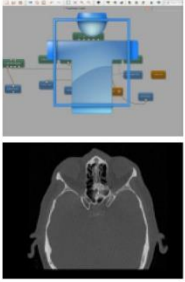
After segmentation of the hard- and soft-tissues, 3D-triangular surface meshes were constructed. This resulted in 400 usable 3D surfaces (200 hard- tissue 3D surfaces and 200 soft-tissue 3D surfaces). Prior to registration, all the surfaces were repositioned into the same coordinate system using an initialisation mesh procedure (Figure 1.b). The initialisation was performed manually with indicating a set of landmarks on floating and target surfaces in order to interactively rotate and translate the surfaces so as to bring them into each other's proximity. These transformations map the coordinates on each point of the floating surface into the coordinate space of the target surface. The results of the non-rigid surface registration depend on the quality of this initialisation procedure.

The automatic landmarking method used in this study was adapted from the procedure introduced by [Claes and colleagues](#) [39-42]. Reference hard- and soft-tissue templates (Figure 1.d) were created using a non-rigid- surfaces registration process (Figure 1.c). During surface registration, the geometrical relationship between surfaces was established, so that surfaces were optimally aligned. Then, every individual surface was 'templated', resulting in a warped surface, so that every point on all 3D surfaces was associated with the anatomically corresponding point on the reference template. Landmarks were then placed on the reference templates (Figure 1.e). Each landmark placed on the reference template was associated to the anatomically corresponding point on the warped surfaces.

During an anatomical templating process, the reference template was warped non-rigidly to every subject's anatomically corresponding surface (target surface). The non-rigid (robust) surface registration software used for this warping was developed using the MeVisLab © v. 2.7.1 software [43]. The warping was performed iteratively starting with a rigid alignment, and gradually following with more flexible registration steps. At the end of this process every landmark of the template was projected onto every subject's surface, thus establishing a dense point-based anatomical correspondence among all subjects (Figure 1.f). Therefore, the coordinates of all subjects were recorded within a common coordinate system which may be used for statistical analysis.

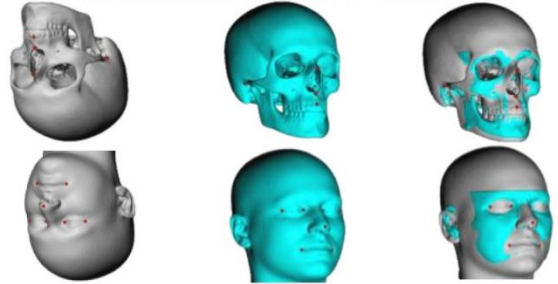
DATABASE

a **Segmentation and construction of surface meshes.**



Hard- and soft- tissue surface meshes.

b **Initialization of surface meshes.**



All surfaces are aligned on the same coordinates system.

TEMPLATE GENERATION

c



Non-rigid surface registration.



d



Templates

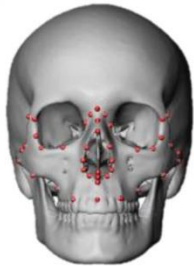


Geometrical relationship between surfaces.

All surfaces are templated (named warped surfaces).

ANATOMICAL TEMPLATING

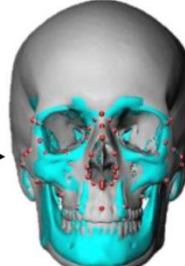
e



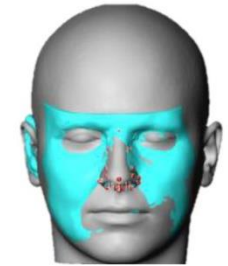
Landmark placements on templates.



f



Automatic landmarking



Landmarks placed on templates are associated with the corresponding points on the warped surfaces.

Figure 1. Workflow of the automatic landmarking procedure. a) segmentation process; b) initialisation process; c) non-rigid surface registration process; d) templates generation; e) definition of the region of interest on templates; f) automatic landmarking.

Following the facial approximation literature [3, 19] and to conserve homology and comparability between studies, classic craniometric and capulometric landmarks (type I, II, and III [3, 19, 44, 45] were used. We selected landmarks on the facial skeleton and the external nose, creating a hard- and soft-tissue region of interest. The hard-tissue region of interest was delimited on the facial skeleton (Figure 2) comprising the nasal bones (Figure 2.b), the anterior nasal aperture (Figure 2.c), the zygomatic bones (Figure 2.d). and the maxillae (Figure 2.e). On the nasal bones, five craniometric landmarks (three median and two bilateral pairs), and on the anterior nasal aperture, eight craniometric landmarks (four median and four bilateral pairs) were recorded. On the zygomatic bone, nine craniometric landmarks (bilateral pairs) and 10 craniometric landmarks (two median and eight bilateral pairs) on the maxillary bone were recorded. A total of 41 craniometric landmarks, 17 bilateral pairs and seven median landmarks, were recorded on the hard-tissue surfaces (Table 1). The soft-tissue region of interest was delimited by the surface anatomy as related to the hard-tissue (Figure 3), including mainly the nares (Figure 3.b) and the external nose (Figure 3 c, d). On the soft-tissue, 21 capulometric landmarks were recorded, eight bilateral pairs and five median landmarks (Table 2).

Table 1. Craniometric landmarks used [3, 19, 44, 45].

Craniometric	Landmarks	Abbreviation	Nature	Definition
	1 Nasion	n	Median	Intersection of the nasofrontal sutures in the median plane.
	2 Mid-nasal	mn	Median	Midline point on the internasal suture midway between nasion and rhinion.
	3 Rhinion	rhi	Median	Most rostral (end) point on the internasal suture. Cannot be determined accurately if nasal bones are broken distally.
	4 Nasospinale	ns	Median	The point where a line drawn between the inferior most points of the nasal aperture crosses the median plane. Note that this point is not necessarily at the tip of the nasal spine.
	5 Subspinale	ss	Median	The deepest point seen in the profile view below the anterior nasal spine (orthodontic point A).
	6 Akanthion	ak	Median	Most anterior midline point of the nasal spine.
	7 Prosthion	pr	Median	Median point between the central incisors on the anterior most margin of the maxillary alveolar rim.
	8/9 Zygotemporale superior	zts	Bilateral	Most superior point of the zygomatico-temporal suture.
	10/11 Zygotemporale inferior	zti	Bilateral	Most inferior point of the zygomatico-temporal suture.
	12/13 Jugale	ju	Bilateral	Vertex of the posterior zygomatic angle, between the vertical edge and horizontal part of the zygomatic arch.
	14/15 Frontomalare temporale	fnt	Bilateral	Most lateral part of the zygomaticofrontal suture.
	16/17 Frontomalare orbitale	fmo	Bilateral	Point on the orbital rim marked by the zygomaticofrontal suture.
	18/19 Nasomaxillofrontale	nmf	Bilateral	Point at the intersection of the frontal, maxillary, and nasal bones.
	20/21 Ectoconchion	ec	Bilateral	Lateral point on the orbit at a line that bisects the orbit transversely.
	22/23 Orbitale	or	Bilateral	Most inferior point on the inferior orbital rim. Usually falls along the lateral half of the orbital margin.
	24/25 Zygo-orbitale	zo	Bilateral	Intersection of the orbital margin and the zygomaticomaxillary suture.
	26/27 Maxillofrontale	mf	Bilateral	Intersection of the anterior lacrimal crest with the frontomaxillary suture.
	28/29 Nasomaxillare	nm	Bilateral	Most inferior point of the nasomaxillary suture on the nasal aperture.
	30/31 Alare	al	Bilateral	Instrumentally determined as the most lateral point on the nasal aperture in a transverse plan.
	32/33 Piriform curvature	cp	Bilateral	Most infero-lateral point of the piriform aperture.
	34/35 Nariale	na	Bilateral	Most inferior point of the piriform aperture.
	36/37 Zygomaxillare	zm	Bilateral	Most inferior point on the zygomaticomaxillary suture.
	38/39 Submaxillare curvature	csm	Bilateral	Most supero-medial point on the maxillary inflexion between the zygomaxillare and the ectomolar.
	40/41 Supra-canine	sc	Bilateral	Point on the superior alveolar ridge superior to the crown of the maxillary canine.

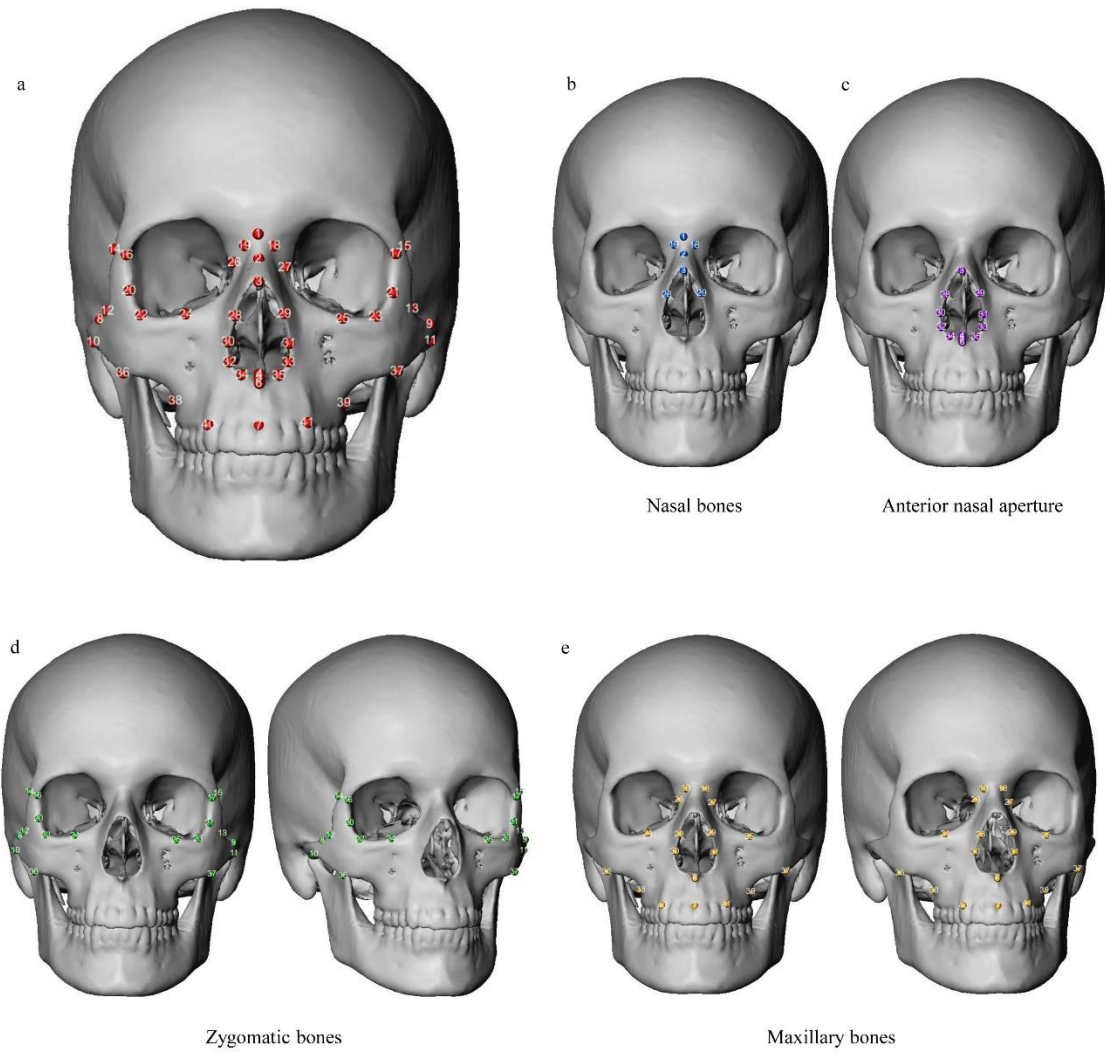


Figure 2. Hard-tissue region of interest. a) frontal view of the mid-facial hard-tissue region of interest; b) nasal bones; c) anterior nasal aperture; d) zygomatic bones; e) maxillary bones (cf. Table 1).

Table 2. Capulometric landmarks used [3, 19, 44, 45].

Capulometric	Landmarks	Abbreviation	Nature	Definition
	1 Pronasale	prn'	Median	The most anteriorly protruded point of the apex nasi. In the case of a bifid nose, the more protruding tip is chosen.
	2 Nasale inferius	ni'	Median	Most inferior point of the apex nasi. Not locatable on upturned noses.
	3 Columella	c'	Median	Midpoint of the nasal columella crest, intersecting a line between the two cs' points.
	4 Subnasale	sn'	Median	Median point at the junction between the lower border of the nasal septum and the philtrum area.
	5 Sellion	se'	Median	Deepest midline point of the nasofrontal angle; not a substitute for n'.
	6/7 External alar curvature	eac	Bilateral	Most anterior point of the nasal wing at the maximum of curvature.
	8/9 Superior alar curvature	sac	Bilateral	Most superior point of the nasal wing.
	10/11 Alagenion	ag	Bilateral	Most posterior point of the nasal wing.
	12/13 Alare	al'	Bilateral	The most lateral point on the nasal ala.
	14/15 Alar curvature point	ac'	Bilateral	The most posterolateral point of the curvature of the base line of each nasal ala.
	16/17 Mid-nostril	mn	Bilateral	Midpoint of maximal nostril width - projected on the transition nostril/philtrum.
	18/19 Mid-columella	mc'	Bilateral	Midpoint of the nasal columella crest on either side, where the columella thickness is measured (equivalent to Subnasale).
	20/21 Nasal-depth	nd	Bilateral	Most medial point of the transition nose/eye.

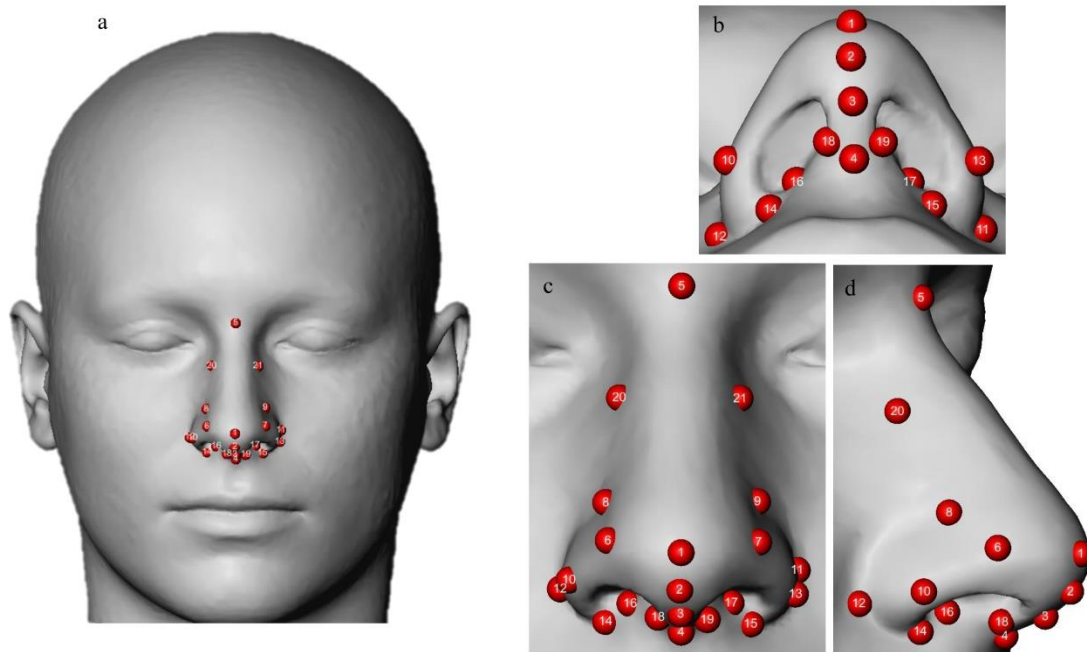


Figure 3. Soft-tissue region of interest. a) frontal view of the soft-tissue region of interest; b) inferior view of the nose; c) anterior view of the nose; d) lateral view of the nose (cf. Table 2).

The procedure of the automatic placement of discrete landmarks was applied using two different templates, one for each sample, namely a black South African template (Figure 4 a,b) and a white South African template (Figure 4 c,d). The landmarks of interest were indicated once on each template for both groups separately, which were then projected each of the 400 surfaces (200 hard-tissue and 200 soft-tissue). The coordinates of the landmarks were then recorded for the statistical analysis.

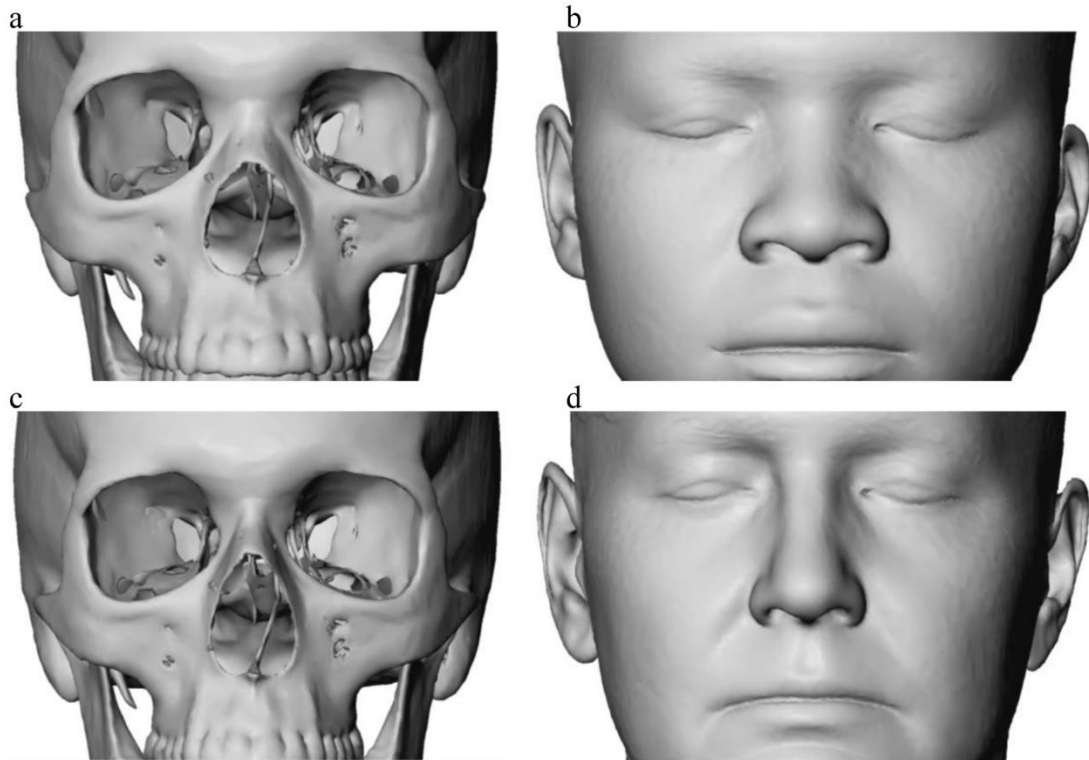


Figure 4. Black and white South African templates. a) black hard-tissue template; b) black soft-tissue template; c) white hard-tissue template; d) white soft-tissue template.

The evaluation and the quantification of shape differences attributed to known factors (ancestry, sex, size and age) and covariates was performed both on hard- and soft-tissue shape using Geometric morphometric method (GMM). Geometric morphometrics considers the geometry of the placed landmarks and allows for effective visual representations of statistical results as actual shapes/forms or shape/form deformations [46-54].

Preceding the statistical analysis, we used a General Procrustes Analysis (GPA) [55, 56] to obtain pose-invariant shape coordinates [57-60] for both the hard- and soft-tissue surfaces. We used Principal Component Analysis (PCA) to reduce data dimensionality and to create independent principal component (PC) scores that quantified the different shapes. Statistical testing was performed using the PC scores covering 95% of the sample's overall variance. Hard and soft tissue PC scores were tested for normality by interpreting Q-Q-plots [61]. All results were double-checked using non parametric testing and only if both tests point into the same direction, results were considered reliable. The GPA, PCA and the multivariate normality testing were performed on the whole sample, on the hard and soft tissue surfaces separately and on the hard and soft tissue surfaces for each population subset, namely black South Africans and white South Africans.

The impact of ancestry, sex, age and allometry on the hard- and soft-tissue within the complete sample was firstly performed. Then, in order to identify significant population-specific differences, the sexual dimorphism expression, the ageing process and the impact of size (allometry) were analysed on each specific subsample (black and white subsamples) separately and on both hard- and soft- tissue. Finally, the analysis of covariation between nasal hard- and soft- tissue and its dependence on ancestry were analyzed.

Multiple analysis of variance (MANOVA) was run to evaluate differences between populations, sexes and with aging on hard and soft tissues. A MANOVA is an extension of the univariate analysis of variance (ANOVA). MANOVA takes into account multiple continuous dependent variables and bundles them together into a weighted linear combination or composite variables. The MANOVA will compare whether or not the newly created combination differs among groups, or levels, of the independent variable. In this way, the MANOVA essentially tests whether or not the independent grouping variable simultaneously explains a statistically significant amount of variance in the dependent variable. We applied MANOVA using the R-packages `geomorph` [62].

Two non parametric-tests were also applied in order to double checked the results from the parametric test: 50-50 MANOVA and permutation testing (all permutation tests were run with 10,000 rounds). 50-50 MANOVA [63, 64] is a modified version of a MANOVA, designed for many (potentially correlated) response variables. We applied 50-50 MANOVA using the R-packages `ffmanova` [65]. Permutation testing permits calculation and comparison to values gained from the same sample where group membership is randomly reassigned over and over again. As a result, the number of resampled values exceeding the “true” one are divided by the number of permutation rounds. If the value to be tested falls within the range of random grouping, the null hypothesis cannot be rejected, because the measured value is not exceeding the one generated by chance. Permutation testing was performed using the R-packages `Morpho` [66]. Significance of age effects were also assessed using standard MANOVA (parametric test) and 50-50 MANOVA (non-parametric test).

Standard discriminant function analysis (DFA) was also performed for ancestry and sex classification purposes. The accuracy of the classification was estimated by conducting a leaving-one-out cross-validation. Discriminant function analysis finds linear variables that describe intergroup differences. These combinations define linear discriminant functions. The

linear discriminant coefficients are defined from the non-null eigenvectors of the between group variance-covariance “scaled” by the within-group variance-covariance. Discriminant function analysis was conducted using the R-packages Morpho [66].

To assess the influence of allometry, we constructed linear models, with hard and soft tissue shape as response variables and, sex and centroid size as predictor variables. Allometry is defined as shape change that can be expressed as a function of size [46, 67]. In this study, we considered allometric effects when dealing with shape differences associated with sex on account of the effect of sexual dimorphism on size [3, 68, 69]. The significance of each variable was tested using MANCOVA using Pillai trace and double checked by applying 50-50 MANOVA (non-parametric test).

We assessed the covariation between the mid-facial hard-tissue elements and the external soft-tissue of the nose on each subsample using Two Blocks Partial Least Squares (PLS) analyses. The two-block partial least squares analysis allows us to assess the degree of association between two block of Procrustes-aligned coordinates [70].

Results

For the complete sample and within ancestral subgroups, the multivariate normality analyses, using Q-Q plots of Mahalanobis distances, revealed non-parametric distributions for some hard-tissue elements such as the anterior nasal aperture and the maxillary shapes. For this reason, all results were examined using both parametric and non-parametric tests and results were only considered reliable if both tests provided a similar outcome.

Complete sample

Ancestry was found to contribute the most to shape variation in the complete sample for both, hard- and soft-tissue shape components (Figure 5). All statistical tests (Table 3), parametric (MANOVA) and non-parametric (Permutation test) confirmed a strong difference between ancestral averages for all hard-tissue and soft-tissue elements. Additionally, the overall classification accuracy was 100%, meaning that none of the 200 specimens were wrongly classified. (Table 3). Judging by visual observation in Figure 9 a,b of the hard- (Figure 9.a) and soft-tissue (Figure 9.c) mean shape representations, the larger shape could be attributed to black South Africans. The boxplots (Figure 6) further also illustrated that the centroid sizes are were slightly larger within black than white South Africans. However, this was a very small variation concerning the groups mean shapes, thus reflecting only minor shape changes attributed to ancestral-specific size. In addition, the interaction between size and ancestry testing reported non-significant differences for the hard-tissue including all the skeletal elements evaluated separately, as well as for the soft-tissue (Table 3).

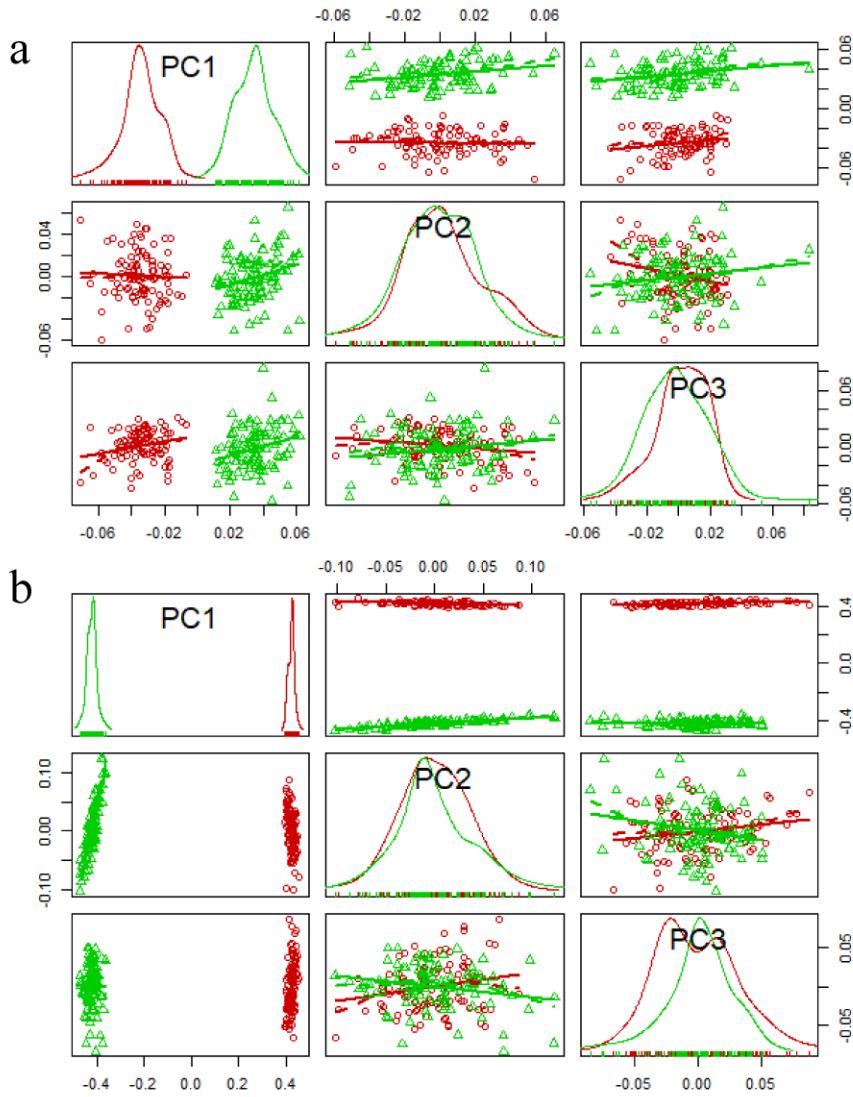


Figure 5. Pairwise scatterplots of the scores from the first three hard-tissue mid facial PCs and the first three external nasal soft-tissue PCs. a) mid-facial hard-tissue; b) external nasal soft-tissue. Red circle: Black South African; Green triangle: White South African.

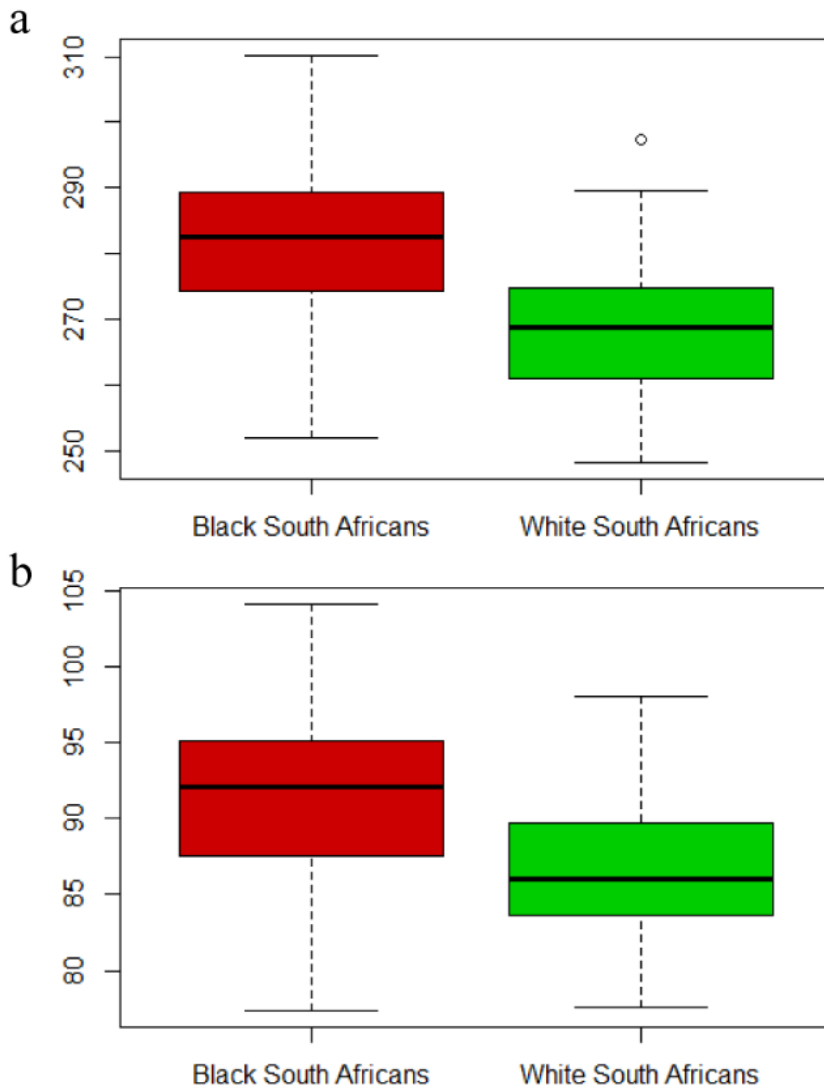


Figure 6. Centroid sizes of the mid facial hard-tissue (a) and the external nasal soft-tissue (b) shape components. Red: Black South African; Green: White South African.

Table 3. Results of hard- and soft-tissue ancestral differences.

	Ancestry			Ancestry*Size
	Test ¹	Test ²	DFA	Test ³
Mid-facial region	0.001	0.001	100%	0.431
Nasal bones	0.001	0.001	100%	0.216
Nasal bone (left)	0.001	0.001	99%	0.554
Nasal bone (right)	0.001	0.001	100%	0.583
Anterior nasal aperture	0.001	0.001	100%	0.623
Anterior nasal aperture (left)	0.001	0.001	99%	0.580
Anterior nasal aperture (right)	0.001	0.001	100%	0.563
Zygoma	0.001	0.001	100%	0.556
Zygomatic bone (left)	0.001	0.001	100%	0.553
Zygomatic bone (right)	0.001	0.001	100%	0.534
Maxilla	0.001	0.001	100%	0.598
Maxillary bone (left)	0.001	0.001	100%	0.627
Maxillary bone (right)	0.001	0.001	100%	0.623
External nose	0.001	0.001	100%	0.615

Test¹: MANOVA; Test²: Permutation test; Test³: ANOVA. Significant p.value (<0.05) are indicated in bold.

The two South African ancestral groups differed also visually in shape variation for the hard and soft-tissue regions of interest (Figure 9 a,b). For example on the soft-tissue of the external nose, black South Africans presented with a flattened and larger external nose, while white South Africans had a longer and more prominent external nose. On the hard-tissue skeletal region of interest, nasal bones of black South Africans were more integrated into the skull (or blunt), whereas nasal bones were more salient in white South Africans. Black South Africans had an anterior nasal aperture rounder and wider than white South Africans, which is narrower and more constricted (or pear-shaped). Concerning, the maxilla, black South Africans exhibit prognathism, unlike the maxilla of white South Africans which exhibits orthognathism. For both ancestral groups, zygomatic bones are retracted, but this tends to be more obvious in the black South African than in the white South African group. White South Africans also present with narrower zygomatic bones than black South Africans.

Sex was observed to have an interaction with ancestry in the complete hard- and soft-tissue sample. The between group PCAs (Figure 7), confirmed a strong separation between ancestral groups and illustrated a similar expression of sexual dimorphism (Figure 9 c, d, e, f) in both populations for both, hard- (Figure 7 a) and soft- tissue (Figure 7 b) shape components. However, when elements of the hard-tissue shape components were considered separately, the interaction of between sex and ancestry was not significant (Table 4), demonstrating the absence of ancestral-specific expression of sexual dimorphism for the hard-tissue shape. On the other hand, for the soft-tissue shape component, the interaction of sex with ancestry was statistically significant, implicating ancestral-specific expression of sexual dimorphism for the external nose (Table 4).

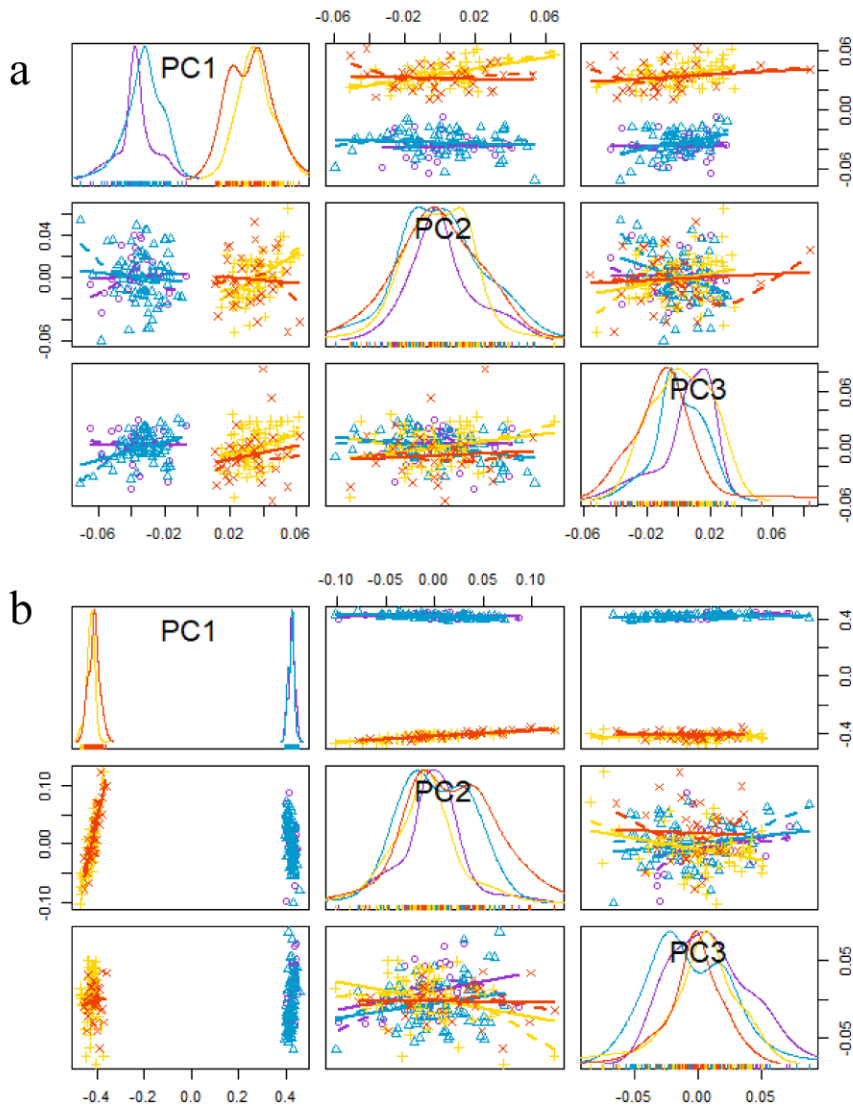
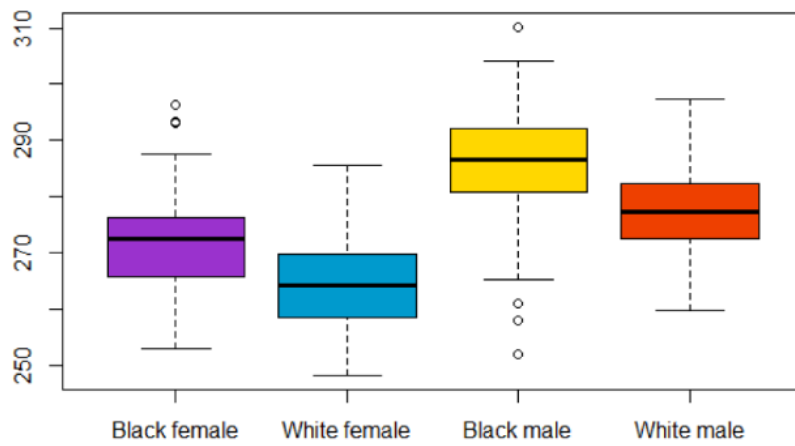


Figure 7. Between group PCA of mid facial hard-tissue and external nasal soft-tissue shape components grouped by sex and ancestry. a) mid facial hard-tissue; b) external nasal soft-tissue. Purple circle: black female; blue triangle: black male; yellow plus: white female; orange cross: white male.

a



b

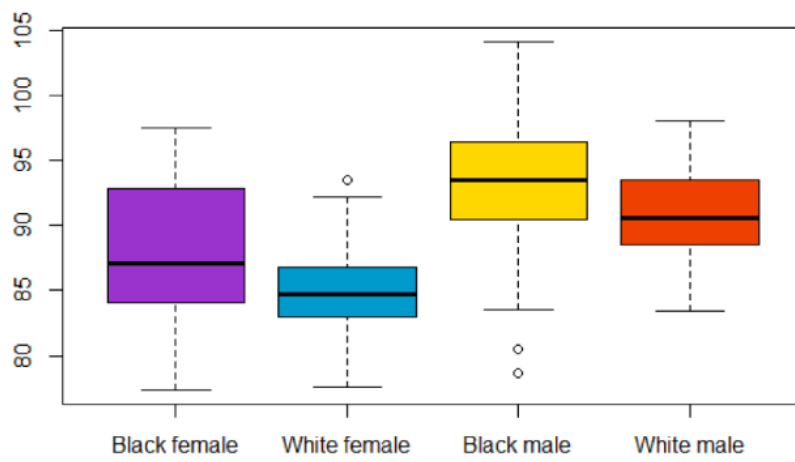


Figure 8. Centroid sizes grouped by sex and ancestry for the mid facial hard-tissue and the external nasal soft-tissue shapes. a) mid facial hard-tissue; b) external nose soft-tissue. Purple: black female; yellow: white female; blue: black male; orange: white male.

Table 4. Hard- and soft-tissue sexual dimorphism in the complete sample and within ancestral groups.

	Complete sample		Black South Africans				White South Africans					
	Ancestry*Sex		Test ¹	Test ²	Test ⁴	DFA	Size*sex Test ³	Test ¹	Test ²	Test ⁴	DFA	Size*sex Test ³
Test ⁴	Test ⁵	Test ¹										
Mid-facial region	0.325	0.253	0.015	0.008	0.008	96%	0.270	0.017	0.019	0.616	93%	0.501
Nasal bones	0.121	0.086	0.053	0.049	0.000	76%	0.631	0.158	0.164	0.000	83%	0.629
Nasal bone (left)	0.364	0.396	0.036	0.034	0.052	71%	0.619	0.068	0.055	0.014	70%	0.620
Nasal bone (right)	0.060	0.082	0.006	0.006	0.000	79%	0.558	0.165	0.178	0.000	80%	0.621
Anterior nasal aperture	0.622	0.562	0.005	0.005	0.003	82%	0.378	0.514	0.516	0.476	79%	0.152
Anterior nasal aperture (left)	0.400	0.097	0.003	0.006	0.002	82%	0.618	0.454	0.424	0.234	68%	0.615
Anterior nasal aperture (right)	0.555	0.495	0.011	0.006	0.001	76%	0.571	0.239	0.214	0.129	76%	0.587
Zygoma	0.249	0.372	0.001	0.001	0.000	91%	0.381	0.001	0.001	0.000	93%	0.593
Zygomatic bone (left)	0.394	0.502	0.002	0.002	0.000	86%	0.088	0.001	0.001	0.000	90%	0.532
Zygomatic bone (right)	0.684	0.765	0.001	0.001	0.000	84%	0.521	0.002	0.001	0.000	94%	0.516
Maxilla	0.397	0.311	0.097	0.107	0.002	88%	0.531	0.029	0.021	0.000	94%	0.579
Maxillary bone (left)	0.173	0.188	0.025	0.032	0.000	82%	0.684	0.034	0.025	0.000	90%	0.378
Maxillary bone (right)	0.275	0.228	0.133	0.147	0.003	82%	0.620	0.013	0.008	0.000	91%	0.641
External nose	0.008	0.008	0.005	0.005	0.014	88%	0.679	0.001	0.001	0.016	90%	0.378

Test¹: MANOVA; Test²: Permutation test; Test³: ANOVA. Test⁴: MANCOVA; Test⁵: 50-50 MANOVA. Significant p-values (<0.05) are indicated in bold.

For an analysis of the ageing process, we observed its interaction with ancestry and sex in the complete hard- and soft-tissue sample. For the hard-tissue shape, both parametric (MANCOVA) and non-parametric (50-50 MANOVA) tests did not reported a similar outcome for the variable age, but significance was reported for the interaction between ancestry and age. (Table 5). Regarding, the soft-tissue shape both parametric and non-parametric tests reported significance for the variable age, and for the interaction between age and ancestry. When we analysed the hard-tissue elements separately, the right anterior nasal aperture and the right maxilla seemed to show a greater variability of shape with aging when compared to the other skeletal elements, as well for the interaction between ancestry and age (Table 5). On the other hand, apart from the right maxillary bone, no parametric and non-parametric testing on individual skeletal elements and on soft-tissue reported significance for the interaction between sex and age, or for the interaction between ancestry, sex and age. Age, and it's interaction between ancestry, were reported to be highly significant contributors to overall hard- and soft-tissue shape variation (Figure 9 g, h, i, j).

Table 5. Hard- and soft-tissue shape change associated with age in the complete sample and within ancestral groups.

	Complete sample								Black South Africans				White South Africans			
	Age		Ancestry*Age		Sex*Age		Ancestry*Sex*Age		Age		Sex*Age		Age		Sex*Age	
	Test ⁴	Test ⁵	Test ⁴	Test ⁵	Test ⁴	Test ⁵	Test ⁴	Test ⁵	Test ⁴	Test ⁵	Test ⁴	Test ⁵	Test ⁴	Test ⁵	Test ⁴	Test ⁵
Mid-facial region	0.054	0.012	0.002	0.000	0.454	0.288	0.317	0.302	0.006	0.000	0.001	0.064	0.001	0.015	0.020	0.015
Nasal bones	0.420	0.309	0.763	0.484	0.501	0.760	0.989	0.996	0.357	0.372	0.880	0.863	0.401	0.429	0.306	0.328
Nasal bone (left)	0.363	0.230	0.740	0.547	0.782	0.632	0.931	0.975	0.670	0.694	0.758	0.770	0.548	0.583	0.565	0.586
Nasal bone (right)	0.507	0.298	0.391	0.266	0.302	0.412	0.981	0.952	0.595	0.581	0.770	0.775	0.548	0.548	0.754	0.797
Anterior nasal aperture	0.109	0.127	0.017	0.003	0.746	0.842	0.687	0.691	0.009	0.000	0.008	0.057	0.134	0.038	0.826	0.901
Anterior nasal aperture (left)	0.112	0.032	0.034	0.011	0.598	0.796	0.348	0.533	0.115	0.057	0.368	0.454	0.282	0.276	0.904	0.934
Anterior nasal aperture (right)	0.024	0.036	0.134	0.108	0.433	0.625	0.081	0.052	0.011	0.002	0.003	0.002	0.080	0.030	0.748	0.731
Zygoma	0.530	0.596	0.014	0.145	0.896	0.791	0.769	0.700	0.040	0.092	0.070	0.151	0.102	0.079	0.521	0.412
Zygomatic bone (left)	0.373	0.450	0.038	0.165	0.737	0.674	0.210	0.193	0.121	0.113	0.153	0.155	0.574	0.408	0.304	0.188
Zygomatic bone (right)	0.190	0.302	0.026	0.060	0.518	0.467	0.151	0.098	0.042	0.023	0.098	0.030	0.159	0.078	0.732	0.518
Maxilla	0.132	0.064	0.015	0.000	0.228	0.370	0.129	0.117	0.149	0.001	0.280	0.028	0.031	0.090	0.119	0.121
Maxillary bone (left)	0.137	0.094	0.079	0.038	0.379	0.279	0.587	0.528	0.016	0.011	0.679	0.720	0.185	0.393	0.566	0.376
Maxillary bone (right)	0.004	0.001	0.101	0.019	0.009	0.020	0.005	0.002	0.109	0.043	0.044	0.046	0.039	0.057	0.075	0.017
External nose	0.001	0.000	0.009	0.010	0.674	0.665	0.723	0.730	0.000	0.000	0.002	0.595	0.007	0.006	0.754	0.876

Test⁴: MANCOVA; Test⁵: 50-50 MANOVA. Significant p.values (<0.05) are indicated in bold.

To create an impression of the extent to which allometry is responsible for hard- and soft-tissue shape variations in the complete sample, all three variables, ancestry, sex and centroid size, were tested. For the hard-tissue shape, all statistical tests (parametric and non-parametric) reported significance for size (Table 6). When we analyzed all elements of the hard-tissue region separately, the nasal bones, the left anterior nasal aperture, the left zygomatic bone and the left maxillary bone showed significance with both parametric and non-parametric tests for the interaction between size and ancestry. On the other hand, no significance was found for the interaction between sex and size, and only the nasal aperture and the maxilla showed a significant interaction among ancestry, sex and size, with both parametric and non-parametric tests. Regarding the soft-tissue shape, both parametric and non-parametric statistical tests, reported significance for size (Table 6). No significance interaction was observed between ancestry and size, or among ancestry, sex and size for soft-tissue shapes. Overall, size is an important contributor to variation found in the hard- and soft-tissue shapes.

Table 6. Hard- and soft-tissue shape changes associated with size in the complete sample and within ancestral groups.

	Complete sample								Black South Africans				White South Africans			
	Size		Ancestry*Size		Sex*Size		Ancestry*Sex*Size		Size		Sex*Size		Size		Sex*Size	
	Test ⁴	Test ⁵	Test ⁴	Test ⁵	Test ⁴	Test ⁵	Test ⁴	Test ⁵	Test ⁴	Test ⁵	Test ⁴	Test ⁵	Test ⁴	Test ⁵	Test ⁴	Test ⁵
Mid-facial region	0.000	0.000	0.527	0.478	0.636	0.728	0.467	0.716	0.000	0.000	0.280	0.277	0.000	0.000	0.124	0.098
Nasal bones	0.000	0.000	0.000	0.002	0.611	0.445	0.313	0.238	0.000	0.000	0.229	0.190	0.000	0.000	0.718	0.676
Nasal bone (left)	0.000	0.000	0.000	0.144	0.312	0.248	0.577	0.476	0.000	0.000	0.142	0.142	0.000	0.000	0.780	0.780
Nasal bone (right)	0.000	0.000	0.014	0.004	0.287	0.208	0.466	0.658	0.000	0.000	0.323	0.324	0.000	0.000	0.632	0.632
Anterior nasal aperture	0.000	0.000	0.263	0.215	0.559	0.444	0.023	0.013	0.000	0.000	0.462	0.406	0.000	0.000	0.090	0.072
Anterior nasal aperture (left)	0.000	0.000	0.000	0.021	0.029	0.122	0.355	0.092	0.000	0.000	0.042	0.065	0.000	0.000	0.135	0.135
Anterior nasal aperture (right)	0.000	0.000	0.460	0.329	0.135	0.099	0.159	0.137	0.000	0.000	0.690	0.629	0.000	0.000	0.106	0.085
Zygoma	0.000	0.000	0.227	0.166	0.405	0.357	0.264	0.212	0.000	0.000	0.125	0.187	0.000	0.000	0.122	0.362
Zygomatic bone (left)	0.000	0.000	0.017	0.010	0.298	0.337	0.552	0.487	0.000	0.000	0.044	0.029	0.000	0.000	0.230	0.375
Zygomatic bone (right)	0.000	0.000	0.149	0.078	0.561	0.482	0.380	0.481	0.000	0.000	0.373	0.558	0.000	0.000	0.856	0.984
Maxilla	0.000	0.000	0.074	0.044	0.718	0.655	0.005	0.012	0.000	0.000	0.135	0.303	0.000	0.000	0.780	0.709
Maxillary bone (left)	0.000	0.000	0.024	0.013	0.911	0.856	0.162	0.127	0.000	0.000	0.829	0.749	0.000	0.000	0.532	0.473
Maxillary bone (right)	0.000	0.000	0.012	0.085	0.610	0.593	0.000	0.000	0.002	0.001	0.006	0.003	0.000	0.000	0.577	0.515
External nose	0.000	0.000	0.167	0.189	0.932	0.932	0.383	0.383	0.000	0.000	0.138	0.191	0.809	0.000	0.047	0.530

Test⁴: MANCOVA; Test⁵: 50-50 MANOVA. Significant p.values (<0.05) are indicated in bold.

Ancestry subsample

As ancestral differences were clearly visible within the data and in order to identify significant ancestral-specific differences, the expression of sexual dimorphism expression, the ageing process and the impact of size (allometry) were analyzed on each ancestry subsample (black and white subsamples) and on both hard- and soft-tissue.

In the black South African sample, the presence of sexual dimorphism was confirmed on all hard-tissue element shapes (Table 4), while only for the maxilla and the right maxilla shapes no significance was found in both parametric and non-parametric tests. Additionally, cross-validated linear discriminant function analysis yielded an accuracy of 96% for the hard-tissue shape component. For the black South African sample, when we analysed the skeletal elements separately, the zygomatic shape presented with the greatest sexual dimorphism, with a cross-validated linear discriminant function analysis of 91%. For the white South African group, the presence of sexual dimorphism was confirmed only on the shape of the zygoma and on the shape of the maxilla, with cross-validated linear discriminant function analysis of 93% and 94 % accuracy, respectively. Sexual dimorphism in the soft-tissue shape was confirmed in both populations (Table 4). Although, sexual dimorphism of the soft-tissue shape was accentuated for the white South African sample, all tests (parametric and non-parametric) also reported significant differences between group means for the black South Africans. Additionally, a cross-validated linear discriminant function analysis on the soft-tissue shape yielded an accuracy of 88% for the black South African sample and 90% for the white South African group, reflecting the discriminative power of sexual dimorphism in both populations.

The hard-tissue and soft-tissue shapes differences between sex averages for black South African (Figure 9 c, d) and white South African (Figure 9 e, f) confirm the statistical findings of sexual dimorphism in each population group. It is important to emphasize that the findings on sexual dimorphism may to some extent be impacted by the sex split in each sample (100 black South Africans (33 females, 67 males) and 100 white South Africans (65 females, 35 males). Non-significant differences to the size variations for the hard-tissue including all the skeletal elements evaluated separately, as well as for the soft-tissue (Table 4) were noted. On the other hand, boxplots (Figure 8) showed that the centroid sizes were slightly larger for males than for the females for both ancestral groups and for both, hard-and soft-tissue shape

components demonstrating that the expression of sexual dimorphism, concerning centroid size, is therefore very similar in each population group for both types of tissue.

In both ancestral groups, the effect of age on the hard-tissue shape was statically significant (Table 5) indicating that age contributes to hard-tissue shape variation in both ancestral groups. In the black South African sample, all statistical testing showed that the shape of the anterior nasal aperture, the shape of the right zygoma and the shape of the left maxilla seemed to indicate a more important influence of age for the explanation of shape variability than in the white South African sample. In both samples, significant interactions between age and sex were found in the hard-tissue shape indicating that sex-dependent ageing processes exist. In addition, parametric and non-parametric testing reported a significant influence for age on the soft-tissue, suggesting that age affects, or at least influences, shape variability of the external nose (Table 5) in both ancestral groups. No significance for the interaction of sex and age were noted on the soft-tissue, indicating that the influence of ageing was independent of sex.

The statistical findings on ageing processes in each ancestral group is confirmed in Figure 9 representing the mid-facial hard-tissue and external soft-tissue shape differences between average age from 18 to 79 years for black South Africans (Figure 9 g, h) and white South Africans (Figure 9 i, j). It is important to emphasize that the findings on the ageing process may to some extent be impacted by the fact that individuals in the white South African sub-sample are slightly older on average compared to the black South African sub-sample.

In the black and white South African sample separately, all parametric and non-parametric tests reported significance for size on all elements of the hard- and soft-tissue. In both ancestral groups, no statistical significance was noted for the interaction between sex and size on the hard- and soft-tissue shapes, indicating a common direction of allometry in both sexes for both types of tissues. Only the left zygomatic bone and the right maxillary bone indicated a significant interaction between sex and size in the black South African sample. (Table 6). In both ancestral groups, size is an important factor for the explanation of hard- and soft-tissue shape variability.

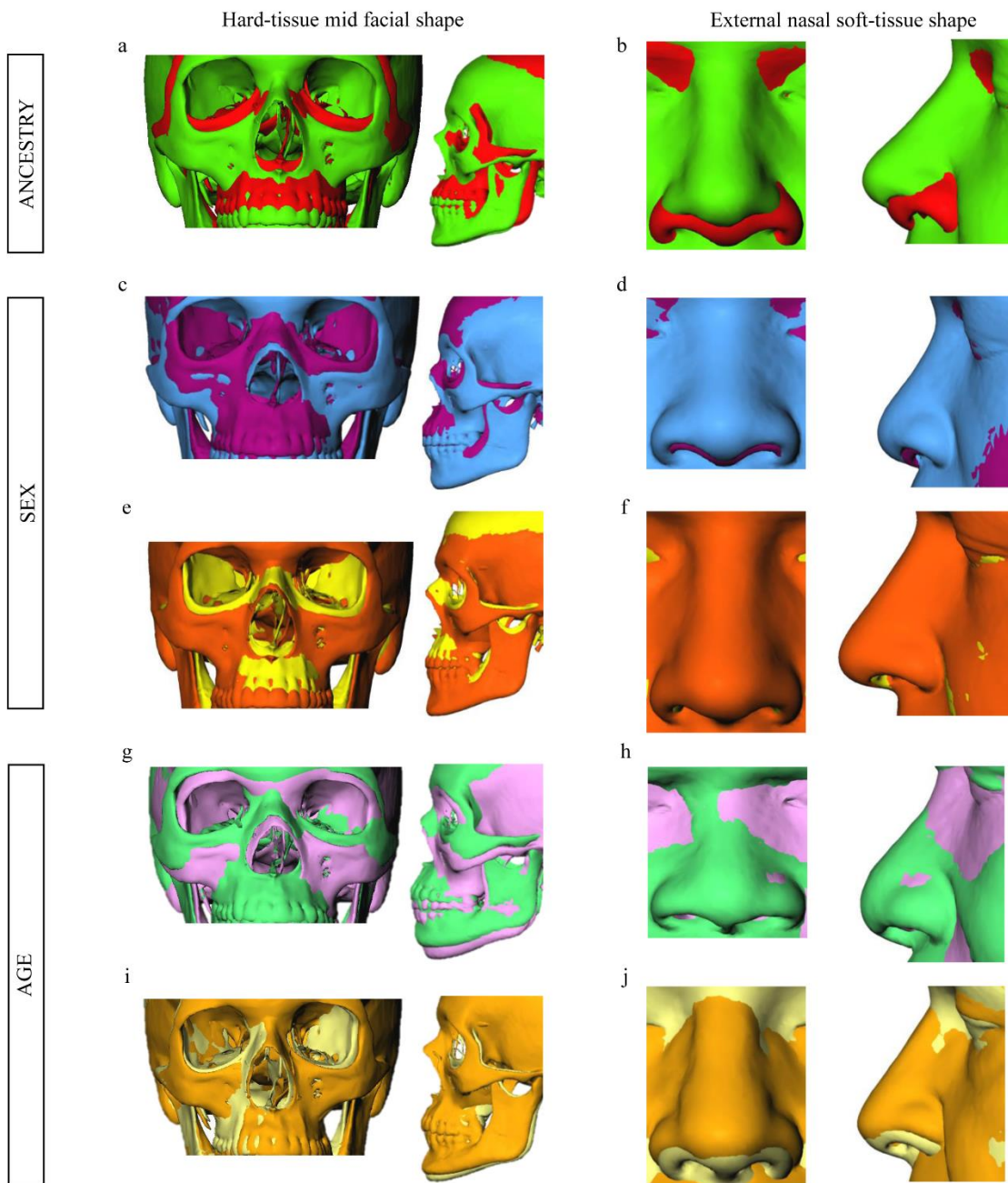


Figure 9. Mid-facial hard-tissue and external nasal soft-tissue shapes differences between ancestry, sex and age averages.

a,b) Mid-facial hard-tissue and external nasal soft-tissue shapes. Red: Black South African; Green: White South African. c,d,e,f) Sexual dimorphism in mid-facial hard-tissue and external nasal soft-tissue shapes differences for the black and white population separately. c,d) black hard- and soft-tissue shape (purple: black female; blue: black male); e,f) white hard- and soft-tissue shape (yellow: white female; orange: white male). g,h,i,j) Hard- and soft-tissue shape ageing differences for the black and white population separately. g,h) black hard- and soft-tissue shape (purple: 18 years; green: 79 years); i,j) white hard- and soft-tissue shape (yellow: 18 years; orange: 79 years).

Covariation between hard- and soft-tissue in each ancestral subsample.

Ancestry is paramount to evaluating shape variation in the hard- and soft-tissue of the nose. Therefore, in order to assess covariation between nasal-hard and soft-tissue shape and its dependence on ancestry, the sample was split into population-specific subsets (black South African and white South African). All correlations between all elements of the hard- and soft-tissue were found to be significant within black South Africans, whereas most variables, excluding zygomatic matrices and the right maxillary component, were significantly correlated within the white South African sample (Table 7).

Table 7. Results of covariation between hard-and soft-tissue and its dependence on ancestry.

Covariation	Black South Africans	White South Africans
	External nose	External nose
Mid-facial region	+	+
Nasal bones	+	+
Nasal bone (left)	+	+
Nasal bone (right)	+	+
Anterior nasal aperture	+	+
Anterior nasal aperture (left)	+	+
Anterior nasal aperture (right)	+	+
Zygoma	+	-
Zygomatic bone (left)	+	+
Zygomatic bone (right)	+	-
Maxilla	+	+
Maxillary bone (left)	+	+
Maxillary bone (right)	+	-

Significant correlation between mid-facial region and external nose tested by Two Blocks Partial Least Square Analyses (+: significant at $p < 0.05$).

Discussion

In this study, we provided a detailed overview of the influence of the factors: ancestry, sex, ageing and allometry, on the variability of the mid-facial skeleton and confirmed that all these variables contributed to the overall variation of the nose.

Our findings confirmed that the external nose is strongly correlated with the underlying skull substrate, which consists of the hard-tissue mid-facial regions including the nasal bones, the anterior nasal aperture, the zygomatic bones and the maxillary bones. These underlying skull elements are influenced by multifactorial processes (sex, age, and ancestry) involving hormonal, genetic and epigenetic factors; and external stimuli (soft tissue growth, dental maturation and biomechanical factors) [21-32]. During human development, and in order to maintain the function and the proportionate growth, the skeletal components of the face involve changes in their shape and size as well as their relative position within the craniofacial complex system [30, 32, 71, 72]. During growth, the skull evolves through two simultaneous and interrelated processes, namely, modelling and displacements of the skeletal components. In general, the adult face shows downward and forward growth directions [73] due to the bone growth dynamics of the facial skeleton, such as the resorption of the nasal area, the canine fossae, and the inferior margin of the zygomatic region. During adulthood, the remodelling of the underlying skeletal structure [20] and changes in the facial musculature resulting from gravity and the effects of hyperdynamic facial expressions may influence the morphology of the nose with advancing aging [20]. According to the literature, differences in the rate of soft tissue facial aging exists that varies according to the decade of life, sex and ancestry [33, 34]. Consequently, our results confirms that during craniofacial development, the morphology of the nose is influenced by the remodelling of the underlying skeletal structure [20] emphasizing the fact that the components of the nose cannot be considered as independent elements of the craniofacial skeleton and the influence of factors such as ancestry, sex and age must be considered.

The influence of environmental factors on nasal shape variation within population has been demonstrated by several bioanthropological studies [74-76]. The general hypothesis is that the shape of the external nose and the nasal aperture plays an important role in climate adaptation by regularising air temperature in order to protect the lungs from temperature and excessive humidity [74-76]. The scientific community has demonstrated that physical

anthropologists can estimate ancestral morphological variation among humans because they are able to translate morphological traits (biological) to a culturally constructed labelling system [77-80]. In addition, Serre and Paabo [81] noted a strong association between culture and biology and stated that, “genetic discontinuities seen between population groups are not racial or continental in nature but depend on historical and cultural factors” [82]. Moreover, Ousley and colleagues [82] have shown that variation among population groups is quantifiable and may be useful in providing a probable classification of an unknown person. While no discrete pattern of biological variation exists among humans, clinal morphological variation is observed in geographical distances which is often driven by social and cultural aptitudes [83-85]. In the South African context, racial classification is no longer legally imposed, but modern South Africans continue to socially self-identify according to the classifications imposed by Apartheid. Indeed, a need to self-identify as one of the previously prescribed groups is pervasive in all aspects of life and is an important part of a person’s cultural place in the country’s citizenship. Therefore, the majority of the population in South Africa self-classifies today as black (80.5%), coloured (8.8%), white (8.3%), and Indian/Asian (2.5%) South Africans [86]. Assortative mating within these groups strengthened the already notable biological variation between and among groups [87] engendering the perpetuation of skeletal variation allowing for forensic anthropologists to classify an unknown deceased individual as most similar to black, coloured, or white South African.

Distinct differences in mid-facial size and shape have already been observed among all South Africans groups (78-80, 88). In several osteometric analyses, some discrete traits from the mid-face, such as nasal width, inter-orbital breadth, nasal bone structure and alveolar prognathism are significantly related to the ancestry of South African groups [78-80, 88]. Cranial variation among modern black, coloured, and white South Africans has shown that cranial geometric morphometrics outperformed the traditional craniometrics, 89% versus 84% total cross-validated correct classification [89]. Variation in nasal hard- and soft-tissue morphologies has been described in other populations as well [3]. For instance, a differences exist for hard- and soft-tissue nasal shapes between Chinese and European groups. While the nasal complexes in Chinese are smoother and incorporated into the skull, the European nasal shapes are quite prominent [3]. In our study, black and white South Africans demonstrate distinct population shape variation in hard- and soft-tissue shapes and this variation must be considered in a CFR.

Accurate sex estimation is based on interpreting and quantifying the expression of sexual dimorphism in a population [90, 91]. These questions of population specific sexual dimorphism expression are of basic anthropological interest as they can provide information about human patterns of sexual selection. From our findings, sexual dimorphism plays an important role in the overall hard- and soft-tissue shape variation of the nose and might therefore be useful in discrimination between the sexes. At birth, babies display a slight sexual dimorphism, with major divergence occurring during puberty, which are also expressed as variations in nasal dimensions [22, 30, 92]. In recent literature, variation in nasal complex shape have been investigated using methods of standard morphometrics, based on distances and angles [93-95] or soft-tissue thickness [96] that address a link between asymmetry and facial masculinity [93, 94, 97]. In CFR, dimensions of the nose are important in distinguishing male and female faces and are useful in establishing an accurate facial approximation of a missing person. [92]. In the literature, only one method developed by Schlager [3] on a Chinese and European sample, related to geometric morphometrics have been applied to these issues for the reconstruction of the nose. Schlager [3] found that the expression of sexual dimorphism in variation of the shape of the nose among Chinese and European groups seemed to be influenced statistically by ancestry, but he emphasized that this influence is small from a biological point of view. In South African research context, distinct differences in facial skeletal morphology (size and shape) between the sexes have been shown in many research studies [78, 80, 98] using standard morphometric methods. In general, sexual dimorphism has been demonstrated to be less pronounced in the black South African population, than in other groups (white and coloured) [78,79]. In our study, visualizations of sexual dimorphism imply that the shape change is consistent between hard- and soft-tissue structure, and that the general similarity seems to outweigh the difference.

Ageing is almost as important as sex when considering variation in both hard- and soft-tissue shapes. Generally, studies concentrate on the analysis of classical metric data [99, 100] and/or additional volume and area measurements [95] of the human soft-tissue nose. These studies report the prolongation and widening of the nose [95,96, 100] and a change in angles during ageing [95] that resemble some geometric features of the external nose. In the craniofacial literature, few studies address age-related shape changes by means of geometric morphometrics. Only two recent studies, one on a French sample [19] and one on a Chinese and a European sample [3] demonstrated the presence of age-related changes of the nasal soft-tissue dimensions in human adults using geometric morphometric analysis. Results from the

soft-tissue analysis of age-induced shape changes in this study are perfectly consistent with previous studies using classic anthropometric methods. Indeed, in both ancestral groups, age had an influence on hard- and soft-tissue shape. In this study we found shape changes associated with age between ancestral groups from 18 years to 79 years which could be explained by weakening of the tissue and the effects of gravity.

Conclusion

We investigated the influence that ancestry, sex, age, and size (allometry) on the variability of the nasal complex, both in hard- and soft-tissue shapes. Ancestry was found to be a very important factor of shape variation within the sample emphasizing ancestral-specific differences. Additionally, within ancestral groups, sexual dimorphism and aging appeared to influence distinct elements of the shape of the mid-facial region. The influence of sex and aging emphasizes that during craniofacial development, the morphology of the nose is influenced by the remodelling of the underlying skeletal structure [20]. From the findings, the two South African groups differed significantly regarding hard- and soft-tissue nasal complex morphology and their correlations, emphasizing the importance of considering ancestry, sex and age as factors in the process of approximating the nose and highlighting the need for population specific accurate and reliable 3D statistical nose prediction methods .

Acknowledgments

The authors would like to thank Dr. André Uys from the Oral and Dental Hospital, University of Pretoria, South Africa and Dr. Sarel Botha from the Life Groenkloof Hospital, Pretoria, South Africa, for providing the CBCT-data. We acknowledge the AESOP+ consortia coordinated by Prof. José Braga from the Computer-assisted Palaeoanthropology Team, UMR 5288 CNRS- Université Paul-Sabatier, 37, allées Jules-Guesde, 31000 Toulouse, and from the Evolutionary Studies Institute and School of Geosciences, University of the Witwatersrand, Johannesburg, South Africa, for the financial support.

References

1. J. Bloom, 1272 Unidentified Bodies in Gauteng Mortuaries in 2014/2015.
2. G.C. Krüger, L. Liebenberg, J. Myburgh, A. Meyer, A.C. Oettlé, D. Botha, D.M. Brits, M.W. Kenyhercz, K.E. Stull, C. Sutherland, E.N. L'Abbé, Forensic Anthropology and the Biological Profile in South Africa, in: *New Perspectives in Forensic Human Skeletal Identification*, Elsevier, 2018: pp. 313–321.
Doi:10.1016/B978-0-12-805429-1.00027-2.
3. S. Schlager, Soft-tissue reconstruction of the human nose : population differences and sexual dimorphism = Weichteilrekonstruktion der menschlichen Nase : Populationsunterschiede und Sexualdimorphismus, Universität, Freiburg, 2013.
4. M. Steyn, E. N. L'Abbé, & J. Myburgh, Forensic Anthropology as Practiced in South Africa. *Handbook of Forensic Anthropology and Archaeology* 2016.
5. C. M. Wilkinson, Virtual sculpture as a method of computerized facial reconstruction. In *Proceedings of the 1st International Conference on Reconstruction of Soft Facial Parts* 2003 (pp. 17-18).
6. W.-J. Lee, C.M. Wilkinson, H.-S. Hwang, An Accuracy Assessment of Forensic Computerized Facial Reconstruction Employing Cone-Beam Computed Tomography from Live Subjects: an accuracy assessment of forensic computerized facial reconstruction, *Journal of Forensic Sciences*. 57 (2012) 318–327.
Doi:10.1111/j.1556-4029.2011.01971.x.
7. V. Bruce, G.W. Humphreys, Recognizing objects and faces, *Visual Cognition*. (1994); Apr 1;1(2–3):141–80.
8. M.M. Gerasimov, Vosstanovlieniia Litsa po Cherapu; Gos Izd-vo Sovetskaia [The reconstruction of the face on the skull]. Unpublished translation (1975) by Tshernezky 1955.
9. W. M. Krogman, *The human skeleton in forensic medicine*. Thomas, Springfield, Ill. 1962
10. W. Krogman, M. İşcan M, *The Human Skeleton in Forensic Medicine*, Charles C. Thomas Springfield IL, 2nd edition, 1986.
11. G.A. Macho, An Appraisal of Plastic Reconstruction of the External Nose, *Journal of Forensic Sciences*. 31 (1986) 11917J. Doi:10.1520/JFS11917J.
12. R. George, The Lateral Craniographic Method of Facial Reconstruction, *Journal of Forensic Sciences*, Vol.32, No.5. (1987); pp.1305-1330.

13. M. Prokopec, D.H. Ubelaker, Reconstructing the shape of the nose according to the skull, *Forensic Science Communications*. (2002); 4(1).
14. C.N. Stephan, M. Henneberg, W. Sampson, Predicting nose projection and pronasale position in facial approximation: a test of published methods and proposal of new guidelines, *American Journal of Physical Anthropology*. (2003);122(3):240–50. [Doi:10.1002/ajpa.10300](https://doi.org/10.1002/ajpa.10300).
15. F. Tilotta, *Contribution à la reconstitution faciale en médecine légale : proposition d'une nouvelle méthode statistique*(Doctoral dissertation) 2008.
16. N. Iblher, E. Gladilin, B.G. Stark, Soft-Tissue Mobility of the Lower Face Depending on Positional Changes and Age: A Three-Dimensional Morphometric Surface Analysis, *Plastic and Reconstructive Surgery*. 131 (2013) 372–381. [Doi:10.1097/PRS.0b013e318278d67c](https://doi.org/10.1097/PRS.0b013e318278d67c).
17. F. Marin, K.B. Mansour, F. Demeter, P. Frey, Displacement of facial soft tissues in upright versus supine positions, *Computer Methods in Biomechanics and Biomedical Engineering*. (2015) 1–2. [Doi:10.1080/10255842.2015.1069590](https://doi.org/10.1080/10255842.2015.1069590).
18. L. Munn, C.N. Stephan, Changes in face topography from supine-to-upright position— And soft tissue correction values for craniofacial identification, *Forensic Science International*. 289 (2018) 40–50. [Doi:10.1016/j.forsciint.2018.05.016](https://doi.org/10.1016/j.forsciint.2018.05.016).
19. P. Guyomarc'h, B. Dutailly, J. Charton, F. Santos, P. Desbarats, H. Coqueugniot, Anthropological Facial Approximation in Three Dimensions (AFA3D): Computer-Assisted Estimation of the Facial Morphology Using Geometric Morphometrics, *Journal of Forensic Sciences*. 59 (2014) 1502–1516. [Doi:10.1111/1556-4029.12547](https://doi.org/10.1111/1556-4029.12547).
20. A.M. Albert, K. Ricanek, E. Patterson, A review of the literature on the aging adult skull and face: Implications for forensic science research and applications, *Forensic Science International*. 172 (2007) 1–9. [Doi:10.1016/j.forsciint.2007.03.015](https://doi.org/10.1016/j.forsciint.2007.03.015).
21. M.L. Moss, R.W. Young, A functional approach to craniology, *American Journal of Physical Anthropology*. (1960);18(4):281–92. [Doi: 10.1002/ajpa.1330180406](https://doi.org/10.1002/ajpa.1330180406).
22. D.H. Enlow, M.G. Hans, *Essentials of facial growth*. W.B. Saunders Company;(1996).
23. M.L. Moss, The functional matrix hypothesis revisited. 1, The role of mechanotransduction, *American Journal of Orthodontics and Dentofacial Orthopedics*. (1997);112(1):8–11. [Doi:10.1016/S0889-5406\(97\)70267-1](https://doi.org/10.1016/S0889-5406(97)70267-1).
24. M.L. Moss, The functional matrix hypothesis revisited. 2, The role of an osseous connected cellular network, *American Journal of Orthodontics and Dentofacial Orthopedics*. (1997a);112(2):221–6. [Doi: 10.1016/S0889-5406\(97\)70249-X](https://doi.org/10.1016/S0889-5406(97)70249-X).

25. M.L. Moss, The functional matrix hypothesis revisited. 3, The genomic thesis, American Journal of Orthodontics and Dentofacial Orthopedics. (1997b);112(3):338–42. [Doi: 10.1016/S0889-5406\(97\)70265-8](https://doi.org/10.1016/S0889-5406(97)70265-8).
26. M.L. Moss, The functional matrix hypothesis revisited. 4, The epigenetic antithesis and the resolving synthesis, American Journal of Orthodontics and Dentofacial Orthopedics. (1997c);112(4):410–7. [Doi: 10.1016/S0889-5406\(97\)70049-0](https://doi.org/10.1016/S0889-5406(97)70049-0).
27. D.E. Lieberman, B.M. McBratney, G. Krovitz, The evolution and development of cranial form in Homo sapiens, Proceeding of the National Academy of Sciences of the United States of America. (2002);99(3):1134–9. [Doi:10.1073/pnas.022440799](https://doi.org/10.1073/pnas.022440799).
28. C.P. Klingenberg, K. Mebus, J. Auffray, Developmental integration in a complex morphological structure: how distinct are the modules in the mouse mandible? Evolution & Development. (2003);5(5):522–31. [Doi: 10.1046/j.1525-142X.2003.03057.x](https://doi.org/10.1046/j.1525-142X.2003.03057.x).
29. Y. Tomoyasu, T. Yamaguchi T, A. Tajima, T. Nakajima, I. Inoue, K. Maki, Further evidence for an association between mandibular height and the growth hormone receptor gene in a Japanese population, American Journal of Orthodontics and Dentofacial Orthopedics. (2009);136(4):53641. [Doi: 10.1016/j.ajodo.2007.10.054](https://doi.org/10.1016/j.ajodo.2007.10.054).
30. D. Lieberman, The evolution of the human head. Harvard University Press; (2011).
31. F. Gröning, M. Fagan, P. O'higgins, Comparing the distribution of strains with the distribution of bone tissue in a human mandible: a finite element study, The Anatomical Record. (2013);296(1):9–18. [Doi:10.1002/ar.22597](https://doi.org/10.1002/ar.22597).
32. W.R. Atchley, B.K. Hall, A model for development and evolution of complex morphological structures, Biological Reviews. (1991);66(2):101–57. [Doi:10.1111/j.1469-185X.1991.tb01138.x](https://doi.org/10.1111/j.1469-185X.1991.tb01138.x).
33. K. Taylor, Forensic Art and Illustration, CRC Press, 2000. [Doi:10.1201/9781420036954](https://doi.org/10.1201/9781420036954).
34. A.A. Akgül, T.U. Toygar, Natural craniofacial changes in the third decade of life: A longitudinal study, American Journal of Orthodontics and Dentofacial Orthopedics. 122 (2002) 512–522. [Doi:10.1067/mod.2002.128861](https://doi.org/10.1067/mod.2002.128861).
35. A.F. Ridel, F. Demeter, J. Liebenberg, E.N. L'Abbé, D. Vandermeulen, A.C. Oettlé, Skeletal dimensions as predictors for the shape of the nose in a South African sample: A cone-beam computed tomography (CBCT) study, Forensic Science International. 289 (2018) 18–26. [Doi:10.1016/j.forsciint.2018.05.011](https://doi.org/10.1016/j.forsciint.2018.05.011).

36. H.-J. Vogel, Mees, F., Swennen, R., Van Geet, M. & Jacobs, P. (eds) Applications of X-ray Computed Tomography in the Geosciences. Geological Society of London, 2003. vi + 243 pp. f65 (US\$108), hardback. ISBN 1-86239-139-4., *European Journal of Soil Science*. 56 (2005) 277–278. [Doi:10.1111/j.1365-2389.2004.0694f.x](https://doi.org/10.1111/j.1365-2389.2004.0694f.x).
37. W.C. Scarfe, A.G. Farman, What is Cone-Beam CT and How Does it Work?, *Dental Clinics of North America*. 52 (2008) 707–730. [Doi:10.1016/j.cden.2008.05.005](https://doi.org/10.1016/j.cden.2008.05.005).
38. C.F. Spoor, F.W. Zonneveld, G.A. Macho, Linear measurements of cortical bone and dental enamel by computed tomography: Applications and problems, *American Journal of Physical Anthropology*. 91 (1993) 469–484. [Doi:10.1002/ajpa.1330910405](https://doi.org/10.1002/ajpa.1330910405).
39. P. Claes, D. Vandermeulen, S. De Greef, G. Willems, P. Suetens, Statistically Deformable Face Models for Cranio-Facial Reconstruction, *Journal of Computing and Information Technology*. 14 (2006) 21. [Doi:10.2498/cit.2006.01.03](https://doi.org/10.2498/cit.2006.01.03).
40. P. Claes, D. Vandermeulen, S. De Greef, G. Willems, P. Suetens, Craniofacial reconstruction using a combined statistical model of face shape and soft tissue depths: Methodology and validation, *Forensic Science International*. 159 (2006) S147–S158. [Doi:10.1016/j.forsciint.2006.02.035](https://doi.org/10.1016/j.forsciint.2006.02.035).
41. P. Claes, A robust statistical surface registration framework using implicit function representations: Application in craniofacial reconstruction. PhD Thesis, K.U. Leuven, Belgium 2007.
42. P. Claes, A robust statistical surface registration framework using implicit function representations: application in craniofacial reconstruction, in: *Faculteit ingenieurswetenschappen, department Elektrotechniek, afdeling PSI, K.U. Leuven, Belgium, Leuven, 2007*.
43. J. Snyders, P. Claes, D. Vandermeulen, P. Suetens, Development and comparison of non-rigid surface registration algorithms and extensions. Technical report KUL/ESAT/PSI/1401, KU Leuven, ESAT, January (2014) Leuven, Belgium.
44. J. Buikstra, D. Ubelaker, Standards for data collection from human skeletal remains: Proceedings of a seminar at the Field Museum of Natural History (Arkansas Archaeology Research Series 44). *Fayetteville Arkansas Archaeological Survey*. (1994).
45. J. Caple, C.N. Stephan, A standardized nomenclature for craniofacial and facial anthropometry, *International Journal of Legal Medicine*. 130 (2016) 863–879. [Doi:10.1007/s00414-015-1292-1](https://doi.org/10.1007/s00414-015-1292-1).

46. F.L. Bookstein, *Morphometric tools for landmark data: geometry and biology*, Cambridge University Press, Cambridge [England]; New York, 1991.
47. F. Bookstein, Biometrics, biomathematics and the morphometric synthesis, *Bulletin of Mathematical Biology*. 58 (1996) 313–365. [Doi:10.1016/0092-8240\(95\)00329-0](https://doi.org/10.1016/0092-8240(95)00329-0).
48. F.L. Bookstein, Shape and the information in medical images: a decade of the morphometric synthesis, in: *IEEE*, 1996, pp. 2–12. [Doi:10.1109/MMBIA.1996.534052](https://doi.org/10.1109/MMBIA.1996.534052).
49. F. James Rohlf, L.F. Marcus, A revolution morphometrics, *Trends in Ecology & Evolution*. 8 (1993) 129–132. [Doi:10.1016/0169-5347\(93\)90024-J](https://doi.org/10.1016/0169-5347(93)90024-J).
50. C.P.E. Zollikofer, M.S. Ponce de Leon, Visualizing patterns of craniofacial shape variation in *Homo sapiens*, *Proceedings of the Royal Society B: Biological Sciences*. 269 (2002) 801–807. [Doi:10.1098/rspb.2002.1960](https://doi.org/10.1098/rspb.2002.1960).
51. D.C. Adams, F.J. Rohlf, D.E. Slice, Geometric morphometrics: Ten years of progress following the ‘revolution,’ *Italian Journal of Zoology*. 71 (2004) 5–16. [Doi:10.1080/11250000409356545](https://doi.org/10.1080/11250000409356545).
52. M.L. Zelditch, D.L. Swiderski, D.S. Sheets, W.L. Fink, *Geometric Morphometrics for Biologists*. Elsevier Academic Press, San Diego 2004.
53. D.E. Slice, Geometric Morphometrics, *Annual Review of Anthropology*. 36 (2007) 261–281. [doi:10.1146/annurev.anthro.34.081804.120613](https://doi.org/10.1146/annurev.anthro.34.081804.120613).
54. P. Mitteroecker, P. Gunz, *Advances in Geometric Morphometrics*, *Evolutionary Biology*. 36 (2009) 235–247. [Doi:10.1007/s11692-009-9055-x](https://doi.org/10.1007/s11692-009-9055-x).
55. C. Goodall Procrustes methods in the statistical analysis of shape. *Journal of the Royal Statistical Society. Series B. Statistical Methodology*, (1991) 53:285–239.
56. L. Dryden and K. V. Mardia, *Statistical shape analysis*. John Wiley and sons, Chichester 1998.
57. D.G. Kendall, Shape Manifolds, Procrustean Metrics, and Complex Projective Spaces, *Bulletin of the London Mathematical Society*. 16 (1984) 81–121. [Doi:10.1112/blms/16.2.81](https://doi.org/10.1112/blms/16.2.81).
58. C.P. Klingenberg, G.S. McIntyre, Geometric morphometric of developmental instability: analysing patterns of fluctuating asymmetry with Procrustes methods, *Evolution*. 52 (1998) 1363–1375. [Doi:10.1111/j.1558-5646.1998.tb02018.x](https://doi.org/10.1111/j.1558-5646.1998.tb02018.x).
59. D.E. Slice, Landmark coordinates aligned by Procrustes analysis do not lie in Kendall’s shape space. *Systematic Biology* 50(1): (2001) 141–149.

60. C.P. Klingenberg, M. Barluenga, A. Meyer, Shape analysis of symmetric structures: quantifying variation among individuals and asymmetry, *Evolution*. 56 (2002) 1909. [Doi:10.1554/00143820\(2002\)056\[1909:SAOSSQ\]2.0.CO;2](https://doi.org/10.1554/00143820(2002)056[1909:SAOSSQ]2.0.CO;2).
61. L. Scrucca, *Assessing Multivariate Normality through Interactive Dynamic Graphics* 2000.
62. Adams, D., Collyer, M., & Kaliontzopoulou, A. *Geometric Morphometric Analyses of 2D/3D Landmark Data* (2018).
63. Ø. Langsrud, 50-50 multivariate analysis of variance for collinear responses, *Journal of the Royal Statistical Society: Series D (The Statistician)*. 51 (2002) 305–317. [Doi:10.1111/1467-9884.00320](https://doi.org/10.1111/1467-9884.00320).
64. Ø. Langsrud, K. Jørgensen, R. Ofstad, T. Næs, Analyzing Designed Experiments with Multiple Responses, *Journal of Applied Statistics*. 34 (2007) 1275–1296. [Doi:10.1080/02664760701594246](https://doi.org/10.1080/02664760701594246).
65. Ø. Langsrud & B. H. Mevik, *ffmanova: Fifty-fifty MANOVA*. URL <http://CRAN.R-project.org/package=ffmanova> (2012).
66. S. Schlager, *Calculations and Visualisations Related to Geometric Morphometrics* (2017).
67. P.N. Gonzalez, S.I. Perez, V. Bernal, Ontogenetic Allometry and Cranial Shape Diversification Among Human Populations From South America, *The Anatomical Record: Advances in Integrative Anatomy and Evolutionary Biology*. 294 (2011) 1864–1874. [Doi:10.1002/ar.21454](https://doi.org/10.1002/ar.21454).
68. A. Rosas, M. Bastir, Thin-plate spline analysis of allometry and sexual dimorphism in the human craniofacial complex, *American Journal of Physical Anthropology*. 117 (2002) 236–245. [Doi:10.1002/ajpa.10023](https://doi.org/10.1002/ajpa.10023).
69. E.H. Kimmerle, A. Ross, D. Slice, Sexual Dimorphism in America: Geometric Morphometric Analysis of the Craniofacial Region, *Journal of Forensic Sciences*. 53 (2008) 54–57. [Doi:10.1111/j.1556-4029.2007.00627.x](https://doi.org/10.1111/j.1556-4029.2007.00627.x).
70. F.J. Rohlf, M. Corti, Use of Two-Block Partial Least-Squares to Study Covariation in Shape, *Systematic Biology*. 49 (2000) 740–753. [Doi:10.1080/106351500750049806](https://doi.org/10.1080/106351500750049806).
71. O’Higgins, P., Bromage, T. G., Johnson, D. R., Moore, W. J., & McPhie, P.. A study of facial growth in the sooty mangabey *Cercocebus atys*. *Folia Primatologica*, 56(2), (1991) 86-94.
72. M.A McCollum Nasomaxillary remodelling and facial form in robust *Australopithecus*: a reassessment. *J Hum Evol* (2008) 54,2–14.

73. M.Bastir, A systems-model for the morphological analysis of integration and modularity in human craniofacial evolution. *J Anthropol Sci*, 86, 2008. 37-58.
74. Thomson, L.H.D Buxton, Man's nasal index in relation to certain climatic conditions. *J R Anthropol Inst* 1923 53: 92–122.
75. J.S. Weiner Nose shape and climate. *Am J Phys Anthropol* 12, (1954) 615–618.
76. R.G. Franciscus, J.C. Long, Variation in human nasal height and breadth. *Am J Phys Anthropol* 85, (1991) 19–427.
77. N.J. Sauer, Forensic anthropology and the concept of race: If races don't exist, why are forensic anthropologists so good at identifying them?, *Social Science & Medicine*. 34 (1992) 107–111. [Doi:10.1016/0277-9536\(92\)90086-6](https://doi.org/10.1016/0277-9536(92)90086-6).
78. E.N. L'Abbé, C. Van Rooyen, S.P. Nawrocki, P.J. Becker, An evaluation of non-metric cranial traits used to estimate ancestry in a South African sample, *Forensic Science International*. (2011);209(1):195-e1. [Doi: 10.1016/j.forsciint.2011.04.002](https://doi.org/10.1016/j.forsciint.2011.04.002).
79. J.L. McDowell, E.N. L'Abbé, M.W. Kenyhercz, Nasal aperture shape evaluation between black and white South Africans, *Forensic Science International*. (2012);222(1):397-e1. [Doi: 10.1016/j.forsciint.2012.06.007](https://doi.org/10.1016/j.forsciint.2012.06.007).
80. J.L. McDowell, M.W. Kenyhercz, E.N. L'Abbé, An evaluation of nasal bone and aperture shape among three South African populations, *Forensic Science International*. (2015); 252:189-e1. [Doi: 10.1016/j.forsciint.2015.04.016](https://doi.org/10.1016/j.forsciint.2015.04.016).
81. D. Serre, S. Paabo, Evidence for gradients of human genetic diversity within and among continents, *Genome Res*. 14 (2004) 1679–1685.
82. S. Ousley, R. Jantz, D. Freid, Understanding race and human variation: Why forensic anthropologists are good at identifying race, *American Journal of Physical Anthropology*. (2009); Feb 18;139(1):68–76. [Doi:10.1002/ajpa.21006](https://doi.org/10.1002/ajpa.21006).
83. M. Hall, A. Morris, Race and iron age human skeletal remains from Southern Africa: an assessment, *Soc. Dyn*. 9 (2) (1983) 29–36.
84. E.N. L'Abbe', M. Kenyhercz, K.E. Stull, S.D. Ousley, Cra S. Dubow, *Scientific racism in modern South Africa*. Cambridge : Cambridge 1995.
85. E.N. L'Abbé, M. Kenyhercz, K.E. Stull, S.D. Ousley Craniometric assessment of modern 20th century black, white and “coloured” South Africans. *Proceedings of the 65th Annual Meeting of the American Academy of Forensic Sciences* 19:444 (2013).
86. Statistics South Africa, 2015. Mid-year Population Estimates (Census No. P0302). South Africa.

87. C. Sutherland, Biological Distance Among Modern and Parental South African Groups Using Discrete Traits of the Skull (M.Sc.). University of Pretoria, Pretoria, South Africa 2016.
88. A.C. Oettlé, F.P. Demeter, E.N. L'abbé, Ancestral Variations in the Shape and Size of the Zygoma: ancestral variations of the zygoma, *The Anatomical Record*. 300 (2017) 196–208. [Doi:10.1002/ar.23469](https://doi.org/10.1002/ar.23469).
89. K.E. Stull, M.W. Kenyhercz, E.N. L'Abbé, Ancestry estimation in South Africa using craniometrics and geometric morphometrics. *Forensic Sci. Int.* 245, 206.e1–206.e7 2014a.
90. S.R. Loth, M.Y. İşcan Sex Determination. In: Siegel J, Knupfer G, Saukko P (eds) *Encyclopedia of forensic sciences*. Academic Press, Waltham, (2000) pp 252–260.
91. R. Gapert, S. Black, J. Last Sex determination from the occipital condyle: discriminant function analysis in an eighteenth and nineteenth century British sample. *Am J Forensic Anthropol* (2008) 138:384–394.
92. E.P. Chronicle, M.Y. Chan, C. Hawkings, K. Mason, K. Smethurst, K. Stallybrass, You can tell by the nose—Judging sex from an isolated facial feature, *Perception*. (1995); 24(8):969–73. [Doi: 10.1068/p240969](https://doi.org/10.1068/p240969).
93. J. A Troncoso Pazos, I. C. Suazo Galdames, M. Cantin Lopez and D.A Zavando Matamata. Sexual Dimorphism in the Nose Morphotype in Adult Chilean. *International Journal of Morphology*, (2008) 26:537 – 542.
94. Rynn, C. Wilkinson and H. Peters, Prediction of nasal morphology from the skull. *Forensic Science, Medicine, and Pathology*, (2009) 6(1):20–34.
95. C. Sforza, G. Grandi, M. De Menezes, G.M. Tartaglia, V.F. Ferrario, Age- and sex-related changes in the normal human external nose, *Forensic Science International*. 204 (2011) 205.e1-205.e9. [Doi:10.1016/j.forsciint.2010.07.027](https://doi.org/10.1016/j.forsciint.2010.07.027).
96. F. Chen, Y. Chen, Y. Yu, Y. Qiang, M. Liu, D. Fulton, T. Chen, Age and sex related measurement of craniofacial soft tissue thickness and nasal profile in the Chinese population, *Forensic Science International*. 212 (2011) 272.e1-272.e6. [Doi:10.1016/j.forsciint.2011.05.027](https://doi.org/10.1016/j.forsciint.2011.05.027).
97. S. De Greef, D. Vandermeulen, P. Claes, P. Suetens, G. Willems, The influence of sex, age and body mass index on facial soft tissue depths, *Forensic Science, Medicine, and Pathology*. 5 (2009) 60–65. [Doi:10.1007/s12024-009-9085-9](https://doi.org/10.1007/s12024-009-9085-9).

98. S. Schlager and A. Rüdell, Analysis of the human osseous nasal shape—population differences and sexual dimorphism. *American Journal of Physical anthropology* (2015); 157:571–581. [Doi: 10.1002/ajpa.22749](https://doi.org/10.1002/ajpa.22749). 2015.
99. L. Zankl, L. Eberle, A. Molinari, Schinzel, Growth charts for nose length, nasal protrusion, and philtrum length from birth to 97 years, *American Journal of Medical Genetics*. 111 (2002) 388–391. [Doi:10.1002/ajmg.10472](https://doi.org/10.1002/ajmg.10472).
100. Damon, C. C Seltzer, H.W Stoudt. and B. Bell. Age and Physique in Healthy White Veterans at Boston. *Journal of Gerontology*, (1972) 27(2):202–208.

Chapter 7

STATISTICAL MODELS FOR SOUTH AFRICAN NOSE RECONSTRUCTION

7.1. Introduction

The purpose of this chapter is to provide statistical models for predicting nasal soft-tissue shape from information about the underlying hard-tissue configuration. Statistical models were calculated using a Projection onto Latent Structures Regression (PLSR) algorithm, that allow for establishing the statistical relationship predictors (hard-tissue shape, age, sex and ancestry) and response variables (soft-tissue information). The validation of prediction models was performed using cross validation testing with the calculation of the Mean Squared Error (MSE) using leave-one-out cross-validation (LOOCV).

Nose approximation among South African groups from Cone-Beam Computed Tomography (CBCT) using a new computer-assisted method based on automatic landmarking.

AF RIDEL, F DEMETER, EN L'ABBÉ, D VANDERMEULEN, AC OETTLÉ.
Manuscript submitted for publication to Forensic Science International.

Abstract

In light of the great demand for the identification of unknown remains in South Africa, a need exists to establish reliable facial approximation techniques that will not only take into account sex and age, but most importantly be specific for the South African population. The aim of this study was to provide accurate statistical models for predicting nasal soft-tissue shape from information about the underlying skull structure among a South African sample.

The database containing 200 cone beam computer tomography scans CBCT belonging to 100 black South Africans and 100 white South Africans were selected from the Oral and Dental Hospital, University of Pretoria, and the Life Groenkloof Hospital, Pretoria, South Africa. The acquisition and extraction of the 3D relevant anatomical structures (hard- and soft-tissue) was performed by an automated three-dimensional (3D) method based on an automatic dense landmarking procedure using MeVisLab © v. 2.7.1 software. An evaluation of shape differences attributed to known factors (ancestry, sex, size and age) were performed using geometric morphometric and, statistical models of prediction were created using a Projection onto Latent Structures Regression (PLSR) algorithm. The accuracy of the estimated soft-tissue nose was evaluated in terms of metric deviations on training and on un-trained datasets. Our findings demonstrated the influence of factors (sex, ageing and allometry) on the variability of the hard- and soft-tissue among two South African population groups.

This research provides accurate statistical models optimised by including additional information such as ancestry, sex and age. When using the landmark-to-landmark distances, the prediction errors ranged between 1.769 mm and 2.164 mm for black South Africans at the tip of the nose and the alae, while they range from 2.068 mm to 2.175 mm for the white subsample. The prediction errors on un-trained data were slightly larger, ranging between 2.139 mm and 2.833 mm for the black South African sample at the tip of the nose and the alae and ranging from 2.575 mm to 2.859 mm for the white South African sample.

This research demonstrates the utilization of an automated three-dimensional (3D) method based on an automatic landmarking method as a convenient prerequisite for providing a valid and reliable nose prediction models meeting population specific standards for South Africans.

Keywords: Statistical models; shape variation; South African standards; predictions errors; non-rigid registration procedure.

Introduction

Each year in the Gauteng province of South Africa, approximately 1300 bodies are incinerated without a known identity [1-2]. Identification is not always possible with conventional methods such as DNA comparisons and fingerprints. The high rate of migrant labour, associated with the country's socio-political and mining history [3], can separate individuals from their relatives and from their documentation.

Additionally, many poor South Africans do not have dental/hospital records or identification documents. Therefore, more creative methods, including facial reconstruction, have been implemented to assist in the identification of unknown persons from their skeletal remains in South Africa. In collaboration with the Victim Identification Centre (VIC) of the South African Police Service (SAPS), the Forensic Anthropology Research Centre (FARC) at the University of Pretoria has worked hard toward finding solutions for many of the challenges in the identification of unknown skeletal remains found within the South African population. In particular, attention has been given to the development of South African standards for establishing a biological profile (age, sex, stature and ancestry) in adults and children; the validation of current research methodologies and improvements of methods used in craniofacial reconstruction (CFR) and skull-to-photo superimposition [2, 4-7].

CFR methods are employed to estimate the ante-mortem appearance of an individual from their skeletal remains, providing information about an individual which can be conveyed to the public. CFR is based on the assumed morphological relationship between the soft-tissue envelope and the underlying skull substrate [8]. CFR is a useful tool in the identification of a corpse that is unrecognizable due to its state of decomposition, soft-tissue mutilation or incineration, and with no other available evidence for positive identification [9]. The history and development of CFR methodology, as well as its applications, has exposed the depth of human variation within and between populations and forms the foundation for the current development of valid and reliable population specific standards.

Yet, prior to reconstructing a face from the cranial substrate, the practitioner needs information as to the individual's biological profiles which includes estimations of ancestry, sex, age and stature. These skeletal estimations are then used to provide a presumptive identification of the deceased. Assortative mating within among South African groups certainly

strengthened the already notable biological variation in the country and engendered the perpetuation of skeletal variation within the population such that forensic anthropologists are able to classify an unknown into one of the three main socially identified groups: black, coloured, or white South Africans [2].

Currently, the craniofacial reconstruction division of the SAPS uses facial sculpting with modelling software to perform three-dimensional (3D) manual approximation of faces following the estimation of the biological profile (sex, age and ancestry) by anthropologists at the FARC, University of Pretoria. The facial reconstruction process involves the 3D surface scanning of the target skull (unidentified skull) with a Metrascan 210, a 3D surface of the target skull which is transposed onto Freeform modelling software, followed the manual application of soft-tissue thicknesses at specific craniometrics points using a 3D stylus. Facial features are adjusted, using the same process, on the skull according to North American databases of soft tissue thicknesses derived from cadaver studies. After the final touches by the forensic artists, the final 3D facial reconstruction is printed and presented to the family for possible recognition. The main critiques of this current CFR techniques are the inherent subjectivity in manual methods, the references used, the non-consideration of population specificities, the lack of standardization, and the poor correlations between facial bony structures and soft-tissue, which limit the objectivity and the accuracy of the estimation.

The scientific community in the field of CFR recognized that manual reconstruction methods require a high degree of anatomical and sculptural expertise and remain difficult and subjective in practice. The manual 3D CFR technique used by the VIC in South Africa relies on the expertise of a forensic artist to manipulate a 3D stylus. Therefore, the interpretations of two different forensic artists from the same skull can result in the creation of two substantially different faces [9-14]. Furthermore, manual reconstructions are time consuming, and are often limited to a single reconstruction. Today, traditional 2D or 3D manual techniques of CFR are considered unsuitable for application to the judicial system, which requires precision, reliability and knowledge of possible quantisation errors [13].

The reliability of the CFR methods used by the VIC in South Africa, is further challenged by the available reference sample. The data in the reference sample is based on soft-tissue depth thicknesses from North American cadavers. The use of cadavers for recording soft-tissue thicknesses has been extensively criticized in recent craniofacial identification literature

with poor relationships having been reported between cadaver-based and in vivo measurements on account of tissue deformation from post-mortem changes [15] namely dehydration and shrinkage as well as swelling with the onset of putrefaction [16-23]. In addition, the utilization of guidelines derived from populations other than South Africans is also problematic. The non-consideration of South African standards, taking into account the population specificities, in current facial features approximation techniques such as for the approximation of the nose, limits the objectivity and the accuracy of the reconstruction, and by extension the success of the recognition.

Following the literature, facial features have been determined to be important for perceiving and remembering faces [24-26]. The nose is of particular interest as it is a projecting feature, displaying much variation and therefore the reconstruction, could be invaluable in the identification of an unknown person. The nose is an important feature to accurately predict in facial recognition especially in profile view and in three-quarter view [24]. However, reconstruction of the nose poses specific challenges, because of its less clear relationship with the underlying skeletal features. The morphology of the nose is often manually reconstructed from the shape and size of the nasal aperture, represented by the position of the pronasale, subnasale, and alare landmarks [27-33]. These nasal profile prediction methods are time consuming, often limited to a single reconstruction, and has been demonstrated to be highly varied and subjective, rendering their applications useless in a court of law [33]. In South Africa, a new approach is needed to address the reliability and validity of CFR, particularly with regard to its overall accuracy and population specificity.

In order to accurately assess, the structural and functional coherence of correlations between facial bony structures and facial soft-tissue, a definition of a biologically meaningful region of interest, not limited to the nasal aperture and the nasal bones, for the approximation of the nose, is proposed in this study. During craniofacial development, from birth to death, the morphology of the nose is influenced by the remodelling of the underlying skeletal structure, [34] emphasizing the fact that the components of the nose cannot be considered as independent elements of the craniofacial skeleton. In addition, in nasal approximation, a biologically meaningful region of interest is rarely considered. A biologically meaningful region of interest is defined as a skeletal region which demonstrates important shape variation, impacting on the external morphology, and is influenced by factors such as sex, age and ancestry. In the scientific literature, it has been demonstrated that the growth and development of the human craniofacial

skeleton results from the interdependence of its different components, which are influenced by multifactorial processes involving hormonal, genetic and epigenetic factors such as ancestry, sex, age and external stimuli [35-46]. According to the literature, differences in the rate of soft-tissue facial aging exists, and varies according to the decade of life, sex and ancestry [47-48]. Recent studies on the facial approximation of the nose among South African groups [49] and on other European and Asian populations [8], demonstrate the importance of considering factors such as sex and ancestry in the approximation of the nose. Nasal shape variations present a challenge for facial reconstruction. Effective techniques taking into account the effects of population, sexual dimorphism and aging on the morphology of the nose, need to be developed. Failure to account for this suite of variations may impact on the accuracy of the final facial reconstruction.

To further improve the accuracy of facial approximation of the nose in the South African population, this study proposes the development of computer-based method using large databases of 3D representations of hard- and soft-tissues of the face. In general, all computer-based methods share the foundational premise that information about the complete skull versus information of the skin is used for mapping a template face onto a dry skull [50]. The prediction is performed by using a soft-tissue representation generated from the database by applying a deformation, based on the correlation between skin and skull-surfaces incorporated in the database. As compared to a human expert, a computer is consistent and objective. The computer integrates all the modelling assumptions and repeatedly generate the same output data. As compared to forensic artists, some procedures can be automated, such as the creation of multiple reconstructions from the same target skull, using different modelling assumptions (ancestry, age, sex). An additional advantage of using computer-based CFR is the convenience of visualization. Furthermore, the CFR process is more accessible to a wide range of forensic experts without the need for extensive expertise in computer science or computer-based CFR fields. In practice, the development of software for computerized facial reconstructions of an individual could benefit law enforcement agencies by allowing faster, easier and more efficient generation of multiple representations of an individual.

Tilotta and colleagues [51] and Schlager [8] developed computer-assisted methods for the prediction of the structure of the external surface of the nose based on conventional computer tomography (CT) scans. Compared to manual methods, automation of facial approximation of the nose, using large 3D surface samples, offered increased objectivity and

the possibility of standardization. However, the use of conventional CT scans as initial references for CFR methods is influenced by supination effects on the face due to the horizontal position of the patient during scanning [52-54]. In addition, the slice thickness of conventional CT scans, which generally ranges from 0.6 mm to 1.5 mm [8, 14, 51], may induce errors in the manual landmark placement on the 3D hard- and soft-tissue surfaces.

Although, automation of facial approximation of the nose increased objectivity as compared to the traditional manual methods, the manual placements of landmarks on large 3D surface samples affected the accuracy of the standardization. Indeed, these methods for approximation of the nose involve manual placements of landmarks for the definition of the region of interest [8, 51]. Manual placement of landmarks is extremely time consuming on large 3D surface samples and may induce important observer subjectivity and errors in placing these landmarks. As a result, manual landmarking may render the analysis less repeatable and accurate for the facial approximation process. To address these shortcoming a new computer-assisted method is proposed in this study

The aim of this study was to provide accurate statistical models for predicting nasal soft-tissue shape from information about the underlying skull subtract among a CBCT South African sample. The acquisition and extraction of the relevant anatomical structures (hard- and soft-tissue) was performed using an automated three-dimensional (3D) method based on an automatic dense landmarking procedure and analysed by geometric morphometric. Firstly, a shape variation analysis was performed in order to provide an overview of the influence of the factors sex, ageing and allometry on the overall hard- and soft-tissue shape variation. Secondly, statistical models for predicting nasal soft-tissue shape from information about the underlying hard-tissue configuration were created and additional factors such as sex and age were added to the models as additional informations in the predictors. In order to compare our results to other research results comparable to the methods proposed in this study, the accuracy of the estimated soft-tissue nose was evaluated in terms of metric deviations.

Materials & Methods

The data used in this study originated from CBCT-scans as retrospective records collected at two institutions: the *Oral and Dental Hospital, University of Pretoria, South Africa* and the *Life Groenkloof Hospital, Pretoria, South Africa*. The data were anonymized, with only details regarding age, sex and ancestry remaining. In order to standardize the acquisition, we selected all subjects scanned in a seated position with their eyes closed and with a relaxed facial expression. Subjects were excluded if they presented with any condition that could affect the morphology of the face (e.g. orthodontic treatment, pathological conditions, facial asymmetry or any facial interventional reconstructive surgery). This resulted in 200 usable datasets (100 black South African and 100 white South African). As the scope of this study did not concern the analysis of ontogenetic processes, only individuals between 18 and 80 years of age were selected. The average age of the complete sample is 40.51 years. The database contains 200 individuals of which 100 are black South Africans (33 females, 67 males) and 100 are white South Africans (65 females, 35 males). The average age of the black South African sample is 36.07 years, with females being slightly older (39.45 years) than males (34.40 years). Individuals in the white South African sub-sample are slightly older on average compared to the black South African sub-sample. The average age of the white South African group is 45.01 years, with females being slightly older (45.78 years) than males (43.60 years). All cone beam computer tomography scans used in this research were obtained using a CBCT scanner (Planmeca ProMax ® 3D, Pretoria, South Africa) with the following properties: 90 kV, 11.2 mA, voxel size of 0.4 mm, and field of view of 230 x 260 mm.

X-ray computed tomography (CT) is a non- destructive technique that allows visualization of the internal structure of objects, determined mainly by variations in density and atomic composition [55]. CBCT imaging is accomplished by using a rotating gantry to which an x-ray source and detector are fixed. A divergent pyramidal- or cone-shaped source of ionizing radiation is directed through the middle of the area of interest onto an area X-ray detector on the opposite side. The X-ray source and detector rotate around a rotation fulcrum fixed within the center of the region of interest. During the rotation, multiple (from 150 to more than 600) sequential planar projection images of the field of view (FOV) are acquired in a complete, or sometimes partial, arc [56]. CBCT images in DICOM format were imported into MeVisLab © v. 2.7.1 software for segmentation and 3D surface mesh generation.

CBCT images in DICOM format were imported into MeVisLab © v. 2.7.1 software for segmentation and 3D surface mesh generation. The grey values encode the density of the material observed - analogous to a common X-ray image: the lighter the grey value, the denser the tissue's intrinsic structure. Based on an initially defined grey value threshold and given all the different layers, MeVisLab © v. 2.7.1 software program estimates a three-dimensional representation of the object in question. As one is dealing with distinct slices, the space between them has to be interpolated by the software. A process called threshold-segmentation allows an observer to define grey value intervals, within which a given tissue (e.g. hard- and soft- tissue) is displayed. The segmentation of different elements (hard- and soft-tissue) were obtained by finding the threshold values between segmented components according to the "Half Maximum Height" (HMH) quantitative iterative thresholding method [57]. For this study, threshold values for hard-tissue varied between 1200-1250 and for the soft-tissue between 400-450. The segmentation process is illustrated in Figure 1. a. After segmentation of hard- and soft-tissues, 3D-triangular surface meshes were constructed. This resulted in 400 usable 3D surfaces (200 hard- tissue 3D surfaces and 200 soft-tissue 3D surfaces). Prior to registration, all the surfaces are repositioned into the same coordinate system using an initialisation mesh procedures (Figure 1.b). The initialisation is performed manually with indicating a set of landmarks on floating and target surfaces in order to interactively rotate and translate the surfaces so as to bring them into each other's proximity. These transformations map the coordinates of each point of the floating surface into the coordinate space of the target surface. The non-rigid surface registration results are dependent on the quality of this initial initialisation procedure.

The automatic landmarking method proposed here is adapted from the procedure introduced by [Claes and colleagues](#) [58-61]. The basic concept involves a reference template of the anatomical surface of interest, containing a dense set of landmarks. These landmarks are a dense equivalent of traditional sparse, discrete, well-defined, anatomical landmarks. Reference hard- and soft-tissue templates (Figure 1.d) are created using a non-rigid- surfaces registration process (Figure 1.c). Surface registration refers to the establishment of the geometrical relationship between surfaces that aligns the surfaces as well as possible between them. Then, every individual surface is 'templated' (named the warped surfaces): every point on all 3D surfaces is associated with the anatomically corresponding point on the reference template. As our main interest is finding a quantitative approach to estimate soft-tissue shape from information given by the underlying bone structure. Therefore, information encoded in 3D-surface representations has to be extracted and made comparable. In a last step, landmarks

are indicated once on the reference templates (Figure 1.e) . Every landmark placed on the template is associated with the anatomically corresponding point on the warped surfaces. During an anatomical templating process, this reference template is warped non-rigidly to every subject's anatomically corresponding surface (target surface). The non-rigid (robust) surface registration software used for this warping was developed using the MeVisLab © v. 2.7.1 software [62]. The warping is performed iteratively starting with a rigid alignment, followed by gradually more flexible registration steps. At the end of this process every landmark of the template is projected onto every subject's surface, thus establishing a dense point-based anatomical correspondence between all subjects (Figure 1.f). Therefore, landmark coordinates are recorded within a common coordinate system which may be used for statistical analysis.

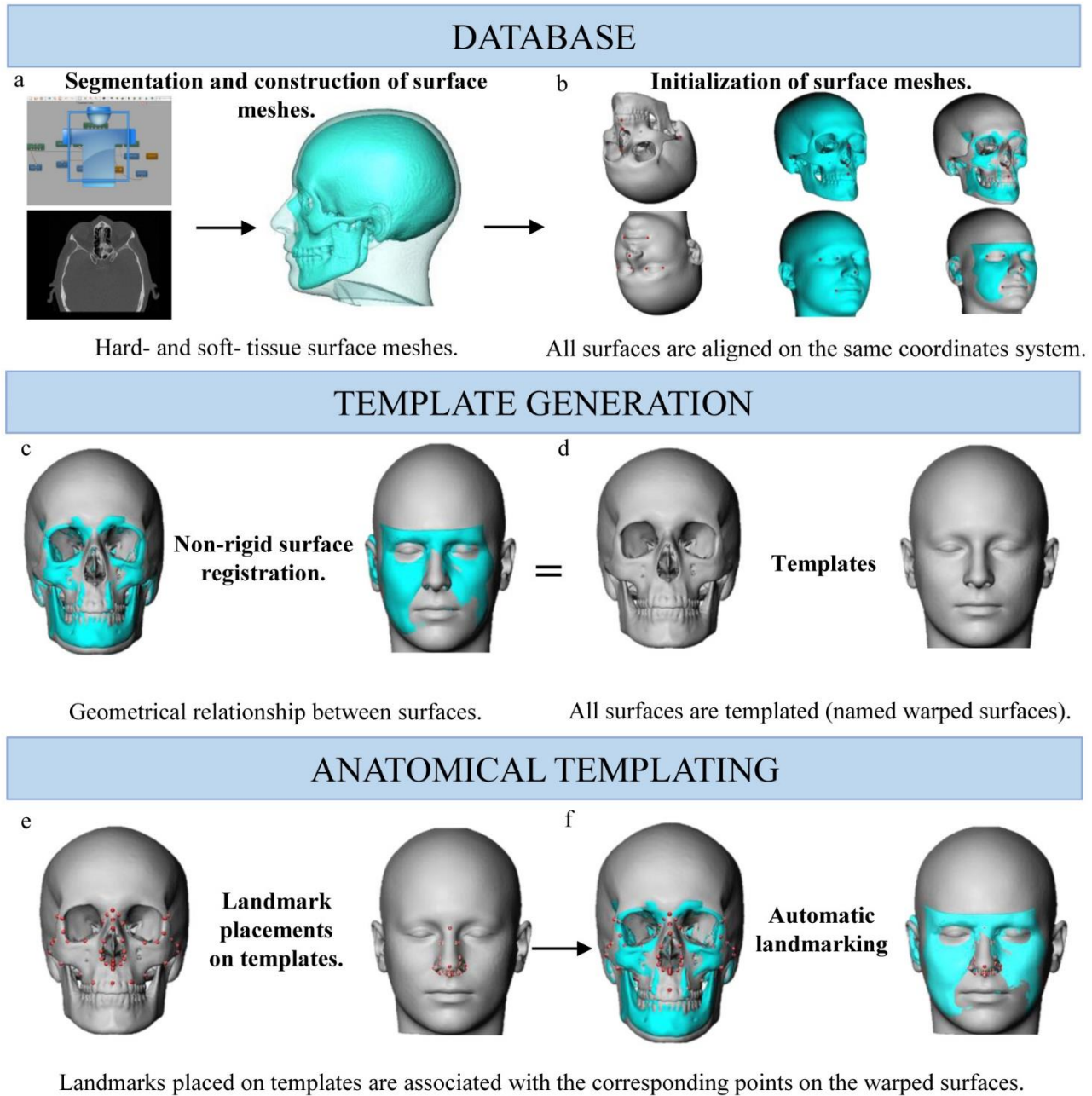


Figure 1. Workflow of the automatic landmarking procedure. a) segmentation process; b) initialisation process; c) non-rigid surface registration process; d) templates generation; e) definition of the region of interest on templates; f) automatic landmarking.

Following the facial approximation literature [8, 14] and in order to conserve homology and comparability between studies, classic craniometric and capulometric landmarks (type I, II, and III [8, 14, 65, 66] were used. The landmarks selected were distributed on the facial skeleton and the external nose, creating a hard- and soft-tissue region of interest. The hard-tissue region of interest was delimited on the facial skeleton (Figure 2 a, c) comprising the nasal bones, the anterior nasal aperture, the zygomatic bones and the maxillae. A total of 41 craniometric landmarks, 17 bilateral pairs and seven median landmarks, were recorded on the hard-tissue surfaces (Table 1). The soft-tissue region of interest was delimited by the surface anatomy as related to the hard-tissue (Figure 2 b, d), including mainly the nares and the external nose. On the soft-tissue, 21 capulometric landmarks were recorded, eight bilateral pairs and five median landmarks (Table 2).

Table 1. Definition and reproducibility of craniometric landmarks placed automatically and used in this study.

Craniometric	Landmarks	Abbreviation	Nature	Definition	Observer errors	
					Black surfaces	White surfaces
	1 Nasion	n	Median	Intersection of the nasofrontal sutures in the median plane.	< 1mm	< 1mm
	2 Mid-nasal	mn	Median	Midline point on the internasal suture midway between nasion and rhinion.	< 1mm	< 1mm
	3 Rhinion	rhi	Median	Most rostral (end) point on the internasal suture. Cannot be determined accurately if nasal bones are broken distally.	< 1mm	< 1mm
	4 Nasospinale	ns	Median	The point where a line drawn between the inferior most points of the nasal aperture crosses the median plane. Note that this point is not necessarily at the tip of the nasal spine.	< 1mm	< 1mm
	5 Subspinale	ss	Median	The deepest point seen in the profile view below the anterior nasal spine (orthodontic point A).	< 1mm	< 1mm
	6 Acanthion	ak	Median	Most anterior midline point of the nasal spine.	< 1mm	< 1mm
	7 Prosthion	pr	Median	Median point between the central incisors on the anterior most margin of the maxillary alveolar rim.	< 1mm	< 1mm
	8/9 Zygotemporale superior	zts	Bilateral	Most superior point of the zygomatico-temporal suture.	< 1mm	< 1mm
	10/11 Zygotemporale inferior	zti	Bilateral	Most inferior point of the zygomatico-temporal suture.	< 1mm	< 1mm
	12/13 Jugale	ju	Bilateral	Vertex of the posterior zygomatic angle, between the vertical edge and horizontal part of the zygomatic arch.	< 1mm	< 1mm
	14/15 Frontomolare temporale	fnt	Bilateral	Most lateral part of the zygomaticofrontal suture.	< 1mm	< 1mm
	16/17 Frontomolare orbitale	fmo	Bilateral	Point on the orbital rim marked by the zygomaticofrontal suture.	< 1mm	< 1mm
	18/19 Nasomaxillofrontale	nmf	Bilateral	Point at the intersection of the frontal, maxillary, and nasal bones.	1-2 mm	1-2 mm
	20/21 Ectoconchion	ec	Bilateral	Lateral point on the orbit at a line that bisects the orbit transversely.	< 1mm	1-2 mm
	22/23 Orbitale	or	Bilateral	Most inferior point on the inferior orbital rim. Usually falls along the lateral half of the orbital margin.	< 1mm	< 1mm
	24/25 Zigo-orbitale	zo	Bilateral	Intersection of the orbital margin and the zygomaticomaxillary suture.	< 1mm	< 1mm
	26/27 Maxillofrontale	mf	Bilateral	Intersection of the anterior lacrimal crest with the frontomaxillary suture.	< 1mm	1-2 mm
	28/29 Nasomaxillare	nm	Bilateral	Most inferior point of the nasomaxillary suture on the nasal aperture.	< 1mm	< 1mm
	30/31 Alare	al	Bilateral	Instrumentally determined as the most lateral point on the nasal aperture in a transverse plan.	< 1mm	< 1mm
	32/33 Piriform curvature	cp	Bilateral	Most infero-lateral point of the piriform aperture.	< 1mm	< 1mm
	34/35 Nariale	na	Bilateral	Most inferior point of the piriform aperture.	< 1mm	< 1mm
	36/37 Zygomaxillare	zm	Bilateral	Most inferior point on the zygomaticomaxillary suture.	1-2 mm	1-2 mm
	38/39 Submaxillare curvature	csm	Bilateral	Most supero-medial point on the maxillary inflexion between the zygomaxillare and the ectomolar.	1-2 mm	< 1mm
	40/41 Supra-canine	sc	Bilateral	Point on the superior alveolar ridge superior to the crown of the maxillary canine.	< 1mm	< 1mm

Table 2. Definition and reproducibility of capulometric landmarks placed automatically and used in this study.

Capulometric	Landmarks	Abbreviation	Nature	Definition	Observer errors	
					Black surfaces	White surfaces
	1 Pronasale	pm'	Median	The most anteriorly protruded point of the apex nasi. In the case of a bifid nose, the more protruding tip is chosen.	< 1 mm	< 1 mm
	2 Nasale inferius	ni'	Median	Most inferior point of the apex nasi. Not locatable on upturned noses.	< 1 mm	< 1 mm
	3 Columella	c'	Median	Midpoint of the nasal columella crest, intersecting a line between the two cs' points.	< 1 mm	< 1 mm
	4 Subnasale	sn'	Median	Median point at the junction between the lower border of the nasal septum and the philtrum area.	1-2 mm	< 1 mm
	5 Sellion	se'	Median	Deepest midline point of the nasofrontal angle; not a substitute for n'.	< 1 mm	< 1 mm
	6/7 External alar curvature	eac	Bilateral	Most anterior point of the nasal wing at the maximum of curvature.	< 1 mm	< 1 mm
	8/9 Superior alar curvature	sac	Bilateral	Most superior point of the nasal wing.	< 1 mm	< 1 mm
	10/11 Alagenion	ag	Bilateral	Most posterior point of the nasal wing.	1-2 mm	< 1 mm
	12/13 Alare	al'	Bilateral	The most lateral point on the nasal ala.	< 1 mm	< 1 mm
	14/15 Alar curvature point	ac'	Bilateral	The most posterolateral point of the curvature of the base line of each nasal ala.	< 1 mm	< 1 mm
	16/17 Mid-nostril	mn	Bilateral	Midpoint of maximal nostril width - projected on the transition nostril/philtrum.	1-2 mm	1-2 mm
	18/19 Mid-columella	mc'	Bilateral	Midpoint of the nasal columella crest on either side, where the columella thickness is measured (equivalent to Subnasale).	< 1 mm	< 1 mm
	20/21 Nasal-depth	nd	Bilateral	Most medial point of the transition nose/eye.	1-2 mm	< 1 mm

The procedure of the automatic placement of discrete landmarks was applied using two different templates, one for each sample: black South African template (Figure 2. a, b) and white South African template (Figure 2. c, d). The landmarks of interest were indicated once on each template for both groups separately, which were then projected on each of the 400 surfaces (200 hard-tissue and 200 soft-tissue). The coordinates of the landmarks were then recorded for the statistical analysis.

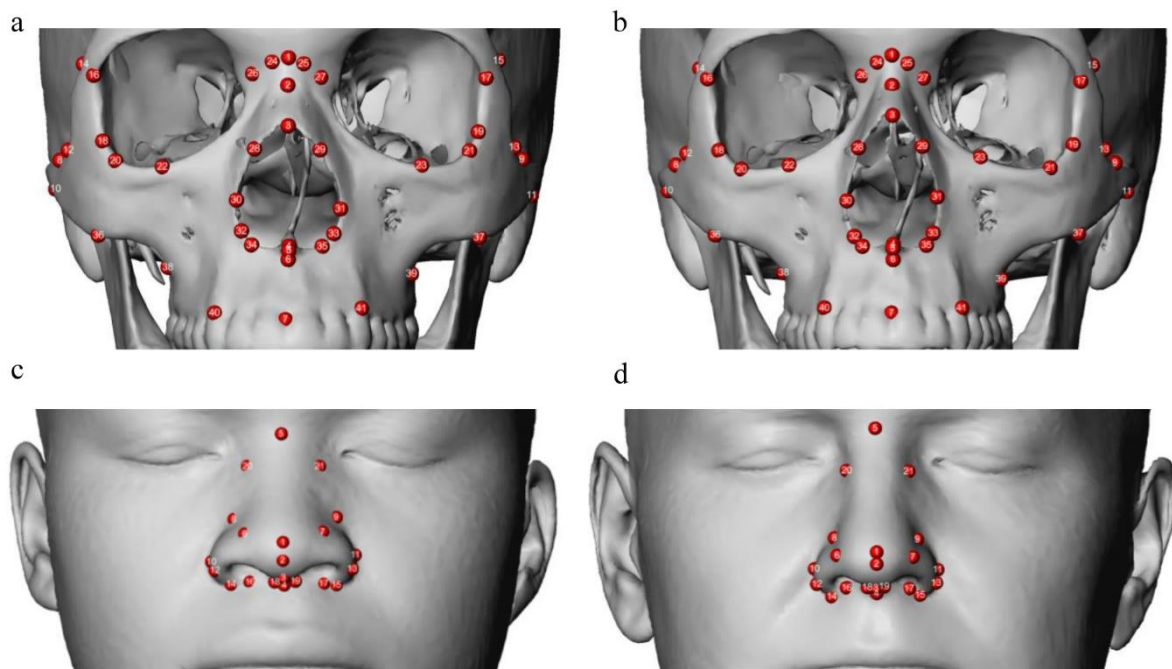


Figure 2. Landmarks placed on hard- and soft-tissue templates. a,b: Hard- and soft-tissue black South African templates; c,d: Hard- and soft-tissue white South African templates.

Statistical analysis

In order to assess reproducibility and to have a quantification of errors induced, a test of the repeatability of the digitization in terms of inter- and intra-observer errors was performed on the complete sample (400 surfaces). The coordinates of the landmarks were then recorded. For the intra-observer errors, the landmark indication on templates was done by the same observer, with an interval of two weeks. For the inter-observer errors, the landmark indication on templates was done independently by two different observers. The precision of the landmark positioning was calculated using the dispersion Δ_{ij} for each landmark i and individual j . Dispersion is defined as the Mean Euclidean Distance (MED) of the sample landmark \mathbf{p}_{ijk} to the mean $\bar{\mathbf{p}}_{ij}$ of the (x,y,z)-coordinates of landmark i over all observations k (INTER, INTRA, resp.) for subject j :

$$\Delta_{ij} = \sum_{k=1}^K \|\mathbf{p}_{ijk} - \bar{\mathbf{p}}_{ij}\|/K, \text{ with } \bar{\mathbf{p}}_{ij} = \sum_{k=1}^K \mathbf{p}_{ijk}/K$$

An evaluation of shape differences attributed to known factors (ancestry, sex, size and age) among the two population groups were performed both on hard- and soft-tissue shape using geometric morphometric methods (GMM) [67-75]. Preceding the statistical analysis, a General Procrustes Analysis (GPA) [76-77] was performed on the complete hard- and soft-tissue raw coordinates separately, to obtain pose-invariant shape coordinates [63, 64, 78, 79]. A data reduction was achieved by Principal Component Analysis (PCA) to reduce data dimensionality and to create independent principal component (PC) scores that quantify the different shapes. Statistical testing was performed using the PC scores covering 95% of the sample's overall variance. Multivariate normality testing was performed on the hard- and soft-tissue PC scores distribution by interpreting Q-Q-plots [80], which allowed the examination of variable distribution.

All results were double-checked using non parametric testing. The results were considered reliable if both tests pointed in the same direction. Multiple analysis of variance (MANOVA) was run to evaluate differences between populations, sexes and with aging on hard and soft tissues [81]. Two non-parametric-tests were also applied: 50-50 MANOVA [82] and permutation testing [83]. Standard discriminant function analysis (DFA) [84] was also

performed for ancestry and sex classification purposes and leaving-one-out cross-validation (LOOCV) was used for classification accuracy. For assessing allometry, linear models (hard- and soft-tissue shape versus factor sex and centroid size) were calculated. Allometry is defined as shape change that can be expressed as a function of size [67, 85]. The significance was tested with a MANCOVA using Pillai trace test (parametric) and 50-50 MANOVA (non-parametric test) were used. The evaluation of covariation between the mid-facial hard-tissue elements and the external soft-tissue of the nose on each subsample was performed with Two Blocks Partial Least Squares (PLS) analyses [86].

In the previous section, the influence of known factors (ancestry, age, sex, allometry) on shape using geometric morphometric methods were analysed using two separate shape spaces, one for each type of tissue (hard- and soft-tissue). In order to create a statistical model for predicting nasal soft-tissue shape from information about the underlying hard-tissue configuration, both types of tissue (hard- and soft-tissue) needed to be scaled, translated, rotated and predicted within the same space using only the initial hard-tissue information.

The adapted GPA used in this study was introduced by Schlager [8] and firstly involved the calculation of a Procrustes fit for hard-tissue configurations and the scaling, translation and rotation of the complete (soft- and hard-tissue) landmark datasets onto the hard-tissue configurations by using corresponding landmarks. In a last step, the data were split up into soft-tissue and hard-tissue configuration again in order to have a predictor hard-tissue shape and a predicted soft-tissue shape already aligned correctly in the same coordinate system.

In order to extract information for the soft-tissue prediction, two types of regression algorithms exist, namely Principal Component Regression and Projection onto Latent Structures Regressions (PLSR). Schlager [8] demonstrated that both types of regression algorithm, PCR and PLSR models, provided similar results in terms of nose prediction accuracies. Projection onto Latent Structures Regressions (PLSR) was used in order to extract information for the soft-tissue prediction and to select those linear combinations relevant for explaining the predictor variables maximizing covariation between predictors (hard- tissue shape and additional factors) and response (soft-tissue shape). [87-89]. PLSR is a method for relating two data matrices, X and Y, by a linear multivariate model. In addition, PLSR goes beyond traditional regression because it models also the structure of X and Y and analyses data with many, noisy, collinear, and even incomplete variables [89]. In this study, all calculation

were performed using the PLSR algorithm, implemented in the R-package “pls” [90-91], for extraction of latent variables.

The accuracy of the predicted soft-tissue nose was evaluated in terms of metric deviations in order to be comparable other research result. The estimation of the Mean Squared Error (MSE) from the training data and from the predicted data (MSEP) were calculated [91]. Then, the validation of prediction models was performed using cross validation testing with the calculation of the (MSE) using LOOCV. The impact of additional information such as ancestry, sex and age is evaluated by adding them to the models as predictors and comparing the resulting MSE/MSEP. The prediction quality per landmark over all subjects was also calculated. In addition, in order to determine if the covariation was significantly population-dependent, the soft-tissue shape of all specimens from one population was estimated by applying a regression model fit by the other population’s data.

Results

The reproducibility of each craniometric and capulometric landmarks is reported in Table 1 and Table 2, respectively. Regarding the mean results of the intra- and inter- dispersion errors of craniometric and capulometric landmark positioning, lower dispersion values were obtained for both black and white surfaces and for both hard- and soft-tissue. On each black and white surface analysed separately, none of the landmarks showed low reproducibility (> 2 mm).

Ancestry was found to contribute the most to shape variation for both, hard- and soft-tissue shape components (Table 3). All statistical tests (Table 3), parametric (MANOVA) and non-parametric (Permutation test) confirmed a strong difference between population averages for all hard-tissue and soft tissue elements. Additionally, the overall classification accuracy was 100%, meaning that none of the 200 specimens were wrongly classified. (Table 3). In the black South African sample, the presence of sexual dimorphism was confirmed on all hard- and soft-tissue shapes (Table 3). Additionally, cross-validated linear discriminant function analysis yielded an accuracy of 96% (hard-tissue) and 88% (soft-tissue) for the black South African sample, and an accuracy of 93% (hard-tissue) and 90% (soft-tissue) for the white South African sample, reflecting the discriminative power of sexual dimorphism in both populations. In both populations, the effect of age and size (allometry) on the hard- and soft-tissue shape was also statistically significant (Table 3) indicating that age and size (allometry) contributes also to the overall shape variation in both population groups. Indeed, in the black and white South African sample separately, all parametric (MANOVA) and non-parametric (50-50 MANOVA) tests reported significant differences for age and size (allometry) on all elements of the hard- and soft-tissue. In addition, all correlations between hard- and soft-tissue were found to be significant within both population groups (Table 3).

Table 3. Hard- and soft-tissue shape analysis results.

	Ancestry			Black South Africans										White South Africans									
				Sexual dimorphism				Age		Alometry		Covariation		Sexual dimorphism				Age		Alometry		Covariation	
	Test ¹	Permu.test	DFA	Test ¹	Test ²	Permu.test	DFA	Test ²	Test ³	Test ²	Test ³	RV-pls	p-value	Test ¹	Test ²	Permu.test	DFA	Test ²	Test ³	Test ²	Test ³	RV-pls	p-value
Mid-facial region	0.001	0.001	100%	0.015	0.008	0.008	96%	0.006	0.000	0.000	0.000	0.613	0.001	0.017	0.616	0.019	93%	0.001	0.015	0.000	0.000	0.563	0.001
Nasal bones	0.001	0.001	100%	0.053	0.000	0.049	76%	0.357	0.372	0.000	0.000	0.562	0.001	0.158	0.000	0.164	83%	0.401	0.429	0.000	0.000	0.545	0.001
Nasal bone (left)	0.001	0.001	99%	0.036	0.052	0.034	71%	0.670	0.694	0.000	0.000	0.549	0.001	0.068	0.014	0.055	70%	0.548	0.583	0.000	0.000	0.492	0.002
Nasal bone (right)	0.001	0.001	100%	0.006	0.000	0.006	79%	0.595	0.581	0.000	0.000	0.584	0.001	0.165	0.000	0.178	80%	0.548	0.548	0.000	0.000	0.515	0.001
Anterior nasal aperture	0.001	0.001	100%	0.005	0.003	0.005	82%	0.009	0.000	0.000	0.000	0.468	0.008	0.514	0.476	0.516	79%	0.134	0.038	0.000	0.000	0.523	0.003
Anterior nasal aperture (left)	0.001	0.001	99%	0.003	0.002	0.006	82%	0.115	0.057	0.000	0.000	0.460	0.007	0.454	0.234	0.424	68%	0.282	0.276	0.000	0.000	0.477	0.008
Anterior nasal aperture (right)	0.001	0.001	100%	0.011	0.001	0.006	76%	0.011	0.002	0.000	0.000	0.467	0.008	0.239	0.129	0.214	76%	0.080	0.030	0.000	0.000	0.468	0.007
Zygoma	0.001	0.001	100%	0.001	0.000	0.001	91%	0.040	0.092	0.000	0.000	0.570	0.001	0.001	0.000	0.001	93%	0.102	0.079	0.000	0.000	0.458	0.022
Zygomatic bone (left)	0.001	0.001	100%	0.002	0.000	0.002	86%	0.121	0.113	0.000	0.000	0.536	0.001	0.001	0.000	0.001	90%	0.574	0.408	0.000	0.000	0.465	0.006
Zygomatic bone (right)	0.001	0.001	100%	0.001	0.000	0.001	84%	0.042	0.023	0.000	0.000	0.577	0.001	0.002	0.000	0.001	94%	0.159	0.078	0.000	0.000	0.414	0.052
Maxilla	0.001	0.001	100%	0.097	0.002	0.107	88%	0.149	0.001	0.000	0.000	0.605	0.001	0.029	0.000	0.021	94%	0.031	0.090	0.000	0.000	0.540	0.001
Maxillary bone (left)	0.001	0.001	100%	0.025	0.000	0.032	82%	0.016	0.011	0.000	0.000	0.587	0.001	0.034	0.000	0.025	90%	0.185	0.393	0.000	0.000	0.518	0.002
Maxillary bone (right)	0.001	0.001	100%	0.133	0.003	0.147	82%	0.109	0.043	0.002	0.001	0.570	0.001	0.013	0.000	0.008	91%	0.039	0.057	0.000	0.000	0.330	0.505
External nose	0.001	0.001	100%	0.005	0.014	0.005	88%	0.000	0.000	0.000	0.000			0.001	0.016	0.001	90%	0.007	0.006	0.809	0.000		

Test¹: MANOVA; Test²: MANCOVA; Test³: 50-50 MANOVA. Significant p.values (<0.05) are indicated in bold.

Table 4. Prediction errors (in mm) of the predicted capulometric landmarks in the complete sample, calculated on 200 individuals, based on training and on non-trained data.

Predicted capulometric landmarks	Plain		Ancestry		Sex		Age		Sex*Age		Ancestry*sex		Ancestry*age		Ancestry*sex*age	
	PE	PE_cv	PE	PE_cv	PE	PE_cv	PE	PE_cv	PE	PE_cv	PE	PE_cv	PE	PE_cv	PE	PE_cv
<i>Pronasale</i>	2.498	2.875	2.497	2.875	2.492	2.877	2.435	2.862	2.487	2.872	2.487	2.872	2.443	2.872	2.451	2.870
<i>Nasale inferius</i>	2.614	3.015	2.614	3.015	2.606	3.014	2.531	2.982	2.598	3.006	2.598	3.006	2.563	3.015	2.573	3.002
<i>Columella</i>	2.479	2.871	2.478	2.871	2.469	2.868	2.385	2.827	2.462	2.865	2.462	2.865	2.431	2.850	2.453	2.861
<i>Subnasale</i>	2.316	2.674	2.316	2.674	2.309	2.670	2.207	2.594	2.300	2.666	2.300	2.666	2.244	2.629	2.301	2.662
<i>Sellion</i>	2.019	2.178	2.019	2.178	2.020	2.174	2.015	2.200	2.017	2.170	2.017	2.170	2.052	2.220	1.990	2.166
<i>External alar curvature L</i>	2.315	2.642	2.315	2.642	2.312	2.641	2.291	2.658	2.307	2.634	2.307	2.634	2.275	2.636	2.278	2.640
<i>External alar curvature R</i>	2.354	2.710	2.354	2.710	2.346	2.706	2.336	2.721	2.338	2.698	2.338	2.698	2.327	2.712	2.339	2.719
<i>Superior alar curvature L</i>	2.118	2.373	2.118	2.373	2.116	2.375	2.087	2.372	2.114	2.375	2.114	2.375	2.078	2.363	2.108	2.373
<i>Superior alar curvature R</i>	2.222	2.517	2.221	2.517	2.208	2.508	2.197	2.501	2.199	2.504	2.199	2.504	2.177	2.495	2.233	2.519
<i>Alagenion L</i>	2.289	2.592	2.289	2.592	2.29	2.592	2.256	2.549	2.289	2.593	2.289	2.593	2.248	2.563	2.273	2.540
<i>Alagenion R</i>	2.437	2.762	2.437	2.762	2.424	2.756	2.398	2.710	2.418	2.76	2.418	2.760	2.399	2.718	2.435	2.720
<i>Alare L</i>	2.413	2.749	2.413	2.749	2.412	2.748	2.342	2.676	2.409	2.743	2.409	2.743	2.329	2.669	2.357	2.680
<i>Alare R</i>	2.506	2.861	2.506	2.861	2.499	2.858	2.457	2.806	2.496	2.859	2.496	2.859	2.448	2.794	2.455	2.802
<i>Alar curvature point L</i>	2.307	2.659	2.307	2.659	2.305	2.657	2.205	2.541	2.299	2.652	2.299	2.652	2.194	2.527	2.247	2.567
<i>Alar curvature point R</i>	2.424	2.790	2.424	2.790	2.413	2.784	2.372	2.731	2.406	2.783	2.406	2.783	2.359	2.722	2.394	2.737
<i>Mid-nostril L</i>	2.205	2.567	2.205	2.567	2.199	2.565	2.086	2.453	2.192	2.563	2.192	2.563	2.079	2.454	2.158	2.495
<i>Mid-nostril R</i>	2.375	2.739	2.375	2.739	2.365	2.735	2.286	2.663	2.357	2.734	2.357	2.734	2.277	2.653	2.321	2.672
<i>Mid-columella L</i>	2.368	2.731	2.368	2.731	2.359	2.729	2.274	2.676	2.348	2.723	2.348	2.723	2.315	2.713	2.359	2.727
<i>Mid-columella R</i>	2.369	2.725	2.369	2.725	2.359	2.719	2.260	2.659	2.347	2.711	2.347	2.711	2.306	2.698	2.345	2.713
<i>Nasal-depth L</i>	1.818	1.986	1.818	1.986	1.816	1.982	1.803	1.996	1.813	1.979	1.813	1.979	1.806	1.983	1.770	1.960
<i>Nasal-depth R</i>	1.862	2.058	1.862	2.058	1.851	2.049	1.829	2.048	1.842	2.047	1.842	2.047	1.860	2.063	1.846	2.047
RMSEP	2.300	2.622	2.300	2.622	2.294	2.619	2.240	2.582	2.288	2.616	2.288	2.616	2.248	2.588	2.271	2.594

PE: Prediction errors on training data; PE_cv: prediction errors on non-trained data. Better predictions are indicated in bold.

Regarding the prediction analysis of the complete sample (Table 4), a prediction errors of 2.300 mm is based on training data and a prediction of 2.622 mm is based on non-trained data. Errors based on training data for each population groups separately, were 2.157 mm for the black South African sample (Table 5), and 2.062 mm for the white south African sample (Table 6). However, when we observed the prediction errors on non-trained data using cross-validation testing we obtained slightly greater errors, with 2.781 mm for black South Africans and 2.748 mm for white South African.

On the complete sample, the prediction errors for the tip of the nose and the alae, (Table 4) showed respectively a prediction errors of 2.498 mm and 2.340 mm on training data, and of 2.875 mm and 2.666 mm on non-trained data. For the black South African sample, the prediction errors for the tip of the nose and the alae on training data showed prediction errors of 1.177 mm and 2.130 mm respectively, while for the white South African sample, a prediction errors of 2.175 and 2.069 mm were observed. However, when we analyzed the prediction errors on non-trained data, we obtained respectively 2.139 mm and 2.733 mm for the black South Africans and 2.700 mm and 2.740 mm for the white South Africans.

Table 5. Prediction errors (in mm) of the predicted capulometric landmarks in the black South African sample, calculated on 200 individuals, based on the training and on the non-trained data.

Black South Africans Predicted capulometric landmarks	Plain		Sex		Age		Sex*Age	
	PE	PE_cv	PE	PE_cv	PE	PE_cv	PE	PE_cv
<i>Pronasale</i>	1.779	2.139	1.777	2.190	1.795	2.179	1.769	2.142
<i>Nasale inferius</i>	2.590	3.392	2.581	3.413	2.504	3.262	2.576	3.520
<i>Columella</i>	2.183	3.087	2.183	2.987	2.177	2.940	2.174	2.968
<i>Subnasale</i>	1.658	1.924	1.658	1.955	1.659	1.946	1.658	1.953
<i>Sellion</i>	2.567	3.348	2.558	3.384	2.473	3.231	2.521	3.455
<i>External alar curvature L</i>	2.215	3.160	2.216	3.053	2.204	3.048	2.206	3.111
<i>External alar curvature R</i>	1.677	1.985	1.677	2.048	1.693	2.030	1.634	1.992
<i>Superior alar curvature L</i>	2.660	3.463	2.652	3.523	2.485	3.242	2.555	3.584
<i>Superior alar curvature R</i>	2.184	3.111	2.185	2.997	2.157	2.928	2.170	3.051
<i>Alagenion L</i>	1.726	2.014	1.725	2.053	1.732	2.079	1.692	2.043
<i>Alagenion R</i>	2.828	3.678	2.823	3.594	2.718	3.459	2.790	3.736
<i>Alare L</i>	2.001	2.762	2.002	2.733	1.987	2.685	1.990	2.728
<i>Alare R</i>	1.651	1.993	1.651	1.979	1.679	1.996	1.608	1.932
<i>Alar curvature point L</i>	2.678	3.408	2.672	3.375	2.629	3.308	2.689	3.563
<i>Alar curvature point R</i>	2.023	2.656	2.023	2.624	2.020	2.558	2.045	2.598
<i>Mid-nostril L</i>	2.100	2.972	2.100	2.851	2.092	2.827	2.086	2.777
<i>Mid-nostril R</i>	1.958	2.274	1.958	2.336	1.968	2.292	1.925	2.302
<i>Mid-columella L</i>	2.080	2.486	2.079	2.483	2.088	2.432	2.030	2.413
<i>Mid-columella R</i>	2.492	3.387	2.479	3.386	2.343	3.117	2.458	3.556
<i>Nasal-depth L</i>	2.543	3.424	2.531	3.455	2.360	3.151	2.491	3.557
<i>Nasal-depth R</i>	2.064	2.950	2.064	2.851	2.057	2.804	2.059	2.803
RMSEP	2.204	2.895	2.200	2.875	2.157	2.781	2.178	2.910

PE: Prediction errors on the training data; *PE_cv*: prediction errors on non-trained data. Better predictions are indicated in bold.

Table 6. Prediction errors (in mm) of the predicted capulometric landmarks in the white South African sample, calculated on 200 individuals, based on the training and on the non-trained data.

White South Africans Predicted capulometric landmarks	Plain		Sex		Age		Sex*Age	
	PE	PE_cv	PE	PE_cv	PE	PE_cv	PE	PE_cv
<i>Pronasale</i>	2.175	2.700	2.170	2.673	2.141	2.701	2.108	2.575
<i>Nasale inferius</i>	2.097	3.212	2.087	3.204	2.085	3.026	2.043	3.198
<i>Columella</i>	2.333	2.993	2.333	2.955	2.206	2.760	2.222	2.823
<i>Subnasale</i>	2.039	2.698	2.036	2.605	2.031	2.659	2.036	2.614
<i>Sellion</i>	2.186	3.320	2.174	3.352	2.154	3.173	2.156	3.383
<i>External alar curvature L</i>	2.336	3.036	2.336	2.972	2.200	2.767	2.218	2.799
<i>External alar curvature R</i>	2.019	2.578	2.015	2.555	1.998	2.565	1.973	2.465
<i>Superior alar curvature L</i>	2.318	3.376	2.308	3.360	2.271	3.234	2.302	3.455
<i>Superior alar curvature R</i>	2.065	2.693	2.064	2.632	1.974	2.494	1.969	2.485
<i>Alagenion L</i>	2.048	2.615	2.045	2.529	2.038	2.602	2.033	2.467
<i>Alagenion R</i>	2.318	3.367	2.309	3.366	2.240	3.276	2.295	3.552
<i>Alare L</i>	1.923	2.550	1.923	2.438	1.860	2.293	1.884	2.339
<i>Alare R</i>	1.860	2.325	1.858	2.270	1.844	2.317	1.821	2.211
<i>Alar curvature point L</i>	2.305	3.366	2.294	3.328	2.242	3.226	2.306	3.449
<i>Alar curvature point R</i>	2.053	2.690	2.052	2.702	2.019	2.624	2.017	2.530
<i>Mid-nostril L</i>	2.054	2.619	2.055	2.639	1.981	2.456	2.008	2.469
<i>Mid-nostril R</i>	2.056	2.619	2.054	2.572	2.024	2.563	1.999	2.485
<i>Mid-columella L</i>	2.172	2.665	2.167	2.636	2.140	2.650	2.096	2.589
<i>Mid-columella R</i>	1.967	2.940	1.961	2.878	1.915	2.745	1.925	2.899
<i>Nasal-depth L</i>	1.941	2.939	1.932	2.954	1.886	2.780	1.927	2.972
<i>Nasal-depth R</i>	2.054	2.622	2.054	2.625	1.974	2.487	1.994	2.494
RMSEP	2.115	2.870	2.111	2.840	2.062	2.748	2.068	2.802

PE: Prediction errors on the training data; *PE_cv*: prediction errors on non-trained data. Better predictions are indicated in bold.

The impact of additional information: ancestry, sex and age were evaluated on the complete sample by adding them to the models as predictors (Table 4). The impact of sex and age was also observed on the black South African sample (Table 5) and on the white South African sample (Table 6). Regarding the complete sample, a better prediction was obtained when the factor age was added to the model as predictors. Indeed, on the training data we obtained prediction errors of 2.240 mm and of 2.582 mm on non-trained data. Similar trends were observed when the two population groups were analysed separately. For both populations, the factor age seemed to improve the prediction accuracy. For the black South African sample we observed a prediction errors of 2.157 mm and 2.062 mm for the white South African sample, both based on training data. The prediction errors based on non-trained data for both population groups is 2.781 mm for the black South Africans and 2.748 mm for the white South Africans.

Regarding the prediction errors on the training data for the tip of the nose, we observed respectively better prediction errors when we added the factors sex and age to the models, for the two population groups separately. Indeed, for the tip of the nose in the two population groups separately, better predictions for the tip of the nose were found when we added the factor sex to the models. Indeed, based on the training data, we observed for the black South African sample, prediction errors of 1.769 mm, and 2.108 mm for the white South African sample. However, when we observed the prediction errors on non-trained data, we obtained 2.142 mm for the black South African sample and 2.375 mm for the white South African sample. On the other hand, for the alae, we observed a better prediction errors when we added the factor age to the models for the complete sample and for both population groups analyzed separately. Indeed, for the alae in the complete sample, we obtained 2.290 mm based on the training data, and 2.627 mm based on the non-trained data. Based on the training data, for the black South African sample, prediction errors of 2.130 mm were observed, and of 2.069 mm for the white South African sample. When we observed the prediction errors on non-trained data, we obtained 2.733 mm for the black South African and 2.740 mm for the white South African.

The predictive performance of the PLSR, tested on predictions obtained from black and white South African models, generated from the training and non-trained data of the other population is detailed in Table 7. As expected, the prediction error was significantly larger than for predictions based on the original population database because the population-specific covariation between both types of tissue cannot be exploited by the prediction algorithm.

Table 7. Population dependent quality of prediction (mm) of the predicted capulometric landmarks, calculated on 200 individuals, on the training and on non-trained data.

Population dependent quality of prediction	Black South Africans predictions based on white South Africans sample data		White South Africans predictions based on black South Africans sample data	
	PE	PE_cv	PE	PE_cv
RMSEP	3.479	10.083	2.733	8.196

PE: Prediction errors on the training data; PE_cv: prediction errors on non-trained data.

Discussion

Statistical models and a detailed overview of the influence of factors (ancestry, sex, ageing) for predicting nasal soft-tissue shape from information about the underlying skull substrate are provided. Ancestry was found to be a very important factor of shape variation within the sample emphasizing population-specific differences. From the findings, sexual dimorphism and ageing also plays an important role in the overall hard- and soft-tissue shape variation of the nose. In addition, when these factors were added as additional information in the models, they appeared to be important to be considered in order to improve the quality of the prediction, for both South African groups.

In this study, the external nose was shown to be strongly correlated with the underlying skull substrate, which are influenced by multifactorial processes (sex, age, and ancestry) involving hormonal, genetic and epigenetic factors; and external stimuli (soft tissue growth, dental maturation and biomechanical factors) [37-46]. During human development, and in order to maintain the function and the proportionate growth, the skeletal components of the face involve changes in their shape and size as well as their relative position within the craniofacial complex system [44, 45, 92, 93]. Consequently, this study supports the notion that during craniofacial development, the morphology of the nose is influenced by the remodelling of the underlying skeletal structure [34] emphasizing that the components of the nose cannot be considered as independent elements of the craniofacial skeleton and the influence of factors such as ancestry, sex and age must be considered. The high prediction errors produced when applying one ancestral-specific information on the other ancestral group, emphasize the need for ancestral-specific guidelines and highlight the importance of considering ancestry as a factor in the process of approximating the nose.

Population specific statistical models were created in order to minimize the influence of ancestry. The influence of environmental factors on nasal shape variation within populations has been demonstrated by several bioanthropological studies [94-96]. The general hypothesis is that the shape of the external nose and the nasal aperture plays an important role in climatic adaptation by regularizing air temperature in order to protect the lungs from temperature and excessive humidity [94-96]. The scientific community has demonstrated that physical anthropologists can estimate ancestral morphological variation among humans because they are able to translate morphological traits (biological) to a culturally constructed labelling

system [97-99]. In addition, Serre and Paabo [100] noted a strong association between culture and biology and stated that, genetic differences between population groups are dependant on historical and cultural factors [101]. In the South African context, racial classification is no longer legally imposed, but modern South Africans continue to socially self-identify according to the classifications imposed by Apartheid. Indeed, a need to self-identify as one of the previously prescribed groups is pervasive in all aspects of life and is an important part of a person's cultural place in the country's citizenship. Therefore, the majority of the population in South Africa self-classifies today as "Black" (80.5%), "Coloured" (8.8%), "White" (8.3%), or "Indian/Asian" (2.5%) South Africans [102]. Assortative mating within these groups strengthened the already notable biological variation between and among groups [2], engendering the perpetuation of skeletal variation allowing for forensic anthropologists to classify an unknown deceased individual as most similar to black, coloured, or white South African.

Sexual dimorphism plays an important role in the overall shape variation of the nose and on the quality of its statistical prediction, mainly regarding the prediction of the tip of the nose and the alae, in both population groups. In CFR, dimensions of the nose are important in distinguishing male and female faces and are useful in establishing an accurate facial approximation of a missing person [103]. In the literature, only one method developed by Schlager [8] on a Chinese and European sample, related to geometric morphometrics have been applied to these issues for the reconstruction of the nose. Schlager [8] found that the expression of dimorphism in variation of the shape of the nose among Chinese and European groups seemed to be influenced statistically by ancestry, but he emphasized that this influence is small from a biological point of view. In the South African research context, distinct differences in facial skeletal morphology (size and shape) between the sexes are shown in many research studies [98, 99, 104] using standard morphometric methods. In general, sexual dimorphism has been demonstrated to be less pronounced in the black South African population, than in other groups (white and coloured) [98, 105].

Ageing is almost as important to the overall shape variation as sex when considering, in both samples. In this study, we found shape changes associated with age between population groups from 18 years to 79 years, which could be explained by general shape differences: as the tissue weakens with age, it follows gravity downwards. In addition, age factors appear to be an important factors to consider in order to improve the quality of the prediction. Research

studies report the prolongation and the widening of the nose (increase of nasal breadth and length) [106-108] during ageing that somewhat resemble some geometric features of the external nose. In the craniofacial literature, few studies address age-related shape changes by means of geometric morphometrics. Only two recent studies, one on a French sample [14] and one on a Chinese and European sample [8] demonstrated the presence of age-related changes of the nasal soft-tissue dimensions in human adults using geometric morphometric analysis. Results from the soft-tissue analysis of age-induced shape changes in this study are consistent with previous studies using classic anthropometric methods.

Population-specific statistical models were created resulting in an error when using the landmark-to-landmark distances on non-trained data ranged between 2.139 mm and 2.833 mm for black South Africans at the tip of the nose and the alae, while they ranged from 2.575 mm to 2.859 mm for the white South Africans. Presently, there are four scientific papers on soft-tissue predictions of the nasal complex region of interest, which will be comparable to the methods proposed in this study: [8, 14, 109, 110]. In Vandermeulen [109], the error distribution based on mesh-to-mesh distances (2006) exhibited an error between 2 and 2.5 mm around the tip of the nose and between 1 and 2 mm for the alae. Tilotta and colleagues [110] reported an average error based on point-to-mesh using a subsample of 49 specimens over the complete surface, of only 1 mm. Guyomarc'h [14] found prediction errors based on point-to-point between 2.7 and 3.1 mm for the respiratory subset [14]. Schlager provides a prediction error when using mesh-to-mesh distances, ranged between 1.2 and 1.4 mm and when considering the landmark-to-landmark distances. In addition, Schlager [8] analyzed two population groups separately. For the European sample, the prediction errors ranged between 2.2 mm and 2.7 mm at the alae and the tip of the nose, while they ranged from 2 mm to 2.4 mm for the Chinese subsample.

The methods used by Vandermeulen [109] and Tilotta [110] differ from our study in the regions being analyzed. When comparing results, one has to take into account that nasal regions with underlying bone tissue can be predicted much better than those lacking such hard-tissue support. Thus, studies concentrating on the nasal tips will lead to significantly higher error rates. In the Tilotta approach [110], the main bias is the utilization of a non-biologically meaningful region as a region of interest. Indeed, the rectangular region is rather based on geometrical factors than biological reasons and therefore does not account for structural or functional coherence. The approach of Schlager [8] and Guyomarc'h [14] approach are close

to the approach taken in this study, involving the definition of a biologically, hence anatomically, meaningful substructure by extracting shape information using landmarks [14] and semi-landmarks [8]. In both studies, correlations between the external shape of the nose and the underlying bone structure were both assessed using GMM.

The comparison between our findings and the results from other studies should however, be performed with caution, because resulting error values are dependent on the metric deviations used: mesh-to-mesh distance [109], point-to-mesh distance [110, 8] or point-to-point distance [8, 14]. Schlager [8], demonstrated how strong the choice of the metric affects the reported prediction error. If the deviation is along the surface of the actual nose (mesh-to-mesh or point-to-mesh), even a large distance will be meaningless, as the discrepancy does not show because the surface model warped onto the estimated landmark configuration would not deviated from the original one. Alternatively, one could calculate the average distance between the predicted point set and the surface model representing the original nose. In the literature, the point-to-mesh is commonly applied when it comes to estimating prediction accuracy [109, 110]. A low error value, however, is not necessarily linked to a pleasing shape: if the prediction fails greatly and heaps all landmarks onto a single location very close to the actual surface, this will result in a low error rate. If the original mesh is used as reference and the distance to the predicted mesh is calculated, this might still be misleading because the closest points are not necessarily homologous. Both scenarios lead to an underestimation (overoptimistic) of prediction error as in Vandermeulen [109] and Tilotta [110] and this is not comparable to the findings in other studies [8, 14] or to our study as well, using point-to-point distances (over-pessimistic). Thus, reconstructions with a relatively high error can still yield a scientifically good prediction [8].

Finally, this research demonstrates the utilization of an automated three-dimensional (3D) method based on an automatic landmarking as a convenient prerequisite for accurate statistical models of nose prediction. Extensive work has been published on 2D landmarks [111-116], whereas limited research has been done on the identification and location of landmarks on 3D surfaces [117]. Only, some recent work on 3D face registration, however, have explored the use of curvature in order to find the tip of the nose [118-122] in combination with an iterative closest point (ICP) alignment algorithm. The ICP is one of most popular techniques for 3D face registration and it has been extensively used as the main procedure or in combination with other methods [118-122].

Finally, we stress that this study is the first attempt at a computer-assisted facial approximation of the nose with an automatic landmarking approach for the South African population using CBCT scans. Compared to manual methods, automation of facial approximation is suitable for application to the judicial system, which requires precision, reliability and knowledge of possible quantization errors. In addition, the automatic placement of landmarks on large 3D surface samples, offers the possibility of standardization, and increased accuracy in the analysis of the correlations between hard- and soft-tissue facial features. When planning future research, it will be fundamental to consider the integration of semi-landmarks as well, in order to describe and to visualise the structures more satisfactory, however, a much denser placement of coordinates would be required. In this research, we specifically used CBCT scans from living patients as we intended to remove the limits generated by the use of dry skulls, cadavers and CT datasets as initial references, such as desiccation and supination effects. A further advantage of CBCT compared to CT includes higher spatial resolution (0.1 mm to 0.4 mm) and isotropic volumetric data for the accurate placement of 3D landmarks [56].

In this study, a statistical model for predicting nasal soft-tissue shape from information about the underlying hard-tissue configuration were created using only the initial hard-tissue information in order to predict the nose in its absolute position. When planning future research, it would be interesting to compare the prediction results with a prediction analysis performed on a non-absolute position. In future research, a quantifying prediction error procedure [8] involving the relaxation of estimated coordinates along the predicted surface will be interesting to perform. Extended analysis of human recognition patterns as well, will be necessary to achieve an improved quantification of similarity, better resembling the human perception. Future work will have to concentrate on acquisition of larger databases, including more populations. In addition, the integration of other parts of the human face in order to generate a soft-tissue prediction for the whole face must be considered, which will require the development of a framework handling the integration of prediction results from different facial areas into the most probable facial surface representation.

Conclusion

This research provided accurate statistical models optimised by including additional information such as ancestry, sex and age. In our study, age and sex factors appeared to be important factors to be considered as additional information in order to improve the quality of the prediction, for both South African samples. This research demonstrates the utilization an automated three-dimensional (3D) method based on an automatic landmarking as a convenient prerequisite for accurate statistical models of nose prediction.

Acknowledgments

The authors would like to thank Dr. André Uys from the Oral and Dental Hospital, University of Pretoria, South Africa and Dr. Sarel Botha from the Life Groenkloof Hospital, Pretoria, South Africa, for providing the CBCT-data. We acknowledge the AESOP+ consortia coordinated by Prof. José Braga from the Computer-assisted Palaeoanthropology Team, UMR 5288 CNRS- Université Paul-Sabatier, 37, allées Jules-Guesde, 31000 Toulouse, and from the Evolutionary Studies Institute and School of Geosciences, University of the Witwatersrand, Johannesburg, South Africa, for the financial support.

References

1. J. Bloom, 1272 Unidentified Bodies in Gauteng Mortuaries in 2014/2015.
2. G.C. Krüger, L. Liebenberg, J. Myburgh, A. Meyer, A.C. Oettlé, D. Botha, D.M. Brits, M.W. Kenyhercz, K.E. Stull, C. Sutherland, E.N. L'Abbé, Forensic Anthropology and the Biological Profile in South Africa, in: *New Perspectives in Forensic Human Skeletal Identification*, Elsevier, 2018: pp. 313–321.
[Doi:10.1016/B978-0-12-805429-1.00027-2](https://doi.org/10.1016/B978-0-12-805429-1.00027-2).
3. E.N. L'Abbé, M. Loots, J.H. Meiring, The Pretoria Bone Collection: A modern South African skeletal sample, *HOMO*. 56 (2005) 197–205. [Doi:10.1016/j.jchb.2004.10.004](https://doi.org/10.1016/j.jchb.2004.10.004).
4. M. Steyn, E.N. L'Abbé, J. Myburgh, Forensic Anthropology as Practiced in South Africa, *Hand book Forensic Anthropol Archaeol.* (2016).
5. C.N. Stephan, Estimating the Skull-to-Camera Distance from Facial Photographs for Craniofacial Superimposition, *Journal of Forensic Sciences*. 62 (2017) 850–860.
[Doi:10.1111/1556-4029.13353](https://doi.org/10.1111/1556-4029.13353).
6. C.N. Stephan, Facial Approximation and Craniofacial Superimposition, in: C. Smith (Ed.), *Encyclopedia of Global Archaeology*, Springer New York, New York, NY, 2014: pp. 2721–2729. [Doi:10.1007/978-1-4419-0465-2_149](https://doi.org/10.1007/978-1-4419-0465-2_149).
7. C. N. Stephan, R. Taylor, & J. Taylor, Methods of facial approximation and skull-face superimposition, with special consideration of method development in Australia. *Forensic Approaches to Death, Disaster and Abuse*, 133 (2008).
8. S. Schlager, Soft-tissue reconstruction of the human nose : population differences and sexual dimorphism = Weichteilrekonstruktion der menschlichen Nase : Populationsunterschiede und Sexualdimorphismus, Universität, Freiburg, 2013.
9. D. Vandermeulen, P. Claes, S. De Greef, G. Willems, J. Clement, P. Suetens, Automated facial reconstruction. *Craniofacial Identification*, (2012) 203.
10. A.J. Tyrrell, M.P. Evison, A.T. Chamberlain, M.A. Green, Forensic Three-Dimensional Facial Reconstruction: Historical Review and Contemporary Developments, *Journal of Forensic Sciences*. 42 (1997) 14176J. [Doi:10.1520/JFS14176J](https://doi.org/10.1520/JFS14176J).
11. C.N. Stephan, Anthropological facial ‘reconstruction’ – recognizing the fallacies, ‘unembracing’ the errors, and realizing method limits, *Science & Justice*. 43 (2003) 193–200. [Doi:10.1016/S1355-0306\(03\)71776-6](https://doi.org/10.1016/S1355-0306(03)71776-6).

12. L. Verzé, History of facial reconstruction, *Acta Bio Medica Atenei Parmensis*, 1. 80 (2009) 5–12.
13. H. Ullrich, C.N. Stephan, On Gerasimov's Plastic Facial Reconstruction Technique: New Insights to Facilitate Repeatability*: Gerasimov's plastic facial reconstruction techniques, *Journal of Forensic Sciences*. 56 (2011) 470–474.
Doi:10.1111/j.1556-4029.2010.01672.x.
14. P.Guyomarc'h, B. Dutailly, J. Charton, F. Santos, P. Desbarats, H. Coqueugniot, Anthropological Facial Approximation in Three Dimensions (AFA3D): Computer-Assisted Estimation of the Facial Morphology Using Geometric Morphometrics, *Journal of Forensic Sciences*. 59 (2014) 1502–1516. Doi:10.1111/1556-4029.12547.
15. T.W. Todd, A. Lindala, Thickness of the subcutaneous tissues in the living and the dead, *American Journal of Anatomy*. (1928);41(2):153–196.
Doi: 10.1002/aja.1000410202.
16. M.H. Manhein, G.A. Listi, R.E. Barsley, R. Musselman, N.E. Barrow, D.H. Ubelaker, In Vivo Facial Tissue Depth Measurements for Children and Adults, *Journal of Forensic Sciences*. 45 (2000) 14640J. Doi:10.1520/JFS14640J.
17. C. M. Wilkinson, In vivo facial tissue depth measurements for white British children. *Journal of Forensic Science*, Vol. 47, No. 3, 2002, pp. 459-465.
Doi: 10.1520/JFS15286J.
18. F. Chen, Y. Chen, Y. Yu, Y. Qiang, M. Liu, D. Fulton, T. Chen, Age and sex related measurement of craniofacial soft tissue thickness and nasal profile in the Chinese population, *Forensic Science International*. 212 (2011) 272.e1-272.e6.
Doi:10.1016/j.forsciint.2011.05.027.
19. C. Wilkinson, *Forensic facial reconstruction*, Cambridge University Press, Cambridge, UK ; New York, 2004.
20. S. De Greef, D. Vandermeulen, P. Claes, P. Suetens, G. Willems, The influence of sex, age and body mass index on facial soft tissue depths, *Forensic Science, Medicine, and Pathology*. 5 (2009) 60–65. Doi:10.1007/s12024-009-9085-9.
21. S.D. Greef, G. Willems, Three-dimensional Cranio-Facial Reconstruction in Forensic Identification: *Latest Progress and New Tendencies in the 21st Century*, *Journal of Forensic Sciences*. 50 (2005) 1–5. Doi:10.1520/JFS2004117.
22. W.J. Lee, S. Mackenzie, C.M. Wilkinson, Facial identification of the dead. In: Black S, Ferguson E, editors. *Forensic anthropology: 2000– 2010*. Boca Raton, FL: CRC Press-Taylor and Francis Group (2011) 363–94.

23. D. Vandermeulen, P. Claes, D. Loeckx, S. De Greef, G. Willems, P. Suetens, Computerized craniofacial reconstruction using CT-derived implicit surface representations, *Forensic Science International*. 159 (2006) S164–S174. [Doi:10.1016/j.forsciint.2006.02.036](https://doi.org/10.1016/j.forsciint.2006.02.036).
24. V. Bruce, G.W. Humphreys, Recognizing objects and faces, *Visual Cognition*. (1994); Apr 1;1(2–3):141–80.
25. J. Shepherd, "Studies of cue saliency." *Perceiving and remembering faces* (1981).
26. W. Zhao, R. Chellappa, P.J. Phillips, A. Rosenfeld, Face recognition: A literature survey, *ACM Computing Surveys*. 35 (2003) 399–458. [Doi:10.1145/954339.954342](https://doi.org/10.1145/954339.954342).
27. M.M. Gerasimov, Vosstanovlieniia Litsa po Cherapu; Gos Izd-vo Sovetskaia [The reconstruction of the face on the skull]. Unpublished translation (1975) by Tshernezky 1955.
28. W. M. Krogman, *The human skeleton in forensic medicine*. Thomas, Springfield, Ill. 1962
29. W. Krogman, M. Işcan M, *The Human Skeleton in Forensic Medicine*, Charles C. Thomas Springfield IL, 2nd edition, 1986.
30. G.A. Macho, An Appraisal of Plastic Reconstruction of the External Nose, *Journal of Forensic Sciences*. 31 (1986) 11917J. [Doi:10.1520/JFS11917J](https://doi.org/10.1520/JFS11917J).
31. R. George, The Lateral Craniographic Method of Facial Reconstruction, *Journal of Forensic Sciences*, Vol.32, No.5. (1987); pp.1305-1330.
32. M. Prokopec, D.H. Ubelaker, Reconstructing the shape of the nose according to the skull, *Forensic Science Communications*. (2002); 4(1).
33. C.N. Stephan, M. Henneberg, W. Sampson, Predicting nose projection and pronasale position in facial approximation: a test of published methods and proposal of new guidelines, *American Journal of Physical Anthropology*. (2003);122(3):240–50. [Doi: 10.1002/ajpa.10300](https://doi.org/10.1002/ajpa.10300).
34. A.M. Albert, K. Ricanek, E. Patterson, A review of the literature on the aging adult skull and face: Implications for forensic science research and applications, *Forensic Science International*. 172 (2007) 1–9. [Doi:10.1016/j.forsciint.2007.03.015](https://doi.org/10.1016/j.forsciint.2007.03.015).
35. M.L. Moss, R.W. Young, A functional approach to craniology, *American Journal of Physical Anthropology*. (1960);18(4):281–92. [Doi: 10.1002/ajpa.1330180406](https://doi.org/10.1002/ajpa.1330180406).
36. D.H. Enlow, M.G. Hans, *Essentials of facial growth*. W.B. Saunders Company;(1996).

37. M.L. Moss, The functional matrix hypothesis revisited. 1, The role of mechanotransduction, *American Journal of Orthodontics and Dentofacial Orthopedics*. (1997);112(1):8–11. [Doi: 10.1016/S0889-5406\(97\)70267-1](https://doi.org/10.1016/S0889-5406(97)70267-1).
38. M.L. Moss, The functional matrix hypothesis revisited. 2, The role of an osseous connected cellular network, *American Journal of Orthodontics and Dentofacial Orthopedics*. (1997a);112(2):221–6. [Doi: 10.1016/S0889-5406\(97\)70249-X](https://doi.org/10.1016/S0889-5406(97)70249-X).
39. M.L. Moss, The functional matrix hypothesis revisited. 3, The genomic thesis, *American Journal of Orthodontics and Dentofacial Orthopedics*. (1997b);112(3):338–42. [Doi: 10.1016/S0889-5406\(97\)70265-8](https://doi.org/10.1016/S0889-5406(97)70265-8).
40. M.L. Moss, The functional matrix hypothesis revisited. 4, The epigenetic antithesis and the resolving synthesis, *American Journal of Orthodontics and Dentofacial Orthopedics*. (1997c);112(4):410–7. [Doi: 10.1016/S0889-5406\(97\)70049-0](https://doi.org/10.1016/S0889-5406(97)70049-0).
41. D.E. Lieberman, B.M. McBratney, G. Krovitz, The evolution and development of cranial form in *Homo sapiens*, *Proceeding of the National Academy of Sciences of the United States of America*. (2002);99(3):1134
<https://doi.org/10.1073/pnas.022440799>.
42. C.P. Klingenberg, K. Mebus, J. Auffray, Developmental integration in a complex morphological structure: how distinct are the modules in the mouse mandible? *Evolution & Development*. (2003);5(5):522–31.
[Doi: 10.1046/j.1525-142X.2003.03057.x](https://doi.org/10.1046/j.1525-142X.2003.03057.x).
43. Y. Tomoyasu, T. Yamaguchi T, A. Tajima, T. Nakajima, I. Inoue, K. Maki, Further evidence for an association between mandibular height and the growth hormone receptor gene in a Japanese population, *American Journal of Orthodontics and Dentofacial Orthopedics*. (2009);136(4):53641.
[Doi: 10.1016/j.ajodo.2007.10.054](https://doi.org/10.1016/j.ajodo.2007.10.054).
44. D. Lieberman, *The evolution of the human head*. Harvard University Press; (2011).
45. F. Gröning, M. Fagan, P. O'higgins, Comparing the distribution of strains with the distribution of bone tissue in a human mandible: a finite element study, *The Anatomical Record*. (2013);296(1):9–18. [Doi: 10.1002/ar.22597](https://doi.org/10.1002/ar.22597).
46. W.R. Atchley, B.K. Hall, A model for development and evolution of complex morphological structures, *Biological Reviews*. (1991);66(2):101–57.
[Doi:10.1111/j.1469-185X.1991.tb01138.x](https://doi.org/10.1111/j.1469-185X.1991.tb01138.x).
47. K. Taylor, *Forensic Art and Illustration*, CRC Press, 2000.
[Doi:10.1201/9781420036954](https://doi.org/10.1201/9781420036954).

48. A.A. Akgül, T.U. Toygar, Natural craniofacial changes in the third decade of life: A longitudinal study, *American Journal of Orthodontics and Dentofacial Orthopedics*. 122 (2002) 512–522. [Doi:10.1067/mod.2002.128861](https://doi.org/10.1067/mod.2002.128861).
49. A.F. Ridel, F. Demeter, J. Liebenberg, E.N. L'Abbé, D. Vandermeulen, A.C. Oettlé, Skeletal dimensions as predictors for the shape of the nose in a South African sample: A cone-beam computed tomography (CBCT) study, *Forensic Science International*. 289 (2018) 18–26. [Doi:10.1016/j.forsciint.2018.05.011](https://doi.org/10.1016/j.forsciint.2018.05.011).
50. Claes, P., Vandermeulen, D., De Greef, S., Willems, G., Clement, J.G. & Suetens, P., 2010. Computerized craniofacial reconstruction: Conceptual framework and review. *Forensic Science International*. 201(1–3):138–145. [Doi:10.1016/j.forsciint.2010.03.008](https://doi.org/10.1016/j.forsciint.2010.03.008).
51. F. Tilotta, *Contribution à la reconstitution faciale en médecine légale : proposition d'une nouvelle méthode statistique* (Doctoral dissertation) 2008.
52. N. Iblher, E. Gladilin, B.G. Stark, Soft-Tissue Mobility of the Lower Face Depending on Positional Changes and Age: A Three-Dimensional Morphometric Surface Analysis, *Plastic and Reconstructive Surgery*. 131 (2013) 372–381. [Doi:10.1097/PRS.0b013e318278d67c](https://doi.org/10.1097/PRS.0b013e318278d67c).
53. F. Marin, K.B. Mansour, F. Demeter, P. Frey, Displacement of facial soft tissues in upright versus supine positions, *Computer Methods in Biomechanics and Biomedical Engineering*. (2015) 1–2. [Doi:10.1080/10255842.2015.1069590](https://doi.org/10.1080/10255842.2015.1069590).
54. L. Munn, C.N. Stephan, Changes in face topography from supine-to-upright position—And soft tissue correction values for craniofacial identification, *Forensic Science International*. 289 (2018) 40–50. [Doi:10.1016/j.forsciint.2018.05.016](https://doi.org/10.1016/j.forsciint.2018.05.016).
55. H.-J. Vogel, Mees, F., Swennen, R., Van Geet, M. & Jacobs, P. (eds) *Applications of X-ray Computed Tomography in the Geosciences*. Geological Society of London, 2003. vi + 243 pp. f65 (US\$108), hardback. ISBN 1-86239-139-4., *European Journal of Soil Science*. 56 (2005) 277–278. [Doi:10.1111/j.1365-2389.2004.0694f.x](https://doi.org/10.1111/j.1365-2389.2004.0694f.x).
56. W.C. Scarfe, A.G. Farman, What is Cone-Beam CT and How Does it Work?, *Dental Clinics of North America*. 52 (2008) 707–730. [Doi:10.1016/j.cden.2008.05.005](https://doi.org/10.1016/j.cden.2008.05.005).
57. C.F. Spoor, F.W. Zonneveld, G.A. Macho, Linear measurements of cortical bone and dental enamel by computed tomography: Applications and problems, *American Journal of Physical Anthropology*. 91 (1993) 469–484. [Doi:10.1002/ajpa.1330910405](https://doi.org/10.1002/ajpa.1330910405).

58. P. Claes, D. Vandermeulen, S. De Greef, G. Willems, P. Suetens, Statistically Deformable Face Models for Cranio-Facial Reconstruction, *Journal of Computing and Information Technology*. 14 (2006) 21. [Doi:10.2498/cit.2006.01.03](https://doi.org/10.2498/cit.2006.01.03).
59. P. Claes, D. Vandermeulen, S. De Greef, G. Willems, P. Suetens, Craniofacial reconstruction using a combined statistical model of face shape and soft tissue depths: Methodology and validation, *Forensic Science International*. 159 (2006) S147–S158. [Doi:10.1016/j.forsciint.2006.02.035](https://doi.org/10.1016/j.forsciint.2006.02.035).
60. P. Claes, A robust statistical surface registration framework using implicit function representations: Application in craniofacial reconstruction. PhD Thesis, K.U. Leuven, Belgium 2007.
61. P. Claes, A robust statistical surface registration framework using implicit function representations: application in craniofacial reconstruction, in: *Faculteit ingenieurswetenschappen, department Elektrotechniek, afdeling PSI, K.U. Leuven, Belgium, Leuven, 2007*.
62. J. Snyders, P. Claes, D. Vandermeulen, P. Suetens, Development and comparison of non-rigid surface registration algorithms and extensions. Technical report KUL/ESAT/PSI/1401, KU Leuven, ESAT, January (2014) Leuven, Belgium.
63. D.G. Kendall, Shape Manifolds, Procrustean Metrics, and Complex Projective Spaces, *Bulletin of the London Mathematical Society*. 16 (1984) 81–121. [Doi:10.1112/blms/16.2.81](https://doi.org/10.1112/blms/16.2.81).
64. D.E. Slice, Landmark coordinates aligned by Procrustes analysis do not lie in Kendall's shape space. *Systematic Biology* 50(1): (2001) 141–149.
65. J. Buikstra, D. Ubelaker, Standards for data collection from human skeletal remains: Proceedings of a seminar at the Field Museum of Natural History (Arkansas Archaeology Research Series 44). *Fayetteville Arkansas Archaeological Survey*. (1994).
66. J. Caple, C.N. Stephan, A standardized nomenclature for craniofacial and facial anthropometry, *International Journal of Legal Medicine*. 130 (2016) 863–879. [Doi:10.1007/s00414-015-1292-1](https://doi.org/10.1007/s00414-015-1292-1).
67. F.L. Bookstein, *Morphometric tools for landmark data: geometry and biology*, Cambridge University Press, Cambridge [England]; New York, 1991.
68. F. Bookstein, Biometrics, biomathematics and the morphometric synthesis, *Bulletin of Mathematical Biology*. 58 (1996) 313–365. [Doi:10.1016/0092-8240\(95\)00329-0](https://doi.org/10.1016/0092-8240(95)00329-0).

69. F.L. Bookstein, Shape and the information in medical images: a decade of the morphometric synthesis, in: IEEE, 1996, pp. 2–12. [Doi:10.1109/MMBIA.1996.534052](https://doi.org/10.1109/MMBIA.1996.534052).
70. F. James Rohlf, L.F. Marcus, A revolution morphometrics, *Trends in Ecology & Evolution*. 8 (1993) 129–132. [Doi:10.1016/0169-5347\(93\)90024-J](https://doi.org/10.1016/0169-5347(93)90024-J).
71. C.P.E. Zollikofer, M.S. Ponce de Leon, Visualizing patterns of craniofacial shape variation in *Homo sapiens*, *Proceedings of the Royal Society B: Biological Sciences*. 269 (2002) 801–807. [Doi:10.1098/rspb.2002.1960](https://doi.org/10.1098/rspb.2002.1960).
72. D.C. Adams, F.J. Rohlf, D.E. Slice, Geometric morphometrics: Ten years of progress following the ‘revolution,’ *Italian Journal of Zoology*. 71 (2004) 5–16. [Doi:10.1080/11250000409356545](https://doi.org/10.1080/11250000409356545).
73. M.L. Zelditch, D.L. Swiderski, D.S. Sheets, W.L. Fink, *Geometric Morphometrics for Biologists*. Elsevier Academic Press, San Diego 2004.
74. D.E. Slice, Geometric Morphometrics, *Annual Review of Anthropology*. 36 (2007) 261–281. [Doi:10.1146/annurev.anthro.34.081804.120613](https://doi.org/10.1146/annurev.anthro.34.081804.120613).
75. P. Mitteroecker, P. Gunz, *Advances in Geometric Morphometrics*, *Evolutionary Biology*. 36 (2009) 235–247. [Doi:10.1007/s11692-009-9055-x](https://doi.org/10.1007/s11692-009-9055-x).
76. C. Goodall Procrustes methods in the statistical analysis of shape. *Journal of the Royal Statistical Society. Series B. Statistical Methodology*, (1991) 53:285–239.
77. L. Dryden and K. V. Mardia, *Statistical shape analysis*. John Wiley and sons, Chichester 1998.
78. C.P. Klingenberg, G.S. McIntyre, Geometric morphometric of developmental instability: analysing patterns of fluctuating asymmetry with Procrustes methods, *Evolution*. 52 (1998) 1363–1375. [Doi:10.1111/j.1558-5646.1998.tb02018.x](https://doi.org/10.1111/j.1558-5646.1998.tb02018.x).
79. C.P. Klingenberg, M. Barluenga, A. Meyer, Shape analysis of symmetric structures: quantifying variation among individuals and asymmetry, *Evolution*. 56 (2002) 1909. [Doi:10.1554/00143820\(2002\)056\[1909:SAOSSQ\]2.0.CO;2](https://doi.org/10.1554/00143820(2002)056[1909:SAOSSQ]2.0.CO;2).
80. L. Scrucca, *Assessing Multivariate Normality through Interactive Dynamic Graphics* 2000.
81. Adams, D., Collyer, M., & Kaliontzopoulou, A.. *Geometric Morphometric Analyses of 2D/3D Landmark Data* (2018).
82. Ø. Langsrud, K. Jørgensen, R. Ofstad, T. Næs, Analyzing Designed Experiments with Multiple Responses, *Journal of Applied Statistics*. 34 (2007) 1275–1296. [Doi:10.1080/02664760701594246](https://doi.org/10.1080/02664760701594246).

83. Ø. Langsrud & B. H. Mevik, *ffmanova: Fifty-fifty MANOVA*. URL <http://CRAN.R-project.org/package=ffmanova> (2012).
84. S. Schlager, 2017, Calculations and Visualisations Related to Geometric Morphometrics
85. P.N. Gonzalez, S.I. Perez, V. Bernal, Ontogenetic Allometry and Cranial Shape Diversification Among Human Populations From South America, *The Anatomical Record: Advances in Integrative Anatomy and Evolutionary Biology*. 294 (2011) 1864–1874. [Doi:10.1002/ar.21454](https://doi.org/10.1002/ar.21454).
86. F.J. Rohlf, M. Corti, Use of Two-Block Partial Least-Squares to Study Covariation in Shape, *Systematic Biology*. 49 (2000) 740–753. [Doi:10.1080/106351500750049806](https://doi.org/10.1080/106351500750049806).
87. H. Abdi, Partial least squares regression and projection on latent structure regression (PLS Regression): PLS REGRESSION, *Wiley Interdisciplinary Reviews: Computational Statistics*. 2 (2010) 97–106. [Doi:10.1002/wics.51](https://doi.org/10.1002/wics.51).
88. H. Martens and T. Naes, *Multivariate Calibration*. John Wiley and Sons 1992.
89. S. Wold, M. Sjöström, L. Eriksson, PLS-regression: a basic tool of chemometrics, *Chemometrics and Intelligent Laboratory Systems*. 58 (2001) 109–130. [Doi:10.1016/S0169-7439\(01\)00155-1](https://doi.org/10.1016/S0169-7439(01)00155-1).
90. B.-H. Mevik, H.R. Cederkvist, Mean squared error of prediction (MSEP) estimates for principal component regression (PCR) and partial least squares regression (PLSR), *Journal of Chemometrics*. 18 (2004) 422–429. [Doi:10.1002/cem.887](https://doi.org/10.1002/cem.887).
91. B.-H. Mevik, R. Wehrens, The **pls** Package: Principal Component and Partial Least Squares Regression in *R*, *Journal of Statistical Software*. 18 (2007). [Doi:10.18637/jss.v018.i02](https://doi.org/10.18637/jss.v018.i02).
92. O'Higgins, T.G. Bromage, D.R. Johnson, W.J. Moore, P. McPhie, A Study of Facial Growth in the Sooty Mangabey *Cercocebus atys*, *Folia Primatologica*. 56 (1991) 86–94. [Doi:10.1159/000156532](https://doi.org/10.1159/000156532).
93. M.A McCollum Nasomaxillary remodelling and facial form in robust *Australopithecus*: a reassessment. *J Hum Evol* (2008) 54,2–14
94. A. Thomson, L.H.D. Buxton, Man's Nasal Index in Relation to Certain Climatic Conditions., *The Journal of the Royal Anthropological Institute of Great Britain and Ireland*. 53 (1923) 92. [Doi:10.2307/2843753](https://doi.org/10.2307/2843753).
95. J.S. Weiner Nose shape and climate. *Am J Phys Anthropol* 12, (1954) 615–618.
96. R.G. Franciscus, J.C. Long, Variation in human nasal height and breadth. *Am J Phys Anthropol* 85, (1991) 19–427.

97. N.J. Sauer, Forensic anthropology and the concept of race: If races don't exist, why are forensic anthropologists so good at identifying them?, *Social Science & Medicine*. 34 (1992) 107–111. [Doi:10.1016/0277-9536\(92\)90086-6](https://doi.org/10.1016/0277-9536(92)90086-6).
98. E.N. L'Abbé, C. Van Rooyen, S.P. Nawrocki, P.J. Becker, An evaluation of non-metric cranial traits used to estimate ancestry in a South African sample, *Forensic Science International*. (2011);209(1):195-e1. [Doi: 10.1016/j.forsciint.2011.04.002](https://doi.org/10.1016/j.forsciint.2011.04.002).
99. J.L. McDowell, M.W. Kenyhercz, E.N. L'Abbé, An evaluation of nasal bone and aperture shape among three South African populations, *Forensic Science International*. (2015); 252:189-e1. [Doi: 10.1016/j.forsciint.2015.04.016](https://doi.org/10.1016/j.forsciint.2015.04.016).
100. D. Serre, S. Paabo, Evidence for gradients of human genetic diversity within and among continents, *Genome Res*. 14 (2004) 1679–1685.
101. S. Ousley, R. Jantz, D. Freid, Understanding race and human variation: Why forensic anthropologists are good at identifying race, *American Journal of Physical Anthropology*. (2009); Feb 18;139(1):68–76. [Doi: 10.1002/ajpa.21006](https://doi.org/10.1002/ajpa.21006).
102. Statistics South Africa, 2015. Mid-year Population Estimates (Census No. P0302). South Africa.
103. E.P. Chronicle, M.Y. Chan, C. Hawkins, K. Mason, K. Smethurst, K. Stallybrass, You can tell by the nose—Judging sex from an isolated facial feature, *Perception*. (1995); 24(8):969–73. [Doi: 10.1068/p240969](https://doi.org/10.1068/p240969).
104. A.C. Oetlé, F.P. Demeter, E.N. L'abbé, Ancestral Variations in the Shape and Size of the Zygoma: ancestral variations of the zygoma, *The Anatomical Record*. 300 (2017) 196–208. [Doi:10.1002/ar.23469](https://doi.org/10.1002/ar.23469).
105. J.L. McDowell, E.N. L'Abbé, M.W. Kenyhercz, Nasal aperture shape evaluation between black and white South Africans, *Forensic Science International*. (2012);222(1):397-e1. [Doi: 10.1016/j.forsciint.2012.06.007](https://doi.org/10.1016/j.forsciint.2012.06.007).
106. A. Damon, C.C. Seltzer, H.W. Stoudt, B. Bell, Age and Physique in Healthy White Veterans at Boston, *Journal of Gerontology*. 27 (1972) 202–208. [Doi:10.1093/geronj/27.2.202](https://doi.org/10.1093/geronj/27.2.202).
107. C. Sforza, G. Grandi, M. De Menezes, G.M. Tartaglia, V.F. Ferrario, Age- and sex-related changes in the normal human external nose, *Forensic Science International*. 204 (2011) 205.e1-205.e9. [Doi:10.1016/j.forsciint.2010.07.027](https://doi.org/10.1016/j.forsciint.2010.07.027).
108. F. Chen, Y. Chen, Y. Yu, Y. Qiang, M. Liu, D. Fulton, T. Chen, Age and sex related measurement of craniofacial soft tissue thickness and nasal profile in the Chinese population, *Forensic Science International*. 212 (2011) 272.e1-272.e6.

Doi:10.1016/j.forsciint.2011.05.027.

109. D. Vandermeulen, P. Claes, D. Loeckx, S. De Greef, G. Willems, & P. Suetens, Computerized craniofacial reconstruction using CT-derived implicit surface representations. *Journal of Forensic Sciences*. 159:S (2006) 164–S174.
110. F.M. Tilotta, J.A. Glaunès, F.J. Richard, Y. Rozenholc, A local technique based on vectorized surfaces for craniofacial reconstruction, *Forensic Science International*. (2010);200(1):50–9. Doi:10.1016/j.forsciint.2010.03.029.
111. L.P. Menéndez, Comparing Methods to Assess Intraobserver Measurement Error of 3D Craniofacial Landmarks Using Geometric Morphometrics Through a Digitizer Arm, *Journal of Forensic Sciences*. 62 (2017) 741–746. Doi:10.1111/1556-4029.13301.
112. T.F. Cootes and C. Taylor. "Active Shape Models Search Using Grey Level Models: A Quantitative Evaluation". In *Proceedings, British Machine Vision Conference*, (1993) 2:639–648.
113. T.F. Cootes, G.J. Edwards, C.J. Taylor, Active appearance models, *IEEE Transactions on Pattern Analysis and Machine Intelligence*. 23 (2001) 681–685. Doi:10.1109/34.927467.
114. Y. Wang, C.-S. Chua, Y.-K. Ho, Facial feature detection and face recognition from 2D and 3D images, *Pattern Recognition Letters*. 23 (2002) 1191–1202. Doi:10.1016/S0167-8655(02)00066-1.
115. D. Xi, S.-W. Lee, Face Detection and Facial Component Extraction by Wavelet Decomposition and Support Vector Machines, in: *Audio- and Video-Based Biometric Person Authentication*, Springer, Berlin, Heidelberg, 2003, pp. 199–207. Doi:10.1007/3-540-44887-X 24.
116. S. Kobayashi, S. Hashimoto, Automated feature extraction of face image and its applications, in: *IEEE*, 1995, pp. 164–169. Doi:10.1109/ROMAN.1995.531954.
117. M.C. Ruiz, J. Illingworth, Automatic landmarking of faces in 3D-ALF, in: *IEE*, 2008, pp. 41–46. Doi:10.1049/cp:20080280.
118. Kyong I. Chang, K.W. Bowyer, P.J. Flynn, Multiple Nose Region Matching for 3D Face Recognition under Varying Facial Expression, *IEEE Transactions on Pattern Analysis and Machine Intelligence*. 28 (2006) 1695–1700. Doi:10.1109/TPAMI.2006.210.
119. G. Zhang, Y. Wang, A 3D Facial Feature Point Localization Method Based on Statistical Shape Model, in: *IEEE*, (2007), p. II-249-II-252. Doi:10.1109/ICASSP.2007.366219.

120.M.P. Segundo, C. Queirolo, O.R.P. Bellon, L. Silva, Automatic 3D facial segmentation and landmark detection, in: IEEE, (2007), pp. 431–436.
[Doi:10.1109/ICIAP.2007.4362816.](https://doi.org/10.1109/ICIAP.2007.4362816)

Chapter 8

CONCLUSION

This research is the first attempt at a computer-assisted facial approximation of the nose with an automatic landmarking approach for the development of valid and reliable South African population specific standards using Cone Beam Computer-Tomography scans.

7.1 Automatic landmarking method

This study provided a validation of the precision of the automatic placement of landmarks and demonstrated its utilisation as a convenient prerequisite for geometric morphometrics based shape analysis of the nasal complex. The automatic landmark positioning on hard- and soft-tissue 3D surfaces offered increased objectivity and the possibility of standardisation. The automatic landmarking, in addition to reducing measurement errors in landmark placements, achieved a better precision for facial approximation, enabling the possibility to include more samples and populations with ease. Furthermore, the automatic placement of landmarks as an accurate alternative to manual landmarking, is envisaged to have many applications in forensic and physical anthropology.

7.2. Linear measurement versus Geometric morphometric techniques

The morphological differences among South African groups was characterised by a preliminary analysis using linear distance measurements. Because linear distance measurements are highly correlated with size, geometric morphometrics techniques were applied on craniometric and capulometric anatomical landmarks, so that size-free shape variables could be extracted, and patterns of shape variation elucidated. The results of the preliminary analysis were confirmed and an accurate quantification of the morphological differences in the nasal complex (hard- and soft-tissue) within population groups was performed using geometric morphometric methods.

7.3. Reference sample used

The CBCT database used, includes higher spatial resolution (0.1 mm to 0.4 mm) and isotropic volumetric data for the accurate placement of 3D landmarks and obviated the limits generated by the use of dry skulls, cadavers and CT datasets as initial references, such as desiccation and postural effects.

7.4. Region of interest

A biologically meaningful region of interest enabled the accurate observation of the influence of the underlying mid-facial skull substrate on the external shape of the nose. For this reason, the landmarks selected were distributed on the facial skeleton (nasal bones, anterior nasal aperture, zygomatic bones and maxillary bones) and the external nose.

7.5. Anthropological study

Our findings provided a detailed overview of the influence of factors (sex, ageing and allometry) on the variability of the mid-facial skeleton among two South African population groups and confirming their contribution to the overall shape variation of the nose. Ancestry was found to be a very important factor in shape variation within the sample emphasising population-specific differences. In addition, the expression of sexual dimorphism and effect of aging appeared to be different on distinct elements of the shape of the mid-facial region. From the findings, the two South African groups differed significantly regarding hard- and soft-tissue nasal complex morphology and their correlations, emphasising the importance of considering ancestry, sex and age as factors in the process of approximating the nose and highlighting the need for population specific accurate and reliable 3D statistical nose prediction methods.

7.6. Model of prediction

This research provided accurate statistical models optimised by including additional information such as ancestry, sex and age. In this study, age and sex factors appeared to be important factors to be considered as additional information in order to improve the quality of the prediction, for both South African samples. The predictions in our study was based on a sample of 200 specimens and taking into account the local structure of the nasal hard-tissue, resulting in an error when using the landmark-to-landmark distances, ranging between 1.769 mm and 2.164 mm for black South Africans at the tip of the nose and the alae, and ranged from 2.068 mm to 2.175 mm for the white subsample. However, the prediction errors were calculated on training data which tends to optimise the model. When we observed the prediction errors on non-trained data, we obtained errors. ranging between 2.139 mm and 2.833 mm for black South Africans at the tip of the nose and the alae, while they ranged from 2.575 mm to 2.859 mm for the white South Africans.

7.7 Future research

When planning future research, it will be fundamental to consider the integration of semi-landmarks as well in order to describe and to visualise the structures more satisfyingly. In addition, a procedure introduced by Schlager (Schlager, 2013) for quantifying prediction error, involving the relaxation of estimated coordinates along the predicted surface in order to maximise homology between true and predicted landmarks will be interesting to perform. Future research studies should concentrate on the acquisition of larger databases, including more populations. In addition, the integration of other parts of the human face in order to generate a soft-tissue prediction for the whole face must be considered, which will require the development of a framework handling the integration of prediction results from different facial areas into one most probable facial surface representation.

Chapter 9

REFERENCES

- Abdi, H. 2010. Partial least squares regression and projection on latent structure regression (PLS Regression): PLS Regression. *Wiley Interdisciplinary Reviews: Computational Statistics*. 2(1):97–106. [Doi: 10.1002/wics.51](https://doi.org/10.1002/wics.51).
- Adams, D.C., Rohlf, F.J. & Slice, D.E. 2004. Geometric morphometrics: Ten years of progress following the ‘revolution’. *Italian Journal of Zoology*. 71(1):5–16. [Doi:10.1080/11250000409356545](https://doi.org/10.1080/11250000409356545).
- Adams, D.C., Collyer, M., & Kaliontzopoulou, A., 2018. Geometric Morphometric Analyses of 2D/3D Landmark Data.
- Akgül, A.A. & Toygar, T.U., 2002. Natural craniofacial changes in the third decade of life: A longitudinal study. *American Journal of Orthodontics and Dentofacial Orthopedics*. 122(5):512–522. [Doi:10.1067/mod.2002.128861](https://doi.org/10.1067/mod.2002.128861).
- Albert, A.M., Ricanek, K. & Patterson, E., 2007. A review of the literature on the aging adult skull and face: Implications for forensic science research and applications. *Forensic Science International*. 172(1):1–9. [Doi: 10.1016/j.forsciint.2007.03.015](https://doi.org/10.1016/j.forsciint.2007.03.015).
- Andersson, B. & Valfridsson, M., 2005. Digital 3D Facial Reconstruction Based on Computed Tomography.
- Archer, K.M., 1997. Craniofacial reconstruction using hierarchical B-Spline interpolation. [Doi:10.14288/1.0065288](https://doi.org/10.14288/1.0065288).
- Archer, K., Coughlan, K., Forsey, D., and Struben, S., 1998. Software tools for craniofacial growth and reconstruction. Graphics Interface. Vancouver, Canada.
- Atchley, W.R. & Hall, B.K., 1991. A model for development and evolution of complex morphological structures. *Biological Reviews*. 66(2):101–157. [Doi:10.1111/j.1469-185X.1991.tb01138.x](https://doi.org/10.1111/j.1469-185X.1991.tb01138.x).
- Baillie, L.J., Muirhead, J.C., Blyth, P., Niven, B.E. & Dias, G.J., 2016. Position Effect on Facial Soft Tissue Depths: A Sonographic Investigation. *Journal of Forensic Sciences*. 61: S60–S70. [Doi:10.1111/1556-4029.12935](https://doi.org/10.1111/1556-4029.12935).

- Bastir, M., 2008. A systems-model for the morphological analysis of integration and modularity in human craniofacial evolution. *J Anthropol Sci*, 86, 37-58.
- Berar, M., Desvignes, M., Bailly, G. & Payan, Y., 2005. 3D statistical facial reconstruction. In Zagreb, Croatia: IEEE ISPA 2005. *Proceedings of the 4th International Symposium on Image and Signal Processing and Analysis, 2005*. 365–370.
Doi:10.1109/ISPA.2005.195439.
- Berar, M., Desvignes, M., Bailly, G. & Payan, Y., 2006a. 3D Semi-Landmarks Based Statistical Face Reconstruction. *Journal of Computing and Information Technology*. 14(1):31.
Doi:10.2498/cit.2006.01.04.
- Berar, M., Desvignes, M., Bailly, G. & Payan, Y., 2006b. Statistical skull models from 3D X-ray images. *arXiv preprint physics/0610182*.
- Bloom, J., 2015. 1272. Unidentified Bodies in Gauteng Mortuaries in 2014/2015.
- Bookstein, F.L., 1991. Morphometric tools for landmark data: geometry and biology, Cambridge University Press, Cambridge [England]; New York.
- Bookstein, F.L. 1996a. Shape and the information in medical images: a decade of the morphometric synthesis. In San Francisco, CA, USA: IEEE *Proceedings of the Workshop on Mathematical Methods in Biomedical Image Analysis*. 2–12.
Doi:10.1109/MMBIA.1996.534052.
- Bookstein, F.L., 1996b. Biometrics, biomathematics and the morphometric synthesis. *Bulletin of Mathematical Biology*. 58(2):313–365. Doi:10.1016/0092-8240(95)00329-0.
- Brant, W. E. & Helms, C. A., 2012. *Fundamentals of diagnostic radiology*. 3d edn. Lippincott Williams & Wilkins.
- Bruce, V., 1989. Recognising faces, Erlbaum, Hove.
- Buikstra, J. E., 1994. Standards for data collection from human skeletal remains. *Arkansas archaeological survey research series*, 44.
- Bullock, W.D., 1999. Computer assisted 3d craniofacial reconstruction.
Doi :10.14288/1.0051482.
- Bulut, O., Sipahioglu, S. & Hekimoglu, B. 2014. Facial soft tissue thickness database for craniofacial reconstruction in the Turkish adult population. *Forensic Science International*. 242:44–61. Doi: 10.1016/j.forsciint.2014.06.012.
- Caple, J. & Stephan, C.N., 2016. A standardized nomenclature for craniofacial and facial anthropometry. *International Journal of Legal Medicine*. 130(3):863–879.
Doi: 10.1007/s00414-015-1292-1.

- Chen, F., Chen, Y., Yu, Y., Qiang, Y., Liu, M., Fulton, D. & Chen, T., 2011. Age and sex related measurement of craniofacial soft tissue thickness and nasal profile in the Chinese population. *Forensic Science International*. 212(1–3): 272.e1-272.e6.
 Doi: [10.1016/j.forsciint.2011.05.027](https://doi.org/10.1016/j.forsciint.2011.05.027).
- Chronicle, E.P., Chan, M.-Y., Hawkings, C., Mason, K., Smethurst, K., Stallybrass, K., Westrope, K. & Wright, K. 1995. You Can Tell by the Nose—Judging Sex from an Isolated Facial Feature. *Perception*. 24(8) :969–973. Doi: [10.1068/p240969](https://doi.org/10.1068/p240969).
- Claes, P., De Greef, S., Willems, G., Vandermeulen, D. & Suetens, P., 2004a. Craniofacial statistical modeling and reconstruction. In *Proceedings 3D modelling* (pp. 1-11).
- Claes, P., Vandermeulen, D., Suetens, P., De Greef, S. & Willems, G., 2004b. Computerized facial approximation using statistical models of tissue depth and 3-D facial outlook. In *Proceedings IACI'2004* (pp. 91-96).
- Claes, P., Vandermeulen, D., De Greef, S., Willems, G. & Suetens, P., (2005a). Combined statistical modeling of tissue depth and 3d facial outlook for computerized facial approximation. In *Facial Reconstruction-Gesichtsrekonstruktion, proceedings RSFP 2005* (pp. 433-449).
- Claes, P., Vandermeulen, D., De Greef, S., Willems, G., Suetens, P., 2005b. Combined statistical modeling of tissue depth and 3d facial outlook for computerized facial approximation, in: 2nd International Conference on Reconstruction of Soft Facial Parts, RSFP, Remagen, Germany.
- Claes, P., Vandermeulen, D., De Greef, S., Willems, G. & Suetens, P., 2006a. Statistically Deformable Face Models for Cranio-Facial Reconstruction. *Journal of Computing and Information Technology*. 14(1):21. <https://doi.org/10.2498/cit.2006.01.03>.
- Claes, P., Vandermeulen, D., De Greef, S., Willems, G. & Suetens, P., 2006b. Craniofacial reconstruction using a combined statistical model of face shape and soft tissue depths: Methodology and validation. *Forensic Science International*. 159: S147–S158.
 Doi : [10.1016/j.forsciint.2006.02.035](https://doi.org/10.1016/j.forsciint.2006.02.035).
- Claes, P., 2007. A robust statistical surface registration framework using implicit function representations: Application in craniofacial reconstruction. PhD Thesis, K.U. Leuven, Belgium.
- Claes, P., Vandermeulen, D., De Greef, S., Willems, G., Clement, J.G. & Suetens, P., 2010a. Computerized craniofacial reconstruction: Conceptual framework and review. *Forensic Science International*. 201(1–3):138–145. Doi: [10.1016/j.forsciint.2010.03.008](https://doi.org/10.1016/j.forsciint.2010.03.008).

- Claes, P., Vandermeulen, D., De Greef, S., Willems, G., Clement, J.G. & Suetens, P., 2010b. Bayesian estimation of optimal craniofacial reconstructions. *Forensic Science International*. 201(1–3):146–152. [Doi: 10.1016/j.forsciint.2010.03.009](https://doi.org/10.1016/j.forsciint.2010.03.009).
- Damon, A., Seltzer, C. C., Stoudt, H. W. & Bell, B., 1972. Age and physique in healthy white veterans at Boston. *Journal of gerontology*, 27(2), 202-208.
- Davy, S., Gilbert, T., Schofield, D. & Evison, M., 2005. Forensic facial reconstruction using computer modeling software. *Computer-Graphic Facial Reconstruction*, 183-194.
- De Greef, S., Claes, P., Mollemans, W., Loubele, M., Vandermeulen, D., Suetens, P. & Willems, G., 2005. Semi-automated Ultrasound Facial Soft Tissue Depth Registration: Method and Validation. *Journal of Forensic Sciences*. 50(6) :1–7.
[Doi : 10.1520/JFS2004547](https://doi.org/10.1520/JFS2004547).
- De Greef, S., Claes, P., Vandermeulen, D., Mollemans, W., Suetens, P. & Willems, G., 2006. Large-scale in-vivo Caucasian facial soft tissue thickness database for craniofacial reconstruction. *Forensic Science International*. 159: S126–S146.
[Doi: 10.1016/j.forsciint.2006.02.034](https://doi.org/10.1016/j.forsciint.2006.02.034).
- De Greef, S., Vandermeulen, D., Claes, P., Suetens, P. & Willems, G., 2009. The influence of sex, age and body mass index on facial soft tissue depths. *Forensic Science, Medicine, and Pathology*. 5(2): 60–65.
[Doi: 10.1016/j.forsciint.2009.06.017](https://doi.org/10.1016/j.forsciint.2009.06.017).
- Dryden, I. L. & Mardia, K. V., 2016. *Statistical shape analysis: with applications in R*. John Wiley & Sons.
- Dubow, S., 1995. *Scientific racism in modern South Africa*. Cambridge University Press.
- Dumont, E.R. 1986. Mid-Facial Tissue Depths of White Children: An Aid in Facial Feature Reconstruction. *Journal of Forensic Sciences*. 31(4):1192-6J.
[Doi: 10.1520/JFS11926J](https://doi.org/10.1520/JFS11926J).
- Enlow, D.H. & Hans, M.G., 1996. *Essentials of facial growth*. Philadelphia: Saunders.
- Evenhouse, R.J., Rasmussen, M. & Sadler, L.L., 1991. Computer-aided forensic facial reconstruction. In R.E. Herron (ed.). Boston, MA. 147–156. [Doi: 10.1117/12.48078](https://doi.org/10.1117/12.48078).
- Evison, M., 1996. Computerised 3D facial reconstruction [Online]. Research School of Archaeology and Archaeological Science, University of Sheffield, UK.
- Evison, M.P., 2001. Modeling age, obesity, and ethnicity in a computerized 3-d facial reconstruction. *Forensic Science Communications*, 3(2).

- Forte, M., 1999. 3D facial reconstruction and visualization of ancient Egyptian mummies using spiral CT data. In Los Angeles, California, United States: ACM Press *ACM SIGGRAPH 99 Conference abstracts and applications on - SIGGRAPH '99*. 223.
 Doi: [10.1145/311625.312106](https://doi.org/10.1145/311625.312106).
- Franciscus, R.G. & Long, J.C., 1991. Variation in human nasal height and breadth. *American Journal of Physical Anthropology*. 85(4):419–427.
 Doi: [10.1002/ajpa.1330850406](https://doi.org/10.1002/ajpa.1330850406).
- Franklin, D., Freedman, L., Milne, N. & Oxnard, C.E. 2007. Geometric morphometric study of population variation in indigenous southern African crania. *American Journal of Human Biology*. 19(1):20–33. Doi: [10.1002/ajhb.20569](https://doi.org/10.1002/ajhb.20569).
- Fraser, I.H. & Parker, D.M., 1986. Reaction Time Measures of Feature Saliency in a Perceptual Integration Task. In H.D. Ellis, M.A. Jeeves, F. Newcombe, & A. Young (eds.). Dordrecht: Springer Netherlands *Aspects of Face Processing*. 45–52.
 Doi:[10.1007/978-94-009-4420-6_4](https://doi.org/10.1007/978-94-009-4420-6_4).
- Gangestad, S. 2003. Facial masculinity and fluctuating asymmetry. *Evolution and Human Behavior*. 24(4):231–241. Doi: [10.1016/S1090-5138\(03\)00017-5](https://doi.org/10.1016/S1090-5138(03)00017-5).
- Gapert, R., Black, S. & Last, J., 2009. Sex determination from the occipital condyle: Discriminant function analysis in an Eighteenth and Nineteenth Century British sample. *American Journal of Physical Anthropology*. 138(4):384–394.
 Doi: [10.1002/ajpa.20946](https://doi.org/10.1002/ajpa.20946).
- Garlie, T.N. & Saunders, S.R., 1999. Midline Facial Tissue Thicknesses of Subadults from a Longitudinal Radiographic Study. *Journal of Forensic Sciences*. 44(1):14412J.
 Doi: [10.1520/JFS14412J](https://doi.org/10.1520/JFS14412J).
- George, R.M., 1987. The Lateral Craniographic Method of Facial Reconstruction. *Journal of Forensic Sciences*. 32(5):11181J. Doi: [10.1520/JFS11181J](https://doi.org/10.1520/JFS11181J). ISSN 0022-1198.
- Gerasimov M.M., 1955. Vosstanovlieniia Litsa po Cherapu; Gos Izd-vo Sovetskaia [The reconstruction of the face on the skull]. Unpublished translation (1975) by Tshernezky.
- Gerasimov M.M., 1971. Face Finder, CRC Press, NY.
- Gonzalez; R.C.; and Woods, R.E., 2008. Digital image Processing, 3,d edn. Upper Sadd le River, NJ: Prentice Hall International.
- Gonzalez, P.N., Perez, S.I. & Bernal, V. 2011. Ontogenetic Allometry and Cranial Shape Diversification Among Human Populations From South America. *The Anatomical Record: Advances in Integrative Anatomy and Evolutionary Biology*. 294(11):1864–1874. Doi:[10.1002/ar.21454](https://doi.org/10.1002/ar.21454).

- Goodall, C., 1991. Procrustes methods in the statistical analysis of shape. *Journal of the Royal Statistical Society. Series B (Methodological)*, 285-339.
- Gower, J. C., 1975. Generalized procrustes analysis. *Psychometrika*, 40(1), 33-51.
- Greef, S.D. & Willems, G., 2005. Three-dimensional Cranio-Facial Reconstruction in Forensic Identification: *Latest Progress and New Tendencies in the 21st Century*. *Journal of Forensic Sciences*. 50(1):1-5.
- Gröning, F., Fagan, M. & O'higgins, P., 2013. Comparing the Distribution of Strains with the Distribution of Bone Tissue in a Human Mandible: A Finite Element Study. *The Anatomical Record: Advances in Integrative Anatomy and Evolutionary Biology*. 296(1) :9-18. Doi : 10.1002/ar.22597.
- Guyomarc'h, P. & Bruzek, J., 2010. Dimorphisme sexuel du crâne de sujets identifiés (collection Olivier, MNHN, Paris) : évaluation par morphométrie géométrique. *Bulletins et mémoires de la Société d'anthropologie de Paris*. 22(3-4) :216-229.
Doi : 10.1007/s13219-010-0019-6. 2010.
- Guyomarc'h, P., Dutailly, B., Charton, J., Santos, F., Desbarats, P. & Coqueugniot, H., 2014. Anthropological Facial Approximation in Three Dimensions (AFA3D): Computer-Assisted Estimation of the Facial Morphology Using Geometric Morphometrics. *Journal of Forensic Sciences*. 59(6):1502-1516. Doi:10.1111/1556-4029.12547.
- Haglund, W.D., and Reay, D.T., 1991. Use of facial approximation techniques in identification of green river serial murder victims. *American Journal of Forensic Medicine and Pathology*, 12(2):132-142.
- Haig, N.D., 1986. Exploring Recognition with Interchanged Facial Features. *Perception*. 15(3):235-247. Doi:10.1068/p150235.
- Haig, N.D., 2013. The Effect of Feature Displacement on Face Recognition. *Perception*. 42(11):1158-1165. Doi:10.1068/p130505n.
- Hall, M. & Morris, A., 1983. Race and Iron age human skeletal remains from Southern Africa: An assessment. *Social Dynamics*. 9(2):29-36.
Doi: 10.1080/02533958308458344.
- Hefner, J.T., 2009. Cranial Nonmetric Variation and Estimating Ancestry. *Journal of Forensic Sciences*. 54(5):985-995. Doi: 10.1111/j.1556-4029.2009.01118.x.
- Helmer, R., 1984. *Schädelidentifizierung durch elektronische Bildmischung: zugleich ein Beitrag zur Konstitutionsbiometrie und Dickenmessung der Gesichtswichteile*. Kriminalistik-Verlag.

- His, W., 1895. Anatomische Forschungen über Johann Sebastian Bach's Gebeine und Antlitz nebst Bemerkungen über dessen Bilder, Abhandlungen der mathematisch-physikalischen Klasse der Königlichen Sächsischen Gesellschaft der Wissenschaften 22. 379–420.
- Hwang, H.-S., Park, M.-K., Lee, W.-J., Cho, J.-H., Kim, B.-K. & Wilkinson, C.M., 2012. Facial Soft Tissue Thickness Database for Craniofacial Reconstruction in Korean Adults: Facial soft tissue thickness database. *Journal of Forensic Sciences*. 57(6):1442–1447.
Doi: 10.1111/j.1556-4029.2012. 02192.x.
- Iblher, N., Gladilin, E. & Stark, B.G., 2013. Soft-Tissue Mobility of the Lower Face Depending on Positional Changes and Age: A Three-Dimensional Morphometric Surface Analysis. *Plastic and Reconstructive Surgery*. 131(2):372–381.
Doi:10.1097/PRS.0b013e318278d67c.
- Jones, M., 2001. Facial reconstruction using volumetric data. Proceedings of the 6th International Vision Modeling and Visualisation Conference in Stuttgart (Germany). pages 21–23.
- Jungers, W. & Baab, K. 2009. The geometry of hobbits: *Homo floresiensis* and human evolution. *Significance*. 6(4):159–164.
- Kähler, K., Haber, J. & Seidel, H.-P. 2003. Reanimating the dead: reconstruction of expressive faces from skull data. In San Diego, California: ACM Press *ACM SIGGRAPH 2003 Papers on - SIGGRAPH '03*. 554. Doi:10.1145/1201775.882307.
- Kendall, D.G., 1984. Shape Manifolds, Procrustean Metrics, and Complex Projective Spaces, *Bulletin of the London Mathematical Society*. 16; 81–121. Doi:10.1112/blms/16.2.81.
- Kimmerle, E.H., Ross, A. & Slice, D. 2008. Sexual Dimorphism in America: Geometric Morphometric Analysis of the Craniofacial Region. *Journal of Forensic Sciences*. 53(1):54–57. Doi:10.1111/j.1556-4029.2007. 00627.x.
- Klingenberg, C.P. & McIntyre, G.S., 1998. Geometric morphometrics of developmental instability: analysing patterns of fluctuating asymmetry with Procrustes methods. *Evolution*. 52(5):1363–1375. Doi:10.1111/j.1558-5646. 1998.tb02018. x.
- Klingenberg, C.P., Barluenga, M. & Meyer, A. 2002. Shape analysis of symmetric structures: quantifying variation among individuals and asymmetry. *Evolution*. 56(10):1909–1920. Doi: 10.1111/j.0014-3820. 2002.tb00117.x.
- Klingenberg, C.P., Mebus, K. & Auffray, J.-C., 2003. Developmental integration in a complex morphological structure: how distinct are the modules in the mouse mandible? *Evolution and Development*. 5(5):522–531. Doi: 10.1046/j.1525-142X.2003. 03057.x.

- Kollmann, J. & Büchly, W., 1898. *Die persistenz der rassen und die reconstruction der physiognomie prähistorischer Schädel*. Archiv f. Anthrop.
- Krogman, W. M., 1962. *The human skeleton in forensic medicine*. Thomas, Springfield, Ill.
- Krogman W., İşcan M., 1986. *The Human Skeleton in Forensic Medicine*, Charles C. Thomas Springfield IL, 2nd edition.
- Krüger, G.C., Liebenberg, L., Myburgh, J., Meyer, A., Oettlé, A.C., Botha, D., Brits, D.M., Kenyhercz, M.W., et al. 2018. Forensic Anthropology and the Biological Profile in South Africa. In Elsevier *New Perspectives in Forensic Human Skeletal Identification*. 313–321.
- L'Abbé, E.N., Loots, M. & Meiring, J.H. 2005. The Pretoria Bone Collection: A modern South African skeletal sample. *HOMO*. 56(2):197–205.
Doi: 10.1016/j.jchb.2004.10.004.
- L'Abbé, E.N., Van Rooyen, C., Nawrocki, S.P. & Becker, P.J., 2011. An evaluation of non-metric cranial traits used to estimate ancestry in a South African sample. *Forensic Science International*. 209(1–3): 195.e1-195.e7. Doi: 10.1016/j.forsciint.2011.04.002.
- L'Abbé, E.N., Kenyhercz, M., Stull, K.E., Ousley, S.D., 2013. Craniometric assessment of modern 20th century black, white and “coloured” South Africans. Proceedings of the 65th Annual Meeting of the American Academy of Forensic Sciences 19:444.
- Langsrud, O., 2002. 50-50 multivariate analysis of variance for collinear responses. *Journal of the Royal Statistical Society: Series D (The Statistician)*. 51(3) :305–317.
Doi :10.1111/1467-9884.00320.
- Langsrud, Ø., JØrgensen, K., Ofstad, R. & Næs, T., 2007. Analyzing Designed Experiments with Multiple Responses. *Journal of Applied Statistics*. 34(10):1275–1296.
Doi:10.1080/02664760701594246.
- Langsrud, Ø. & Mevik, B. H., 2012. ffmanova: Fifty-fifty MANOVA. URL <http://CRAN.R-project.org/package=ffmanova>.
- Lebedinskaya, G., Balueva, T., and Veselovskaya, E., 1993. Development of methodological principles for reconstruction of the face on the basis of skull material. In M. Y. İşcan and R. P. Helmer (Eds.), *Forensic Analysis of the Skull: Craniofacial Analysis, Reconstruction, and Identification*. New York, NY: Wiley-Liss.
- Lee, K.-M., Lee, W.-J., Cho, J.-H. & Hwang, H.-S. 2014. Three-dimensional prediction of the nose for facial reconstruction using cone-beam computed tomography. *Forensic Science International*. 236:194. e1-194.e5. Doi: 10.1016/j.forsciint.2013.12.035.

- Lee, W.J., Mackenzie, S., Wilkinson, C.M., 2011. Facial identification of the dead. In: Black S, Ferguson E, editors. *Forensic anthropology: 2000– 2010*. Boca Raton, FL: CRC Press-Taylor and Francis Group ;363–94.
- Lee, W.-J., Wilkinson, C.M. & Hwang, H.-S., 2012. An Accuracy Assessment of Forensic Computerized Facial Reconstruction Employing Cone-Beam Computed Tomography from Live Subjects: An Accuracy Assessment of Forensic Computerized Facial Reconstruction. *Journal of Forensic Sciences*. 57(2):318–327.
Doi:10.1111/j.1556-4029.2011.01971. x.
- Lemon., 2002. Residential Segregation: apartheid. In: Smith SJ (ed) *International Encyclopedia of Housing and Home*. Elsevier, pp111-120.
- Liebenberg, L., 2015. Postcranial Assessment of Ancestry in among Modern South Africans (M.Sc.). University of Pretoria, Pretoria, South Africa.
- Lieberman, D.E., McBratney, B.M. & Krovitz, G., 2002. The evolution and development of cranial form in Homo sapiens. *Proceedings of the National Academy of Sciences*. 99(3):1134–1139. Doi: 10.1073/pnas.022440799.
- Lieberman, D., 2011. *The evolution of the human head*. Cambridge, Mass: Belknap Press of Harvard University Press.
- Loth, S.R., İşcan, M.Y., 2000. Sex Determination. In: Siegel J, Knupfer G, Saukko P (eds) *Encyclopedia of forensic sciences*. Academic Press, Waltham, pp 252–260.
- Macho, G.A., 1986. An Appraisal of Plastic Reconstruction of the External Nose. *Journal of Forensic Sciences*. 31(4):11917J. Doi:10.1520/JFS11917J.
- Mang, A., Muller, J. & Buzug, T.M., 2006. A Multi-Modality Computer-Aided Framework Towards Postmortem Identification. *Journal of Computing and Information Technology*. 14(1):7. Doi:10.2498/cit.2006.01.02.
- Manhein, M.H., Listi, G.A., Barsley, R.E., Musselman, R., Barrow, N.E. & Ubelaker, D.H., 2000. In Vivo Facial Tissue Depth Measurements for Children and Adults. *Journal of Forensic Sciences*. 45(1):14640J. Doi: 10.1520/JFS14640J.
- Marin, F., Mansour, K.B., Demeter, F. & Frey, P., 2015. Displacement of facial soft tissues in upright versus supine positions. *Computer Methods in Biomechanics and Biomedical Engineering*. (August 20):1–2. Doi:10.1080/10255842.2015.1069590.
- Martens H. and Naes T. 1992. *Multivariate Calibration*. John Wiley and Sons.
- McCollum, M.A. 2008., Nasomaxillary remodeling and facial form in robust Australopithecus: a reassessment. *Journal of Human Evolution*. 54(1):2–14.
Doi: 10.1016/j.jhevol.2007.05.013.

- McDowell, J.L., L'Abbé, E.N. & Kenyhercz, M.W., 2012. Nasal aperture shape evaluation between black and white South Africans. *Forensic Science International*. 222(1–3): 397.e1-397.e6. [Doi: 10.1016/j.forsciint.2012.06.007](https://doi.org/10.1016/j.forsciint.2012.06.007).
- McDowell, J.L., Kenyhercz, M.W. & L'Abbé, E.N., 2015. An evaluation of nasal bone and aperture shape among three South African populations. *Forensic Science International*. 252:189. e1-189.e7. [Doi: 10.1016/j.forsciint.2015.04.016](https://doi.org/10.1016/j.forsciint.2015.04.016).
- Mevik, B.-H. & Cederkvist, H.R. 2004. Mean squared error of prediction (MSEP) estimates for principal component regression (PCR) and partial least squares regression (PLSR). *Journal of Chemometrics*. 18(9):422–429. [Doi: 10.1002/cem.887](https://doi.org/10.1002/cem.887).
- Mevik, B.-H. & Wehrens, R. 2007. The pls Package: Principal Component and Partial Least Squares Regression in R. *Journal of Statistical Software*. 18(2).
- Michael, S., and Chen, M., 1996. The 3D reconstruction of facial features using volume distortion. 14th Eurographics UK Conference. London.
- Mitteroecker, P. & Gunz, P. 2009. Advances in Geometric Morphometrics. *Evolutionary Biology*. 36(2):235–247. [Doi:10.1007/s11692-009-9055-x](https://doi.org/10.1007/s11692-009-9055-x).
- Moss, M.L. & Young, R.W., 1960. A functional approach to craniology. *American Journal of Physical Anthropology*. 18(4):281–292. [Doi: 10.1002/ajpa.1330180406](https://doi.org/10.1002/ajpa.1330180406).
- Moss, M.L. 1997a. The functional matrix hypothesis revisited. 1. The role of mechanotransduction. *American Journal of Orthodontics and Dentofacial Orthopedics*. 112(1):8–11. [Doi: 10.1016/S0889-5406\(97\)70267-1](https://doi.org/10.1016/S0889-5406(97)70267-1).
- Moss, M.L., 1997b. The functional matrix hypothesis revisited. 2. The role of an osseous connected cellular network. *American Journal of Orthodontics and Dentofacial Orthopedics*. 112(2):221–226. [Doi: 10.1016/S0889-5406\(97\)70249-X](https://doi.org/10.1016/S0889-5406(97)70249-X).
- Moss, M.L., 1997c. The functional matrix hypothesis revisited. 3. The genomic thesis. *American Journal of Orthodontics and Dentofacial Orthopedics*. 112(3):338–342. [Doi: 10.1016/S0889-5406\(97\)70265-8](https://doi.org/10.1016/S0889-5406(97)70265-8).
- Moss, M.L., 1997d. The functional matrix hypothesis revisited. 4. The epigenetic antithesis and the resolving synthesis. *American Journal of Orthodontics and Dentofacial Orthopedics*. 112(4):410–417. [Doi: 10.1016/S0889-5406\(97\)70049-0](https://doi.org/10.1016/S0889-5406(97)70049-0).
- Muller, J., Mang, A. & Buzug, T.M., 2005. A template-deformation method for facial reproduction. In Zagreb, Croatia: IEEE ISPA 2005. *Proceedings of the 4th International Symposium on Image and Signal Processing and Analysis, 2005*. 359–364. [Doi:10.1109/ISPA.2005.195438](https://doi.org/10.1109/ISPA.2005.195438).

- Munn, L. & Stephan, C.N., 2018. Changes in face topography from supine-to-upright position—And soft tissue correction values for craniofacial identification. *Forensic Science International*. 289:40–50. [Doi: 10.1016/j.forsciint.2018.05.016](https://doi.org/10.1016/j.forsciint.2018.05.016).
- Nelson, L. & Michael, S., 1998. The application of volume deformation to three-dimensional facial reconstruction: A comparison with previous techniques. *Forensic Science International*. 94(3):167–181. [Doi:10.1016/S0379-0738\(98\)00066-8](https://doi.org/10.1016/S0379-0738(98)00066-8).
- O’Higgins, P., Bromage, T.G., Johnson, D.R., Moore, W.J. & McPhie, P., 1991. A Study of Facial Growth in the Sooty Mangabey *Cercocebus atys*. *Folia Primatologica*. 56(2):86–94. [Doi: 10.1159/000156532](https://doi.org/10.1159/000156532).
- Oppelt, A., 2011. *Imaging systems for medical diagnostics: fundamentals, technical solutions and applications for systems applying ionizing radiation, nuclear magnetic resonance and ultrasound*. John Wiley & Sons.
- Ousley, S., Jantz, R. & Freid, D., 2009. Understanding race and human variation: Why forensic anthropologists are good at identifying race. *American Journal of Physical Anthropology*. 139(1):68–76. [Doi:10.1002/ajpa.21006](https://doi.org/10.1002/ajpa.21006).
- Paysan, P., Lüthi, M., Albrecht, T., Lerch, A., Amberg, B., Santini, F. & Vetter, T., 2009. Face Reconstruction from Skull Shapes and Physical Attributes. In Vol. 5748. J. Denzler, G. Notni, & H. Süße (eds.). Berlin, Heidelberg: Springer Berlin Heidelberg *Pattern Recognition*. 232–241. [Doi:10.1007/978-3-642-03798-6_24](https://doi.org/10.1007/978-3-642-03798-6_24).
- Pei, Y., Zha, H. & Yuan, Z., 2008. The Craniofacial Reconstruction from the Local Structural Diversity of Skulls. *Computer Graphics Forum*. 27(7):1711–1718. [Doi:10.1111/j.1467-8659.2008.01315.x](https://doi.org/10.1111/j.1467-8659.2008.01315.x).
- Petersen, D.C., Libiger, O., Tindall, E.A., Hardie, R.-A., Hannick, L.I., Glashoff, R.H., Mukerji, M., Indian Genome Variation Consortium, et al. 2013. Complex Patterns of Genomic Admixture within Southern Africa. *PLoS Genetics*. 9(3): e1003309. [Doi: 10.1371/journal.pgen.1003309](https://doi.org/10.1371/journal.pgen.1003309).
- Powell N, Humphreys B. 1984. Proportions of the aesthetic face. New York: Thieme-Stratton.
- Prag, J. & Neave, R., 1997. Making faces: using forensic and archaeological evidence [Bodies from the Bog]. London: British Museum, ISBN 0-7141-1743, 9.
- Prokopec, M. & Ubelaker, D. H., 2002. Reconstructing the shape of the nose according to the skull. *Forensic Sci Commun*, 4(1).

- Quatrehomme, G., Cotin, S., Subsol, G., Delingette, H., Garidel, Y., Grévin, G., Fidrich, M., Bailet, P., et al. 1997. A Fully Three-Dimensional Method for Facial Reconstruction Based on Deformable Models. *Journal of Forensic Sciences*. 42(4):14175J. [Doi:10.1520/JFS14175J](https://doi.org/10.1520/JFS14175J).
- R Core Team., 2002. R: a language and environment for statistical computing. Vienna, Austria: R Foundation for Statistical Computing. <http://www.R-project.org>.
- Ridel, A.F., Demeter, F., Liebenberg, J., L'Abbé, E.N., Vandermeulen, D. & Oettlé, A.C., 2018. Skeletal dimensions as predictors for the shape of the nose in a South African sample: A cone-beam computed tomography (CBCT) study. *Forensic Science International*. 289:18–26. [Doi: 10.1016/j.forsciint.2018.05.011](https://doi.org/10.1016/j.forsciint.2018.05.011).
- Rohlf, F.J. & Slice, D. 1990. Extensions of the Procrustes Method for the Optimal Superimposition of Landmarks. *Systematic Zoology*. 39(1):40. [Doi:10.2307/2992207](https://doi.org/10.2307/2992207).
- Rohlf, F.J. & Marcus, L.F. 1993. A revolution morphometrics. *Trends in Ecology & Evolution*. 8(4):129–132. [Doi:10.1016/0169-5347\(93\)90024-J](https://doi.org/10.1016/0169-5347(93)90024-J).
- Rohlf, F.J. & Corti, M., 2000. Use of Two-Block Partial Least-Squares to Study Covariation in Shape. *Systematic Biology*. 49(4):740–753. [Doi:10.1080/106351500750049806](https://doi.org/10.1080/106351500750049806).
- Rosas, A. & Bastir, M. 2002. Thin-plate spline analysis of allometry and sexual dimorphism in the human craniofacial complex. *American Journal of Physical Anthropology*. 117(3):236–245. [Doi:10.1002/ajpa.10023](https://doi.org/10.1002/ajpa.10023).
- Rynn, C., Wilkinson, C., and Peters, H., 2009. Prediction of nasal morphology from the skull. *Forensic Science, Medicine, and Pathology*, 6(1):20–34.
- Sahni, D., Jit, I., Gupta, M., Singh, P., Suri, S. & Sanjeev, K., 2002. Preliminary study on facial soft tissue thickness by magnetic resonance imaging in Northwest Indians. *Forensic Science Communications*, 4(1).
- Sahni, D., Sanjeev, Singh, G., Jit, I. & Singh, P., 2008. Facial soft tissue thickness in northwest Indian adults. *Forensic Science International*. 176(2–3):137–146. [Doi: 10.1016/j.forsciint.2007.07.012](https://doi.org/10.1016/j.forsciint.2007.07.012).
- Sauer, N.J. 1992. Forensic anthropology and the concept of race: If races don't exist, why are forensic anthropologists so good at identifying them? *Social Science & Medicine*. 34(2):107–111. [Doi:10.1016/0277-9536\(92\)90086-6](https://doi.org/10.1016/0277-9536(92)90086-6).
- Scarfe, W.C. & Farman, A.G., 2008. What is Cone-Beam CT and How Does it Work? *Dental Clinics of North America*. 52(4):707–730. [Doi: 10.1016/j.cden.2008.05.005](https://doi.org/10.1016/j.cden.2008.05.005).

- Scheib, J. E., Gangestad, S.W., and Thornhill, R., 1999. Facial attractiveness, symmetry and cues of good genes. *Proceedings of the Royal Society of London. Series B: Biological Sciences*, 266(1431):1913–1917.
- Schimmler, J.B., Helmer, R.P., and Rieger, J., 1993. Craniometric individuality of human skulls, in M.Y, Iscan and R.P. Helmer, *Forensic analysis of the skull*, pages 89–96. New York: Wiley-Liss, Inc.
- Schlager S., 2013. Soft-tissue reconstruction of the human nose: population differences and sexual dimorphism = Weichteilrekonstruktion der menschlichen Nase: Populationsunterschiede und Sexualdimorphismus, Universität, Freiburg.
- Schlager, S. & Rüdell, A., 2015. Analysis of the human osseous nasal shape-population differences and sexual dimorphism: Human Osseous Nasal Shape. *American Journal of Physical Anthropology*. 157(4):571–581. [Doi: 10.1002/ajpa.22749](https://doi.org/10.1002/ajpa.22749). 2015.
- Schlager, S. 2017. Calculations and Visualisations Related to Geometric Morphometrics. *R package version 0.23*, 3.
- Schneider, P. J., and Eberly, D., 2002. *Geometric Tools for Computer Graphics*. Elsevier Science Inc., New York, NY, USA.
- Scrucca, L., 2000. Assessing multivariate normality through interactive dynamic graphics. *Quaderni di Statistica*, 2, 221-240.
- Sforza, C., Grandi, G., De Menezes, M., Tartaglia, G.M. & Ferrario, V.F., 2011. Age- and sex-related changes in the normal human external nose. *Forensic Science International*. 204(1–3): 205.e1-205.e9. [Doi: 10.1016/j.forsciint.2010.07.027](https://doi.org/10.1016/j.forsciint.2010.07.027).
- Shahrom, A.W., Vanezis, P., Chapman, R.C., Gonzales, A., Blenkinsop, C. & Rossi, M.L., 1996. Techniques in facial identification: Computer-aided facial reconstruction using a laser scanner and video superimposition. *International Journal of Legal Medicine*. 108(4):194–200. [Doi:10.1007/BF01369791](https://doi.org/10.1007/BF01369791).
- Shepherd, John., 1981. "Studies of cue saliency." *Perceiving and remembering faces*.
- Sipahioğlu, S., Ulubay, H. & Diren, H.B., 2012. Midline facial soft tissue thickness database of Turkish population: MRI study. *Forensic Science International*. 219(1–3): 282.e1-282.e8. [Doi: 10.1016/j.forsciint.2011.11.017](https://doi.org/10.1016/j.forsciint.2011.11.017).
- Slice, D. E., 2001. Landmark coordinates aligned by Procrustes analysis do not lie in Kendall's shape space. *Systematic biology*, 50(1), 141-149.
- Slice, D.E. 2007. Geometric Morphometrics. *Annual Review of Anthropology*. 36(1):261–281. [Doi: 10.1146/annurev.anthro.34.081804.120613](https://doi.org/10.1146/annurev.anthro.34.081804.120613).

- Snow, C.C., Gatliff, B.P. & McWilliams, K.R., 1970. Reconstruction of facial features from the skull: An evaluation of its usefulness in forensic anthropology. *American Journal of Physical Anthropology*. 33(2):221–227. [Doi:10.1002/ajpa.1330330207](https://doi.org/10.1002/ajpa.1330330207).
- Snyders, J., Claes, P., Vandermeulen, D. & Suetens, P., 2014. Development and comparison of non-rigid surface registration algorithms and extensions.
- Spoor, C.F., Zonneveld, F.W. & Macho, G.A. 1993. Linear measurements of cortical bone and dental enamel by computed tomography: Applications and problems. *American Journal of Physical Anthropology*. 91(4) :469–484.
- Standring, S., Gray, H., 2009. Gray's anatomy: the anatomical basis of clinical practice, 40. ed., reprinted, Churchill Livingstone Elsevier, Edinburgh.
- Statistics South Africa, 2015. Mid-year Population Estimates (Census No. P0302). South Africa.
- Stephan, C.N., 2003. Anthropological facial 'reconstruction' – recognizing the fallacies, 'unembracing' the errors, and realizing method limits. *Science & Justice*. 43(4):193–200. [Doi:10.1016/S1355-0306\(03\)71776-6](https://doi.org/10.1016/S1355-0306(03)71776-6).
- Stephan, C.N., Henneberg, M. & Sampson, W., 2003. Predicting nose projection and pronasale position in facial approximation: A test of published methods and proposal of new guidelines. *American Journal of Physical Anthropology*. 122(3):240–250. [Doi: 10.1002/ajpa.10300](https://doi.org/10.1002/ajpa.10300).
- Stephan, C.N., 2006. Beyond the Sphere of the English Facial Approximation Literature: Ramifications of German Papers on Western Method Concepts*. *Journal of Forensic Sciences*. 51(4):736–739. [Doi:10.1111/j.1556-4029.2006.00175.x](https://doi.org/10.1111/j.1556-4029.2006.00175.x).
- Stephan, C. N., Taylor, R. & Taylor, J., 2008. Methods of facial approximation and skull-face superimposition, with special consideration of method development in Australia. *Forensic Approaches to Death, Disaster and Abuse*, 133.
- Stephan, C.N. 2014. Facial Approximation and Craniofacial Superimposition. In C. Smith (ed.). New York, NY: Springer New York *Encyclopedia of Global Archaeology*. 2721–2729. [Doi:10.1007/978-1-4419-0465-2_149](https://doi.org/10.1007/978-1-4419-0465-2_149).
- Stephan, C.N. 2015. Facial Approximation-From Facial Reconstruction Synonym to Face Prediction Paradigm. *Journal of Forensic Sciences*. 60(3):566–571. [Doi: 10.1111/1556-4029.12732](https://doi.org/10.1111/1556-4029.12732).
- Stephan, C.N. 2017. Estimating the Skull-to-Camera Distance from Facial Photographs for Craniofacial Superimposition. *Journal of Forensic Sciences*. 62(4):850–860. [Doi:10.1111/1556-4029.13353](https://doi.org/10.1111/1556-4029.13353).

- Stephan, C.N. & Preisler, R., 2018. In vivo facial soft tissue thicknesses of adult Australians. *Forensic Science International*. 282:220. e1-220.e12.
Doi: 10.1016/j.forsciint.2017.11.014.
- Stephan, C.N. & Sievwright, E., 2018. Facial soft tissue thickness (FSTT) estimation models— And the strength of correlations between craniometric dimensions and FSTTs. *Forensic Science International*. 286:128–140. Doi: 10.1016/j.forsciint.2018.03.011.
- Steyn, M., L'Abbé, E. N. & Myburgh, J., 2016. Forensic Anthropology as Practiced in South Africa. *Handbook of Forensic Anthropology and Archaeology*.
- Suazo Galdames, I.C., Cantín López, M., Zavando Matamala, D.A., Perez Rojas, F.J. & Torres Muñoz, S.R. 2008. Comparisons in Soft-Tissue Thicknesses on the Human Face in Fresh and Embalmed Corpses Using Needle Puncture Method. *International Journal of Morphology*. 26(1).
- Subsol G., and Quatrehomme G., 2005. Automatic 3D facial reconstruction by feature-based registration of a reference head. In Clement J. G. and Marks M. K., editors, Computergraphic facial reconstruction. Elsevier Academic Press, Amsterdam u.a, pp. 79–101.
- Sutherland, C., 2016. Biological Distance Among Modern and Parental South African Groups Using Discrete Traits of the Skull (M.Sc.). University of Pretoria, Pretoria,
- Taylor, K. 2000. *Forensic Art and Illustration*. CRC Press. Doi:10.1201/9781420036954.
- Thompson, L. M., 2001. *A history of South Africa*. Yale University Press.
- Thomson, A. & Buxton, L. D., 1923. Man's Nasal Index in Relation to Certain Climatic Conditions. *Journal of the Anthropological Institute of Great Britain and Ireland*, 92–122.
- Tilotta F., 2008. *Contribution à la reconstitution faciale en médecine légale : proposition d'une nouvelle méthode statistique* (Doctoral dissertation).
- Tilotta, F., Richard, F., Glaunès, J., Berar, M., Gey, S., Verdeille, S., Rozenholc, Y. & Gaudy, J.F., 2009. Construction and analysis of a head CT-scan database for craniofacial reconstruction. *Forensic Science International*. 191(1–3): 112.e1-112.e12.
- Tilotta, F.M., Glaunès, J.A., Richard, F.J.P. & Rozenholc, Y., 2010. A local technique based on vectorized surfaces for craniofacial reconstruction. *Forensic Science International*. 200(1–3):50–59. Doi: 10.1016/j.forsciint.2010.03.029.
- Todd, T.W. & Lindala, A. 1928. Thickness of the subcutaneous tissues in the living and the dead. *American Journal of Anatomy*. 41(2):153–196.

- Tomoyasu, Y., Yamaguchi, T., Tajima, A., Nakajima, T., Inoue, I. & Maki, K., 2009. Further evidence for an association between mandibular height and the growth hormone receptor gene in a Japanese population. *American Journal of Orthodontics and Dentofacial Orthopedics*. 136(4):536-541. [Doi: 10.1016/j.ajodo.2007.10.054](https://doi.org/10.1016/j.ajodo.2007.10.054).
- Troncoso Pazos, J.A., Suazo Galdames, I.C., Cantin Lopez, M., and Zavando Matamata, D.A., 2008. Sexual Dimorphism in the Nose Morphotype in Adult Chilean. *International Journal of Morphology*, 26:537 – 542.
- Tu, P.H., Kelliher, T.P., Miller, K.W.P., Taister, M.A., 2003. Towards a statistical basis for facial deformation modes in reconstruction, *Forensic Sci. Int.* 136S 168– 169.
- Tu, P., Hartley, R., Lorensen, W. E., Allyassin, M., Gupta, R. & Heier, L., 2005. *Face reconstruction using flesh deformation modes* (pp. 145-162). Elsevier Academic Press.
- Tu, P., Book, R., Liu, X., Krahnstoeber, N., Adrian, C. & Williams, P., 2007. Automatic Face Recognition from Skeletal Remains. In Minneapolis, MN, USA: *IEEE 2007 IEEE Conference on Computer Vision and Pattern Recognition*. 1–7. [Doi:10.1109/CVPR.2007.383060](https://doi.org/10.1109/CVPR.2007.383060).
- Turner, W.D., Brown, R.E.B., Kelliher, T.P., Tu, P.H., Taister, M.A. & Miller, K.W.P., 2005. A novel method of automated skull registration for forensic facial approximation. *Forensic Science International*. 154(2–3):149–158. [Doi: 10.1016/j.forsciint.2004.10.003](https://doi.org/10.1016/j.forsciint.2004.10.003).
- Tyrrell, A.J., Evison, M.P., Chamberlain, A.T. & Green, M.A., 1997. Forensic Three-Dimensional Facial Reconstruction: Historical Review and Contemporary Developments. *Journal of Forensic Sciences*. 42(4):1417-6J. [Doi:10.1520/JFS14176J](https://doi.org/10.1520/JFS14176J).
- Ullrich, H. & Stephan, C.N., 2011. On Gerasimov's Plastic Facial Reconstruction Technique: New Insights to Facilitate Repeatability*: Gerasimov's plastic facial reconstruction technique. *Journal of Forensic Sciences*. 56(2) :470–474. [Doi :10.1111/j.1556-4029.2010.01672. x](https://doi.org/10.1111/j.1556-4029.2010.01672.x).
- Vandermeulen, D., Claes, P., Suetens, R., De Greef, S. & Willems, G., 2005a. Volumetric deformable face models for cranio-facial reconstruction. In Zagreb, Croatia: *IEEE ISPA 2005. Proceedings of the 4th International Symposium on Image and Signal Processing and Analysis, 2005*. 353–358. [Doi :10.1109/ISPA.2005.195437](https://doi.org/10.1109/ISPA.2005.195437).
- Vandermeulen, D., Loubelle, M., Claes, P., Wang, Q., Mollemans, W., Srivastava, S. & Suetens, P., 2005b. Low-dose ct based soft tissue modeling for craniofacial reconstruction. In *Facial Reconstruction-Gesichtsrekonstruktion, proceedings RSFP 2005* (pp. 127-140).

- Vandermeulen, D., Claes, P., Loeckx, D., De Greef, S., Willems, G. & Suetens, P. 2006. Computerized craniofacial reconstruction using CT-derived implicit surface representations. *Forensic Science International*. 159: S164–S174.
- Vandermeulen, D., Claes, P., De Greef, S., Willems, G., Clement, J. & Suetens, P., 2012. Automated facial reconstruction. In C. Wilkinson & C. Rynn (eds.). Cambridge: Cambridge University Press *Craniofacial Identification*. 203–221.
- Vanezis, P., Blowes, R.W., Linney, A.D., Tan, A.C., Richards, R. & Neave, R., 1989. Application of 3-D computer graphics for facial reconstruction and comparison with sculpting techniques. *Forensic Science International*. 42(1–2):69–84. [Doi:10.1016/0379-0738\(89\)90200-4](https://doi.org/10.1016/0379-0738(89)90200-4).
- Vanezis, M. & Vanezis, P., 2000. Cranio-Facial Reconstruction in Forensic Identification — Historical Development and a Review of Current Practice. *Medicine, Science and the Law*. 40(3):197–205. [Doi:10.1177/002580240004000303](https://doi.org/10.1177/002580240004000303).
- Verzé, L., 2009. History of facial reconstruction. *Acta Bio Medica Atenei Parmensis*, 80(1), 5–12.
- Vogel, H.-J. 2005. Mees, F., Swennen, R., Van Geet, M. & Jacobs, P. (eds) Applications of X-ray Computed Tomography in the Geosciences. Geological Society of London, 2003. vi + 243 pp. f65 (US\$108), hardback. ISBN 1-86239-139-4. *European Journal of Soil Science*. 56(2):277–278. [Doi:10.1111/j.1365-2389.2004.0694f.x](https://doi.org/10.1111/j.1365-2389.2004.0694f.x).
- Weiner J.S., 1954. Nose shape and climate. *Am J Phys Anthropol* 12, 615–618.
- Welcker, H., 1883. *Schiller's Schädel und Todtenmaske: nebst Mittheilungen über Schädel und Todtenmaske Kant's. Mit einem Titelbilde, 6 Lithographirten Tafeln und 29 in den Text Eingedruckten Holzstichen*. Friedrich Vieweg und Sohn.
- White, T. D., Black, M. T. & Folkens, P. A., 2011. *Human osteology*. Academic press.
- Wilkinson, C. M., 2002. In vivo facial tissue depth measurements for white British children. *Journal of Forensic Science*, 47(3), 459-465.
- Wilkinson, C. M., 2003. Virtual sculpture as a method of computerized facial reconstruction. In *Proceedings of the 1st International Conference on Reconstruction of Soft Facial Parts* (pp. 17-18).
- Wilkinson, CM., Motwani, M., Chiang, E., 2003. The relationship between the soft tissues and the skeletal detail of the mouth. *J Forensic Sci*;48(4):728–32.
- Wilkinson C., 2004. *Forensic facial reconstruction*, Cambridge University Press, Cambridge, UK; New York.

- Wilkinson, C., 2010. Facial reconstruction – anatomical art or artistic anatomy? *Journal of Anatomy*. 216(2):235–250. [Doi:10.1111/j.1469-7580.2009.01182.x](https://doi.org/10.1111/j.1469-7580.2009.01182.x).
- Wittwer-Backofen, U., Gampe, J. & Vaupel, J.W. 2004. Tooth cementum annulation for age estimation: Results from a large known-age validation study. *American Journal of Physical Anthropology*. 123(2):119–129. [Doi: 10.1002/ajpa.10303](https://doi.org/10.1002/ajpa.10303).
- Wittwer-Backofen, U., Prieels, F., and Hering, P., 2007. Improvements in soft tissue data for facial reconstructions. In Buzug T., Sigl K., Bongartz J. and Prüfer K., editors, *Facial Reconstruction. Forensic, Medical and Archaeological Methods of the Reconstruction of Soft Facial Parts*, volume 35, pages 145–150.
- Wold, S., Sjöström, M. & Eriksson, L. 2001. PLS-regression: a basic tool of chemometrics. *Chemometrics and Intelligent Laboratory Systems*. 58(2):109–130. [Doi: 10.1016/S0169-7439\(01\)00155-1](https://doi.org/10.1016/S0169-7439(01)00155-1).
- Zankl, A., Eberle, L., Molinari, L. & Schinzel, A. 2002. Growth charts for nose length, nasal protrusion, and philtrum length from birth to 97 years. *American Journal of Medical Genetics*. 111(4):388–391. [Doi:10.1002/ajmg.10472](https://doi.org/10.1002/ajmg.10472).
- Zelditch, M., Swiderski, D., Sheets, D. H. & Fink, W., 2004. *Geometric morphometrics for biologists*. Elsevier: Acad. Press. 416 p.
- Zhao, W., Chellappa, R., Phillips, P.J. & Rosenfeld, A. 2003. Face recognition: A literature survey. *ACM Computing Surveys*. 35(4):399–458. [Doi: 10.1145/954339.954342](https://doi.org/10.1145/954339.954342).
- Zollikofer, C.P.E. & Ponce de Leon, M.S. 2002. Visualizing patterns of craniofacial shape variation in *Homo sapiens*. *Proceedings of the Royal Society B: Biological Sciences*. 269(1493):801–807. [Doi:10.1098/rspb.2002.1960](https://doi.org/10.1098/rspb.2002.1960).

Appendix A

LIST OF SPECIMENS

1. Specimens used for the validation of the automatic landmarking analysis (chapter 4).

Table 1. Sample details of 10 CBCT scans used for the validation of the automatic landmarking analysis.

N°	From	Ancestry	Age	Sex
1	Oral and Dental Hospital, University of Pretoria, South Africa	Black South African	29	F
2	Oral and Dental Hospital, University of Pretoria, South Africa	Black South African	21	F
3	Oral and Dental Hospital, University of Pretoria, South Africa	Black South African	28	F
4	Oral and Dental Hospital, University of Pretoria, South Africa	Black South African	27	F
5	Oral and Dental Hospital, University of Pretoria, South Africa	Black South African	25	F
6	Oral and Dental Hospital, University of Pretoria, South Africa	Black South African	23	M
7	Oral and Dental Hospital, University of Pretoria, South Africa	Black South African	21	M
8	Oral and Dental Hospital, University of Pretoria, South Africa	Black South African	29	M
9	Oral and Dental Hospital, University of Pretoria, South Africa	Black South African	26	M
10	Oral and Dental Hospital, University of Pretoria, South Africa	Black South African	28	M

92	Life Groenkloof Hospital, Pretoria, South Africa.	White South African	19	F
93	Life Groenkloof Hospital, Pretoria, South Africa.	White South African	22	F
94	Life Groenkloof Hospital, Pretoria, South Africa.	White South African	23	F
95	Life Groenkloof Hospital, Pretoria, South Africa.	White South African	18	F
96	Life Groenkloof Hospital, Pretoria, South Africa.	White South African	18	F
97	Life Groenkloof Hospital, Pretoria, South Africa.	White South African	24	M
98	Life Groenkloof Hospital, Pretoria, South Africa.	White South African	29	M
99	Life Groenkloof Hospital, Pretoria, South Africa.	White South African	18	M
100	Life Groenkloof Hospital, Pretoria, South Africa.	White South African	24	M
101	Life Groenkloof Hospital, Pretoria, South Africa.	White South African	25	F
102	Life Groenkloof Hospital, Pretoria, South Africa.	White South African	24	F
103	Life Groenkloof Hospital, Pretoria, South Africa.	White South African	24	F
104	Life Groenkloof Hospital, Pretoria, South Africa.	White South African	18	F
105	Life Groenkloof Hospital, Pretoria, South Africa.	White South African	19	F
106	Life Groenkloof Hospital, Pretoria, South Africa.	White South African	18	M
107	Life Groenkloof Hospital, Pretoria, South Africa.	White South African	18	M
108	Life Groenkloof Hospital, Pretoria, South Africa.	White South African	18	M
109	Life Groenkloof Hospital, Pretoria, South Africa.	White South African	20	M
110	Life Groenkloof Hospital, Pretoria, South Africa.	White South African	21	M
111	Oral and Dental Hospital, University of Pretoria, South Africa	White South African	29	M
112	Oral and Dental Hospital, University of Pretoria, South Africa	White South African	18	M
113	Oral and Dental Hospital, University of Pretoria, South Africa	White South African	24	M
114	Oral and Dental Hospital, University of Pretoria, South Africa	White South African	24	M
115	Oral and Dental Hospital, University of Pretoria, South Africa	White South African	29	M
116	Oral and Dental Hospital, University of Pretoria, South Africa	White South African	24	M
117	Oral and Dental Hospital, University of Pretoria, South Africa	White South African	27	M
118	Oral and Dental Hospital, University of Pretoria, South Africa	White South African	18	M
119	Oral and Dental Hospital, University of Pretoria, South Africa	White South African	18	M
120	Oral and Dental Hospital, University of Pretoria, South Africa	White South African	24	M

3. Specimens used for the nasal complex shape variation (chapter 6) and for the statistical modelling (chapter 7).

Table 3. Sample details of 200 CBCT scans used in this thesis.

N°	From	Ancestry	Age	Sex
1	Oral and Dental Hospital, University of Pretoria, South Africa	Black South African	29	F
2	Oral and Dental Hospital, University of Pretoria, South Africa	Black South African	21	F
3	Oral and Dental Hospital, University of Pretoria, South Africa	Black South African	28	F
4	Oral and Dental Hospital, University of Pretoria, South Africa	Black South African	27	F
5	Oral and Dental Hospital, University of Pretoria, South Africa	Black South African	25	F
6	Oral and Dental Hospital, University of Pretoria, South Africa	Black South African	23	M
7	Oral and Dental Hospital, University of Pretoria, South Africa	Black South African	21	M
8	Oral and Dental Hospital, University of Pretoria, South Africa	Black South African	29	M
9	Oral and Dental Hospital, University of Pretoria, South Africa	Black South African	26	M
10	Oral and Dental Hospital, University of Pretoria, South Africa	Black South African	28	M
11	Oral and Dental Hospital, University of Pretoria, South Africa	Black South African	27	M
12	Oral and Dental Hospital, University of Pretoria, South Africa	Black South African	18	M
13	Oral and Dental Hospital, University of Pretoria, South Africa	Black South African	21	M
14	Oral and Dental Hospital, University of Pretoria, South Africa	Black South African	20	M
15	Oral and Dental Hospital, University of Pretoria, South Africa	Black South African	21	M
16	Oral and Dental Hospital, University of Pretoria, South Africa	Black South African	25	M
17	Oral and Dental Hospital, University of Pretoria, South Africa	Black South African	18	M
18	Oral and Dental Hospital, University of Pretoria, South Africa	Black South African	25	M
19	Oral and Dental Hospital, University of Pretoria, South Africa	Black South African	37	F
20	Oral and Dental Hospital, University of Pretoria, South Africa	Black South African	34	F
21	Oral and Dental Hospital, University of Pretoria, South Africa	Black South African	41	F
22	Oral and Dental Hospital, University of Pretoria, South Africa	Black South African	41	F
23	Oral and Dental Hospital, University of Pretoria, South Africa	Black South African	31	F
24	Oral and Dental Hospital, University of Pretoria, South Africa	Black South African	36	F
25	Oral and Dental Hospital, University of Pretoria, South Africa	Black South African	33	F
26	Oral and Dental Hospital, University of Pretoria, South Africa	Black South African	31	M
27	Oral and Dental Hospital, University of Pretoria, South Africa	Black South African	34	M
28	Oral and Dental Hospital, University of Pretoria, South Africa	Black South African	31	M
29	Oral and Dental Hospital, University of Pretoria, South Africa	Black South African	44	M
30	Oral and Dental Hospital, University of Pretoria, South Africa	Black South African	35	M
31	Oral and Dental Hospital, University of Pretoria, South Africa	Black South African	33	M
32	Oral and Dental Hospital, University of Pretoria, South Africa	Black South African	37	M
33	Oral and Dental Hospital, University of Pretoria, South Africa	Black South African	38	M
34	Oral and Dental Hospital, University of Pretoria, South Africa	Black South African	32	M
35	Oral and Dental Hospital, University of Pretoria, South Africa	Black South African	40	M
36	Oral and Dental Hospital, University of Pretoria, South Africa	Black South African	44	M
37	Oral and Dental Hospital, University of Pretoria, South Africa	Black South African	40	M
38	Oral and Dental Hospital, University of Pretoria, South Africa	Black South African	32	M
39	Oral and Dental Hospital, University of Pretoria, South Africa	Black South African	44	M
40	Oral and Dental Hospital, University of Pretoria, South Africa	Black South African	34	M

164	Life Groenkloof Hospital, Pretoria, South Africa.	White South African	47	F
165	Life Groenkloof Hospital, Pretoria, South Africa.	White South African	55	F
166	Life Groenkloof Hospital, Pretoria, South Africa.	White South African	51	F
167	Life Groenkloof Hospital, Pretoria, South Africa.	White South African	57	F
168	Life Groenkloof Hospital, Pretoria, South Africa.	White South African	58	F
169	Life Groenkloof Hospital, Pretoria, South Africa.	White South African	50	F
170	Life Groenkloof Hospital, Pretoria, South Africa.	White South African	53	M
171	Life Groenkloof Hospital, Pretoria, South Africa.	White South African	49	M
172	Life Groenkloof Hospital, Pretoria, South Africa.	White South African	48	M
173	Life Groenkloof Hospital, Pretoria, South Africa.	White South African	48	M
174	Life Groenkloof Hospital, Pretoria, South Africa.	White South African	47	M
175	Life Groenkloof Hospital, Pretoria, South Africa.	White South African	45	M
176	Life Groenkloof Hospital, Pretoria, South Africa.	White South African	52	M
177	Life Groenkloof Hospital, Pretoria, South Africa.	White South African	76	F
178	Life Groenkloof Hospital, Pretoria, South Africa.	White South African	68	F
179	Life Groenkloof Hospital, Pretoria, South Africa.	White South African	87	F
180	Life Groenkloof Hospital, Pretoria, South Africa.	White South African	62	F
181	Life Groenkloof Hospital, Pretoria, South Africa.	White South African	66	F
182	Life Groenkloof Hospital, Pretoria, South Africa.	White South African	65	F
183	Life Groenkloof Hospital, Pretoria, South Africa.	White South African	66	F
184	Life Groenkloof Hospital, Pretoria, South Africa.	White South African	54	F
185	Life Groenkloof Hospital, Pretoria, South Africa.	White South African	63	F
186	Life Groenkloof Hospital, Pretoria, South Africa.	White South African	61	F
187	Life Groenkloof Hospital, Pretoria, South Africa.	White South African	77	F
188	Life Groenkloof Hospital, Pretoria, South Africa.	White South African	60	F
189	Life Groenkloof Hospital, Pretoria, South Africa.	White South African	69	F
190	Life Groenkloof Hospital, Pretoria, South Africa.	White South African	61	M
191	Life Groenkloof Hospital, Pretoria, South Africa.	White South African	72	M
192	Life Groenkloof Hospital, Pretoria, South Africa.	White South African	60	M
193	Life Groenkloof Hospital, Pretoria, South Africa.	White South African	79	M
194	Life Groenkloof Hospital, Pretoria, South Africa.	White South African	60	M
195	Life Groenkloof Hospital, Pretoria, South Africa.	White South African	20	M
196	Life Groenkloof Hospital, Pretoria, South Africa.	White South African	21	M
197	Oral and Dental Hospital, University of Pretoria, South Africa	White South African	29	M
198	Oral and Dental Hospital, University of Pretoria, South Africa	White South African	68	F
199	Oral and Dental Hospital, University of Pretoria, South Africa	White South African	75	F
200	Oral and Dental Hospital, University of Pretoria, South Africa	White South African	18	F

Appendix B

RESEARCH OUTPUT

1. Abstracts published in a journal as a conference proceeding.

- A.F. Ridel, F. Demeter, E.N. L'Abbé, J. Liebenberg, D.Vandermeulen, A.C. Oettlé, A computer-assisted method for approximation of the nose in South Africans from Cone Beam Computed Tomography (CBCT) scans. Colloque annuel de la Société d'anthropologie de Paris, 1843^e réunion scientifique : 27-29 janvier 2017, Poitiers. *Bulletins et Mémoires de la Société d'Anthropologie de Paris*, (2018) ; 30, S9-S31. SNIP 2016: 0.300, SJR 2016: 0.404.
- A.F. Ridel, F. Demeter, E.N. L'Abbé, J. Liebenberg, D.Vandermeulen, A.C. Oettlé, Skeletal dimensions as predictors of the external morphology of the nose using cone beam computed tomography (CBCT) in a South Africans sample. 45th Annual Conference of the Anatomical Society of Southern Africa (ASSA), 23-26 April 2017, Club Mykonos, Langebaan, Western Cape, South Africa. *Clinical Anatomy*, (2018) (in press). IF: 1.824.
- A.F. Ridel, F. Demeter, E.N. L'Abbé, D.Vandermeulen, A.C. Oettlé, A computer-assisted method for approximation of the nose in South Africans from Cone Beam Computed Tomography (CBCT) scans. 45th Annual Conference of the Anatomical Society of Southern Africa (ASSA), 23-26 April 2017, Club Mykonos, Langebaan, Western Cape, South Africa. *Clinical Anatomy*, (2018) (in press). IF: 1.824
- A.F. Ridel, F. Demeter, M. Galland, E.N. L'Abbé, D.Vandermeulen, A.C. Oettlé, Validation of the automatic landmarking for facial approximation using Cone Beam Computed Tomography (CBCT) scans. Colloque annuel de la Société d'anthropologie de Paris, 1843^e réunion scientifique : 24-26 janvier 2018, Poitiers. *Bulletins et Mémoires de la Société d'Anthropologie de Paris*, (2018) ; 30, S9-S31. SNIP 2016: 0.300, SJR 2016: 0.4.

2. Article.

- Ridel, A.F., Demeter, F., Liebenberg, J., L'Abbé, E.N., Vandermeulen, D. & Oettlé, A.C., 2018. Skeletal dimensions as predictors for the shape of the nose in a South African sample: A cone-beam computed tomography (CBCT) study. *Forensic Science International*. 289:18–26. [Doi:10.1016/j.forsciint.2018.05.011](https://doi.org/10.1016/j.forsciint.2018.05.011).

3. Conferences.

Paris (France), January 2017-Anthropological society of Paris:

- A computer-assisted method for approximation of the nose in South Africans from Cone Beam Computed Tomography (CBCT) scans.
AF RIDEL, F DEMETER , EN L'ABBÉ, D VANDERMEULEN , AC OETTLÉ.

Cape Town (South Africa), April 2017-Anatomical society of Southern Africa:

- Skeletal dimensions as predictors of the external morphology of the nose using cone beam computed tomography (CBCT) in a South Africans sample.
AF RIDEL, F DEMETER, EN L'ABBÉ, J LIEBENBERG, D VANDERMEULEN, AC OETTLÉ.
- A computer-assisted method for approximation of the nose in South Africans from Cone Beam Computed Tomography (CBCT) scans.
AF RIDEL, F DEMETER, EN L'ABBÉ, D VANDERMEULEN, AC OETTLÉ.

Brisbane (Australia), July 2017- International Association of,Craniofacial Identification Meeting:

- The variation of the shape of the nose among South African groups based on an automatic landmarking method from Cone Beam Computed Tomography (CBCT).
AF RIDEL, F DEMETER, EN L'ABBÉ, D VANDERMEULEN, AC OETTLÉ.
- Dimensions of the nasal skeleton to predict the shape and size of the nose on a South African sample.
AF RIDEL, F DEMETER, EN L'ABBÉ, D VANDERMEULEN, AC OETTLÉ.

- Approximation of the nose in South Africans by a new computer-assisted method.
AF RIDEL, F DEMETER, EN L'ABBÉ, D VANDERMEULEN, AC OETTLÉ.
- New Statistical Method for Estimate the Demic Origin of an Unidentified Skull.
PY LABLANCHE, A FROMENT, AC OETTLE, AF RIDEL, D VANDERMEULEN,
F DEMETER.

Pretoria (South Africa), August 2017- Sefako Makgatho University Research day:

- The variation of the shape of the nose among South African groups based on an automatic landmarking method from Cone Beam Computed Tomography (CBCT).
AF RIDEL, F DEMETER , EN L'ABBÉ, D VANDERMEULEN , AC OETTLÉ.

Pretoria (South Africa), August 2017- University of Pretoria Faculty day:

- The variation of the shape of the nose among South African groups based on an automatic landmarking method from Cone Beam Computed Tomography (CBCT).
AF RIDEL, F DEMETER, EN L'ABBÉ, D VANDERMEULEN, AC OETTLÉ.

Johannesburg (South Africa), September 2017- IMGRAD2017:

- Shape variation of the nose in a South African sample: A Cone Beam Computed Tomography study.
AF RIDEL, F DEMETER, EN L'ABBÉ, D VANDERMEULEN, AC OETTLÉ.

Paris (France), January 2018-Anthropological society of Paris:

- Validation of the automatic landmarking for facial approximation using South African Cone Beam Computed Tomography (CBCT) scans.
AF RIDEL, F DEMETER, M GALLAND, EN L'ABBÉ, D VANDERMEULEN, AC OETTLÉ.

Pretoria (South Africa), August 2018- Sefako Makgatho University Research day:

- Validation of the automatic landmarking for facial approximation using South African Cone Beam Computed Tomography (CBCT) scans.
AF RIDEL, F DEMETER , EN L'ABBÉ, D VANDERMEULEN , AC OETTLÉ.
- Application of automatic landmarking on Cone Beam Computed Tomography (CBCT) scans-based shape analysis of the nasal complex among South African groups.
AF RIDEL, F DEMETER , EN L'ABBÉ, D VANDERMEULEN , AC OETTLÉ.

Pretoria (South Africa), August 2018- University of Pretoria Faculty day:

- Application of automatic landmarking on Cone Beam Computed Tomography (CBCT) scans-based shape analysis of the nasal complex among South African groups.

AF RIDEL, F DEMETER , EN L'ABBÉ, D VANDERMEULEN , AC OETTLÉ.